



1-1-2014

# The Protein Tyrosine Phosphatase SHP2 as a Mediator of Differential Cellular Sensitivity to EGFR Kinase Inhibitors

Christopher Furcht

*University of Pennsylvania*, [chris.furcht@gmail.com](mailto:chris.furcht@gmail.com)

Follow this and additional works at: <http://repository.upenn.edu/edissertations>

 Part of the [Chemical Engineering Commons](#)

---

## Recommended Citation

Furcht, Christopher, "The Protein Tyrosine Phosphatase SHP2 as a Mediator of Differential Cellular Sensitivity to EGFR Kinase Inhibitors" (2014). *Publicly Accessible Penn Dissertations*. 1279.  
<http://repository.upenn.edu/edissertations/1279>

This paper is posted at ScholarlyCommons. <http://repository.upenn.edu/edissertations/1279>  
For more information, please contact [libraryrepository@pobox.upenn.edu](mailto:libraryrepository@pobox.upenn.edu).

---

# The Protein Tyrosine Phosphatase SHP2 as a Mediator of Differential Cellular Sensitivity to EGFR Kinase Inhibitors

## Abstract

SRC homology 2 domain-containing phosphatase 2 (SHP2) is a ubiquitously expressed cytosolic protein tyrosine phosphatase. Downstream of epidermal growth factor receptor (EGFR) and other receptors, SHP2 is activated by binding to phosphotyrosine-containing receptors and adapter proteins, is required for complete extracellular regulated kinase 1/2 (ERK) pathway activity, which promotes cellular proliferation and survival, and regulates other signaling processes. In this thesis, we explored the signaling functions of SHP2 in lung and brain cancer cell systems with or without clinically relevant mutations that render EGFR constitutively active and developed computational models of EGFR-mediated SHP2 activation. In non-small cell lung cancer cells, SHP2 promoted ERK-dependent resistance to EGFR inhibition, but in cells with EGFR kinase-activating mutations this SHP2 functional role was impaired through sequestration of biochemically active SHP2 with internalization-impaired EGFR mutants. In glioblastoma multiforme cells, SHP2 simultaneously promoted ERK activity and antagonized STAT3 phosphorylation such that SHP2 drove proliferation while also promoting sensitivity to EGFR and c-MET co-inhibition. These SHP2 functions were perturbed by sufficiently high expression of the EGFR variant III mutant. Furthermore, SHP2 was found to regulate EGFRvIII and c-MET phosphorylation and control hypoxia-inducible factor expression in a way that may regulate tumorigenesis. We next developed computational models and associated quantitative experimental data sets to gain quantitative understanding of the regulation of protein complexes containing SHP2 and GRB2-associated binder 1 (GAB1), the primary phosphorylated adapter with which SHP2 associates following EGFR activation. Our analysis revealed that in some cell settings EGFR activity is amplified by intermediary SRC family kinases (SFKs) which drive GAB1 phosphorylation and enable GAB1-SHP2 complexes to persist in the cytosol distal from EGFR. A reaction-diffusion model further predicted that EGFR-initiated GAB1-SHP2 complexes persist over the entire cell length scale, which could permit membrane-localized EGFR to regulate signaling events through SHP2 at subcellular locations where EGFR itself is not present. Overall, these results motivate the continued search for specific SHP2 inhibitors, while providing a contextual basis for predicting when such interventions may be particularly effective, and establish a quantitative framework for understanding EGFR's ability to activate SHP2 and how this might be perturbed in different pathological contexts.

## Degree Type

Dissertation

## Degree Name

Doctor of Philosophy (PhD)

## Graduate Group

Chemical and Biomolecular Engineering

## First Advisor

Matthew J. Lazzara

---

**Keywords**

extracellular signal-regulated kinase, gefitinib, glioblastoma multiforme, GRB2-associated binder 1, non-small cell lung cancer

**Subject Categories**

Chemical Engineering

THE PROTEIN TYROSINE PHOSPHATASE SHP2 AS A MEDIATOR OF  
DIFFERENTIAL CELLULAR SENSITIVITY TO EGFR KINASE INHIBITORS

Christopher Mark Furcht

A DISSERTATION

in

Chemical and Biomolecular Engineering

Presented to the Faculties of the University of Pennsylvania

in

Partial Fulfillment of the Requirements for the

Degree of Doctor of Philosophy

2014

---

Matthew J. Lazzara, Assistant Professor, Chemical and Biomolecular Engineering  
Supervisor of Dissertation

---

Raymond J. Gorte, Professor, Chemical and Biomolecular Engineering  
Graduate Group Chairperson

Dissertation Committee:

Dr. Scott L. Diamond, Professor, Chemical and Biomolecular Engineering

Dr. Dennis E. Discher, Professor, Chemical and Biomolecular Engineering

Dr. Jeffrey M. Field, Professor, Pharmacology

THE PROTEIN TYROSINE PHOSPHATASE SHP2 AS A MEDIATOR OF  
DIFFERENTIAL CELLULAR SENSITIVITY TO EGFR KINASE INHIBITORS

COPYRIGHT

2014

Christopher Mark Furcht

## **ACKNOWLEDGEMENT**

I would first like to thank Matt, both for his never-ending willingness to guide me throughout my studies and for his mentoring which shaped me into the scientist I am today. I would also like to thank Cal, Alice, Janine, Nick, and Andres for their camaraderie, which truly made my thesis experience a much more enjoyable one. I am also grateful to my other colleagues at Penn for their friendship over the years. Lastly, I would like to thank my parents and Alli for their love and patience throughout this process; your support made this all possible.

# ABSTRACT

## THE PROTEIN TYROSINE PHOSPHATASE SHP2 AS A MEDIATOR OF DIFFERENTIAL CELLULAR SENSITIVITY TO EGFR KINASE INHIBITORS

Christopher Mark Furcht

Matthew J. Lazzara

SRC homology 2 domain-containing phosphatase 2 (SHP2) is a ubiquitously expressed cytosolic protein tyrosine phosphatase. Downstream of epidermal growth factor receptor (EGFR) and other receptors, SHP2 is activated by binding to phosphotyrosine-containing receptors and adapter proteins, is required for complete extracellular regulated kinase 1/2 (ERK) pathway activity, which promotes cellular proliferation and survival, and regulates other signaling processes. In this thesis, we explored the signaling functions of SHP2 in lung and brain cancer cell systems with or without clinically relevant mutations that render EGFR constitutively active and developed computational models of EGFR-mediated SHP2 activation. In non-small cell lung cancer cells, SHP2 promoted ERK-dependent resistance to EGFR inhibition, but in cells with *EGFR* kinase-activating mutations this SHP2 functional role was impaired through sequestration of biochemically active SHP2 with internalization-impaired EGFR mutants. In glioblastoma multiforme cells, SHP2 simultaneously promoted ERK activity and antagonized STAT3 phosphorylation such that SHP2 drove proliferation while also promoting sensitivity to EGFR and c-MET co-inhibition. These SHP2 functions were

perturbed by sufficiently high expression of the EGFR variant III mutant. Furthermore, SHP2 was found to regulate EGFRvIII and c-MET phosphorylation and control hypoxia-inducible factor expression in a way that may regulate tumorigenesis. We next developed computational models and associated quantitative experimental data sets to gain quantitative understanding of the regulation of protein complexes containing SHP2 and GRB2-associated binder 1 (GAB1), the primary phosphorylated adapter with which SHP2 associates following EGFR activation. Our analysis revealed that in some cell settings EGFR activity is amplified by intermediary SRC family kinases (SFKs) which drive GAB1 phosphorylation and enable GAB1-SHP2 complexes to persist in the cytosol distal from EGFR. A reaction-diffusion model further predicted that EGFR-initiated GAB1-SHP2 complexes persist over the entire cell length scale, which could permit membrane-localized EGFR to regulate signaling events through SHP2 at subcellular locations where EGFR itself is not present. Overall, these results motivate the continued search for specific SHP2 inhibitors, while providing a contextual basis for predicting when such interventions may be particularly effective, and establish a quantitative framework for understanding EGFR's ability to activate SHP2 and how this might be perturbed in different pathological contexts.

# TABLE OF CONTENTS

<b>ACKNOWLEDGEMENT.....</b>	<b>III</b>
<b>ABSTRACT.....</b>	<b>IV</b>
<b>TABLE OF CONTENTS .....</b>	<b>VI</b>
<b>LIST OF TABLES .....</b>	<b>X</b>
<b>LIST OF FIGURES .....</b>	<b>XI</b>
<b>CHAPTER 1: INTRODUCTION.....</b>	<b>1</b>
1-1 RECEPTOR TYROSINE KINASE-MEDIATED CELL SIGNALING.....	1
1-2 EPIDERMAL GROWTH FACTOR RECEPTOR AND CANCER.....	2
1-3 SHP2 ACTIVATION AND FUNCTION .....	5
1-4 GAB1-SHP2 ASSOCIATION DYNAMICS AND LOCALIZATION .....	7
1-5 IMPLICATIONS OF SHP2 IN CANCER AND DISEASE .....	10
1-6 THESIS SUMMARY .....	11
<b>CHAPTER 2: DIMINISHED FUNCTIONAL ROLE AND ALTERED LOCALIZATION OF SHP2 IN NON-SMALL CELL LUNG CANCER CELLS WITH EGFR-ACTIVATING MUTATIONS .....</b>	<b>15</b>
2-1 ABSTRACT .....	15
2-2 INTRODUCTION .....	17
2-3 MATERIALS AND METHODS .....	20
Cell culture.....	20
Cell proliferation assay .....	20
shRNA and expression constructs .....	20
Immunoblotting .....	21
Immunoprecipitation.....	21
SHP2 activity assay .....	22
Immunofluorescence.....	22
Subcellular fractionation.....	23
Quantitative polymerase chain reaction (qPCR).....	23
Antibodies and other reagents.....	24
Statistics.....	24
IC50 calculations .....	24
2-4 RESULTS.....	25
Effects of SHP2 knockdown on ERK phosphorylation .....	25
Effects of SHP2 knockdown on cellular response to gefitinib .....	27
SHP2 association with GAB1 and EGFR and subcellular compartmentalization.....	31
Intracellular distribution of SHP2.....	33
Role of GAB1 in SHP2 localization and EGF-mediated effects .....	35
SHP2 activity .....	37
Effects of <i>SHP2</i> mutation .....	39

Importance of SHP2-mediated effects downstream of MET .....	41
2-5 DISCUSSION.....	42
2-6 ACKNOWLEDGEMENTS .....	48
2-7 SUPPLEMENTAL MATERIAL .....	49

### **CHAPTER 3: MULTIVARIATE SIGNALING REGULATION BY SHP2 DIFFERENTIALLY CONTROLS PROLIFERATION AND THERAPEUTIC RESPONSE IN GLIOMA CELLS.....63**

3-1 ABSTRACT .....	63
3-2 INTRODUCTION .....	64
3-3 MATERIALS AND METHODS .....	67
Cell culture.....	67
shRNA and stable expression constructs .....	67
Transient expression of wild-type or substrate-trapping SHP2 .....	68
Inhibitors.....	68
Cell death quantification .....	69
Proliferation measurements .....	69
XTT viability assay.....	69
Tumor xenografts.....	69
Subcellular fractionation.....	70
EGF internalization assay .....	71
Western blotting.....	71
Immunofluorescence.....	71
Immunoprecipitation.....	72
Antibodies.....	72
Statistics.....	73
3-4 RESULTS.....	74
SHP2 depletion differentially impacts key GBM cell phenotypes and associated signaling pathways .....	74
ERK and STAT3 pathways control cellular proliferation and survival in GBM cells.....	77
SHP2's ability to regulate signaling and phenotypes is modulated by elevated EGFRvIII expression .....	80
SHP2 can be sequestered with EGFRvIII at high receptor expression levels.....	84
SHP2 negatively regulates EGFRvIII and c-MET phosphorylation.....	87
SHP2 knockdown impedes tumor xenograft growth and expression of hypoxia-inducible factors .....	90
3-5 DISCUSSION.....	93
3-6 ACKNOWLEDGEMENTS.....	100
3-7 SUPPLEMENTAL MATERIAL .....	101

### **CHAPTER 4: EGFR-ACTIVATED KINASES COUNTERACT GAB1 DEPHOSPHORYLATION TO MAINTAIN GAB1-SHP2 COMPLEXES DISTAL FROM EGFR .....108**

4-1 ABSTRACT .....	108
4-2 INTRODUCTION .....	109
4-3 MATERIALS AND METHODS .....	112
Cell culture.....	112
Immunoblotting .....	112
Immunoprecipitation.....	112

Stable shRNA and expression constructs .....	112
Transient expression constructs .....	113
Antibodies and other reagents.....	113
Subcellular fractionation.....	114
Statistics.....	114
General model considerations and topology .....	114
EGF binding and concentration .....	115
ATP and inhibitor binding .....	115
EGFR dimerization.....	115
EGFR phosphorylation .....	115
GAB1 phosphorylation .....	115
PTP activity .....	116
EGFR degradation .....	116
GRB2, GAB1, and SHP2 binding.....	116
SFK activation .....	116
Parameter fitting .....	117
Sensitivity analysis .....	117
Representative H1666 cell.....	117
Model implementation.....	118
Process timescale calculations .....	118
4-4 RESULTS.....	119
In response to EGF, SHP2 remains in complex with GAB1 longer than with EGFR, and GAB1-SHP2 maintenance requires kinase activity to counteract multiple rounds of GAB1 dephosphorylation.....	119
Src family kinases are required for EGFR-initiated GAB1 phosphorylation and maintenance of GAB1-SHP2 association .....	122
GAB1-SHP2 complexes exist mainly in the cytosol .....	124
EGF and HGF promote different dynamics of GAB1-SHP2 complex persistence.....	126
A computational model reveals that SFKs amplify EGFR activity to maintain GAB1-SHP2 complexes distal from EGFR.....	128
Robustness and sensitivity analyses confirm the need for an SFK-mediated amplification mechanism and reveal key process controlling system behavior .....	133
4-5 DISCUSSION.....	138
4-6 ACKNOWLEDGEMENTS.....	143
4-7 SUPPLEMENTAL MATERIAL .....	144

## **CHAPTER 5: A REACTION-DIFFUSION MODEL PREDICTS THE INTRACELLULAR LENGTH SCALE OVER WHICH EGFR-INITIATED GAB1-SHP2 COMPLEXES PERSIST .....**

5-1 ABSTRACT .....	153
5-2 INTRODUCTION .....	155
5-3 MATERIALS AND METHODS .....	159
General model considerations and topology.....	159
Boundary conditions .....	161
Example equations.....	161
EGFR phosphorylation .....	162
GAB1 phosphorylation .....	163
SFK activation .....	163

GRB2, GAB1, and SHP2 binding.....	163
Phosphatase activity.....	163
EGFR inhibition.....	163
Protein diffusivity .....	163
Parameter fitting .....	164
Sensitivity analysis .....	164
Representative cell.....	164
Model implementation.....	164
5-4 RESULTS .....	167
Model predictions with baseline parameterization .....	167
Model parameter sensitivity.....	169
EGFR pulse-chase dynamics .....	173
Model extensions .....	175
5-5 DISCUSSION.....	178
5-6 ACKNOWLEDGEMENTS.....	183
5-7 SUPPLEMENTAL MODEL DEVELOPMENT .....	184
Reaction-diffusion equations and initial and boundary conditions.....	184
Discretization scheme using finite difference methods .....	189
<b>CHAPTER 6: IMPLICATIONS AND FUTURE WORK .....</b>	<b>193</b>
6-1 SUMMARY .....	193
6-2 DEVELOPMENT AND APPLICATION OF SHP2 INHIBITORS .....	194
6-3 INVOLVEMENT OF SHP2 IN EPITHELIAL-TO-MESENCHYMAL TRANSITION .....	197
6-4 INDUCIBLE KNOCKDOWN OF SHP2 IN GLIOBLASTOMA XENOGRAFTS .....	199
6-5 ROLE OF SHP2 PHOSPHORYLATION.....	200
6-6 LOCALIZATION OF SHP2 COMPLEXES IN MUTANT EGFR-EXPRESSING CELLS .....	201
6-7 CYTOSOLIC DISTRIBUTION OF GAB1-SHP2 COMPLEXES .....	204
<b>BIBLIOGRAPHY .....</b>	<b>207</b>

## LIST OF TABLES

Table S4-1: Model parameters.....	152
Table 5-1: Model parameters .....	166

## LIST OF FIGURES

Figure 1-1: Activation of SHP2 .....	6
Figure 1-2: Function of SHP2 downstream of EGFR.....	7
Figure 1-3: Example for the importance of SHP2 activity distal from EGFR.....	9
Figure 2-1: SHP2 knockdown reduces ERK phosphorylation more in NSCLC cells expressing wild-type EGFR than in those expressing EGFR mutants .....	26
Figure 2-2: Knockdown of SHP2 enhances cellular sensitivity to gefitinib in subsets of NSCLC cells .....	28
Figure 2-3: Observed effects of SHP2 knockdown on ERK phosphorylation and gefitinib response are specific to SHP2.....	30
Figure 2-4: GAB1 and EGFR are basally associated with SHP2 in NSCLC cells expressing EGFR mutants and are induced to associate with SHP2 by EGF in NSCLC cells expressing wild-type EGFR.....	32
Figure 2-5: Intracellular redistribution of SHP2 in response to EGF is observed in H1666 cells, but not in H3255 cells.....	34
Figure 2-6: GAB1 knockdown alters EGF-mediated ERK phosphorylation and response to gefitinib in H1666 cells.....	36
Figure 2-7: SHP2 is active in H1666 and H3255 cells, and EGF increases SHP2 activity in H1666 cells .....	38
Figure 2-8: Ectopic expression of SHP2 mutants alters cellular response to gefitinib in H1666 and H3255 cells.....	40
Figure 2-9: Sequestration of SHP2 at the plasma membrane may enhance gefitinib response in cells expressing EGFR mutants by reducing ERK activity .....	45
Figure S2-10: SHP2 knockdown reduces ERK phosphorylation more in NSCLC cells expressing wild-type, versus mutant, EGFR.....	49
Figure S2-11: EGF-mediated phosphorylation of SHP2 at Y542 is impaired in H3255 and HCC827 cells relative to H1666 cells.....	51
Figure S2-12: SHP2 knockdown more strongly influences the phosphorylation of ERK than phosphorylation of AKT or STAT3 in NSCLC cells expressing wild-type EGFR...	52

Figure S2-13: H292 cells are significantly growth inhibited by SHP2 knockdown, while HCC827 cells are not .....	54
Figure S2-14: EGF promotes membrane localization of SHP2 in H1666 cells, but not in H3255 cells .....	55
Figure S2-15: EGF promotes the formation of EGFR-positive endocytic vesicles in H1666 cells, but not in H3255 cells.....	56
Figure S2-16: GAB1 does not influence the localization of SHP2 in H1666 or H3255 cells, but does alter EGF-mediated ERK phosphorylation and response to gefitinib in H1666 cells .....	58
Figure S2-17: SHP2 is not required for HGF-mediated rescue of ERK phosphorylation in NSCLC cells treated with gefitinib.....	61
Figure S2-18: SHP2 is basally associated with GAB1 and pEGFR in H1781 cells.....	62
Figure 3-1: SHP2 knockdown differentially impacts GBM cell proliferation and survival.....	76
Figure 3-2: ERK and STAT3 pathways both control proliferation and survival of GBM cells .....	79
Figure 3-3: Sufficiently high EGFRvIII expression diminishes the ability of SHP2 to promote ERK activity and to reduce STAT3 phosphorylation in the presence of EGFR and c-MET inhibitors.....	83
Figure 3-4: Sufficiently high EGFRvIII expression suppresses EGF-mediated ERK phosphorylation by SHP2 sequestration .....	86
Figure 3-5: SHP2 mutant expression reveals negative regulation of EGFRvIII, c-MET, and STAT3 phosphorylation.....	89
Figure 3-6: Gefitinib and PHA665752 co-treatment or SHP2 knockdown impairs U87MG tumor xenograft growth .....	91
Figure 3-7: Summary of SHP2's oncogenic and anti-survival functions in GBM cells....	94
Figure S3-8: ERK and STAT3 inhibition differentially regulate GBM cell phenotype..	101
Figure S3-9: SHP2's abilities to promote ERK phosphorylation in resting cells and to antagonize STAT3 phosphorylation in drug-treated cells are diminished with sufficiently high EGFRvIII expression .....	102

Figure S3-10: With high levels of EGFRvIII expression, SHP2 becomes increasingly basally associated with EGFRvIII, SHP2 intracellular distribution is perturbed, and EGF-mediated ERK induction becomes impaired.....	104
Figure S3-11: SHP2 regulatory roles identified by SHP2 knockdown are confirmed by ectopic expression of SHP2 mutants.....	106
Figure 4-1: Timescales of protein dephosphorylation and signaling complex disassembly .....	120
Figure 4-2: Requirement of SFKs for EGF-initiated GAB1 phosphorylation and GAB1-SHP2 binding.....	123
Figure 4-3: Subcellular localization of GAB1-SHP2 complexes .....	125
Figure 4-4: Sustained association of GAB1 and SHP2 downstream of c-MET .....	127
Figure 4-5: Model topology and validation .....	129
Figure 4-6: Model requirement for SFK-mediated amplification of EGFR and model sensitivity .....	134
Figure 4-7: Schematic of EGFR-mediated GAB1-SHP2 complex maintenance .....	138
Figure S4-8: Differential rates of EGFR-SHP2 and GAB1-SHP2 complex disassemblies.....	144
Figure S4-9: SFK-mediated GAB1 phosphorylation and GAB1-SHP2 binding .....	146
Figure S4-10: Sustained HGF-mediated association of GAB1 and SHP2 .....	148
Figure S4-11: Model fitting to experimental data.....	149
Figure S4-12: Effect of variations in GAB1 phosphorylation ( $k_{G1p}$ ) and dephosphorylation ( $k_{G1dp}$ ) rate constants on model error.....	151
Figure 5-1: Base model predictions and fits .....	168
Figure 5-2: Model sensitivity analysis .....	171
Figure 5-3: EGF-pulse EGFR inhibition-chase predictions .....	174
Figure 5-4: Model predictions for SFKs only existing at the cell surface .....	176
Figure 5-5: Cytosolic SRC family kinases (SFks) extend the intracellular GAB1-SHP2 length scale by rephosphorylating GAB1. ....	179

# **Chapter 1: Introduction**

## **1-1 RECEPTOR TYROSINE KINASE-MEDIATED CELL SIGNALING**

The process of cell signaling enables the coordination of complex cellular decision-making, both within an individual cell and among several cells, through the sequential transfer of information between cellular proteins by processes such as protein modification and protein-protein binding, which ultimately influence cellular outcomes by altering gene transcription [1]. One key protein modification process involved in many aspects of cell signaling is phosphorylation, which is the covalent addition of a phosphate to a serine, threonine, or tyrosine residue on a substrate protein by enzymes known as kinases [2]. These phosphorylated residues can either alter the intrinsic activity of a phosphorylated protein, or activate other proteins by serving as binding sites for proteins containing phosphotyrosine binding (PTB) or Src-homology 2 (SH2) domains [3]. Both protein phosphorylation and binding are reversible processes, however, as bound proteins can dissociate from one another and phosphorylated proteins can have a phosphate removed through the process of dephosphorylation, which is catalyzed by enzymes known as phosphatases [4, 5].

Some of the major cellular components that initiate phosphorylation-dependent cell signaling pathways are receptor tyrosine kinases (RTKs), a family of transmembrane proteins that can translate extracellular cues into intracellular responses such as growth, differentiation, migration, and apoptosis [6]. RTKs typically function by binding extracellular ligands, which subsequently promotes the intrinsic kinase activity of these receptors. These activated RTKs are then able to phosphorylate various tyrosine residues

on their cytoplasmic tails, which serve as binding sites for cytosolic adapter proteins that ultimately promote the activity of numerous downstream signaling pathways such as the extracellular signal-regulated kinase (ERK), phosphoinositide 3-kinase (PI3K)/AKT, and signal transducer and activator of transcription (STAT) pathways [6]. This thesis specifically focuses on the epidermal growth factor receptor (EGFR), which binds ligands such as epidermal growth factor (EGF). For the case of EGFR, ligand binding promotes dimerization of two receptors, which activates the kinase activity of each receptor by relieving kinase domain auto-inhibition and subsequently permits trans-auto-phosphorylation of EGFR's C-terminal tyrosine residues [6].

## 1-2 EPIDERMAL GROWTH FACTOR RECEPTOR AND CANCER

While EGFR plays an important role in normal physiology, because signaling initiated by EGFR is typically associated with promoting cellular growth and survival, EGFR-mediated signaling is also frequently dysregulated in cancer as a result of EGFR overexpression or *EGFR* mutation [7]. Examples of cancers where EGFR is frequently overexpressed or mutated include non-small cell lung carcinoma (NSCLC), where 70-80% of tumors display elevated EGFR expression and 10-20% of tumors possess EGFR-activating mutations [8, 9], and glioblastoma multiforme (GBM), a common and aggressive form of brain cancer where EGFR is overexpressed in ~50% of cases and mutated in 30-40% of cases [10, 11].

As a way of combating EGFR-driven cancers, pharmaceutical companies have developed several classes of therapeutics targeted against EGFR [7]. One class of therapeutics is monoclonal antibodies that bind EGFR extracellular epitopes. For

example, cetuximab inhibits EGFR activity by preventing EGFR from binding ligands [12]. Another class of therapeutics is EGFR tyrosine kinase inhibitors such as gefitinib, which function as ATP analogues and block the intrinsic kinase activity of EGFR by competing with ATP for binding [13]. Although these therapeutics have had remarkable success in certain NSCLC patients, generally response is limited to 10% of patients, who are typically those with EGFR-activating mutations [9, 14, 15]. Conversely, GBM patients generally do not respond at all to EGFR-targeted therapeutics except in rare cases [16, 17]. Furthermore, cancers from patients who initially respond well to these therapeutics often become resistant to therapy over time [18], which can result from secondary mutations in *EGFR* which inhibit the binding of tyrosine kinase inhibitors to EGFR, such as the T790M point mutation [19, 20], or overexpression of other RTKs including c-MET, which can compensate for reduced EGFR function [21].

The aforementioned NSCLC-associated EGFR mutants display enhanced kinase activity relative to wild-type EGFR [22], and are also endocytosis-impaired [23, 24], suggesting they remain in a hyper-active state at the plasma membrane with the inability to be efficiently degraded through internalization. Consistent with these findings, NSCLC cells harboring *EGFR* mutations often display elevated phosphorylation of EGFR itself, as well as AKT, STAT3/5, ERBB3, and c-MET [15, 25, 26]. However, it was recently shown that these *EGFR* mutations surprisingly impair the phosphorylation of ERK, an important regulator of cell proliferation and survival whose activity can dampen cellular response to EGFR inhibition [24, 27]. These mutations were also shown to impair the phosphorylation of the protein tyrosine phosphatase SHP2, which is required for complete ERK activation downstream of EGFR and other RTKs [24, 28].

As phosphorylation of SHP2 is suggested to positively regulate its activity, these results imply that impaired function of SHP2 could potentially enhance sensitivity to EGFR-targeted therapies by rendering cells in a less survival-prone state due to diminished SHP2-mediated ERK activity [28, 29]. Conversely, the normal function of SHP2 in promoting ERK activity in wild-type EGFR-expressing cells may be at least partially responsible for the resistance of these cells to EGFR-targeted therapies.

The most frequent *EGFR* mutation in GBM is the in-frame deletion of exons 2-7, which encode a large portion of the extracellular domain, leading to expression of the EGFR variant III mutant (EGFRvIII) [11, 30-32]. EGFRvIII is found in ~50% of GBM with *EGFR* amplification [10, 11], and in other cancers, but not in normal tissues [33, 34], making it an ideal therapeutic target. In patients who have undergone major tumor resection followed by radiation, EGFRvIII expression is a negative indicator of  $\geq 1$  year survival [35]. The current standard of care for GBM involves tumor resection, followed by radiotherapy and subsequent temozolomide adjuvant chemotherapy [36-38]. Though *EGFR* amplification and EGFRvIII expression are observed in subsets of GBM, current clinical strategies are the same across GBM tumor sub-types because targeted therapeutic approaches have not produced substantial benefits. Since c-MET amplification and pathway activation promote resistance to therapy, c-MET pathway-targeted therapeutics are being evaluated in clinical trials in glioma patients [39], but initial results do not suggest great promise [40]. In contrast, the VEGF-targeted monoclonal antibody, bevacizumab, was approved in 2009 for use in GBM following primary therapy [41].

In intracranial murine xenograft models, EGFRvIII expression promotes enhanced tumorigenicity compared to cells expressing wild-type EGFR [42, 43].

EGFRvIII does not bind EGF with high affinity [44] but displays low constitutive phosphorylation compared to wild-type EGFR phosphorylation induced by EGF in PTEN-deficient U87MG glioblastoma cells [45]. EGFRvIII also potentiates downstream signaling differently than wild-type EGFR in ways that promote tumor aggressiveness. Similar to NSCLC-associated EGFR mutants, EGFRvIII expression impairs EGF-mediated receptor internalization [45, 46]. In murine xenografts, EGFRvIII expression dampens response to erlotinib and sustains ERK and AKT activity in the presence of erlotinib or a monoclonal antibody against hepatocyte growth factor [43], compared to wild-type EGFR. The STAT3 pathway may be over-activated in GBM cells, including those expressing EGFRvIII, and STAT3 inhibition can sensitize these cells to EGFR inhibition [47]. Such signaling perturbations may depend on EGFRvIII expression levels, as in U87MG cells where sufficiently high EGFRvIII expression drives AKT activation preferentially over the ERK and STAT3 pathways and results in c-MET phosphorylation [48]. When GBM cells from EGFRvIII transgenic mice are cultured *ex vivo*, EGFRvIII promotes AKT phosphorylation but impairs EGF-mediated ERK activation compared to wild-type EGFR [49], but the underlying mechanism remains unknown. ERK impairment has also been observed in NIH3T3 cells expressing EGFRvIII versus wild-type EGFR [50, 51], which may be related to the phenomenon of impaired phosphorylation of ERK and SHP2 observed in the context of NSCLC-associated EGFR mutants.

### 1-3 SHP2 ACTIVATION AND FUNCTION

The protein tyrosine phosphatase (PTP) SHP2 is an important signaling intermediate downstream of most RTKs, including EGFR [28]. Receptor activation

results in recruitment of SHP2 to receptors, either by direct binding to the receptor or through adapter proteins, which activates SHP2 through relief of auto-inhibitory interactions between its N-terminal SH2 domain and its catalytic PTP domain (Figure 1-1 ; [28]). A primary route of SHP2 recruitment to EGFR is through binding to GRB2-associated binder 1 (GAB1) phosphorylated at Y627 and Y659 [52], an adapter protein whose association with EGFR is mediated by GRB2 upon EGFR phosphorylation at either Y1068 and Y1086 [7]. RTK activation also results in phosphorylation of SHP2 at Y542 and Y580, which is required for full function of SHP2 downstream of some but not all RTKs [29].

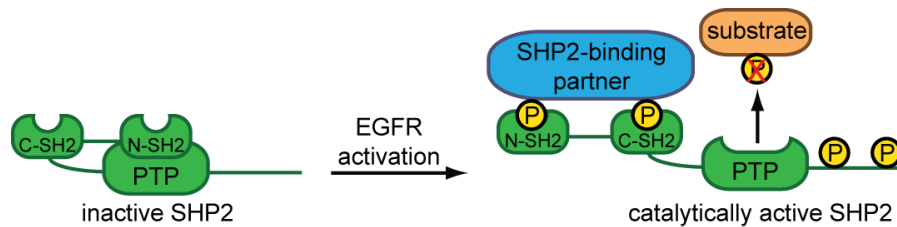


**Figure 1-1: Activation of SHP2.**

Basally, SHP2 is stabilized in an inactive state through binding of its N-terminal SH2 domain to its catalytic PTP domain. Upon activation of receptor tyrosine kinases including EGFR, SHP2 binding partners such as receptors or cytosolic adapter proteins become tyrosine phosphorylated. These tyrosines serve as binding sites for SHP2's N- and C-terminal SH2 domains, which when bound relieve basal auto-inhibition of SHP2 and allow access of SHP2's PTP domain to substrates.

SHP2's most well-studied functional role downstream of EGFR is to activate ERK by positively regulating RAS [53], via dephosphorylation of a RAS GTPase-activating protein (RASGAP) binding site on GAB1 (Figure 1-2 ; [54]) and c-SRC tyrosine kinase (CSK) binding sites on both paxillin [55] and phosphoprotein associated with glycolipid-enriched membranes (PAG), also known as CSK-binding protein (CBP)

[56]. Additionally, SHP2 is in some cases a regulator of the PI3K/AKT, c-Jun N-terminal kinase (JNK), and STAT signaling pathways [57-59].

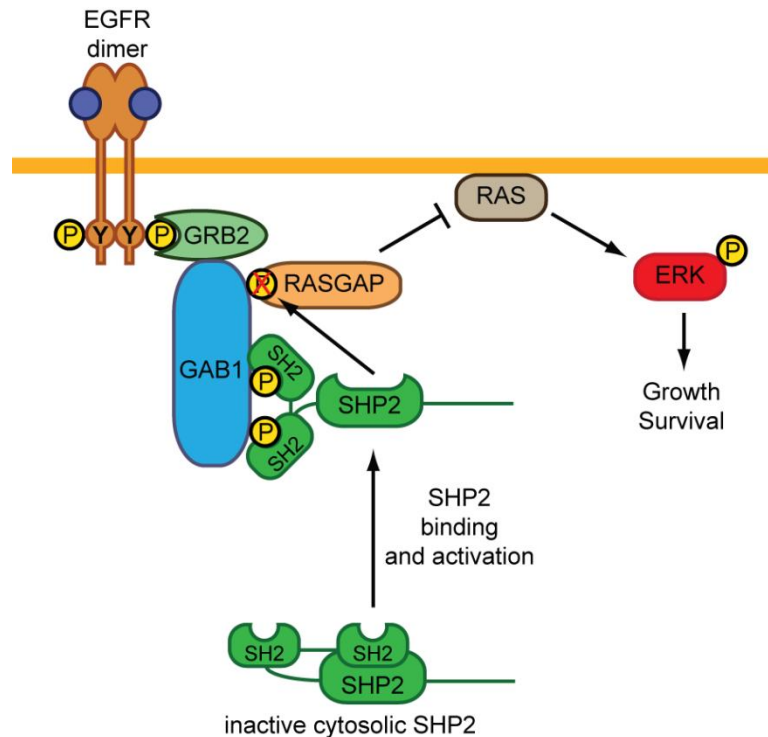


**Figure 1-2: Function of SHP2 Downstream of EGFR.**

Phosphorylation of EGFR at a representative tyrosine (Y) results in recruitment of the adapter protein GRB2, which binds GAB1. Following GAB1 phosphorylation, SHP2 is recruited to this EGFR-GRB2-GAB1 complex through interactions between GAB1 phosphotyrosines and SHP2 SH2 domains. Activated SHP2 is then able to promote the activation of RAS and subsequently ERK by several mechanisms including dephosphorylating RASGAP binding sites on GAB1.

#### 1-4 GAB1-SHP2 ASSOCIATION DYNAMICS AND LOCALIZATION

As previously noted, SHP2 is stabilized in an active state when it is bound with adapter proteins such as GAB1 [28]. Because cell phenotype can be determined by both the duration of a signaling protein's activity as well as the specific cellular localization of that protein [60], it is important to appreciate the dynamics and cellular distribution of

GAB1-SHP2 complexes to fully understand SHP2-mediated signaling. While GAB1-SHP2 complexes can be detected for at least 30 min following activation of growth factor receptors such as EGFR [55], these complexes are unlikely to remain statically associated for this period of time due to rate constants which suggest that phosphotyrosine-SH2 domain interactions fall apart on the order of seconds [61, 62]. This apparent discrepancy is resolved by similarly rapid rates of binding between phosphotyrosines and SH2 domains, which also occur on the order of seconds [61, 62]. Thus, while SHP2 may generally exist in an active, GAB1-bound state on a time scale of ~1 hr, it rapidly cycles between GAB1-bound and –unbound states on a time scale of ~1 sec. This notion is analogous to previous reports that suggest that protein post-translational modifications such as phosphorylation also frequently cycle between an “on” state (i.e. phosphorylated) and an “off” state (i.e. dephosphorylated) [63, 64].

While GAB1 and SHP2 are both cytosolic proteins, RTKs including EGFR have been reported to phosphorylate GAB1 and promote GAB1-SHP2 association [65]. Other possibilities may exist, however, as it has also been found that cytosolic Src family kinases (SFK) members can phosphorylate GAB1 [52, 66], although it has not been determined whether SFKs phosphorylate GAB1 on the specific tyrosines responsible for binding SHP2. Given that GAB1 and SHP2 rapidly dissociate, cytosolic kinases could play an important role in maintaining SHP2’s association with GAB1 distal from the plasma membrane due to the potential for cytosolic GAB1 to be quickly dephosphorylated. This could be an important mechanism for allowing EGFR to regulate SHP2 activity at sites distal from EGFR, such as focal adhesions (Figure 1-3; [55]).

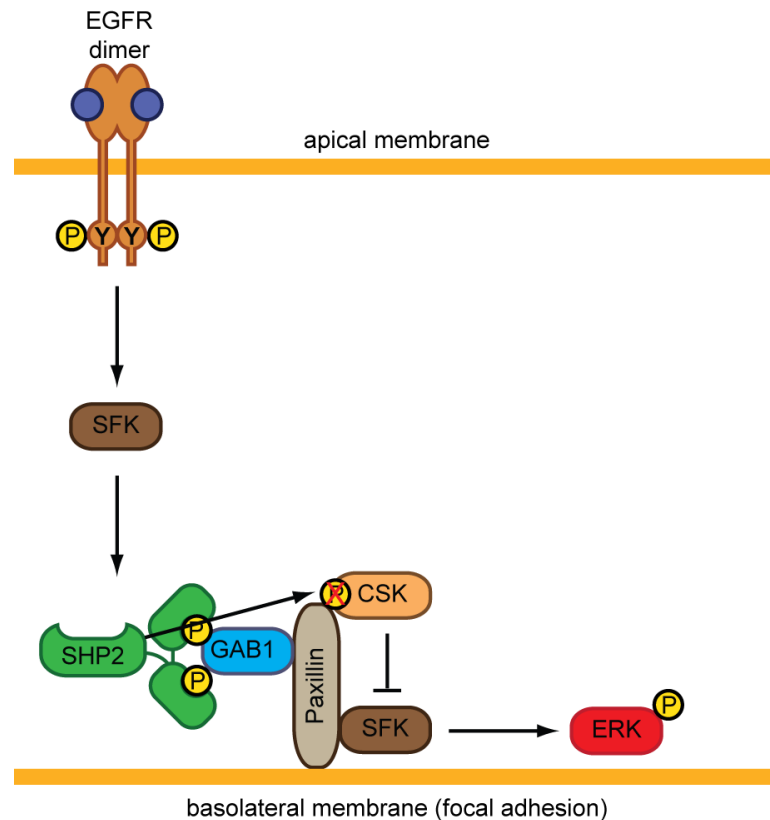


**Figure 1-3: Example for the importance of SHP2 activity distal from EGFR.**

A study from Ren et al. showed that downstream of EGFR, SHP2 is required to function at focal adhesions, where SHP2 dephosphorylates a tyrosine residue on the adapter protein paxillin. This tyrosine serves as a binding site for c-Src kinase (CSK), which negatively regulates the activity of Src family kinases (SFks) by phosphorylating them on an inhibitory tyrosine. As focal adhesions could be far from EGFR if EGFR were localized to the apical rather than the basolateral membrane, EGFR itself might not be able to maintain the association of GAB1 and SHP2 over the entire cellular length scale. Conversely, if EGFR were able to activate intermediary cytosolic kinases such as SFks, EGFR could distally maintain SHP2 activity by allowing SFks to phosphorylate GAB1 within the cytosol. This example also illustrates a potential mechanism by which SHP2 and SFks can act in a positive feedback loop.

In addition to the possibility for cytosolic kinases to extend the length scale over which GAB1 and SHP2 remain associated throughout the cytosol, the internalization of

RTKs may also permit GAB1-SHP2 complex nucleation to occur further from the plasma membrane. EGFR has recently been shown to remain phosphorylated and associated with GRB2 in endosomes following EGF stimulation [67], suggesting that RTKs can remain active and signaling-competent inside the cell. Indeed, recent evidence suggests that EGFR internalization is important for promoting SHP2-mediated signaling, as HeLa cells with a defect in clathrin-mediated endocytosis display impaired phosphorylation of both SHP2 and ERK in response to EGFR activation [24].

## 1-5 IMPLICATIONS OF SHP2 IN CANCER AND DISEASE

Based on the important role SHP2 has in regulating pro-survival signaling pathways such as ERK/MAPK, it is not surprising that SHP2 has been implicated in tumorigenesis. In fact, *PTPN11*, the gene encoding SHP2, was the first identified proto-oncogene encoding a tyrosine phosphatase [68]. Expression of SHP2 has been found to be elevated in several different cancers, including lung cancer and breast cancer [69, 70]. Additionally, SHP2 has been shown to be required for transformation downstream of oncoproteins such as CagA, Bcr-Abl, and EGFRvIII [71-73]. SHP2 has also recently been implicated in promoting epithelial-to-mesenchymal transition (EMT) in breast cancer cells [74], a process that is associated with cancer progression and metastasis [75, 76].

SHP2-activating mutations have been identified in several cancers including lung cancer, neuroblastoma, juvenile myelomonocytic leukemias, and acute myelogenous leukemias [77]. These mutations, which typically occur within the N-SH2 domain of SHP2, disrupt the basal auto-inhibition of SHP2 and render it constitutively active even in the absence of SHP2 binding partners [78]. Active SHP2 mutants also contribute to

other diseases such as Noonan syndrome, an autosomal dominant disorder, which is caused by SHP2-activating mutations in approximately 50% of diagnosed cases [78, 79].

Despite SHP2's well-defined role as an oncogene, in some cancer contexts SHP2 serves as a tumor suppressor. Hepatocyte-specific deletion of SHP2 can promote spontaneous tumor growth due to SHP2's negative regulatory role in IL-6-mediated STAT3 activation [59]. In GBM cells, SHP2 was also found to negatively regulate STAT3 [80], an important pro-survival signaling intermediate in GBM [47, 81], although the implications of this negative regulation were not explored. SHP2-inactivating mutations, which typically occur within the PTP domain of SHP2 and diminish the phosphatase activity of SHP2, can also promote diseases associated with diminished ERK activity such as LEOPARD syndrome [82].

## 1-6 THESIS SUMMARY

In this thesis, we explore the role of SHP2 in determining response to EGFR-targeted therapeutics using experimental techniques, and build upon these findings by analyzing the spatiotemporal activation of SHP2 downstream of EGFR using experimental methods paired with computational modeling techniques. In Chapter 2, we study the role of SHP2 in NSCLC cells with or without *EGFR* mutation. We find that SHP2 depletion in wild-type EGFR-expressing cells reduces ERK phosphorylation and enhances cellular response to the EGFR inhibitor gefitinib, confirming that SHP2-mediated ERK activity promotes resistance to EGFR inhibition. We also find that the functional role of SHP2 in mediating ERK phosphorylation is impaired in NSCLC cells expressing EGFR mutants compared to cells expressing wild-type EGFR, and that

impaired function of SHP2 at least partially contributes to the enhanced sensitivity of EGFR mutant-expressing cells to gefitinib. Our findings also reveal that the mechanism by which SHP2's function is impaired in the context of *EGFR* mutation is through apparent sequestration of biochemically active SHP2 at the plasma membrane with endocytosis-impaired EGFR mutants.

Based on these findings from Chapter 2, we sought to determine whether SHP2 function could also mediate resistance to targeted therapeutics in another cancer. In Chapter 3, we study the role of SHP2 in glioblastoma cells with or without expression of the constitutively active EGFRvIII mutant. While SHP2 is required for ERK phosphorylation and proliferation, consistent with our findings in NSCLC cells, SHP2 also simultaneously antagonizes STAT3 phosphorylation and promotes cell death response to gefitinib in combination with the c-MET inhibitor PHA665752. These regulatory roles of SHP2 are diminished with sufficiently high expression of EGFRvIII, analogous to our finding of an impaired functional role of SHP2 in NSCLC cells expressing EGFR mutants. SHP2 also antagonizes the phosphorylation of EGFRvIII and c-MET but concurrently promotes the expression of hypoxia inducible factors, thus providing further insight into SHP2's capacity to serve as both an oncogene and a tumor suppressor in glioblastoma cells.

In Chapter 4, we explore the dynamic regulation of SHP2's association with GAB1 downstream of EGFR. Experimental studies show that constant kinase activity is required to maintain the association of GAB1 and SHP2, due to the rapid rate at which SHP2 dissociates from GAB1, which itself is rapidly dephosphorylated when not bound with SHP2. Despite the rapid dephosphorylation of GAB1 following EGFR inactivation,

we find that GAB1 dephosphorylates more slowly relative to EGFR and can remain associated with SHP2 in the absence of EGFR's presence within the complex. To explain this apparent discrepancy, we go on to identify cytosolic SFKs as the primary kinases responsible for phosphorylating GAB1 and promoting GAB1-SHP2 association downstream of EGFR. To interpret our experimental data we construct a computational model trained against our experimental data. In order to best explain our data, the model requires that SFKs effectively amplify EGFR activity to buffer GAB1 phosphorylation, and thus GAB1-SHP2 association, when EGFR activity levels are diminished. This amplification is required even with perturbations to the model parameters and topology, confirming the robustness of this finding.

In Chapter 5, we expand upon the findings of Chapter 4 by developing a computational reaction-diffusion model that includes the reactions contained in the mechanistic model from Chapter 4 but also accounts for the process of protein diffusion in order to predict where GAB1-bound SHP2 is distributed throughout a representative lung cancer cell. While the concentration of active SFKs is predicted to quickly diminish distal from the plasma membrane, the concentration of phospho-GAB1 and GAB1-SHP2 complexes are predicted to remain essentially constant throughout the entire cell volume. This finding is dependent on the capacity for SFKs to phosphorylate GAB1 throughout the cytosol, as changing the model topology to permit SFKs to only be active at the plasma membrane results in steep declines in the predicted concentrations of phospho-GAB1 and GAB1-SHP2 complexes away from the plasma membrane. A parameter sensitivity analysis identifies protein diffusion as the most important model process for dictating the length scale of GAB1-SHP2 association distal from the plasma membrane.

The relationships between model processes on determining the GAB1-SHP2 complex length scale are also explored, which identifies that SFK overexpression can compensate for a faster rate of GAB1 dephosphorylation throughout the cytosol to maintain GAB1-SHP2 complexes distal from the plasma membrane, while SFK overexpression cannot compensate for a faster rate of SFK inactivation.

In Chapter 6, we discuss the implications of our findings, which offer support for both furthering the current understanding of SHP2 function in cancer as well as developing and testing SHP2-specific inhibitors for clinical applications. Our findings, of specific importance to SHP2-containing protein complexes, also highlight the broad need to better understand the dynamics and spatial regulation of phospho-protein complex assemblies initiated downstream of RTKs.

## **Chapter 2: Diminished Functional Role and Altered Localization of SHP2 in Non-small Cell Lung Cancer Cells with EGFR-activating Mutations<sup>1</sup>**

### **2-1 ABSTRACT**

Non-small cell lung cancer (NSCLC) cells harboring activating mutations of the epidermal growth factor receptor (EGFR) tend to display elevated activity of several survival signaling pathways. Surprisingly, these mutations also correlate with reduced phosphorylation of ERK and SHP2, a protein tyrosine phosphatase required for complete ERK activation downstream of most receptor tyrosine kinases. Since ERK activity influences cellular response to EGFR inhibition, altered SHP2 function could play a role in the striking response to gefitinib witnessed with *EGFR* mutation. Here, we demonstrate that impaired SHP2 phosphorylation correlates with diminished SHP2 function in NSCLC cells expressing mutant, versus wild-type, EGFR. In NSCLC cells expressing wild-type EGFR, SHP2 knockdown decreased ERK phosphorylation, basally and in response to gefitinib, and increased cellular sensitivity to gefitinib. In cells expressing EGFR mutants, these effects of SHP2 knockdown were less substantial, but expression of constitutively active SHP2 reduced cellular sensitivity to gefitinib. In cells expressing EGFR mutants, which do not undergo efficient ligand-mediated endocytosis, SHP2 was basally associated with GAB1 and EGFR, and SHP2's presence in membrane fractions was dependent on EGFR activity. Whereas EGF promoted a more uniform intracellular distribution of initially centrally localized SHP2 in cells expressing wild-

<sup>1</sup> A version of Chapter 2 was published as: Furcht, C. M., Muñoz Rojas, A. M., Nihalani, D., & Lazzara, M. J. (2013). Diminished Functional Role and Altered Localization of SHP2 in Non-Small Cell Lung Cancer Cells with EGFR-activating Mutations. *Oncogene*, 32(18), 2346-2356. (PMID: 22777356)

type EGFR, SHP2 was basally evenly distributed and did not redistribute in response to EGF in cells with *EGFR* mutation. Thus, *EGFR* mutation may promote association of a fraction of SHP2 at the plasma membrane with adapters which promote SHP2 activity. Consistent with this, SHP2 immunoprecipitated from cells with *EGFR* mutation was active, and EGF treatment did not change this activity. Overall, our data suggest that a fraction of SHP2 is sequestered at the plasma membrane in cells with *EGFR* mutation in a way that impedes SHP2's ability to promote ERK activity and identify SHP2 as a potential target for co-inhibition with EGFR in NSCLC.

## 2-2 INTRODUCTION

In non-small cell lung cancer (NSCLC), tumor response to the EGFR inhibitors gefitinib and erlotinib is generally limited to the 10-20% of NSCLCs carrying kinase-activating *EGFR* mutations [9, 14, 15]. NSCLC cells harboring these mutations often display elevated phosphorylation of EGFR, AKT, signal transducer and activator of transcription 3/5 (STAT3/5), ERBB3, and MET [15, 25, 26, 83]. Recently, it was shown that these *EGFR* mutations also surprisingly result in impaired EGFR-mediated phosphorylation of both ERK, an important determinant of cell response to gefitinib, and the protein tyrosine phosphatase SHP2 [24], which is required for complete ERK activation by most receptor tyrosine kinases [28]. Thus, the striking responsiveness of tumors with *EGFR* mutation to EGFR inhibition may result from an imbalance in EGFR oncogenic signaling wherein activating mutations promote some signaling pathways while simultaneously impairing others.

Activation of receptor tyrosine kinases, including EGFR, results in SHP2 phosphorylation at Y542, which is required for normal SHP2-mediated ERK activation in response to many growth factors [29]. Receptor activation and phosphorylation also results in SHP2 recruitment to receptors via direct binding or through adapters, which activates SHP2 through relief of auto-inhibitory intramolecular interactions [28]. SHP2 is recruited to EGFR through binding to phosphorylated adapter proteins including GRB2-associated binder 1 (GAB1) [52], whose association with EGFR is mediated by GRB2 upon EGFR phosphorylation at Y1068 and Y1086 [7]. Downstream of EGFR, SHP2 is primarily associated with promoting ERK activity by regulating RAS [53]. SHP2-activating mutations have been identified in Noonan syndrome, juvenile

myelomonocytic leukemia, and acute myelogenous leukemia [82, 84]. SHP2-activating mutations have also been found in lung cancer, although the consequences of these mutations are not fully understood [77].

The aforementioned differences in SHP2 and ERK phosphorylation in NSCLC cells with *EGFR* mutation suggest SHP2 function may be perturbed in this setting. However, the role of SHP2 in NSCLC has not been thoroughly evaluated. In previous studies, HeLa cells expressing dominant-negative dynamin [85], a GTPase required for clathrin-mediated EGFR endocytosis, displayed diminished EGF-mediated phosphorylation of SHP2 and ERK.[24] Since the EGFR-activating mutations observed in NSCLC result in impaired EGFR endocytosis [23, 24], differential EGFR trafficking may explain the defects in SHP2 and ERK phosphorylation in NSCLC cells expressing EGFR mutants. SHP2 localization could also be altered in the context of *EGFR* mutation via association with internalization-impaired EGFR.

In this study, we find diminished SHP2 function in NSCLC cells expressing mutant versus wild-type EGFR. In cells expressing wild-type EGFR, SHP2 knockdown reduced ERK phosphorylation and increased cellular sensitivity to gefitinib. In cells expressing EGFR mutants, the effects of SHP2 knockdown were less pronounced, but expression of constitutively active SHP2 reduced cellular sensitivity to gefitinib. In cells expressing EGFR mutants, SHP2 was basally associated with GAB1 and EGFR, and the presence of SHP2 in membrane fractions was dependent on EGFR activity. In cells expressing wild-type EGFR, EGF promoted redistribution of initially centrally localized SHP2, but SHP2 was basally evenly distributed and did not redistribute in response to EGF in cells expressing EGFR mutants. SHP2 was catalytically active in cells

expressing EGFR mutants, consistent with the finding that SHP2 association with adapters was not impaired, but rather basally elevated, in these cells. Overall, our data suggest that a fraction of SHP2 is sequestered at the plasma membrane in cells with *EGFR* mutation in a way that interferes with SHP2-mediated ERK activation and promotes cellular sensitivity to EGFR inhibition.

## 2-3 MATERIALS AND METHODS

**Cell culture.** H1666 and H3255 cells were maintained in ACL4 [24]. All others were maintained in RPMI 1640 supplemented with 100 units/mL penicillin, 100 µg/mL streptomycin, 1 mM L-glutamine, and 10% fetal bovine serum (FBS). H1666 cells were obtained from the American Type Culture Collection. H3255, H322, and H1781 cells were provided by Dr. Pasi Jänne (Dana-Farber Cancer Institute). H292 and HCC827 cells were provided by Dr. Eric Haura (Moffitt Cancer Center). For serum starvation, cells were switched to media containing 0.1% FBS for 16-18 hrs.

**Cell proliferation assay.** Proliferative response to gefitinib was measured by XTT assay according to manufacturer's specifications (Roche, Indianapolis, IN, USA). Cells seeded in 96-well plates were treated with up to 10 µM gefitinib for 4 days. Subsequently, fresh media and XTT reagent were added to wells, and plates were incubated for 2-4 hrs at 37°C to maximize signal-to-background. Wells containing only media were used for background correction. Each experiment was performed at least three times with each condition plated in three replicate wells on each day.

**shRNA and expression constructs.** Sequences encoding short hairpins targeting human *SHP2* and *GAB1* were cloned in the pSicoR vector (Tyler Jacks, MIT; [86]). The *SHP2* shRNA targeted nucleotides 1780-1798 of *SHP2* mRNA (GGACGTTTCATTGTGATTGA) or, for reconstitution experiments, 5890-5908 (GTATTGTACCAGAGTATTA). The *GAB1* shRNA targeted nucleotides 987-1005 of *GAB1* mRNA (GAAACAGACTGCAATGATA). Lentivirus was produced by calcium phosphate-mediated transfection of 293FT cells (Invitrogen, Carlsbad, CA, USA) with vector and the packaging plasmids pCMV-VSVG, pMDL-gp-RRE, and pRSV-Rev

(Marilyn Farquhar, UCSD). Virus was harvested 48 and 72 hrs post-transfection and used to infect target cells, which were selected in puromycin.

SHP2 cDNAs encoding wild-type, D61A, E76A, Y542F, and C459S SHP2 (Ben Neel, Ontario Cancer Institute) were inserted at the EcoRI site of the pBabe vector. Retrovirus was produced by calcium phosphate-mediated transfection of amphotropic Phoenix cells (Gary Nolan, Stanford University) with vector. Virus was harvested 24, 30, and 48 hrs post-transfection and used to infect target cells, which were selected in puromycin or hygromycin.

Constructs were validated by sequencing. SHP2 and GAB1 knockdowns were validated by Western blot and qPCR, respectively.

***Immunoblotting.*** Cell lysates were prepared using cell extraction buffer (Invitrogen; #FNN0011) supplemented with 1 mM PMSF, additional protease inhibitors (Sigma, St. Louis, MO, USA), and phosphatase inhibitors (Sigma). Proteins were resolved by SDS-PAGE and transferred to nitrocellulose membranes, which were blocked in Odyssey Blocking Buffer (OBB; LI-COR, Lincoln, NE, USA) and stripped with 0.2 M NaOH as needed. Images were obtained using a LI-COR Odyssey Infrared Imaging System.

***Immunoprecipitation.*** Cell lysates were prepared with immunoprecipitation lysis buffer (Cell Signaling Technology, Danvers, MA, USA; #9803) supplemented with 1 mM PMSF, additional protease inhibitors, and phosphatase inhibitors. 500 µg of total protein was precleared with Dynabeads (Invitrogen) for 4 hrs and subsequently incubated with Dynabeads conjugated to SHP2 or control antibody at 4°C overnight. Beads were

washed with lysis buffer, re-suspended in LDS sample buffer (Invitrogen), and boiled before SDS-PAGE.

***SHP2 activity assay.*** 500 µg of total protein from cell lysates was incubated overnight with agarose beads conjugated to an SHP2 antibody. Beads were washed with lysis buffer and split into two equal fractions. One fraction was reserved for immunoblotting. Beads from the other fraction were washed with assay buffer (Millipore, Billerica, MA, USA; #20-180) and resuspended in assay buffer containing 100 µM 6,8-difluoro-4-methylumbelliferyl phosphate (Invitrogen). The reaction was performed at 37°C for 30 min with occasional mixing, and reaction product fluorescence was measured at excitation and emission wavelengths of 360 nm and 460 nm, respectively. Linearity of signal with respect to time and protein concentration was validated for both cell lines.

***Immunofluorescence.*** Serum starved cells on coverslips were treated with EGF, fixed in 4% paraformaldehyde in PBS for 20 min, and permeabilized with 0.25% Triton X-100 for 5 min. Coverslips were incubated with primary antibodies diluted in OBB (EGFR, SHP2) or 1% BSA/0.3% Triton X-100 in PBS (RAB5) for 3 hrs at 37°C. Coverslips were washed with 0.1% Tween-20 in PBS and incubated with Alexa Fluor 488- and 594-conjugated secondary antibodies and Hoechst (Invitrogen) in the same diluents used for primary antibodies for 1 hr at 37°C. Coverslips were washed again, mounted on glass slides, and treated with Prolong Gold antifade (Invitrogen). Specificity of the SHP2 antibody was confirmed by comparison with SHP2 knockdown cells. Epifluorescence images were obtained with a Zeiss Axiovert 40 CFL microscope (100X

objective). Confocal images were obtained with a Nikon Eclipse TE-300 microscope (60X objective).

To analyze individual cells from these images, MATLAB was used to determine pixel intensities as a function of distance from the cell center. This was done by outlining individual cells, locating cell centers, and generating lines from the center to the cell periphery in all angular directions, along which pixel intensities were quantified. Data were averaged and normalized to obtain a vector of intensities versus normalized distances from the cell center.

***Subcellular fractionation.*** Serum starved cells were treated with 0 or 5  $\mu$ M gefitinib, washed, and collected in hypotonic buffer (10 mM Tris-HCl, pH 7.4, 1 mM  $MgCl_2$ , 1 mM EDTA) supplemented with 1 mM PMSF, additional protease inhibitors, and phosphatase inhibitors. Crude lysates were generated with a Dounce homogenizer and centrifuged at 3000 and 9300 rpm, for 5 min at each speed, to remove nuclei and mitochondria, respectively. Cleared lysates were centrifuged at 100 000 g for 60 min to separate membrane and cytosol fractions. Membrane pellets were washed with PBS, resuspended in hypotonic buffer, and centrifuged again at 100 000 g. After additional washes, membrane pellets were resuspended in immunoprecipitation lysis buffer to solubilize proteins before SDS-PAGE.

***Quantitative polymerase chain reaction (qPCR).*** Cellular RNA was isolated using an RNEasy kit (Qiagen, Valencia, CA, USA), and cDNA was transcribed using a High-Capacity cDNA Reverse Transcription Kit (Applied Biosciences, Foster City, CA, USA). Using the cDNA as a template, qPCR was performed with previously developed primers for *GAB1* mRNA using SYBR Green Master Mix (Applied Biosciences).[87]

Reactions were monitored on a Model 7300 Real Time PCR System (Applied Biosciences). RNA polymerase II mRNA was quantified as a normalization control using 5'-GCACCACGTCCAATGACAT-3' as the forward primer and 5'-GTGCGGCTGCTTCCATAA-3' as the reverse primer.

***Antibodies and other reagents.*** EGFR (immunoblotting; #2232), pAKT S473 (#9271), AKT (#9272), pERK T202/Y204 (#4377), ERK (#4695), RAB5 (#3547), pSTAT3 Y705 (#9138), and pGAB1 Y627 (#3233) antibodies were from Cell Signaling Technology. SHP2 (sc-280) and EGFR (immunofluorescence; sc-81449) antibodies were from Santa Cruz Biotechnology (Santa Cruz, CA, USA). Actin (MAB 1501) and GAB1 (#06-579) antibodies were from Millipore. pEGFR Y1068 (#1727) and pSHP2 Y542 (#2184) antibodies were from Epitomics (Burlingame, CA, USA), unless otherwise noted. Infrared dye- and Alexa Fluor-conjugated secondary antibodies were from Rockland Immunochemicals (Gilbertsville, PA, USA) and Invitrogen, respectively.

Gefitinib (LC Laboratories, Woburn, MA, USA) was diluted in DMSO. Recombinant human EGF was from Peprotech (Rocky Hill, NJ, USA). Recombinant human HGF (R&D Systems, Minneapolis, MN, USA) was generously provided by Dr. Anil Rustgi (University of Pennsylvania).

***Statistics.*** Statistical analyses were performed using a paired two-tailed student's t-test.

***IC<sub>50</sub> calculations.*** Gefitinib IC<sub>50</sub> values were determined by fitting a four parameter logistic function to normalized data.

## 2-4 RESULTS

***Effects of SHP2 knockdown on ERK phosphorylation.*** To assess the signaling role of SHP2 in NSCLC cells, we examined the effects of SHP2 knockdown on ERK phosphorylation in response to gefitinib in a panel of cell lines (Figures 2-1 and S2-10). In H322 and H292 cells (EGFR<sup>WT</sup>), SHP2 knockdown reduced ERK phosphorylation in untreated cells by more than 90%. In H1666 and H1781 cells (EGFR<sup>WT</sup>), SHP2 knockdown resulted in notable, but more modest, reductions in baseline ERK phosphorylation of ~60% and 20%, respectively, as well as reductions in the gefitinib IC<sub>50</sub> values for ERK phosphorylation. In H3255 cells (EGFR<sup>L858R</sup>), which display impaired EGF-mediated SHP2 phosphorylation relative to cells expressing wild-type EGFR (Figure S2-11; [24]), SHP2 knockdown had no substantial effect on ERK phosphorylation at any concentration of gefitinib. In HCC827 cells (EGFR<sup>delE746-A750</sup>), which also display impaired SHP2 phosphorylation (Figure S2-11; [24]), there was a reduction in baseline ERK phosphorylation with SHP2 knockdown compared to controls, but the effect was less substantial than that observed in cells expressing wild-type EGFR, other than H1781. There was also no enhancement in gefitinib's ability to inhibit ERK phosphorylation in SHP2-depleted HCC827 cells relative to controls. Relative to ERK phosphorylation, SHP2 knockdown produced smaller changes in AKT and STAT3 phosphorylation in H1666 and H292 cells (Figure S2-12).

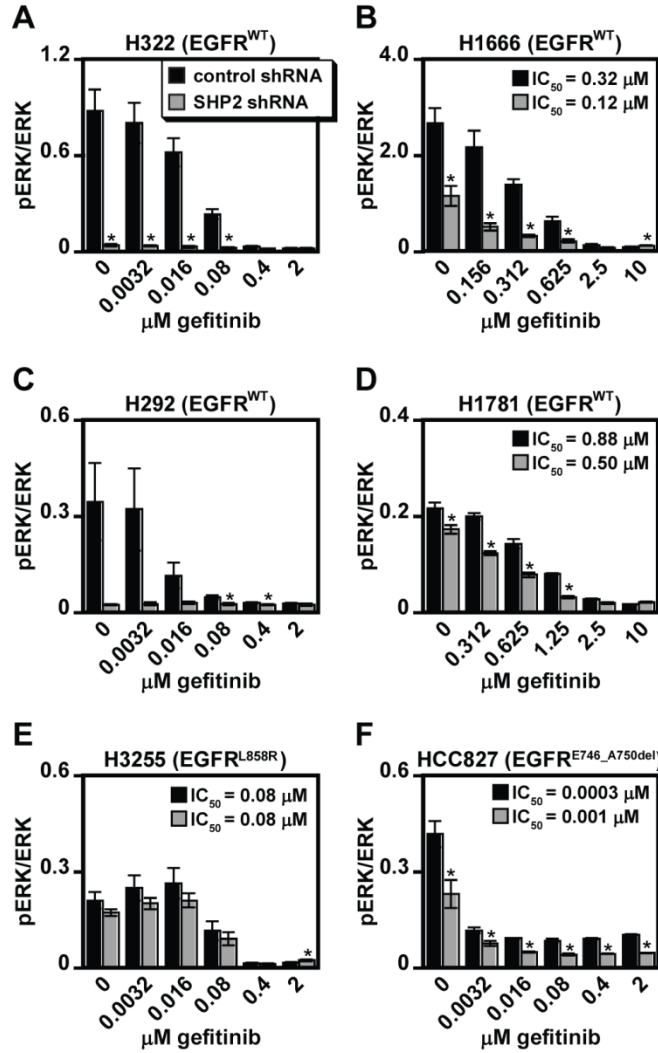


**Figure 2-1: SHP2 knockdown reduces ERK phosphorylation more in NSCLC cells expressing wild-type EGFR than in those expressing EGFR mutants.**

SHP2 knockdown reduces ERK phosphorylation more in NSCLC cells expressing wild-type EGFR than in those expressing EGFR mutants. H322 (A), H1666 (B), H292 (C), H1781 (D), H3255 (E), and HCC827 (F) cells expressing SHP2-targeting or non-targeting control shRNA were treated with 0-10 μM gefitinib for 48 hrs, and lysates were analyzed by Western blotting with antibodies against phosphorylated and total ERK. Densitometry data are represented as mean ± s.e.m. ( $n = 3$ ); \* denotes  $p < 0.05$  relative to controls.

***Effects of SHP2 knockdown on cellular response to gefitinib.*** In H322 and H1666 cells, SHP2 knockdown reduced gefitinib IC<sub>50</sub> values for cell proliferation by 15- and 3-fold, respectively (Figure 2-2). In H1781 cells, a gefitinib-resistant cell line, the IC<sub>50</sub> was reduced from > 10  $\mu$ M to 2.55  $\mu$ M. SHP2-depleted H292 cells were only modestly sensitized to gefitinib but were significantly growth inhibited in the absence of gefitinib (Figure S2-13A). Thus, gefitinib may have been unable to enhance the already striking effects of SHP2 knockdown on H292 proliferation. In contrast, H3255 cells showed virtually no effect of SHP2 knockdown on sensitivity to gefitinib (Figure 2-2E). HCC827 cells displayed a small shift in sensitivity to gefitinib in response to SHP2 knockdown (Figure 2-2F), but we measured no proliferative effect in the absence of gefitinib (Figure S2-13B).

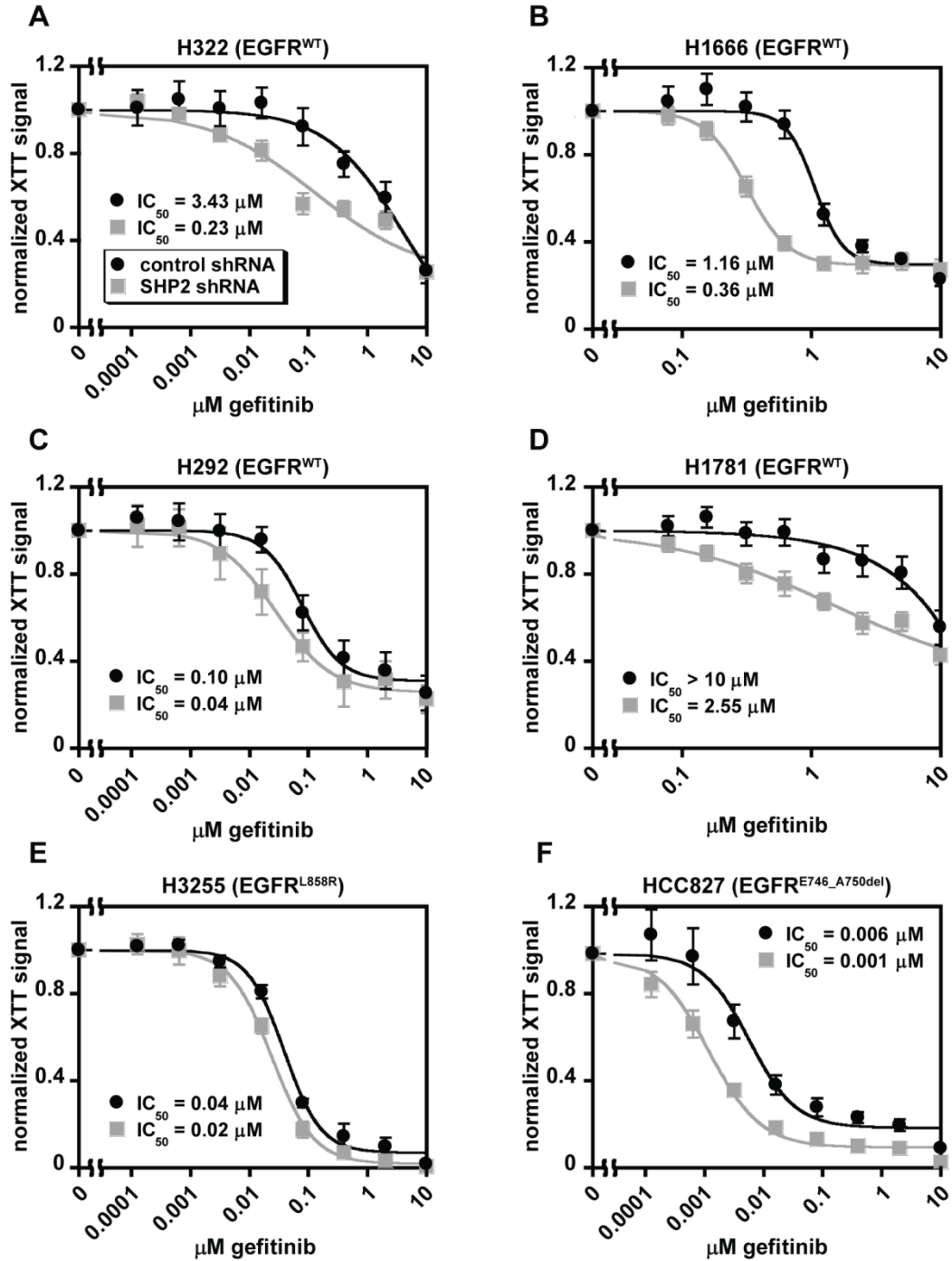


**Figure 2-2: Knockdown of SHP2 enhances cellular sensitivity to gefitinib in subsets of NSCLC cells.**

H322 (A), H1666 (B), H292 (C), H1781 (D), H3255 (E), and HCC827 (F) cells expressing SHP2-targeting or non-targeting control shRNA were treated with 0-10  $\mu M$  gefitinib for four days, and cell proliferation was measured by XTT assay. Normalized

XTT signal values (y-axis) were computed at a given gefitinib concentration by dividing absorbances by those measured for cells treated with DMSO as a control. Data are represented as mean  $\pm$  s.e.m. for three experiments with three replicate wells in each experiment ( $n = 3$ ).

To ensure the measured effects were specific for SHP2, we knocked down SHP2 in a representative cell line expressing wild-type EGFR using an independent hairpin targeting the 3' untranslated region of *SHP2* and reconstituted cells with SHP2<sup>WT</sup> or SHP2<sup>Y542F</sup> (Figure 2-3). As before, SHP2-depleted cells displayed impaired ERK phosphorylation and enhanced sensitivity to gefitinib. These effects were partially rescued by reconstitution with SHP2<sup>WT</sup> or SHP2<sup>Y542F</sup>.

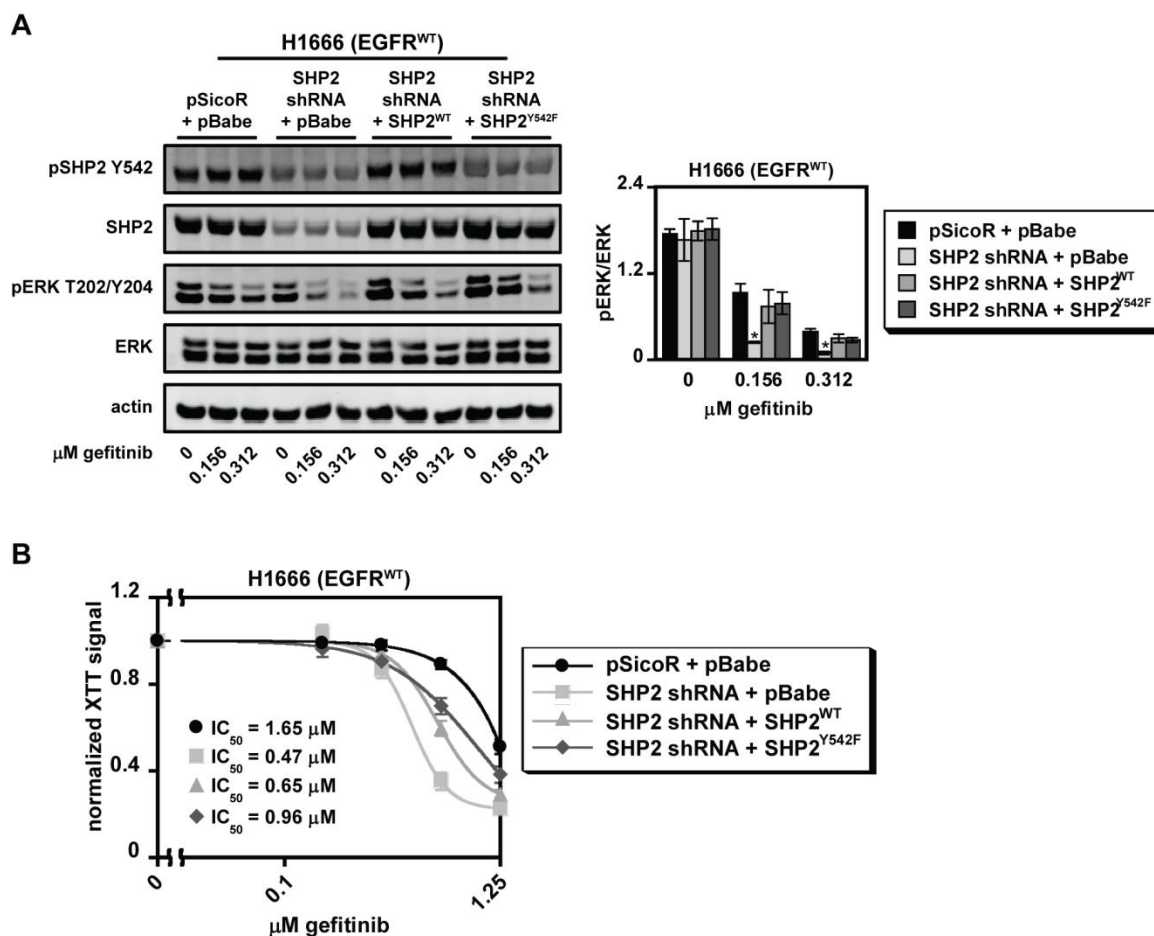


**Figure 2-3: Observed effects of SHP2 knockdown on ERK phosphorylation and gefitinib response are specific to SHP2.**

H1666 cells expressing SHP2-targeting shRNA or an empty pSicoR vector were transduced with SHP2<sup>WT</sup>, SHP2<sup>Y542F</sup>, or an empty pBabe vector. **(A)** Cells were treated with 0-10 μM gefitinib for 48 hrs, and lysates were analyzed by Western blotting with antibodies against indicated proteins. Images are representative of three sets of biological replicates. Densitometry data for ERK are represented as mean ± s.e.m. ( $n = 3$ ); \* denotes  $p < 0.05$  relative to pSicoR and pBabe controls. **(B)** Cells were treated with 0-10 μM gefitinib for four days, and cell proliferation was measured by XTT assay. Normalized XTT signal values (y-axis) were computed at a given gefitinib concentration by dividing absorbances by those measured for cells treated with DMSO as a control. Data points are represented as mean ± s.e.m. for three replicate wells from at least three experiments.

***SHP2 association with GAB1 and EGFR and subcellular compartmentalization.*** To investigate the mechanism underlying apparent differential SHP2 function in cells with or without *EGFR* mutation, we examined SHP2 association with GAB1 and EGFR. In H3255 and HCC827 cells, SHP2 was basally associated with GAB1 and phosphorylated EGFR to a significantly greater degree than in either H322 or H1666 cells (Figure 2-4A). In H3255 cells, these associations were diminished by gefitinib (Figure 2-4B). EGF enhanced SHP2 association with GAB1 and EGFR in all cell lines, but the fold increases in association were generally smaller in H3255 and HCC827 cells (Figure 2-4A). Since EGFR mutants fail to undergo efficient EGF-mediated endocytosis [23, 24], we interpreted these findings as indicating that a fraction of SHP2 was sequestered at the plasma membrane in cells with *EGFR* mutation. To further substantiate this, we analyzed SHP2's distribution in a subset of these cells by subcellular fractionation. In H1666 and H3255 cells, the majority of SHP2 was cytosolic. Only in H3255 cells, however, did gefitinib reduce SHP2 levels in crude membrane fractions, suggesting that SHP2 was membrane-localized in an EGFR-dependent manner (Figure 2-4C). The EGFR activity-independent presence of SHP2 in H1666 membrane fractions could be explained by SHP2 localization to membrane compartments which settle with plasma membrane in the crude membrane fraction generated by our protocol. This possibility is suggested by previous studies [88].

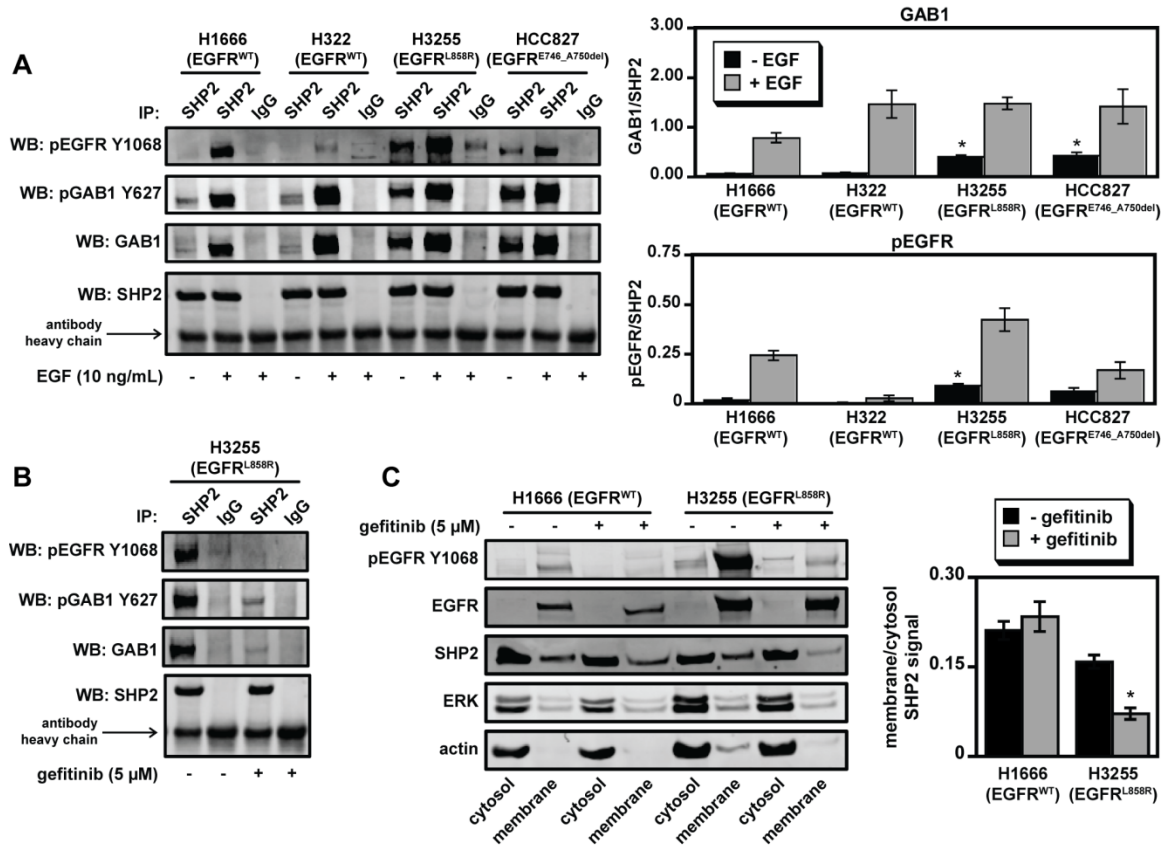


**Figure 2-4: GAB1 and EGFR are basally associated with SHP2 in NSCLC cells expressing EGFR mutants and are induced to associate with SHP2 by EGF in NSCLC cells expressing wild-type EGFR.**

Serum-starved cells treated with or without 10 ng/mL EGF for 5 min (**A**), or serum-starved H3255 cells treated with or without 5  $\mu$ M gefitinib for 15 min (**B**), were lysed. Lysates were immunoprecipitated with either an SHP2 or control antibody, and immunoprecipitates were analyzed by Western blotting using antibodies against the indicated proteins. Images are representative of three sets of biological replicates. Densitometry data in (**A**) are represented as mean  $\pm$  s.e.m. ( $n = 3$ ); \* denotes  $p < 0.05$  relative to wild-type EGFR-expressing cells not stimulated with EGF. (**C**) Subcellular fractions were prepared from H1666 and H3255 cells treated with or without gefitinib, as described in *Materials and Methods* (Section 2-3), and equivalent relative amounts of the fractions for both cell lines were analyzed by Western blotting using antibodies against indicated proteins. To improve signals, membrane fractions were 10 $\times$  more concentrated than cytosolic fractions in terms of the relative amount of total lysate loaded. Images are

representative of three sets of biological replicates. Blots were quantified to determine the relative difference in membrane-localized SHP2 in H1666 versus H3255 cells. For each condition, SHP2 signal from the membrane fraction was divided by the SHP2 signal from the cytosol fraction to determine a membrane/cytosol SHP2 signal. Data are represented as mean  $\pm$  s.e.m. ( $n = 4$ ); \* denotes  $p < 0.05$  relative to untreated cells.

***Intracellular distribution of SHP2.*** We further examined EGF's ability to alter the intracellular distribution of SHP2 in H1666 and H3255 cells by immunofluorescence. In H1666 cells, the distribution shifted from one where SHP2 was concentrated around the cell center to one where some SHP2 moved toward the cell periphery and SHP2 was distributed more uniformly (Figure 2-5). Similar changes were noted by confocal microscopy, including movement of SHP2 to membrane ruffles (Figure S2-14). EGF also caused the formation of EGFR- and RAB5-positive endocytic vesicles in H1666 cells (Figure S2-15). In H3255 cells, SHP2 was basally uniformly distributed. EGF did not alter this distribution or generate endocytic vesicles (Figures 2-5, S2-14, and S2-15), consistent with previous reports of impaired EGFR internalization in these cells.

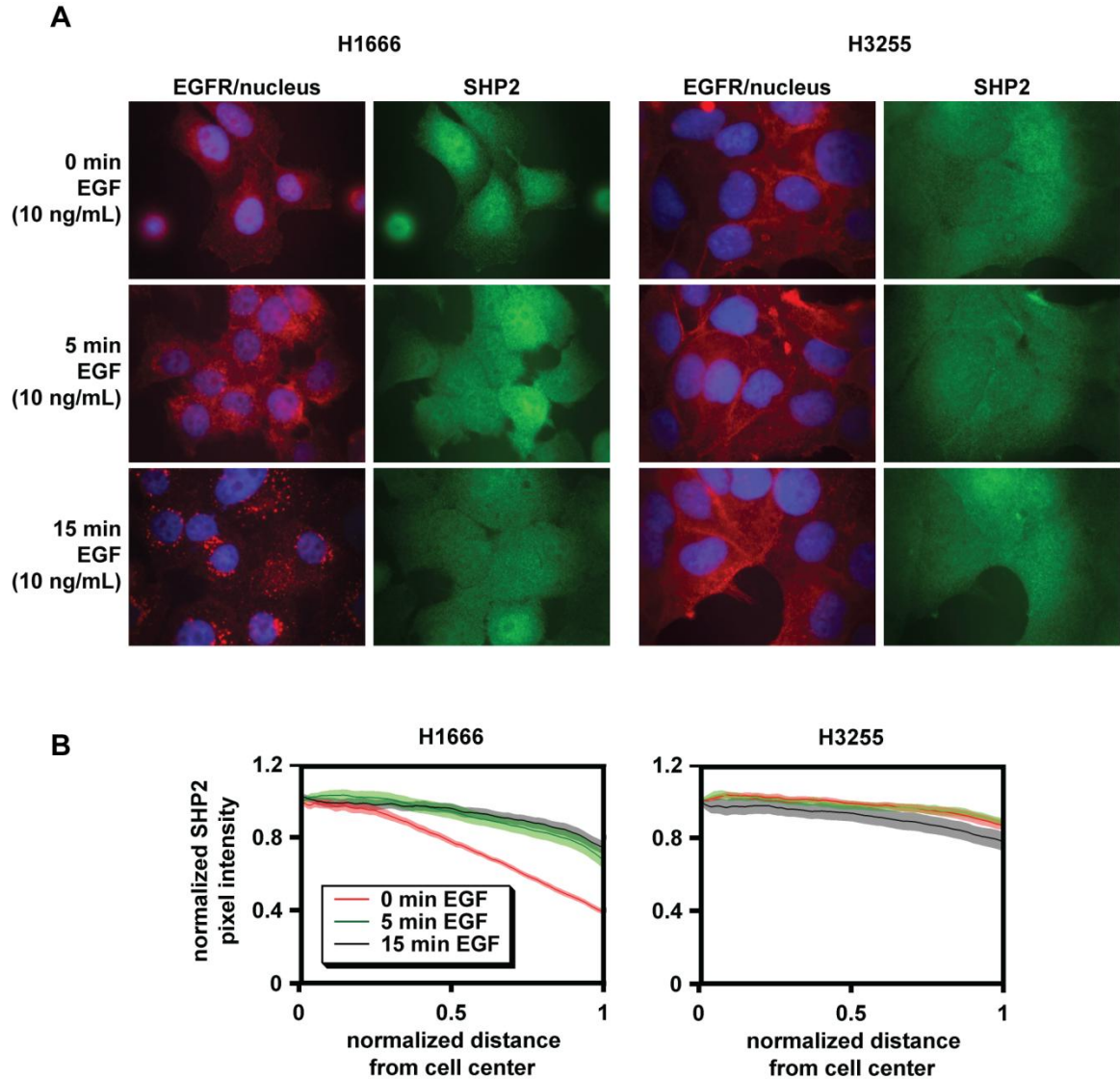


**Figure 2-5: Intracellular redistribution of SHP2 in response to EGF is observed in H1666 cells, but not in H3255 cells.**

(A) Serum-starved H1666 and H3255 cells were treated with 10 ng/mL EGF for up to 15 min, fixed, and stained with Hoechst (nucleus) and antibodies against EGFR and SHP2. Images are representative of three biological replicates. (B) As described in *Materials and Methods* (Section 2-3), intracellular SHP2 pixel intensities were quantified as a function of normalized radial distance from cell centers ( $x = 0$ ) to the cell periphery ( $x = 1$ ). Three images for each condition were used for this analysis, in which all cells entirely contained within the image were analyzed. Data are represented as mean (solid line)  $\pm$  s.e.m. (shaded area;  $n \geq 7$  cells).

***Role of GAB1 in SHP2 localization and EGF-mediated effects.*** GAB1 knockdown (Figure S2-16A) did not alter basal association of SHP2 with Y1068-phosphorylated EGFR in H3255 cells (Figure 2-6A), nor did it alter SHP2's intracellular distribution in either H1666 or H3255 cells (Figure S2-16B), suggesting that recruitment of SHP2 to EGFR and the cell periphery can be accomplished independent of GAB1 binding, potentially through GAB2. GAB1 knockdown did, however, diminish EGF-mediated ERK and SHP2 phosphorylation, reduce ERK and AKT phosphorylation in response to gefitinib, and increase cellular sensitivity to gefitinib in H1666 cells (Figures 2-6B-D and S2-16C-D). Although GAB1-depleted H3255 cells displayed a modest reduction in SHP2 phosphorylation, there was no effect on ERK phosphorylation (Figure 2-6B), suggesting that the mechanism by which SHP2 function is impaired in these cells may simultaneously perturb GAB1 function.

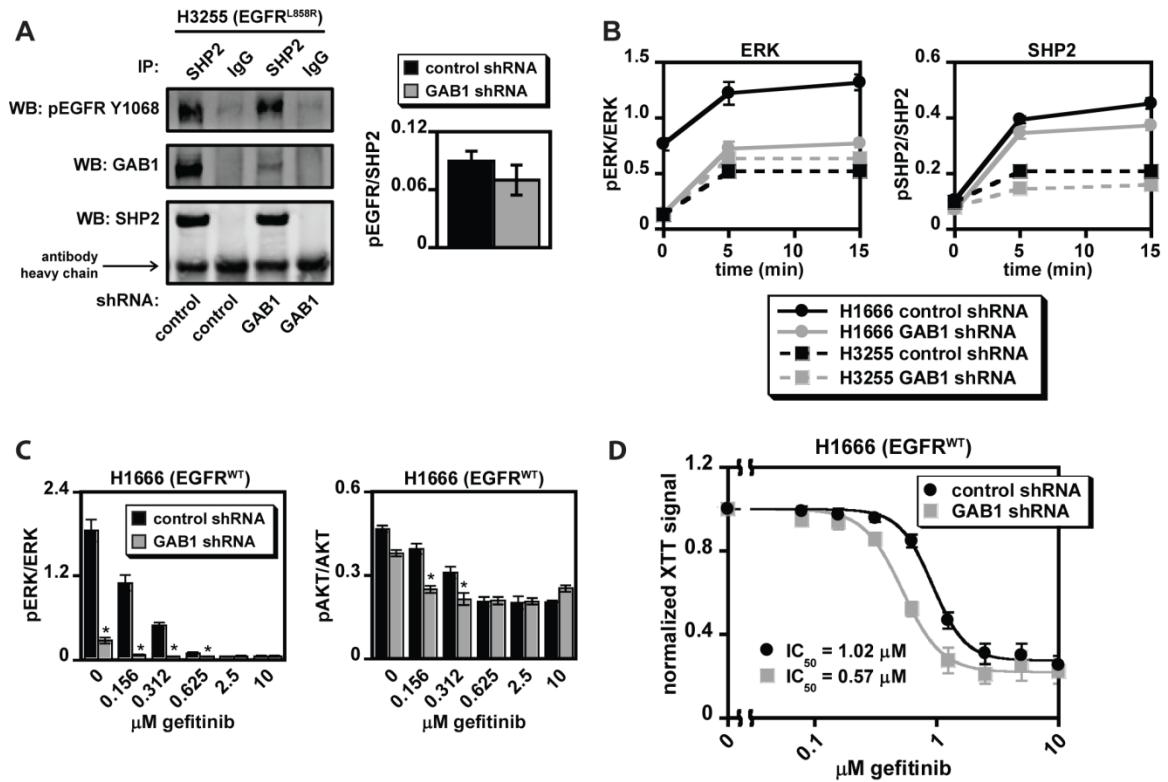


**Figure 2-6: GAB1 knockdown alters EGF-mediated ERK phosphorylation and response to gefitinib in H1666 cells.**

In H1666 and H3255 cells expressing GAB1-targeting or non-targeting control shRNA: (A) Serum-starved H3255 cells were lysed, and lysates were immunoprecipitated with either an SHP2 or control antibody. Immunoprecipitates were analyzed by Western blotting using antibodies against indicated proteins. Images are representative of three sets of biological replicates, and densitometry data are represented as mean  $\pm$  s.e.m. ( $n = 3$ ). (B) Serum-starved cells were treated with or without 10 ng/mL EGF for up to 15 min, and lysates were analyzed by Western blotting using antibodies against phosphorylated and total ERK and SHP2. Densitometry data are represented as mean  $\pm$  s.e.m. ( $n = 3$ ). (C) H1666 cells were treated with 0-10  $\mu$ M gefitinib for 48 hrs, and lysates were analyzed by Western blotting with antibodies against phosphorylated and total ERK and AKT. Densitometry data are represented as mean  $\pm$  s.e.m. ( $n = 3$ ); \* denotes  $p < 0.05$  relative to controls. (D) H1666 cells were treated with 0-10  $\mu$ M gefitinib for four days, and cell proliferation was measured by XTT assay. Normalized XTT signal (y-axis) represents the normalization of values obtained from cells at a given gefitinib

concentration by dividing these values by those obtained from cells treated with DMSO as a control. Data are represented as mean  $\pm$  s.e.m. for three experiments with three replicate wells in each experiment ( $n = 3$ ).

***SHP2 activity.*** SHP2 knockdown in H1666 and H3255 cells resulted in fractional reductions of measured phosphatase activities comparable to the reductions in immunoprecipitated SHP2 levels (Figure 2-7A), indicating that SHP2 was active in both cell lines. In response to EGF, SHP2 activity increased in H1666 cells, with  $p = 0.08$  for this comparison (Figure 2-7B). EGF elicited no change in SHP2 activity in H3255 cells ( $p = 0.50$ ). Note that comparison of activity between cell lines is not straightforward because more SHP2 was immunoprecipitated from H3255 lysates, lysates were not controlled for cell numbers due to proliferation differences, and only a fraction of SHP2 was adapter-bound in each cell line. Thus, the lower apparent normalized SHP2 activity in H3255 versus H1666 cells may not necessarily reflect a lower total SHP2 activity level on a per cell basis.

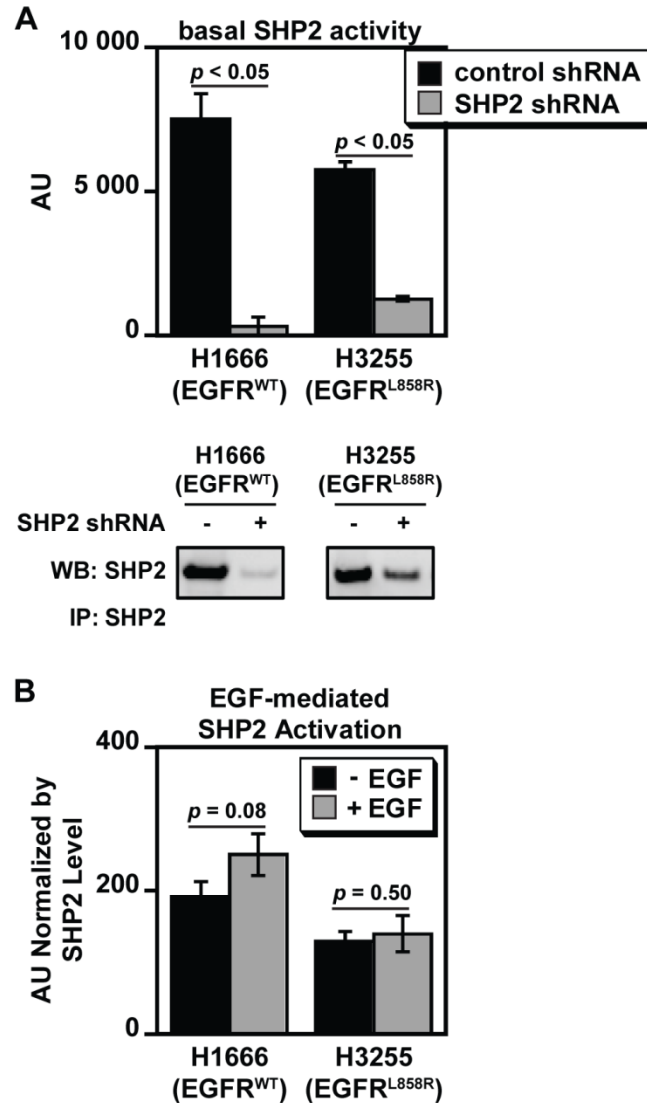


**Figure 2-7: SHP2 is active in H1666 and H3255 cells, and EGF increases SHP2 activity in H1666 cells.**

H1666 and H3255 cells expressing SHP2-targeting or non-targeting control shRNA (**A**), and serum-starved H1666 and H3255 cells treated with or without 10 ng/mL EGF for 5 min (**B**) were lysed, and SHP2 was immunoprecipitated from whole cell lysates. Half of each immunoprecipitate was used to determine phosphatase activity, as described in *Materials and Methods* (Section 2-3), while the remainder was used to determine SHP2 levels by immunoblot. Data are represented as mean  $\pm$  s.e.m. ( $n = 3$ ); AU, arbitrary units. Blot images in (**A**) are representative of three sets of biological replicates. Values

reported in (B) were determined by dividing AU values from the phosphatase activity assay by the quantified SHP2 levels obtained from immunoblots.

***Effects of SHP2 mutation.*** In H1666 cells, expression of constitutively active SHP2<sup>D61A</sup> or SHP2<sup>E76A</sup> mitigated gefitinib-mediated reductions in ERK phosphorylation, and expression of catalytically-inactive SHP2<sup>C459S</sup> reduced ERK phosphorylation basally and in response to gefitinib (Figure 2-8A). Despite increased ERK phosphorylation in H1666 cells expressing SHP2<sup>D61A</sup> or SHP2<sup>E76A</sup>, there was no change in gefitinib sensitivity in these cells (Figure 2-8B), suggesting that the parental cell line's capacity to activate ERK was at a threshold level for maintaining cell survival. However, H1666 cells expressing SHP2<sup>C459S</sup> were more responsive to gefitinib, mirroring the effects of SHP2 knockdown. In H3255 cells, expression of SHP2<sup>E76A</sup> augmented ERK phosphorylation in the presence of gefitinib and substantially decreased cellular sensitivity to gefitinib (Figure 2-8C-D). As expected, SHP2<sup>C459S</sup> expression had little effect on ERK phosphorylation or gefitinib response in H3255 cells.

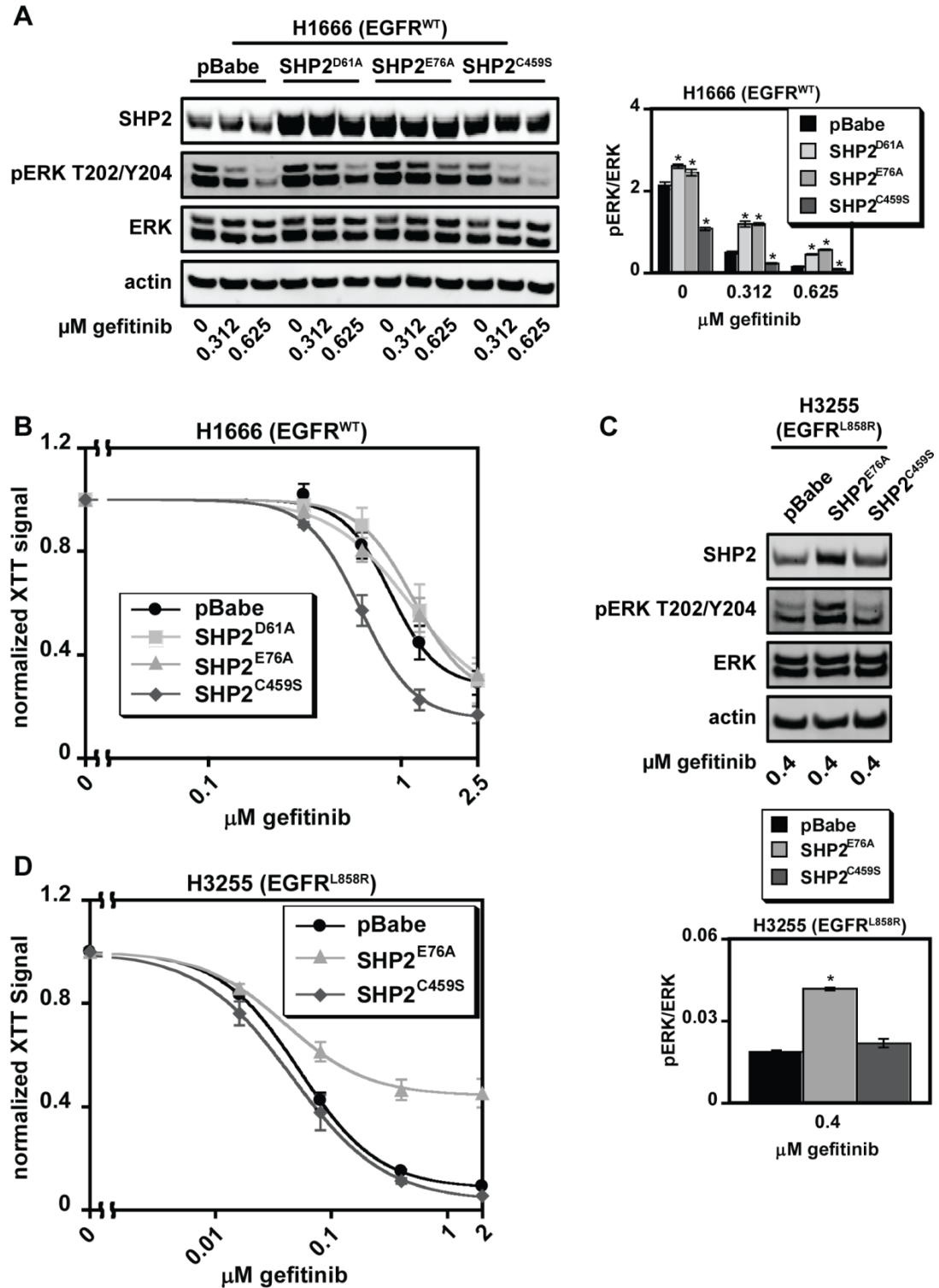


**Figure 2-8: Ectopic expression of SHP2 mutants alters cellular response to gefitinib in H1666 and H3255 cells.**

The following experiments were carried out with H1666 and H3255 cells transduced with SHP2<sup>D61A</sup> (H1666 only), SHP2<sup>E76A</sup>, SHP2<sup>C459S</sup>, or an empty pBabe vector: (A and C) H1666 and H3255 cells were treated with the indicated concentrations of gefitinib for 48 hrs, and lysates were analyzed by Western blotting with antibodies against indicated proteins. Images for (A) and (C) are representative of three sets of biological replicates. Densitometry data for ERK are represented as mean  $\pm$  s.e.m. ( $n = 3$ ); \* denotes  $p < 0.05$  relative to controls. (B and D) H1666 and H3255 cells were treated with up to 2.5  $\mu$ M gefitinib for four days, and cellular proliferation was measured by XTT assay. Normalized XTT signal values (y-axis) were computed at a given gefitinib concentration by dividing absorbances by those measured for cells treated with DMSO as a control. Data are represented as mean  $\pm$  s.e.m. for three experiments with three replicate wells in each experiment ( $n = 3$ ).

***Importance of SHP2-mediated effects downstream of MET.*** Since SHP2-GAB1 association is required for sustained ERK activation downstream of MET [89], we hypothesized that SHP2 could play a role in hepatocyte growth factor (HGF)-mediated resistance to EGFR inhibition in NSCLC cells by maintaining GAB1-mediated signaling in the presence of gefitinib [90, 91]. To explore this idea, we treated SHP2-depleted H1666 and HCC827 cells with gefitinib in the presence or absence of HGF. Although HGF sustained phosphorylated GAB1 Y627, a SHP2 binding site, in the presence of gefitinib, SHP2 knockdown did not affect HGF-mediated rescue of ERK phosphorylation in either cell line (Figure S2-17).

## 2-5 DISCUSSION

Other than in H292 cells, where SHP2 knockdown substantially inhibited cell growth, SHP2 depletion in cells expressing wild-type EGFR increased sensitivity to gefitinib by 3- to 15-fold, as measured by XTT assay. Gefitinib IC<sub>50</sub> values for cells expressing wild-type or mutant EGFR typically differ by a factor of ten or more [92]. Thus, SHP2 depletion in cells expressing wild-type EGFR generally produced an effect consistent with differences on the lower end of what is observed among NSCLC cells with or without *EGFR* mutation. Of course, other factors contribute to differences in NSCLC cellular sensitivity to gefitinib, including differential regulation of phosphatidylinositol 3-kinase (PI3K)/AKT and STAT3/5 [15, 25, 83]. Our study appears to be the first, however, to identify a mechanism wherein a survival signaling pathway is impaired by EGFR-activating mutations in a way which impacts cellular response to EGFR inhibition.

We also found that SHP2 depletion most strongly impaired ERK phosphorylation in cells expressing wild-type versus mutant EGFR. However, H1781 (EGFR<sup>WT</sup>) cells were an outlier in terms of the relatively modest effect of SHP2 knockdown on ERK phosphorylation. Despite this, there was a substantial effect of SHP2 knockdown on cellular response to gefitinib. H1781 cells express a constitutively active HER2 mutant (VC insertion at G776) and are dependent on HER2 for ERK and AKT phosphorylation [93]. Since HER2 can sequester EGFR at the plasma membrane [94, 95], the possibility exists for SHP2 to be sequestered with EGFR in these cells as well. Indeed, this appeared to occur (Figure S2-18). However, as SHP2 promotes RAS activity downstream of HER2 [96], HER2-mediated SHP2 function may contribute to the modest effect of SHP2

knockdown on ERK phosphorylation in these cells. Further studies are needed to parse the effects of SHP2 downstream of EGFR and HER2 in these cells.

A previous study demonstrated impaired SHP2 phosphorylation in NSCLC cells expressing EGFR mutants [24], but the phenotypic implications of SHP2 phosphorylation status were not directly evaluated. Our finding that reconstitution of SHP2<sup>Y542F</sup> in SHP2-depleted H1666 cells rescued ERK phosphorylation as efficiently as SHP2<sup>WT</sup> suggests that SHP2 Y542 phosphorylation is dispensable for SHP2-mediated activation of ERK, consistent with previous findings regarding EGF-mediated ERK activation in 3T3 fibroblasts [29]. Thus, impaired SHP2 phosphorylation with *EGFR* mutation may not be the cause, but rather a result, of a mechanism whereby SHP2 function (but not activity) is diminished by SHP2 sequestration. We also note that despite the lack of an effect of SHP2 knockdown in H3255 cells (EGFR<sup>L858R</sup>), there were small effects of SHP2 knockdown in HCC827 cells (EGFR<sup>E746\_A750del</sup>). This difference between H3255 and HCC827 cells could reflect a functional difference between the two EGFR mutants or a differential role of receptors such as MET, which is basally phosphorylated to a higher degree in HCC827 cells [26].

Based on our studies of GAB1 knockdown, GAB1 function may also be perturbed by *EGFR* mutation. GAB1 also appears to be an important determinant of cellular response to gefitinib in an NSCLC cell line expressing wild-type EGFR. This could be due to the function of GAB1 upstream of SHP2 in regulating ERK phosphorylation, the function of GAB1 in promoting AKT phosphorylation by recruiting PI3K, or both. Additional work is needed to clarify the role and regulation of GAB1.

Our data suggest that *EGFR* mutation promotes constitutive binding of a fraction of SHP2 to EGFR through GAB1 and other adapters. Since adapter engagement of SHP2's SH2 domains promotes SHP2 activity, it is perhaps not surprising that SHP2 was biochemically active in cells with *EGFR* mutation. Given these findings, our immunofluorescence microscopy and subcellular fractionation results, and previous findings that EGFR mutants are endocytosis-impaired, *EGFR* mutation appears to result in sequestration of at least some SHP2 at the plasma membrane in a state where it should be biochemically active. The finding that not all SHP2 was sequestered at the plasma membrane in cells with *EGFR* mutation (as observed by immunofluorescence and fractionation) could be a stoichiometric effect. Indeed, in A431 cells, with over  $3 \times 10^6$  EGFR/cell, a more complete redistribution of SHP2 to the cell periphery was observed in response to EGF than we observed [97]. Moreover, in EGFR mutant cells, the SHP2 which is not sequestered, and less likely to be adapter-bound, should be at a lower activity and therefore less functionally relevant. This model is consistent with our findings that in EGFR mutant cells, where only a fraction of SHP2 was sequestered, SHP2 depletion had relatively small effects, but expression of constitutively active SHP2 rescued ERK phosphorylation and sensitivity to gefitinib. The reason why SHP2 sequestration may impede SHP2's ability to promote ERK phosphorylation could be related to previous findings that normal EGFR endocytosis is required for complete ERK activation in some cellular contexts [85]. This coupling between endocytosis and ERK could involve a role for SHP2 localization wherein normal trafficking of SHP2-containing complexes promotes ERK activity by allowing complex access to substrates in the cell interior (Figure 2-9).

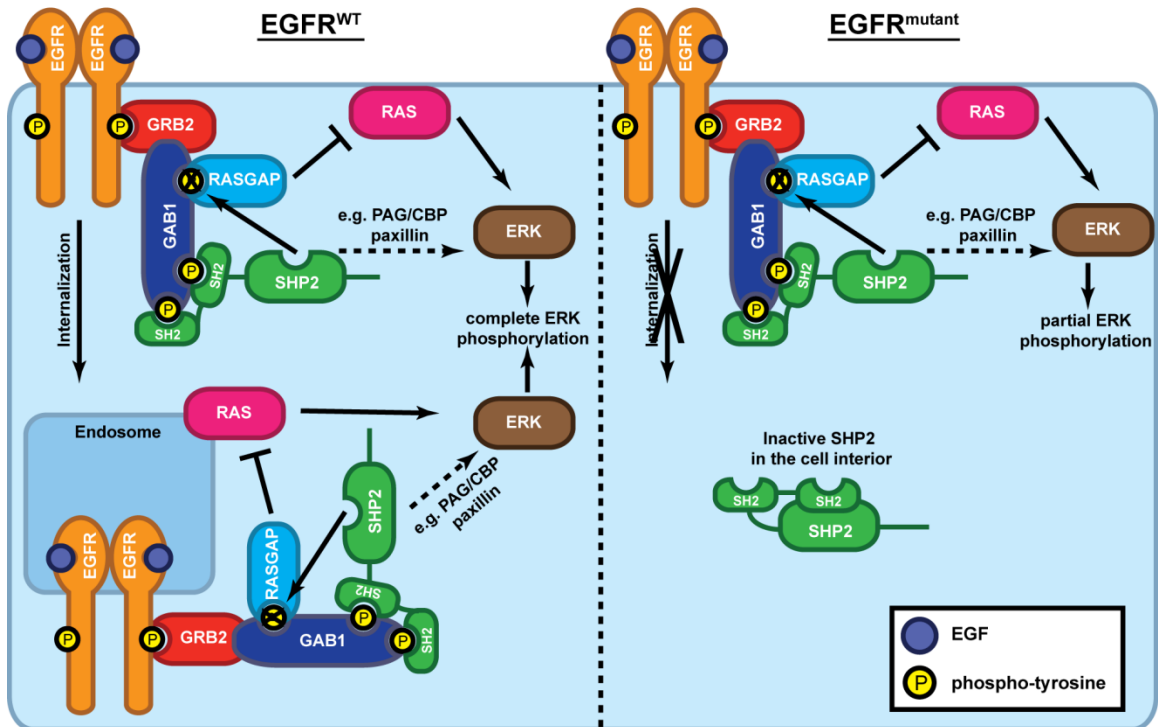


**Figure 2-9: Sequestration of SHP2 at the plasma membrane may enhance gefitinib response in cells expressing EGFR mutants by reducing ERK activity.**

In the proposed mechanism, EGFR activation and phosphorylation leads to recruitment of GRB2, which is constitutively bound with GAB1 via an SH3 domain-mediated interaction. Phosphorylated GAB1 (and possibly other adapters) recruits SHP2, whose activity leads to ERK activation through dephosphorylation of a RASGAP binding site on GAB1 (as shown) or through other mechanisms (as depicted by dotted arrow), such as dephosphorylation of CSK binding sites on PAG/CBP and paxillin. The function of SHP2 in this complex at both the plasma membrane and the cell interior leads to complete ERK phosphorylation. When SHP2 is sequestered at the plasma membrane in complex with internalization-impaired mutant EGFR (e.g. EGFR<sup>L858R</sup>), ERK phosphorylation is impaired. Due in part to impaired ERK activity resulting from sequestration of SHP2, cells with EGFR mutants display increased sensitivity to EGFR inhibition.

SHP2 knockdown in an NSCLC cell line was previously shown to slow xenograft growth in mice [98]. In addition, SHP2-activating mutations have been found in solid

tumors, including NSCLC [77]. As far as we are aware, however, the effects of SHP2 expression and mutation on cellular response to EGFR inhibition have not previously been evaluated. Our finding that SHP2 knockdown in NSCLC cells expressing wild-type EGFR enhanced cellular response to gefitinib suggests that combined inhibition of EGFR and SHP2 may improve response in tumors that are unresponsive to EGFR inhibition alone. The largest effects of SHP2 knockdown on enhancing response to EGFR inhibition in cells with wild-type EGFR tended to occur at or below 1  $\mu$ M gefitinib, the maximum achievable plasma concentration at a clinically relevant dose [99]. Thus, it is conceivable that such a co-inhibition strategy could have clinical impact. Our finding that expression of constitutively active SHP2 mutants mitigated the effects of gefitinib on ERK phosphorylation in H1666 and H3255 cells suggests that SHP2 activity can maintain the activity of ERK in the presence of EGFR inhibitors. Although we noted no major effect of ectopic expression of these mutants on sensitivity to gefitinib in H1666 cells, H3255 cells expressing SHP2<sup>E76A</sup> displayed decreased sensitivity to gefitinib. It would therefore be interesting to explore the implications for drug resistance in cells with *SHP2* mutation.

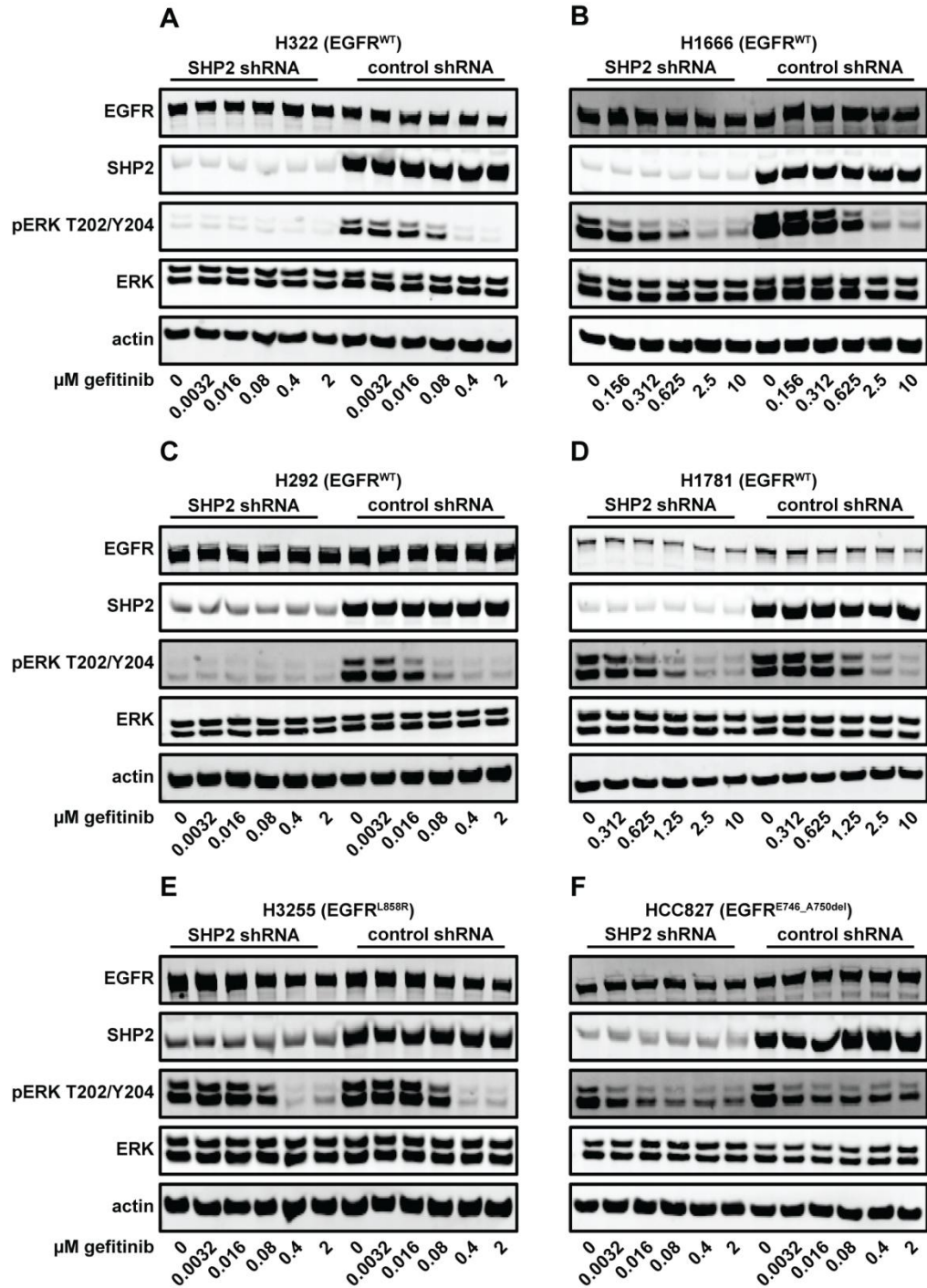
Our findings point to SHP2 as a potential target to be co-inhibited with EGFR in the treatment of NSCLC cells expressing wild-type EGFR. Expanding these studies to an *in vivo* model would be helpful in determining if a clinical benefit for combined SHP2/EGFR inhibition exists, although such studies would be hampered by the present lack of effective and specific SHP2 inhibitors. Our findings also highlight the non-intuitive possibility for activating mutations of receptors such as EGFR to impair the

function of specific signaling pathways in ways which promote cellular response to receptor-targeting therapeutics.

## 2-6 ACKNOWLEDGEMENTS

We thank Dr. Ben Neel, Dr. Eric Haura, Dr. Pasi Jänne, Dr. Tyler Jacks, Dr. Marilyn Farquhar, Dr. Gary Nolan, Dr. Anil Rustgi, and Dr. Susan Margulies for generously providing reagents and instrumentation. We also thank Ms. Gladys Gray Lawrence, Dr. Ranganath Parthasarathy, Mr. Calixte Monast, and Ms. Alice Macdonald Walsh for technical assistance.

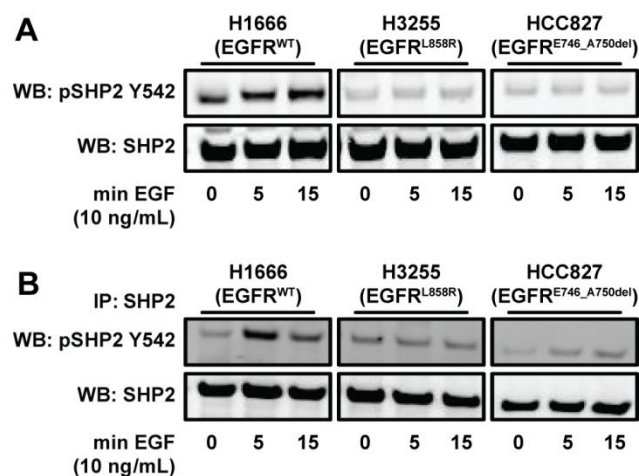
## 2-7 SUPPLEMENTAL MATERIAL



**Figure S2-10: SHP2 knockdown reduces ERK phosphorylation more in NSCLC cells expressing wild-type, versus mutant, EGFR.**

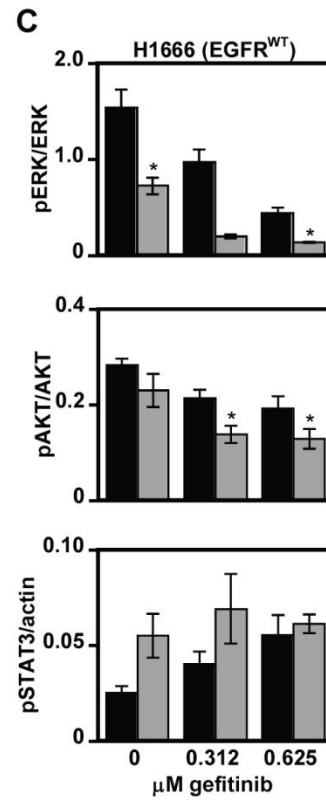
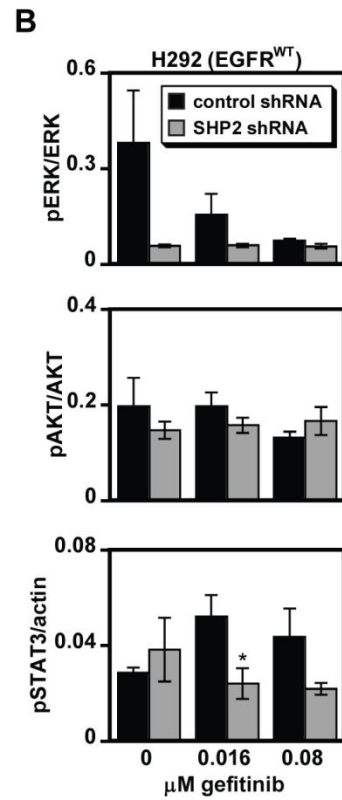
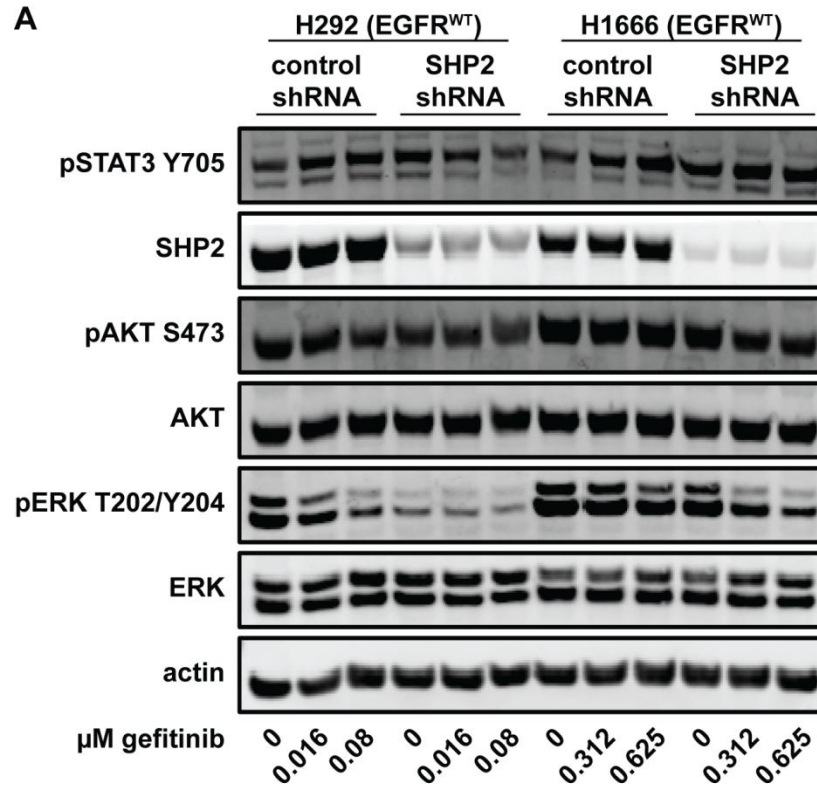
H322 (A), H1666 (B), H292 (C), H1781 (D), H3255 (E), and HCC827 (F) cells expressing control or SHP2-targeting shRNA were treated with up to 10  $\mu$ M gefitinib for

48 hrs. Lysates were analyzed by Western blotting with antibodies against indicated proteins. Images are representative of three sets of biological replicates. EGFR was probed to ensure there was no significant change in its expression due to SHP2 knockdown.



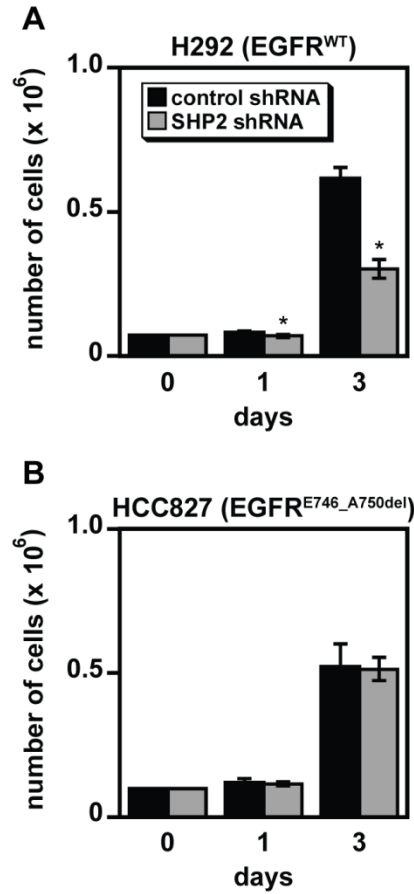
**Figure S2-11: EGF-mediated phosphorylation of SHP2 at Y542 is impaired in H3255 and HCC827 cells relative to H1666 cells.**

Serum-starved cells were treated with 10 ng/mL EGF for up to 15 min and lysed. Whole cell lysates (**A**) or SHP2 immunoprecipitates from whole cell lysates (**B**) were then analyzed by Western blotting using antibodies against the indicated proteins. For each panel, images for different cell lines were obtained from the same membrane; the cropping is due to removal of irrelevant lanes. The pSHP2 Y542 antibody was from Cell Signaling Technology for the analysis in (**A**) and from Epitomics for the analysis in (**B**). The specificity of both antibodies for SHP2 was validated by comparisons with lysates from cells with SHP2 knockdown.



**Figure S2-12: SHP2 knockdown more strongly influences the phosphorylation of ERK than phosphorylation of AKT or STAT3 in NSCLC cells expressing wild-type EGFR.**

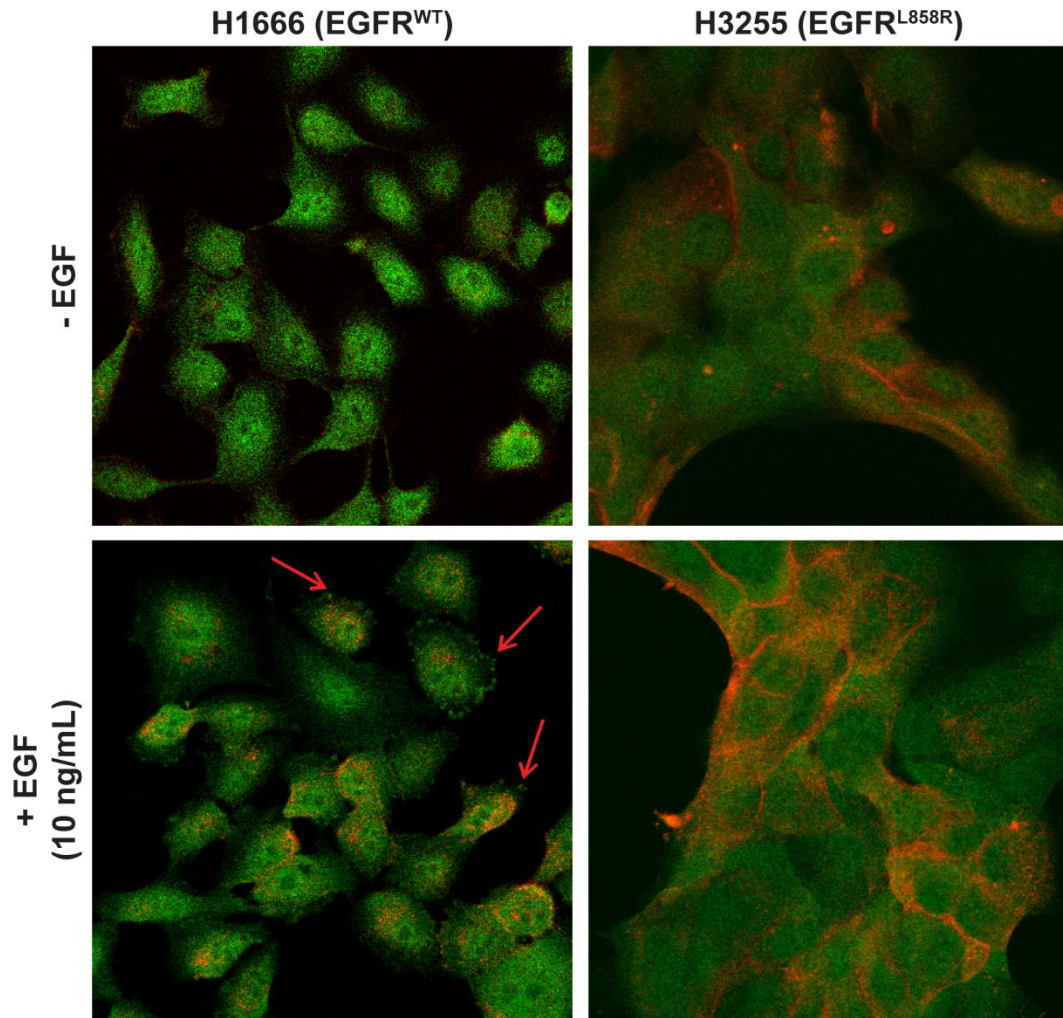
(A) H292 and H1666 cells expressing control or SHP2-targeting shRNA were treated with the indicated concentrations of gefitinib for 48 hrs, and lysates were analyzed by Western blotting with antibodies against indicated proteins. Images are representative of three sets of biological replicates. Densitometry data for H292 (B) and H1666 (C) blots from (A) are represented as mean  $\pm$  s.e.m. ( $n = 3$ ); \* denotes  $p < 0.05$  relative to controls.



**Figure S2-13: H292 cells are significantly growth inhibited by SHP2 knockdown, while HCC827 cells are not.**

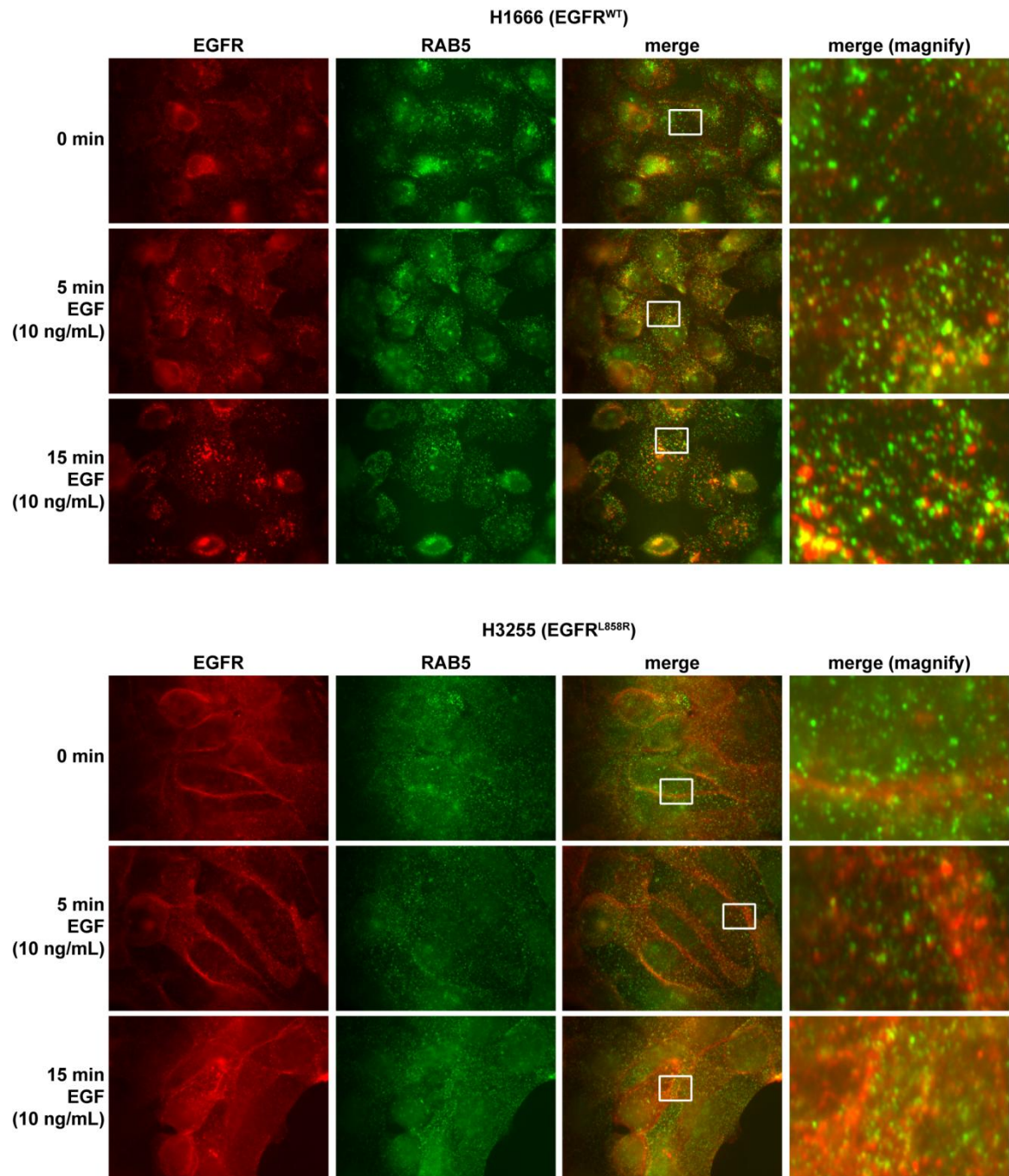
H292 (**A**) and HCC827 (**B**) cells expressing control or SHP2-targeting shRNA were plated in 6-well plates at 75 000 and 100 000 cells per well, respectively. Cells were counted by hemocytometer one day after plating to ensure similar numbers of adherent cells had been plated. Cells were also counted three days after plating to determine the difference in proliferation between cells with or without knockdown of SHP2. Data are represented as mean  $\pm$  s.e.m. of two replicate wells from two distinct experiments ( $n = 4$ ).

\* denotes  $p < 0.05$  relative to controls.



**Figure S2-14: EGF promotes membrane localization of SHP2 in H1666 cells, but not in H3255 cells.**

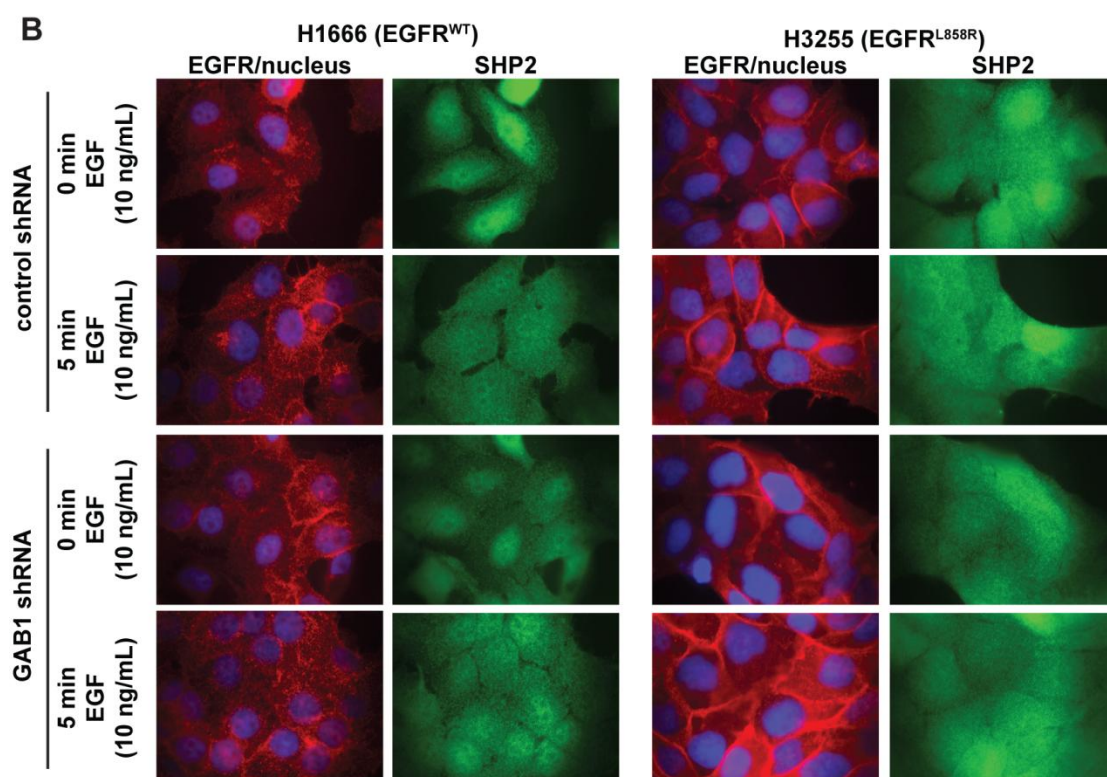
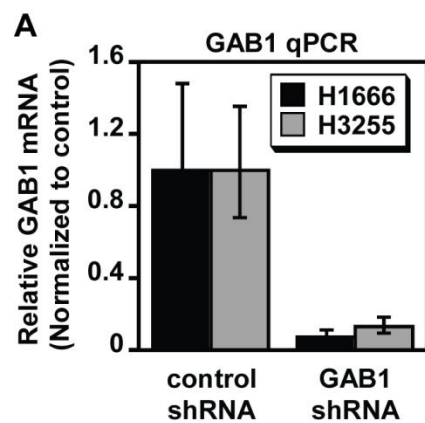
Serum-starved H1666 and H3255 cells were treated with or without 10 ng/mL EGF for 5 min (H1666) or 15 min (H3255), and subsequently fixed and stained with antibodies against EGFR (red) and SHP2 (green). Images represent single frames from *z*-stacks obtained on a confocal microscope. Red arrows denote localization of SHP2 at membrane ruffles.



**Figure S2-15: EGF promotes the formation of EGFR-positive endocytic vesicles in H1666 cells, but not in H3255 cells.**

Serum-starved H1666 and H3255 cells were treated with or without 10 ng/mL EGF for up to 15 min, fixed, and stained with antibodies against EGFR (red) and RAB5 (green), a marker for early endosomes. Sections of merged images (white rectangles) were magnified to show co-localization of EGFR and RAB5 (yellow vesicles), which were

present in EGF-treated H1666 cells. Images are representative of three separate pictures taken from three biological replicates.



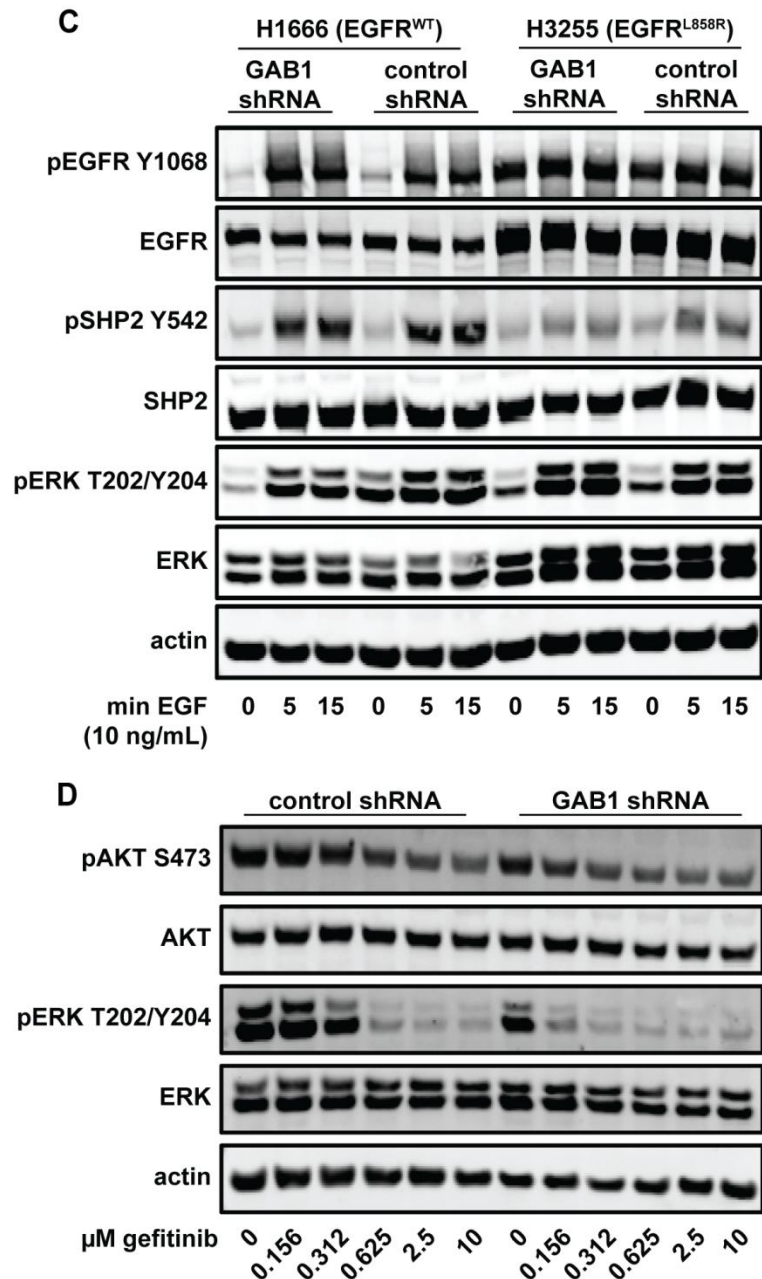


**Figure S2-16: GAB1 does not influence the localization of SHP2 in H1666 or H3255 cells, but does alter EGF-mediated ERK phosphorylation and response to gefitinib in H1666 cells.**

In H1666 and H3255 cells expressing GAB1-targeting or non-targeting control shRNA: (A) RNA was isolated from cells, and relative levels of GAB1 mRNA were determined by qPCR as described in *Materials and Methods* (Section 2-3). (B) Serum-starved cells were treated with or without 10 ng/mL EGF for 5 min, and subsequently fixed and

stained with Hoescht nuclear stain (blue) and antibodies against EGFR (red) and SHP2 (green). Images are representative of three separate pictures taken from three biological replicates. **(C)** Cells were treated with 10 ng/mL EGF for up to 15 min, and lysates were analyzed by Western blotting with antibodies against the indicated proteins. Images are representative of three biological replicates. **(D)** H1666 cells were treated with up to 0-10  $\mu$ M gefitinib for 48 hrs, and lysates were analyzed by Western blotting with antibodies against indicated proteins. Images are representative of three biological triplicates.

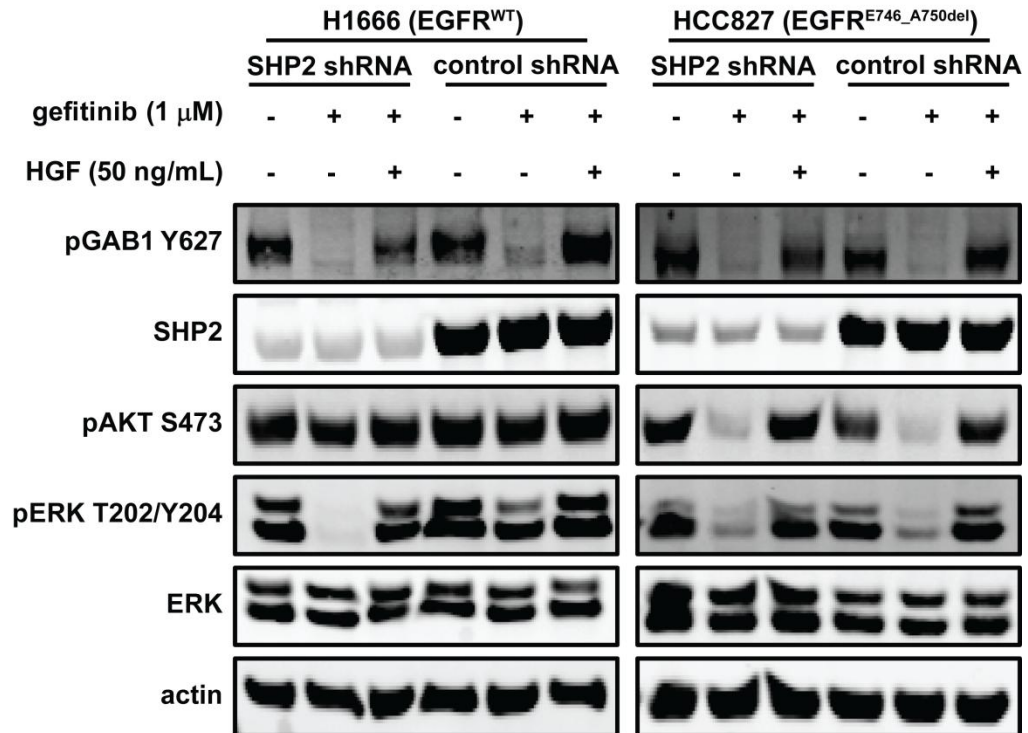


**Figure S2-17: SHP2 is not required for HGF-mediated rescue of ERK phosphorylation in NSCLC cells treated with gefitinib.**

H1666 and HCC827 cells expressing SHP2-targeting or control shRNA were treated with 1  $\mu$ M gefitinib, with or without 50 ng/mL HGF, for 6 hrs. Lysates were analyzed by Western blotting with antibodies against indicated proteins.

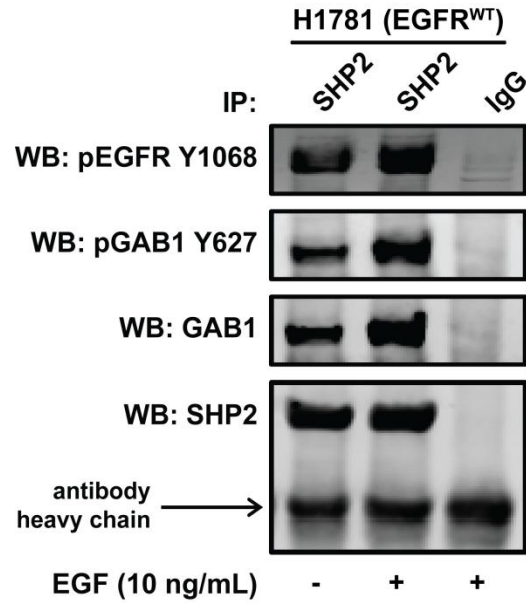


**Figure S2-18: SHP2 is basally associated with GAB1 and pEGFR in H1781 cells.** Serum-starved H1781 cells were treated with or without 10 ng/mL EGF for 5 min and lysed. SHP2 was immunoprecipitated from whole cell lysates, and immunoprecipitates were analyzed by Western blotting using antibodies against the indicated proteins. Images are representative of three biological replicates.

# **Chapter 3: Multivariate Signaling Regulation by SHP2**

## **Differentially Controls Proliferation and Therapeutic Response in Glioma Cells<sup>2</sup>**

### **3-1 ABSTRACT**

Information from multiple signaling axes is integrated in the determination of cellular phenotypes. Here, we demonstrate this aspect of cellular decision making in glioblastoma multiforme (GBM) cells by investigating the multivariate signaling regulatory functions of the protein tyrosine phosphatase SHP2. Specifically, we demonstrate that SHP2's ability to simultaneously drive ERK and antagonize STAT3 pathway activities produces qualitatively different effects on the phenotypes of proliferation and resistance to EGFR and c-MET co-inhibition. While the ERK and STAT3 pathways independently promote proliferation and resistance to EGFR and c-MET co-inhibition, SHP2-driven ERK activity is dominant in driving cellular proliferation, and SHP2's antagonism of STAT3 phosphorylation prevails in promoting GBM cell death in response to EGFR and c-MET co-inhibition. Interestingly, the extent of these SHP2 signaling regulatory functions is diminished in glioblastoma cells expressing sufficiently high levels of the EGFR variant III (EGFRvIII) mutant, which is commonly expressed in GBM. In cells and tumors expressing EGFRvIII, SHP2 also antagonizes EGFRvIII and c-MET phosphorylation and drives expression of HIF-1/2 $\alpha$ , adding complexity to the evolving understanding of SHP2's regulatory functions in GBM.

### 3-2 INTRODUCTION

Cells integrate information from multiple signaling pathways to execute decision-making processes [100-103]. While some signaling pathway intermediates act predominantly in one pathway, others exert substantial effects in multiple pathways, thus expanding their ability to control cell fate determination. One such protein is SH2 domain-containing phosphatase-2 (SHP2), which plays key roles in development, homeostatic maintenance, and disease. Here, we investigate SHP2's ability to simultaneously regulate the extracellular signal-regulated kinase (ERK) and signal transducer and activator of transcription-3 (STAT3) pathways, as well as other signaling events that we identify as SHP2-regulated for the first time, and the net effect of this regulation on cellular proliferation and response to co-inhibition of EGFR and the HGF receptor c-MET.

SHP2 was the first phosphatase to be identified as a proto-oncogene [68, 84], and it is primarily regarded as a mediator of pro-survival signaling. Indeed, SHP2's most well-studied signaling role is to promote ERK activity [28]. SHP2's catalytic activity, which is required for this function, is promoted through engagement of its N-terminal SH2 domains by phosphotyrosines on various receptor tyrosine kinases or adapter proteins such as GRB2 associated binding protein-1 (GAB1) [28, 52]. SHP2 can also negatively regulate STAT3 activation downstream of the interleukin-6 receptor [104], and one recent study even described a "tumor-suppressor" role for SHP2 in hepatocellular carcinoma through its regulation of STAT3 [105]. SHP2 can also positively or negatively impact AKT pathway activity [58, 106]. Through these signaling regulatory functions, the magnitude of which may depend on cell type or disease context,

SHP2 is able to control cellular phenotypes including proliferation [107, 108], oncogenic transformation [73], tumor progression [109], response to therapeutics [108], and senescence [80].

A specific setting of interest where SHP2 influences multiple complex phenotypes is glioblastoma multiforme (GBM), the most common and lethal form of adult brain cancer [36]. One study described SHP2's ability to suppress cellular senescence in the GBM cell lines U87MG and A172 and reported simultaneous SHP2-mediated ERK activation and STAT3 inhibition, though no causal relationships between ERK or STAT3 signaling and the senescence phenotype were established [80]. SHP2 function has also been linked to tumorigenicity of GBM cells expressing EGFR variant III (EGFRvIII), a mutant prevalent in GBM [73]. Of course, ERK and STAT3 are both well-described as promoting proliferation and survival across cancer types [110, 111]. For example, in GBM cells, ERK activity promotes resistance to cisplatin [112], and STAT3 is an important regulator of proliferation that has been recognized as a potential therapeutic target [47, 81]. Since SHP2 regulates the ERK and STAT3 pathways in qualitatively different ways, and since the ERK and STAT3 signaling pathways promote qualitatively similar effects across multiple phenotypes, how SHP2's multivariate signaling roles are integrated to determine phenotype in GBM cells remains unclear. A more complete understanding of this could help address a number of outstanding issues, including the identification of ways to overcome GBM resistance to targeted inhibitors [37, 113, 114] and the potential efficacy of targeting SHP2 in glioblastoma.

Here, we evaluate the effects of SHP2's signaling roles on GBM cell proliferation and resistance to inhibitors of EGFR and c-MET, oncogenic receptors that drive GBM

progression and chemoresistance. In a panel of GBM cells, SHP2 depletion reduced cellular proliferation but surprisingly also promoted resistance to EGFR and c-MET co-inhibition. These results appear to derive from SHP2's ability to drive ERK and antagonize STAT3 pathway activities in the panel of cell lines and the differential abilities of those pathways to control different phenotypes. That is, even though ERK and STAT3 both promote proliferation and survival, SHP2-mediated ERK activity is dominant in determining cellular proliferation rates, while SHP2 suppression of STAT3 phosphorylation exerts the dominant effect in determining response to EGFR and c-MET co-inhibition. Interestingly, SHP2's ability to regulate these pathways was greatly diminished in cells with sufficiently high EGFRvIII expression, where SHP2 became basally sequestered with the receptor. We further found that SHP2 negatively regulates EGFRvIII and c-MET phosphorylation and drives expression of hypoxia-inducible factors 1 and 2 alpha (HIF-1/2 $\alpha$ ) in cultured cells and tumor xenografts. These results expand our understanding of SHP2 as a multivariate regulator of signaling and GBM cell phenotype and raise additional questions about how SHP2 function may be perturbed in different GBM contexts.

### 3-3 MATERIALS AND METHODS

**Cell culture.** LN18, T98G, and U118MG cells were obtained from the American Type Culture Collection (Manassas, VA, USA). U87MG parental cells and cells expressing low ( $1 \times 10^6$  receptors/cell), medium ( $1.5 \times 10^6$  receptors/cell), or high ( $2 \times 10^6$  receptors/cell) levels of EGFRvIII (U87MG-L, -M, and -H, respectively) or a dead kinase mutant of EGFRvIII (U87MG-DK,  $2 \times 10^6$  receptors/cell) were a generous gift from Dr. Frank Furnari (University of California San Diego). All cells were maintained in DMEM supplemented with 10% FBS, 1 mM L-glutamine, 100 units/mL penicillin, and 100  $\mu$ g/mL streptomycin. U87MG cells expressing EGFRvIII were cultured with 400  $\mu$ g/mL G418. Where indicated, cells were treated with EGF (Peprotech, Rocky Hill, NJ, USA) following 8-16 hrs starvation in media containing 0.1% FBS. All cell culture reagents were from Life Technologies (Carlsbad, CA, USA). For experiments in hypoxic conditions, cells were cultured for 24 hrs in 0.5% O<sub>2</sub> using an Invivo<sub>2</sub> 400 hypoxia workstation (Ruskin Technology, Grandview, MO, USA) prior to lysis.

**shRNA and stable expression constructs.** DNA oligonucleotides encoding short hairpins targeting human *SHP2* (Integrated DNA Technologies, San Jose, CA, USA) were cloned into the pSicoR vector (Tyler Jacks, MIT; [86]). The main shRNA targeted nucleotides 1780-1798 of *SHP2* mRNA (5'-GGACGTTTCATTGTGATTGA-3'). Control vectors were created using shRNA sequences that do not target a known human mRNA. We also used an alternative, non-overlapping *SHP2* shRNA targeting nucleotides 5890-5908 (5'-GTATTGTACCAGAGTATTA-3') of human *SHP2* in a cell proliferation experiment in the presence of drugs (Figure S3-9A). Combined with the data showing the effects of *SHP2*<sup>E76A</sup> expression, the data in Figure S3-9A help to demonstrate the

SHP2 specificity of effects observed using the primary SHP2-targeting hairpin. To engineer cells with shRNA expression, lentivirus was produced by calcium phosphate-mediated transfection of 293FT cells (Life Technologies) with pSicoR plasmids along with the packaging plasmids pCMV-VSV-G, pMDL-gp-RRE, and pRSV-Rev (Dr. Marilyn Farquhar, University of California San Diego). Virus was collected 48 and 72 hrs post-transfection and filtered using 0.45 µm syringe filters prior to infecting target cells.

SHP2 cDNA encoding SHP2<sup>E76A</sup> (Ben Neel, Ontario Cancer Institute) was inserted at the EcoRI site of the pBabe vector. Retrovirus was produced by calcium phosphate-mediated transfection of amphotropic Phoenix cells (Dr. Gary Nolan, Stanford University) with vector. Virus was harvested 24, 30, and 48 hrs post-transfection and used to infect target cells, which were selected in 2 µg/mL puromycin (Sigma-Aldrich, St. Louis, MO, USA). All expression and shRNA constructs were validated by sequencing, and protein knockdown was validated by western blot.

***Transient expression of wild-type or substrate-trapping SHP2.*** Expression constructs for wild-type and substrate-trapping double mutant (DM; D425A/C459S) SHP2 in the pMT2 vector backbone were provided by Dr. Yehenew Agazie (West Virginia University). U87MG cells were transfected with pMT2 plasmids using calcium phosphate. Cells were lysed in immunoprecipitation lysis buffer (Cell Signaling Technology, Danvers, MA, USA; #9803) 48 hrs after transfection.

***Inhibitors.*** Stocks of gefitinib (LC Laboratories, Woburn, MA, USA), U0126 (LC Laboratories), CI-1040 (LC Laboratories), PHA665752 (Santa Cruz Biotechnologies, Dallas, TX, USA), and Stattic (Sigma-Aldrich) were prepared in DMSO.

***Cell death quantification.*** Cells were seeded at a density of 75,000-100,000 cells/well in six-well dishes and treated 24 hrs later with different combinations of gefitinib, PHA665752, CI-1040, and Stattic or DMSO (control). After 72-96 hrs, floating and adherent cells were pooled and stained for permeability to TO-PRO-3 (Life Technologies). Cells were analyzed by flow cytometry within 1 hr of resuspension. Flow cytometry was performed on a Becton Dickinson Biosciences FACSCalibur cytometer, and data were analyzed using FlowJo.

***Proliferation measurements.*** Cells were seeded at an initial density of 75,000 or 100,000 cells/well in six-well dishes. After growing for 72 hrs, cells were trypsinized, suspended in complete media, and counted using a hemocytometer.

***XTT viability assay.*** Cell proliferation in the presence of inhibitors was assessed using the XTT Cell Proliferation Assay (Roche, Indianapolis, IN, USA). Cells were seeded in 96-well plates, grown for 16-24 hrs, and switched to complete media containing up to 20  $\mu$ M gefitinib and/or 1  $\mu$ M PHA665752 for an additional 3 days. Subsequently, fresh media and XTT reagent were added to wells, and plates were incubated for 2-4 hrs at 37°C to maximize signal-to-background. Absorbance was measured at 450 nm with a reference wavelength at 660 nm. The percentage of viable cells was determined by normalizing absorbance to that of cells treated with DMSO. Each experiment was performed on at least three separate days with each condition plated in three replicate wells on each day, except where noted.

***Tumor xenografts.*** Female Nu/Nu mice (Charles River, Wilmington, MA, USA) were subcutaneously injected in both flanks with control or SHP2-depleted U87MG-M cells (control shRNA: 750,000 cells; SHP2 shRNA: 2,500,000 cells). The difference in

injected cell numbers was based upon observations of different rates of proliferation *in vivo* and *in vitro* with or without SHP2 knockdown. When tumors reached an average size of 50 mm<sup>3</sup> (achieved by control tumors only), 7 day treatment with gefitinib and PHA665752 (Selleck Chemicals, Houston, TX, USA) began. Gefitinib was resuspended in an aqueous solution containing 0.5% hydroxypropylmethylcellulose (Sigma-Aldrich) and 0.1% Tween-80 (Sigma-Aldrich), and was delivered at 100 mg/kg/day daily by oral gavage. PHA665752 was resuspended in an aqueous solution containing 1% dimethyl acetamide (Sigma-Aldrich), 10% propylene glycol (Sigma-Aldrich), and 1.05 moles L-lactic acid (Sigma-Aldrich) per mole of PHA665752, and was delivered at 30 mg/kg/day daily by intraperitoneal injection. Tumors were measured with a caliper before and throughout treatment, and tumor volume was calculated as  $\pi/6 \times A \times 2B$ , where *A* and *B* are the larger and smaller tumor diameters, respectively. Excised tumors were homogenized in immunoprecipitation lysis buffer before proceeding with western blotting. All experiments were approved by the University of Pennsylvania Institutional Animal Care and Use Committee and performed in accordance with NIH guidelines.

***Subcellular fractionation.*** Serum-starved cells were washed with PBS and collected in hypotonic buffer (10 mM Tris-HCl, pH 7.4, 1 mM MgCl<sub>2</sub>, 1 mM EDTA) supplemented with 1 mM PMSF, additional protease inhibitors, and phosphatase inhibitors. Crude lysates were generated with a Dounce homogenizer and centrifuged at 3,000 and 9,300 rpm, for 5 min at each speed, to remove nuclei and mitochondria, respectively. Cleared lysates were centrifuged at 100,000 *g* for 60 min to separate membrane and cytosol fractions. Membrane pellets were washed with PBS, resuspended in hypotonic buffer, and centrifuged again at 100,000 *g*. After additional washes,

membrane pellets were resuspended in immunoprecipitation lysis buffer to solubilize proteins. To improve signals, membrane fractions were 10× more concentrated than cytosolic fractions in terms of the relative amount of total lysate loaded.

***EGF internalization assay.*** EGF-mediated EGFR endocytosis rate constants ( $k_e$ ) were measured using  $^{125}\text{I}$ -EGF as described previously [115, 116].

***Western blotting.*** Whole cell lysates were prepared in a standard cell extraction buffer (Life Technologies; FNN0011) prepared with protease inhibitors and phosphatase inhibitors (Sigma-Aldrich). Lysates were cleared by centrifugation at 13,200 rpm for 10 min, and total protein concentrations were determined by micro-bicinchoninic acid (BCA) assay (Thermo Fisher Scientific, Waltham, MA, USA). Proteins were resolved on 4-12% gradient polyacrylamide gels (Life Technologies) under denaturing and reducing conditions and transferred to 0.2  $\mu\text{m}$  nitrocellulose membranes (Bio-Rad Laboratories, Hercules, CA, USA). Membranes were imaged using a LI-COR Odyssey Imaging System. As needed, membranes were stripped with 0.2 M NaOH.

***Immunofluorescence.*** Cells were seeded at 150,000 cells/well on 18 mm glass coverslips in six-well culture dishes. After serum starvation for 16 hrs, cells were treated with 10 ng/mL EGF for up to 30 min. Cells were then washed and fixed for 20 min in 4% paraformaldehyde and permeabilized with 0.25% Triton X-100 in PBS for 5 min. Coverslips were again washed and incubated with the SHP2 antibody in a humidified chamber for 3 hrs at 37°C. Washed coverslips were incubated with Alexa Fluor 488-conjugated secondary antibody (Life Technologies) and Hoechst DNA stain (Sigma-Aldrich) for 1 hr at 37°C. Coverslips were mounted on microscope slides using Prolong Gold Antifade mounting media (Life Technologies) and dried overnight. Fixed slides

were imaged on a Zeiss Axiovert 40 CFL microscope using an A-Plan 100X oil objective and a SPOT Insight CCD camera. Specificity of the SHP2 antibody for immunofluorescence was verified using U87MG-M cells with or without SHP2 knockdown (supplementary material Fig. S3C).

**Immunoprecipitation.** Cells were lysed in immunoprecipitation lysis buffer, with 1 mM PMSF, protease inhibitors, and phosphatase inhibitors. After lysate centrifugation at 13,200 rpm and 4°C for 10 min and determination of protein concentrations by BCA assay, 400-500 µg of protein was incubated with agarose beads conjugated to SHP2 or STAT3 antibodies at 4°C overnight. Beads were washed three times with cold lysis buffer, re-suspended in LDS sample buffer (Life Technologies) and boiled before western blotting. Immunoprecipitation specificity was validated with comparisons to a rabbit control antibody (IgG; Santa Cruz Biotechnology) (supplementary material Fig. S2D, S3A, S4C).

**Antibodies.** EGFR (#2232), c-MET pY1234/1235 (#3126), STAT3 pY705 (#9145), ERK (#4695), and ERK pT202/Y204 (#4377) antibodies were from Cell Signaling Technology. SHP2 (sc-280) and STAT3 (sc-482) antibodies were from Santa Cruz Biotechnology. Actin (MAB1501) and GAB1 (#06-579) were from Millipore (Billerica, MA, USA). EGFR pY1068 (#1727) was from Epitomics (Burlingame, CA, USA). Antibodies against HIF-1α (#10006421) and HIF-2α (NB100-122) were from Cayman Chemical (Ann Arbor, MI, USA) and Novus Biologicals (Littleton, CO, USA), respectively. Infrared dye-conjugated secondary antibodies were from Rockland Immunochemicals (Gilbertsville, PA, USA). All antibodies were used according to manufacturers' recommendations.

*Statistics.* Statistical analyses were performed using a paired two-tailed student's t-test.

### 3-4 RESULTS

***SHP2 depletion differentially impacts key GBM cell phenotypes and associated signaling pathways.*** In the GBM cell lines U87MG, LN18, T98G, and U118MG, we first evaluated the effect of shRNA-mediated SHP2 knockdown on cellular proliferation. As expected based on reports in other glioblastoma cells [73] and numerous other cell settings, SHP2 knockdown reduced cellular proliferation rates in all four cell lines (Figure 3-1A). Interestingly, SHP2 knockdown also promoted cell survival in response to co-inhibition of EGFR and c-MET using the inhibitors gefitinib and PHA665752 (Figure 3-1B). Thus, in response to SHP2 knockdown, cells were generally less proliferative, but significantly more resistant to EGFR and c-MET co-inhibition. The latter effect was unexpected given previous findings that SHP2 knockdown enhances death response to EGFR inhibition in non-small cell lung cancer (NSCLC) cells [108] and that SHP2 antagonizes p73-dependent apoptosis [117]. Western blot analysis revealed that SHP2 knockdown was accompanied by decreases in ERK phosphorylation and simultaneous increases in STAT3 phosphorylation (Figure 3-1C), which could explain how proliferation was impeded while survival in response to EGFR and c-MET co-inhibition could be enhanced. That is, ERK activity could contribute more significantly to determining proliferation rates, and STAT3 activity could contribute more significantly to survival response to EGFR and c-MET co-inhibition.

To explore that idea further, we used the data from Figures 3-1A-C to assign quantitative values to the individual contributions of SHP2-controlled ERK and STAT3 activation toward cellular proliferation and survival. We assumed that the quantitative measure of a particular phenotype  $X_i$  for a particular cellular condition  $i$  (in this case,

control or SHP2 knockdown) can be described as a linear combination of the phosphorylation levels of ERK and STAT3,  $p_{E,i}$  and  $p_{S,i}$ , respectively, where the contribution of each pathway to  $X_i$  is determined as the product of a weighting coefficient for ERK or STAT3,  $w_E$  or  $w_S$ , respectively, and the phosphorylation level of the protein. With these assumptions,  $X_i$  takes the form:

$$X_i = w_E(p_{E,i}) + w_S(p_{S,i})$$

To evaluate pathway contributions to survival response to therapeutics, the percentages of dead cells shown in Figure 3-1B were subtracted from 100%. Phosphorylated ERK and STAT3 signals were normalized to the corresponding total protein signals, as in Figure 3-1C. Finally, phosphorylation and phenotype data were normalized to values from control shRNA cells for each cell line, which leads to  $w_E$  and  $w_S$  summing to unity when the equation above is evaluated for the control condition. Performing the analysis for the proliferation phenotype for each cell line and averaging, we found average  $w_E$  and  $w_S$  values of 0.77 and 0.23, respectively. For cell survival response to combined EGFR and c-MET inhibition, we found average  $w_E$  and  $w_S$  values of -0.14 and 1.14, respectively. These results suggest that ERK and STAT3 play dominant roles in proliferation and survival responses, respectively. We note that a negative value for  $w_E$  in the survival analysis may seem to suggest that ERK activity somehow negatively contributes to cell survival, but this is not the case. Rather, this result arises due to the form of our model structure, which produces a  $w_E < 0$  whenever the fold-increase in survival exceeds the fold-increase in STAT3 phosphorylation and the fold-increase in ERK phosphorylation

does not exceed that for STAT3 phosphorylation, which is the case for three of the four cell lines analyzed.

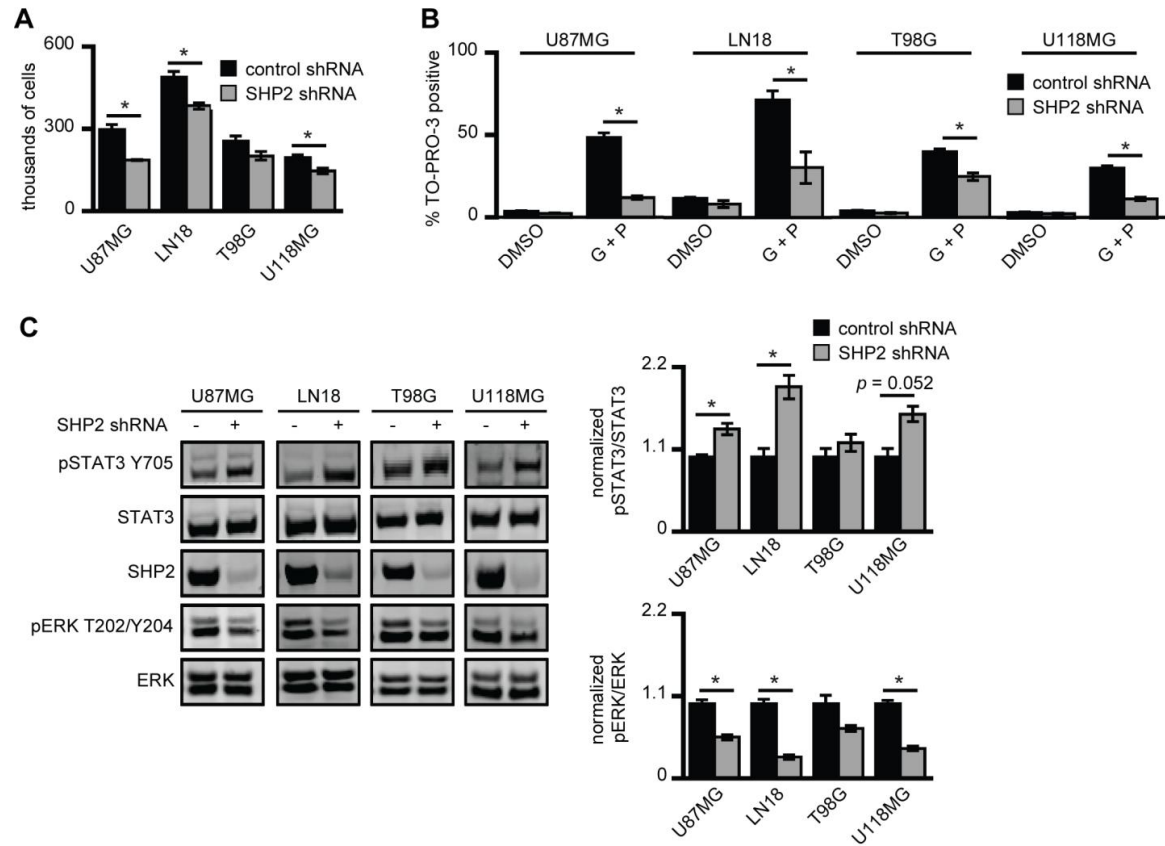


**Figure 3-1: SHP2 knockdown differentially impacts GBM cell proliferation and survival.**

(A) U87MG, LN18, T98G, and U118MG cells expressing control or SHP2-targeting shRNA were seeded at 100,000 cells/well and cells were counted 72 hrs later. Counts are represented as mean  $\pm$  s.e.m. ( $n = 3$ ); \* denotes  $p < 0.05$ . (B) The indicated cell lines were co-treated with 20  $\mu$ M gefitinib (G) and 1  $\mu$ M PHA665752 (P). After 72 hrs, the percentage of TO-PRO-3-positive cells was measured by flow cytometry ( $n = 3$ ); \* denotes  $p < 0.05$ . (C) The indicated cell lines were maintained in complete media, and lysates were analyzed by western blotting using antibodies against the indicated proteins. Densitometry data are represented as mean  $\pm$  s.e.m. ( $n = 3$ ); \* denotes  $p < 0.05$ .

***ERK and STAT3 inhibition further suggests differential pathway control of proliferation and survival in GBM cells.*** We next used the ERK and STAT3 inhibitors CI-1040 and Stattic to confirm experimentally the pathways' relative contributions to cell phenotypes. Cellular proliferation was reduced with either ERK or STAT3 pathway inhibition (Figures 3-2A-B and S3-8A). Note that the incomplete inhibition of STAT3 Y705 phosphorylation (37% reduction) observed in Figure 3-2B resulted from our selection of a STAT3 inhibitor concentration that was low enough to produce relatively low cell death as a single agent across the panel of cell lines. Using a lower concentration of gefitinib than in Figure 3-1B to reduce baseline cell death, we also found that ERK or STAT3 inhibition promoted cell death response to EGFR and c-MET co-inhibition (Figure 3-2C). With the exception of U118MG cells where Stattic produced a substantial amount of cell death by itself, the effect of ERK inhibition on proliferation was generally greater than that of STAT3 inhibition. Conversely, the effect of STAT3 inhibition on death response to gefitinib and PHA665752 was larger than that of ERK inhibition. Given that the same concentrations of CI-1040 and Stattic were used in Figures 3-2A and 3-2C, we interpret these data as indicating that both the ERK and STAT3 pathways participate in regulating cellular proliferation and survival, but confirming the weighting coefficient analysis that ERK is the stronger determinant of proliferation and STAT3 the stronger determinant of survival response to EGFR and c-MET co-inhibition. This suggests that the elevated phosphorylated STAT3 levels observed with SHP2 knockdown promoted resistance to EGFR and c-MET co-inhibition despite the impairment of ERK activity. To confirm this, we demonstrated that

combining Stattic with the concentrations of gefitinib and PHA665752 used in Figure 3-1B increased cell death response of cells with SHP2 knockdown (Figure 3-2D).

We note as well that, in some cell lines, increases in STAT3 Y705 phosphorylation may involve a mechanism wherein ERK negatively regulates STAT3 Y705 phosphorylation by phosphorylating STAT3 S727 [118]. Evidence for this potential connectivity between ERK and STAT3 is provided by our finding that MEK inhibition promoted STAT3 phosphorylation in some cell lines (Figure S3-8B).

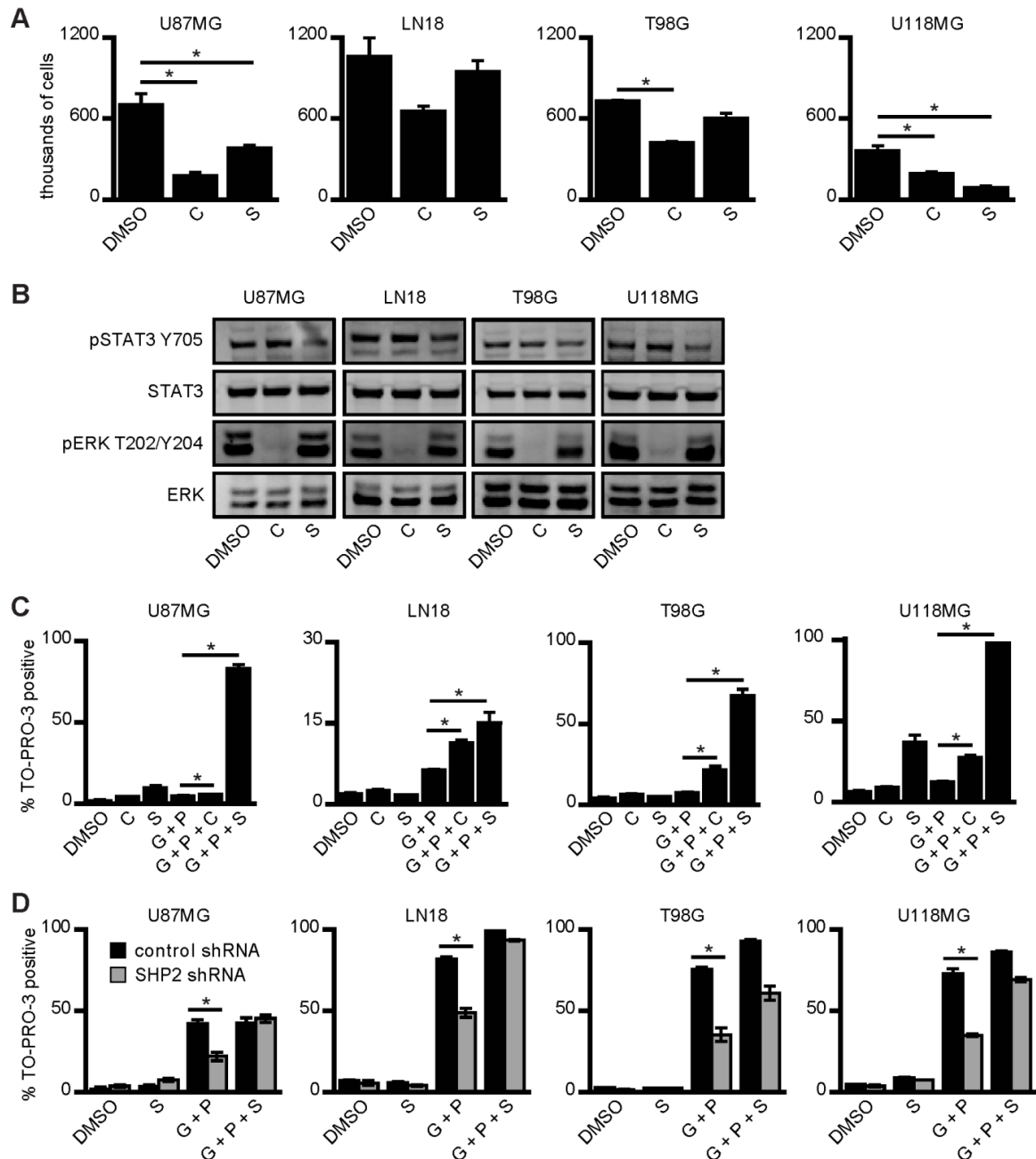


**Figure 3-2: ERK and STAT3 pathways both control proliferation and survival of GBM cells.**

(A) U87MG, LN18, T98G, and U118MG cells were seeded at 100,000 cells/well and treated 24 hrs later with 6  $\mu$ M CI-1040 (C), 4  $\mu$ M Stattic (S), or DMSO control for 72 hrs prior to cell counting. Counts are represented as mean  $\pm$  s.e.m. ( $n = 3$ ); \* denotes  $p < 0.05$ . (B) The indicated cell lines were treated with the same inhibitor concentrations as in panel (A) for 30 min prior to lysis. Lysates were analyzed by western blotting with

antibodies against the indicated proteins. Images are representative of three sets of biological replicates. (C) The indicated cell lines were treated with the indicated combinations of 10  $\mu$ M gefitinib (G) and 1  $\mu$ M PHA665752 (P), 6  $\mu$ M CI-1040 (C), 4  $\mu$ M Stattic (S), or DMSO. Gefitinib concentration was lower compared to Figure 3-1 and (D) below to reduce cellular death in response to G and P. After 96 hrs, the percentage of TO-PRO-3-positive cells was measured by flow cytometry ( $n = 3$ ); \* denotes  $p < 0.05$ . (D) The indicated cell lines expressing control or SHP2-targeting shRNA were treated with the indicated combinations of 20  $\mu$ M gefitinib (G) and 1  $\mu$ M PHA665752 (P), 4  $\mu$ M Stattic (S), or DMSO. After 72 hrs, the percentage of TO-PRO-3-positive cells was measured by flow cytometry ( $n = 3$ ); \* denotes  $p < 0.05$ .

***SHP2's ability to regulate signaling and phenotypes is modulated by elevated EGFRvIII expression.*** To evaluate SHP2's regulatory functions in the context of EGFRvIII expression, we stably depleted SHP2 in a panel of U87MG cells expressing low, medium, or high levels of EGFRvIII or a high level of kinase-dead EGFRvIII (U87MG-L, -M, -H, and -DK, respectively) [48]. SHP2 depletion reduced proliferation in all four cell lines (Figure 3-3A). Similar to effects observed in Figure 3-1B, SHP2 knockdown also promoted survival in response to EGFR and c-MET co-inhibition in U87MG-DK, -L, and -M cells, but there was no effect in U87MG-H cells Figure 3-3B). To confirm specificity of the effects of SHP2 knockdown, we used an additional, non-overlapping SHP2 shRNA to deplete SHP2 in U87MG-M cells, where cells with SHP2 knockdown were once again more resistance to EGFR and c-MET co-inhibition (Figure S3-9A). To understand the basis for the lack of effect of SHP2 knockdown on survival response in U87MG-H cells, we first probed signaling pathways by western blot in resting cells (Figures 3-3C and S3-9B). STAT3 phosphorylation was increased by SHP2 depletion in all cell lines, including U87MG-H, which was surprising given our previous

findings that STAT3 controls survival response and that SHP2 knockdown did not rescue U87MG-H cells from gefitinib and PHA665752 co-treatment. We also noticed reduced ERK phosphorylation in all cell lines with SHP2 knockdown, although the reduction in ERK phosphorylation in U87MG-H cells was very modest, an effect which we explore further in Figure 3-4. In addition, we noticed potential effects of SHP2 knockdown on the expression and phosphorylation of EGFRvIII and on phosphorylation of c-MET, findings which we also revisit later.

To delve further into the lack of effect of SHP2 knockdown on cellular response to inhibitors in U87MG-H cells, we compared the effects of SHP2 knockdown in U87MG-M and -H cells co-treated with gefitinib and PHA665752 (Figures 3-3D and S3-9C). Interestingly, in the presence of the inhibitors, SHP2 depletion significantly increased STAT3 phosphorylation in U87MG-M cells, but had essentially no effect in U87MG-H cells. Since STAT3 can be activated through direct binding with EGFR [81, 119] or EGFRvIII [120], we hypothesized that elevated STAT3 Y705 phosphorylation is EGFRvIII-dependent in SHP2-depleted U87MG-H cells but potentially EGFRvIII-independent in SHP2-depleted U87MG-M cells. This scenario would lead to a preferential reduction in STAT3 phosphorylation with EGFR inhibition in U87MG-H cells. Consistent with this model, STAT3-pEGFRvIII association was much higher in U87MG-H cells than in any other line (Figures 3-3E and S3-9D). In U87MG-H cells, STAT3-pEGFRvIII association was further promoted by SHP2 knockdown, presumably because of the concomitant increase in phosphorylated EGFRvIII levels observed in that cell line with SHP2 depletion. The unchanged STAT3-pEGFRvIII association for SHP2-depleted U87MG-M cells is consistent with the notion that EGFRvIII is not a primary

driver of STAT3 phosphorylation below a threshold level of EGFRvIII expression. Moreover, co-treatment with gefitinib and PHA665752 eliminated STAT3-pEGFRvIII association in U87MG-H cells, consistent with reduced STAT3 phosphorylation in response to gefitinib and PHA665752 co-treatment (Figure 3-3E). It should also be noted that EGFRvIII and c-MET phosphorylation were greatly reduced in cells co-treated with gefitinib and PHA665752 relative to DMSO-treated cells with or without SHP2 knockdown, which eliminates the possibility that a failure to reduce receptor phosphorylation was responsible for resistance to EGFR and c-MET co-inhibition with SHP2 knockdown (Figure S3-9E). Finally, as in parental U87MG cells, combining Stattic with gefitinib and PHA665752 enhanced cell death in SHP2-depleted U87MG-M cells (Figure 3-3F).

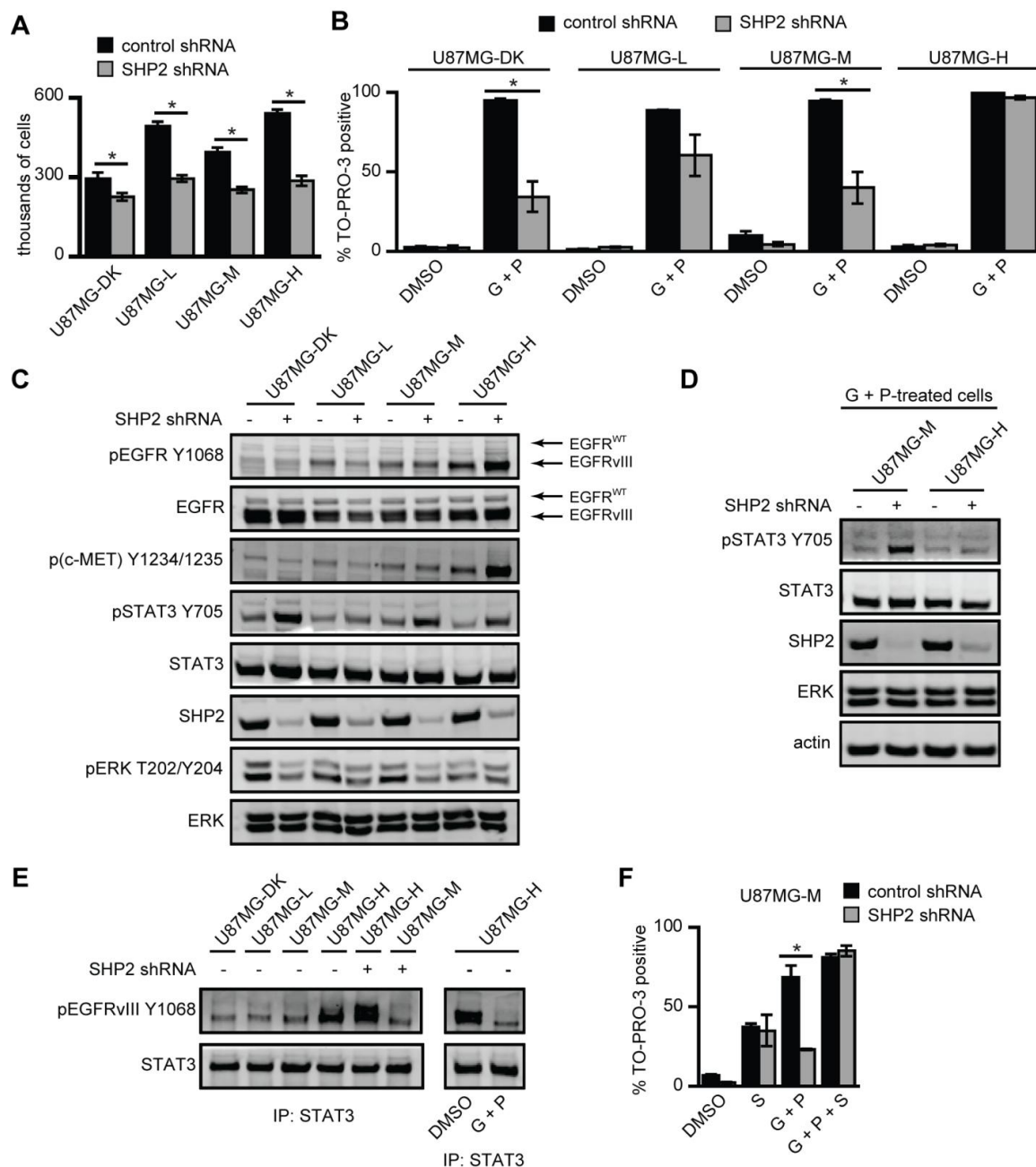


**Figure 3-3: Sufficiently high EGFRvIII expression diminishes the ability of SHP2 to promote ERK activity and to reduce STAT3 phosphorylation in the presence of EGFR and c-MET inhibitors.**

(A) U87MG-DK, -L, -M, and -H cells expressing control or SHP2-targeting shRNA were seeded at 75,000 cells/well and were counted 72 hrs later. Counts are represented as mean  $\pm$  s.e.m. ( $n = 3$ ); \* denotes  $p < 0.05$ . (B) The indicated cell lines were co-treated with 20  $\mu$ M gefitinib (G) and 1  $\mu$ M PHA665752 (P). After 72 hrs, the percentage of TO-PRO-3-

positive cells was measured by flow cytometry ( $n = 3$ ); \* denotes  $p < 0.05$ . (C) The indicated cell lines were grown in complete media for 72 hrs, and lysates were analyzed by western blotting using antibodies against the indicated proteins. Images are representative of five sets of biological replicates. (D) U87MG-M and -H cells were co-treated with 20  $\mu$ M gefitinib (G) and 1  $\mu$ M PHA665752 (P) for 24 hrs were analyzed by western blotting using antibodies against the indicated proteins. Images are representative of three sets of biological replicates. (E) The indicated cell lines were treated with or without 20  $\mu$ M gefitinib (G) and 1  $\mu$ M PHA665752 (P) for 24 hrs and lysed. STAT3 immunoprecipitates were analyzed by western blotting using antibodies against the indicated proteins. Images are representative of three sets of biological replicates. (F) U87MG-M cells were analyzed as in panel (B) with the addition of 4  $\mu$ M Stattic (S) where indicated ( $n = 3$ ); \* denotes  $p < 0.05$ .

***SHP2 can be sequestered with EGFRvIII at high receptor expression levels.*** In the same way that STAT3 can become preferentially bound with EGFRvIII, other proteins may become EGFRvIII-sequestered when the receptor is expressed at high levels. We hypothesized that such a preferential binding effect for SHP2 might explain the modest effect of SHP2 knockdown on ERK phosphorylation in U87MG-H cells as well as the gradual reduction in basal ERK phosphorylation in control cells with increasing EGFRvIII expression in Figure 3-3C. Such an effect for SHP2 would be analogous to one we described in lung cancer cells wherein kinase-activated and internalization-impaired EGFR mutants appear to sequester adapter-bound SHP2 in such a way that full ERK activation is prevented [108]. To explore this, we first probed the basal and EGF-induced associations of SHP2 with GAB1 and EGFRvIII. Increasing EGFRvIII expression clearly promoted GAB1-SHP2 association (Figure 3-4A and S3-10A), as well as pEGFRvIII-SHP2 association as previously reported [73]. Although

GAB1-SHP2 association was EGF-inducible in U87MG-DK, -L, and -M cells, the high basal association observed in U87MG-H cells was so elevated that it was not augmented by EGF. We further noted a larger fraction of SHP2 in the membrane compartment along with EGFRvIII in U87MG-H cells than in -DK cells (Figures 3-4B and S3-10B) with an approximately 1.5-fold increase in SHP2 signal in the membrane compartment in U87MG-H cells relative to U87MG-DK cells. Thus, the activity of the EGFRvIII receptor can promote sequestration of SHP2 in the membrane fraction. We also found that elevated EGFRvIII expression altered the basal intracellular distribution of SHP2, as observed by immunofluorescence. Whereas SHP2 moved from the cell interior toward the cell periphery in response to EGF in U87MG-L cells, SHP2 was already more peripherally distributed in U87MG-H cells in the basal condition and did not redistribute in response to EGF (Figures 3-4C and S3-10C-D). Given that EGF-mediated endocytosis of wild-type EGFR was significantly reduced in U87MG-H cells (Figure 3-4D), and that EGFRvIII itself is also endocytosis impaired [45, 46], our data are indeed consistent with the notion that active adapter- and EGFRvIII-bound SHP2 is sequestered at the plasma membrane in U87MG-H cells. The effect of this on ERK activation is apparently so pronounced that ERK phosphorylation cannot be induced in U87MG-H cells by exogenous EGF, whereas ERK induction does occur in U87MG-DK, -L, and -M cells (Figures 3-4E and S3-10E). To explore the possibility that altered expression of MKP3, the primary phosphatase for ERK, was responsible for the failure of ERK to be induced by EGF in U87MG-H cells, we probed for MKP3 expression across the panel of cells. However, we observed no trends in MKP3 expression that would explain our data (Figure S3-10F).

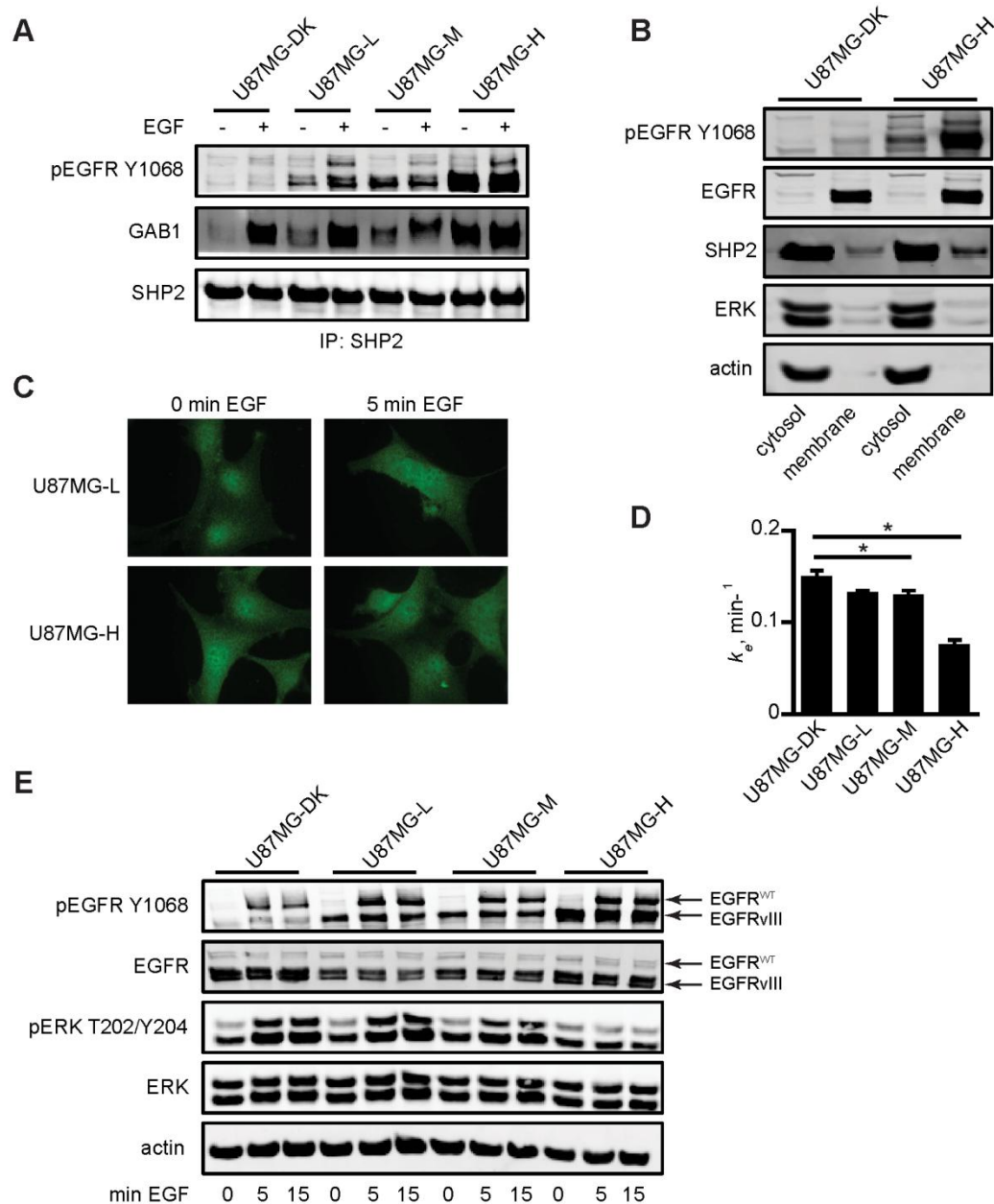


**Figure 3-4: Sufficiently high EGFRvIII expression suppresses EGF-mediated ERK phosphorylation by SHP2 sequestration.**

(A) Serum-starved U87MG-DK, -L, -M, and -H cells were treated with or without 10 ng/mL EGF for 5 min and lysed. SHP2 immunoprecipitates were analyzed by western blotting using antibodies against the indicated proteins. Images are representative of three sets of biological replicates. (B) Membrane and cytosolic fractions from serum-starved U87MG-DK and -H cells were analyzed by western blotting using antibodies

against indicated proteins. Images are representative of four sets of biological replicates. (C) Serum-starved U87MG-L and -H cells were treated with or without 10 ng/mL EGF for 5 min, and slides were prepared for SHP2 immunofluorescence. Images are representative of multiple frames from three biological replicates. (D) EGF endocytosis rate constants ( $k_e$ ) were measured for the indicated cell lines using  $^{125}$ I-EGF. Data are represented as mean  $\pm$  s.e.m. ( $n = 6$ ); \* denotes  $p < 0.05$ . (E) The indicated serum-starved cell lines were treated with 10 ng/mL EGF for up to 15 min and lysates were analyzed by western blotting using antibodies against the indicated proteins. Images are representative of three sets of biological replicates.

*SHP2 negatively regulates EGFRvIII and c-MET phosphorylation.* As previously noted, the results of Figure 3-3C suggest the potential ability for SHP2 to regulate EGFRvIII and c-MET phosphorylation. Specifically, the data showed that total levels of phosphorylated EGFRvIII and c-MET were increased by SHP2 knockdown in U87MG-H cells, but that EGFRvIII phosphorylation was reduced by SHP2 knockdown in U87MG-L and -M cells. The apparent effect in U87MG-L and -M cells may arise because of the concomitant decrease in EGFRvIII expression with SHP2 knockdown, which may result from impaired ERK activity (Figure S3-11A). To clarify this further, we ectopically expressed a constitutively active SHP2 (SHP2<sup>E76A</sup>) in all four cell lines. This had a minimal effect on EGFRvIII expression, but increased ERK phosphorylation and reduced EGFRvIII, c-MET, and STAT3 phosphorylation (Figures 3-5A and S3-11B). SHP2<sup>E76A</sup> expression also promoted cell sensitivity to gefitinib and PHA665752 co-treatment in U87MG-M cells (Figure 3-5B). To further probe SHP2's regulation of EGFRvIII, c-MET, and STAT3, we transiently expressed SHP2<sup>WT</sup> or the substrate-trapping SHP2 double mutant SHP2<sup>D425A/C459S</sup> (SHP2<sup>DM</sup>; [121]) in all four U87MG cell lines. This double point mutation abrogates SHP2's catalytic activity and causes

irreversible binding of the catalytic domain to its substrates. Importantly, expression and immunoprecipitation of SHP2<sup>DM</sup> has previously allowed for the identification of direct substrates of SHP2 including receptors such as EGFR<sup>WT</sup> and HER2 [96, 121]. Phosphorylated EGFRvIII and c-MET co-immunoprecipitated with SHP2<sup>DM</sup> (Figures 3-5C and S3-11C), but STAT3 did not (Figure S3-11D), suggesting that EGFRvIII and c-MET may be substrates of SHP2. These specific interactions have not been reported previously, but it has been reported that SHP2 can directly dephosphorylate other receptors, including HER2 [96], based on experiments using SHP2<sup>DM</sup>.

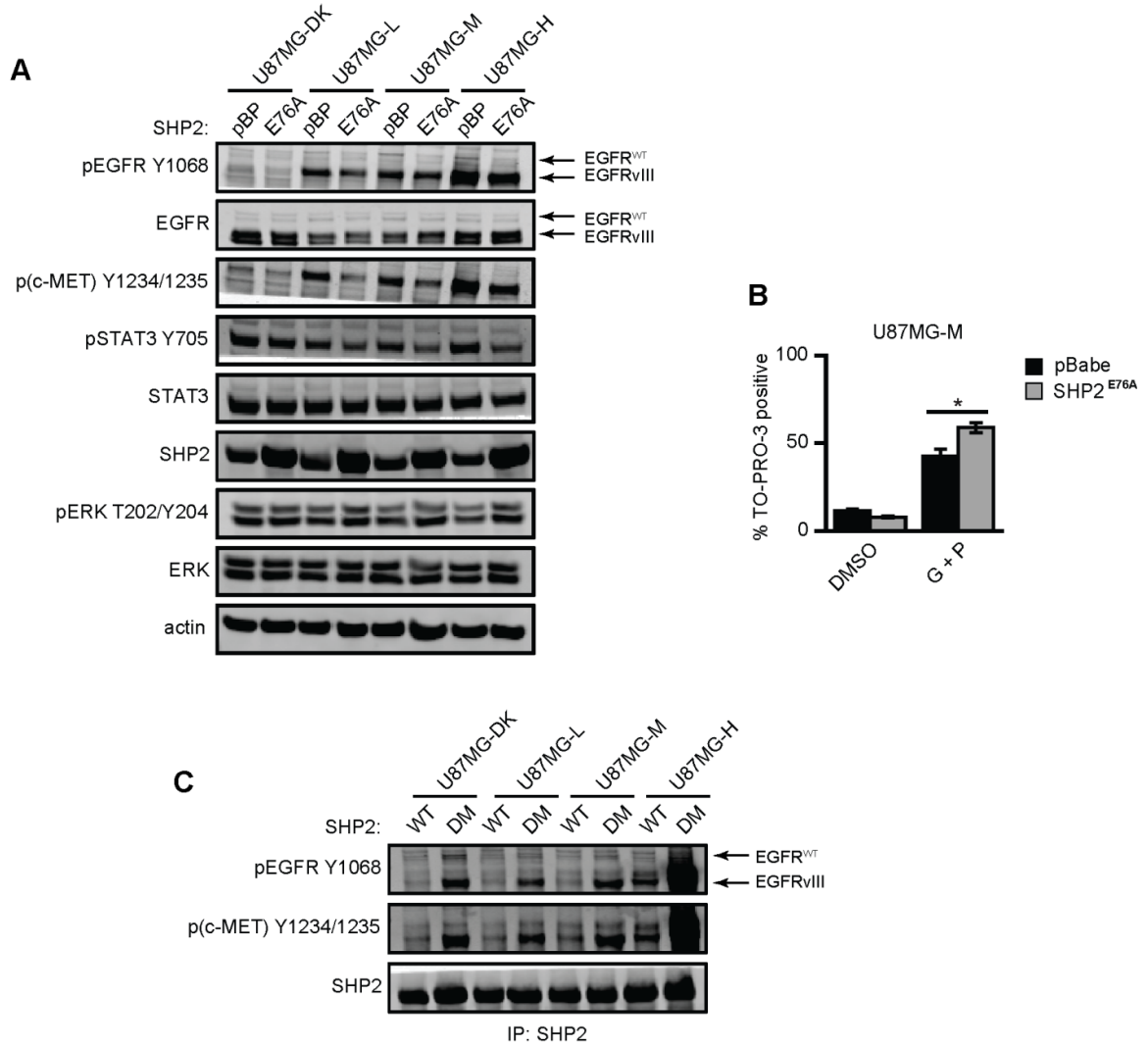


**Figure 3-5: SHP2 mutant expression reveals negative regulation of EGFR<sup>vIII</sup>, c-MET, and STAT3 phosphorylation.**

(A) Lysates of U87MG-DK, -L, -M, and -H cells transduced with an empty pBabe vector (pBP) or SHP2<sup>E76A</sup> (E76A) and grown in full media for 72 hrs were analyzed by western blotting using antibodies against the indicated proteins. Images are representative of three sets of biological replicates. (B) U87MG-M cells transduced with pBP or SHP2<sup>E76A</sup> were co-treated with 20  $\mu$ M gefitinib (G) and 1  $\mu$ M PHA665752 (P). After 72 hrs, the percentage of TO-PRO-3-positive cells was measured by flow cytometry (n = 3); \* denotes p < 0.05. (C) Serum-starved cells of the indicated cell lines transiently transfected with SHP2<sup>WT</sup> or the double mutant SHP2<sup>D425A/C459S</sup> (SHP2<sup>DM</sup>) were lysed.

SHP2 immunoprecipitates were analyzed by western blotting using antibodies against the indicated proteins. Images are representative of three sets of biological replicates.

***SHP2 knockdown impedes tumor xenograft growth and expression of hypoxia-inducible factors.*** Female Nu/Nu mice were injected subcutaneously in both flanks with U87MG-M control or SHP2 knockdown cells. Tumors arising from control cells grew well and were highly responsive to gefitinib and PHA665752 co-treatment (Figures 3-6A-B), suggesting that this co-treatment strategy can be effective in EGFRvIII-expressing GBM. We had hoped to be able to grow tumors arising from SHP2 knockdown cells to probe for the potential ability of SHP2 depletion to promote tumor resistance to gefitinib and PHA665752 co-treatment. However, after reaching an average maximum volume of 40 mm<sup>3</sup>, tumors arising from cells with SHP2 knockdown gradually shrank and never reached a sufficient size to begin treatment (Figure 3-6B). Interestingly, HIF-1 $\alpha$  and HIF-2 $\alpha$  expression was reduced in tumors arising from SHP2 knockdown cells compared to controls (Figure 3-6C), which may explain their failure to form tumors. *In vitro* studies revealed a similar effect of SHP2 knockdown on HIF-2 $\alpha$  expression under hypoxic and normoxic conditions and on HIF-1 $\alpha$  expression for normoxic culture (Figure 3-6D). Control cells treated with the MEK inhibitor U0126 displayed diminished HIF-1 $\alpha$  expression in normoxia and HIF-2 $\alpha$  expression in both normoxia and hypoxia, suggesting that SHP2's regulation of ERK is involved in controlling HIF-1/2 $\alpha$  expression.

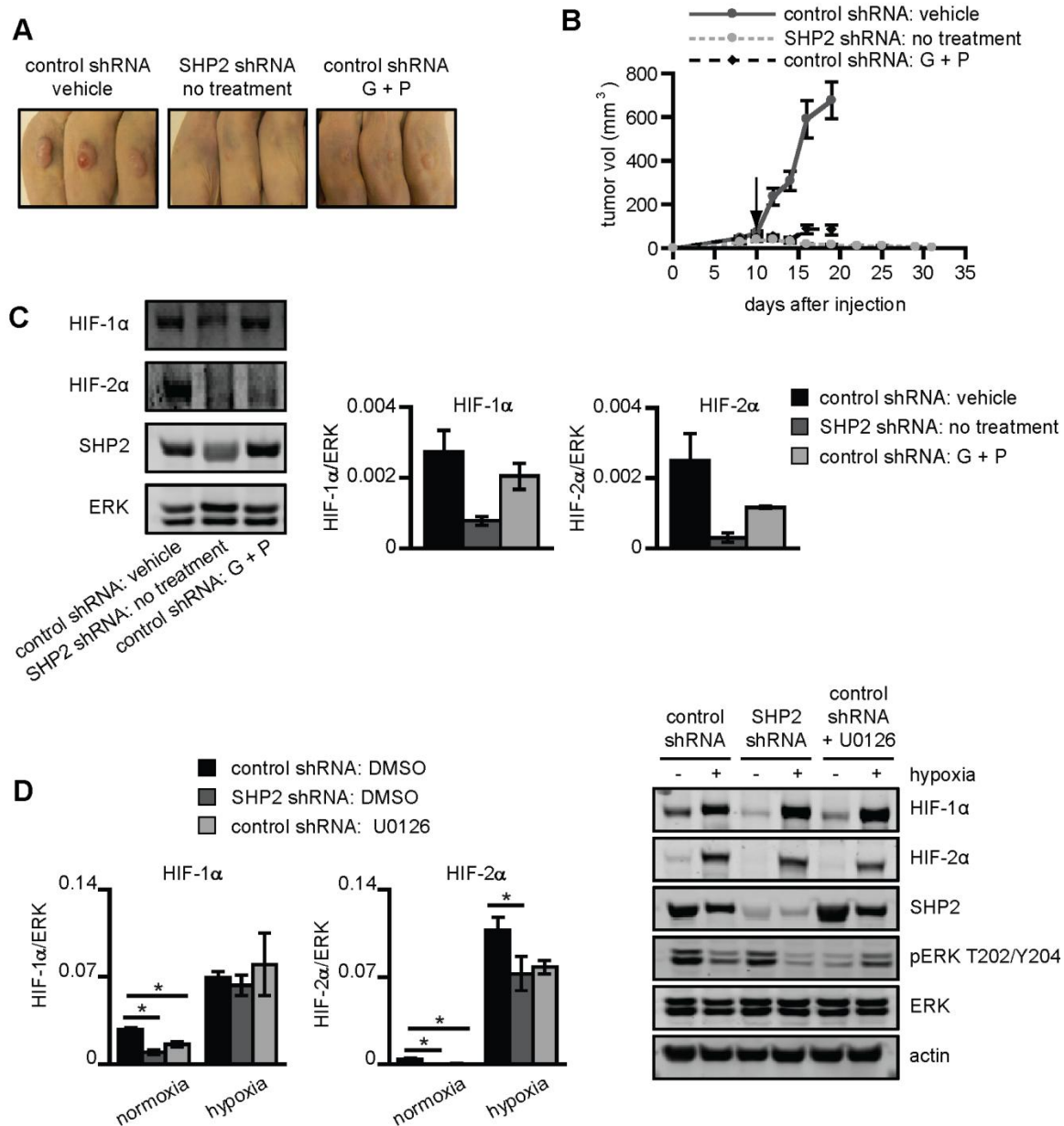


**Figure 3-6: Gefitinib and PHA665752 co-treatment or SHP2 knockdown impairs U87MG tumor xenograft growth.**

Mice were subcutaneously injected with control or SHP2-depleted U87MG-M cells. When tumors reached an average size of 50 mm<sup>3</sup> (control shRNA only), mice were treated with vehicle or 100 mg/kg gefitinib (*G*) and 30 mg/kg PHA665752 (*P*) daily for 7 days (treatment initiation indicated by black arrow). (**A**) After treatment concluded, pictures were taken and tumors were harvested. (**B**) Tumor volumes were measured before and throughout treatment. Data are shown as mean  $\pm$  s.e.m. (control shRNA:

vehicle, SHP2 shRNA: no treatment, control shRNA: G + P;  $n = 12, 26$ , and  $14$  tumors, respectively). **(C)** Tumor lysates were analyzed by western blotting using antibodies against the indicated proteins. Densitometry data are shown as mean  $\pm$  s.e.m. ( $n = 3$ ). **(D)** U87MG-M cells with control or SHP2-targeting shRNA were pretreated with DMSO or  $40 \mu\text{M}$  U0126 (control shRNA only) for  $24$  hrs prior to hypoxic culture for  $24$  hrs. Lysates were analyzed by western blotting using antibodies against the indicated proteins. Densitometry data are shown as mean  $\pm$  s.e.m. ( $n = 3$ ); \* denotes  $p < 0.05$ .

### 3-5 DISCUSSION

Our results demonstrate for the first time that SHP2's ability to exert multivariate control over signaling in GBM cells enables it to regulate simultaneously and differentially the phenotypes of proliferation and resistance to therapy. This effect arises, at least in part, because ERK and STAT3, which are regulated in qualitatively different ways by SHP2, play dominant roles in the regulation of proliferation and therapeutic resistance, respectively. We uncovered a number of other previously undocumented SHP2 regulatory functions, including SHP2-mediated antagonism of EGFRvIII and c-MET phosphorylation and regulation of HIF-1/2 $\alpha$  expression, which may also play roles in determining GBM cell and tumor phenotypes. These integrated SHP2 signaling mechanisms and the ways they impact GBM cell phenotypes are summarized in Figure 3-7.

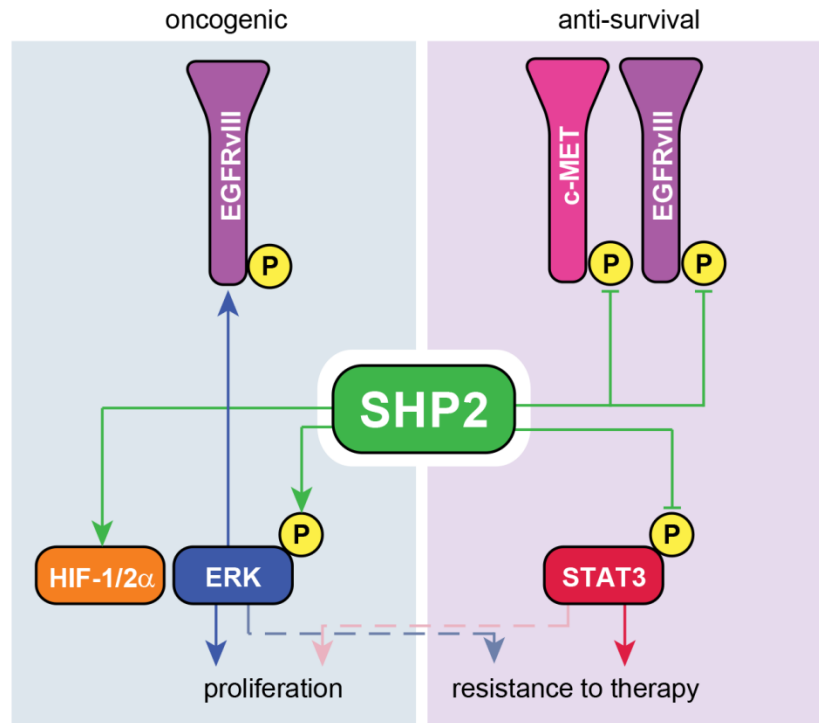


**Figure 3-7: Summary of SHP2's oncogenic and anti-survival functions in GBM cells.**

Consistent with its most well described role, SHP2 has oncogenic functions by promoting the phosphorylation of ERK, which augments expression of EGFRvIII and HIF-1/2 $\alpha$ . Conversely, SHP2 antagonizes survival signaling by apparent activity against EGFRvIII and c-MET as well as negative regulation of multiple modes of STAT3 phosphorylation.

A focus of our study is the impact of SHP2's ability to simultaneously promote ERK activity and suppress STAT3 phosphorylation. It has been shown in other contexts, and we show it explicitly for GBM cells, that the ERK and STAT3 pathways both promote proliferation and survival (here in response to EGFR and c-MET co-inhibition). Overlap in the control of transcriptional events by ERK and STAT3 helps to explain their overlapping control of phenotypes. For example, ERK and STAT3 both drive expression of proteins that promote cell cycle progression and proliferation, promote expression of anti-apoptotic proteins, and down-regulate proteins in apoptotic pathways [122-126].

This functional overlap in the regulation of broad classes of genes also contains overlap of specific gene products such as VEGF [122, 124] and c-MYC [124, 126]. Even with this partial overlap, in GBM cell lines SHP2's positive regulation of ERK is dominant in determining the effect of SHP2 expression on cellular proliferation while SHP2-mediated suppression of STAT3 dominates in determining the effect of SHP2 expression on cellular sensitivity to EGFR and c-MET co-inhibition. This updated view of the consequences of SHP2's multivariate control of signaling and phenotype fits within the general paradigm that cells integrate and interpret multivariate signaling information in different ways in the execution of cellular decisions [100-102].

Other novel aspects of our findings include the discovery that sufficiently high expression of EGFRvIII diminishes the antagonism of STAT3 phosphorylation in the presence of kinase inhibitors, in addition to diminishing SHP2's contributions to ERK activation, and the mechanisms underlying these effects. Others have noted a suppression of ERK activity with EGFRvIII expression [51], but the mechanistic basis for this had not previously been explored. Our data suggest this effect may be related to a mechanism we previously elucidated for structurally distinct EGFR mutants in NSCLC cells wherein the kinase-activated EGFR mutants, which display a reduced ability to activate ERK and a reduced rate of ligand-mediated endocytosis, also promote basal sequestration of SHP2 with EGFR and GAB1 at the cell periphery [24, 108]. It is also interesting to note that in NSCLC cells expressing wild-type EGFR, SHP2 knockdown promotes response to gefitinib [108], rather than resistance. This presumably occurs because SHP2 knockdown produces generally small effects on STAT3 Y705 phosphorylation in NSCLC cells [108] by comparison to what we observed here in GBM

cell lines, further highlighting the contextual dependence of SHP2's functions. Interestingly, the ability of EGFRvIII to sequester proteins also underlies loss of SHP2 control of STAT3 phosphorylation in the presence of EGFR and c-MET inhibitors at high EGFRvIII levels. As we demonstrate in Figure 3-3E, this effect involves a shift in EGFRvIII's ability to bind STAT3 when EGFRvIII is expressed at the highest levels. It is also worth noting that SHP2's ability to negatively regulate EGFR and c-MET phosphorylation was most apparent with high EGFRvIII expression. This could also result from sequestration of active SHP2 at the plasma membrane where it has ready access to these receptors. We also note that the range of EGFRvIII expression explored here is consistent with that observed in tumors [34]. Thus, the dependence of SHP2 functions on EGFRvIII expression may be clinically relevant.

There are of course additional signaling pathways regulated by EGFRvIII and SHP2 that have not been explored here but which could play roles in some apparent quantitative inconsistencies between the effects of altered SHP2 expression on signaling pathways and the phenotypic roles we have ascribed to those pathways. One example pertains to our observations in Figure 3-3 in U87MG-H cells, where control cells were highly proliferative despite displaying relatively low basal ERK phosphorylation and SHP2 knockdown produced a modest effect on ERK phosphorylation but a large effect on proliferation. As just one possible explanation for this, we note that the increased abundance of EGFRvIII in U87MG-H cells could drive other pathways which may compensate for ERK in promoting proliferation. If the activities of those other pathways are also regulated by SHP2 in a way that promotes proliferation, a large drop in proliferation could still accompany SHP2 knockdown with only a modest effect on ERK.

In the future, it will be important to probe these issues more broadly and quantitatively in order to more fully understand the potential impact of targeting SHP2 or EGFRvIII in GBM.

Our data on the effects of SHP2 knockdown, expression of constitutively active SHP2, and expression of substrate-trapping SHP2 all suggest that SHP2 negatively regulates EGFRvIII phosphorylation, potentially through direct interaction. This contrasts with previous reports that SHP2-mediated ERK activity increases levels of phosphorylated EGFRvIII [112]. This discrepancy may be explained by our additional finding that SHP2-mediated ERK activity enhances EGFRvIII expression, an effect which has also been noted by others with SHP2 knockdown in certain GBM cell lines [73]. Thus, SHP2 appears to exert two countervailing effects, either of which may be dominant, in the determination of total cellular phosphorylated EGFRvIII levels. The notion that SHP2 can negatively regulate EGFRvIII phosphorylation may seem at odds with our finding that SHP2 knockdown impairs xenograft growth or the analogous findings of Zhan et al. (2009) where a catalytically inactive SHP2 was expressed in an EGFRvIII-positive tumor model. We interpret these aggregate results as indicating that any potential ability for SHP2 to impair tumorigenesis by negatively regulating EGFRvIII phosphorylation is trumped by SHP2's positive regulatory functions in tumorigenesis, including its apparent ability to control HIF-1/2 $\alpha$  expression, at least in the cell line model used here.

Given ongoing efforts to develop specific SHP2 inhibitors for clinical use, it is worth noting that two distinct effects of SHP2 inhibition could arise in GBM cells and tumors. Based on our results, SHP2 inhibition would be expected to inhibit ERK

activity, but simultaneously to promote STAT3 phosphorylation. In cell culture, the integrated effect of these signaling perturbations was to slow cell growth while simultaneously promoting resistance to EGFR and c-MET co-inhibition. Based on this alone, it is unclear if SHP2 inhibition would be a useful therapeutic approach. Our finding that SHP2 controls HIF-1/2 $\alpha$  expression and GBM tumor xenograft growth may obviate potential concerns about the ability of SHP2 inhibition to promote survival signaling through the STAT3 pathway, but this remains to be demonstrated in more detailed GBM tumor models that include exploration of the potential ability of very high EGFRvIII expression to modulate SHP2 function. Assuming that SHP2 function is indeed controlled by EGFRvIII levels *in vivo*, recent advances in detecting EGFRvIII protein through magnetic resonance imaging [127], as opposed to traditional tumor tissue biopsy approaches, may eventually advance our ability to predict the impact of SHP2 inhibition.

It should also be noted that our xenograft studies suggest promise for combining EGFR and c-MET inhibitors in EGFRvIII-positive GBM. This has not been previously demonstrated *in vivo*, but a previous study did demonstrate the utility of combining an HGF-targeted antibody with an EGFR inhibitor [43]. Interestingly, the utility of certain irreversible EGFR inhibitors in EGFRvIII-positive GBM may obviate the need to combine c-MET and EGFR inhibitors [128]. Whether or not c-MET inhibitors are needed moving forward, SHP2 inhibitors may eventually be an attractive alternative for treating GBM where resistance to other inhibitors arises. Of course, our data support the potential utility of STAT3 inhibitors in treating GBM. STAT3 has previously been identified as a key regulator of GBM cell survival [47, 81], and at least one clinical trial

(ClinicalTrials.gov NCT01904123) is scheduled to begin recruiting patients later this year to test the efficacy of STAT3 inhibition in cancers including GBM.

### 3-6 ACKNOWLEDGEMENTS

We thank Janine Buonato for equally contributing to the completion of this work. We also thank Dr. Donald M. O'Rourke for providing helpful feedback. We thank Drs. Ben Neel, Tyler Jacks, Marilyn Farquhar, Gary Nolan, Frank Furnari, and Yehenew Agazie for generously providing reagents.

### 3-7 SUPPLEMENTARY MATERIAL

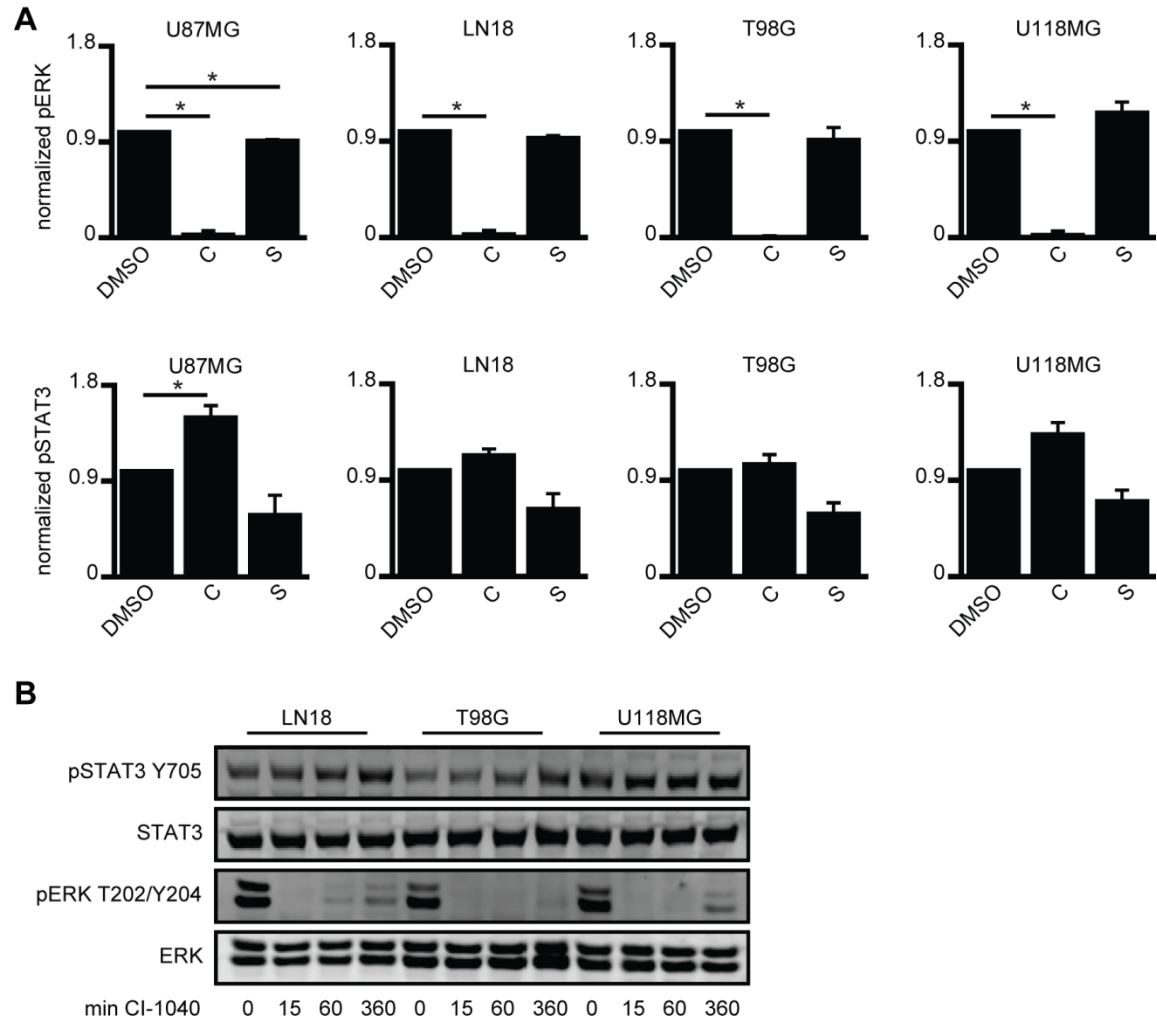


**Figure S3-8: ERK and STAT3 inhibition differentially regulate GBM cell phenotype.**

(A) The indicated cell lines were treated with 6  $\mu$ M CI-1040 (C), 4  $\mu$ M Stattic (S), or DMSO control for 30 min prior to lysis. Lysates were analyzed by western blotting using antibodies against the indicated proteins. Densitometry data are represented as mean  $\pm$  s.e.m. ( $n = 3$ ); \* denotes  $p < 0.05$ . (B) LN18, T98G, and U118MG cells were treated with 3  $\mu$ M CI-1040 for up to 360 min, and lysates were analyzed by western blotting using antibodies against the indicated proteins.

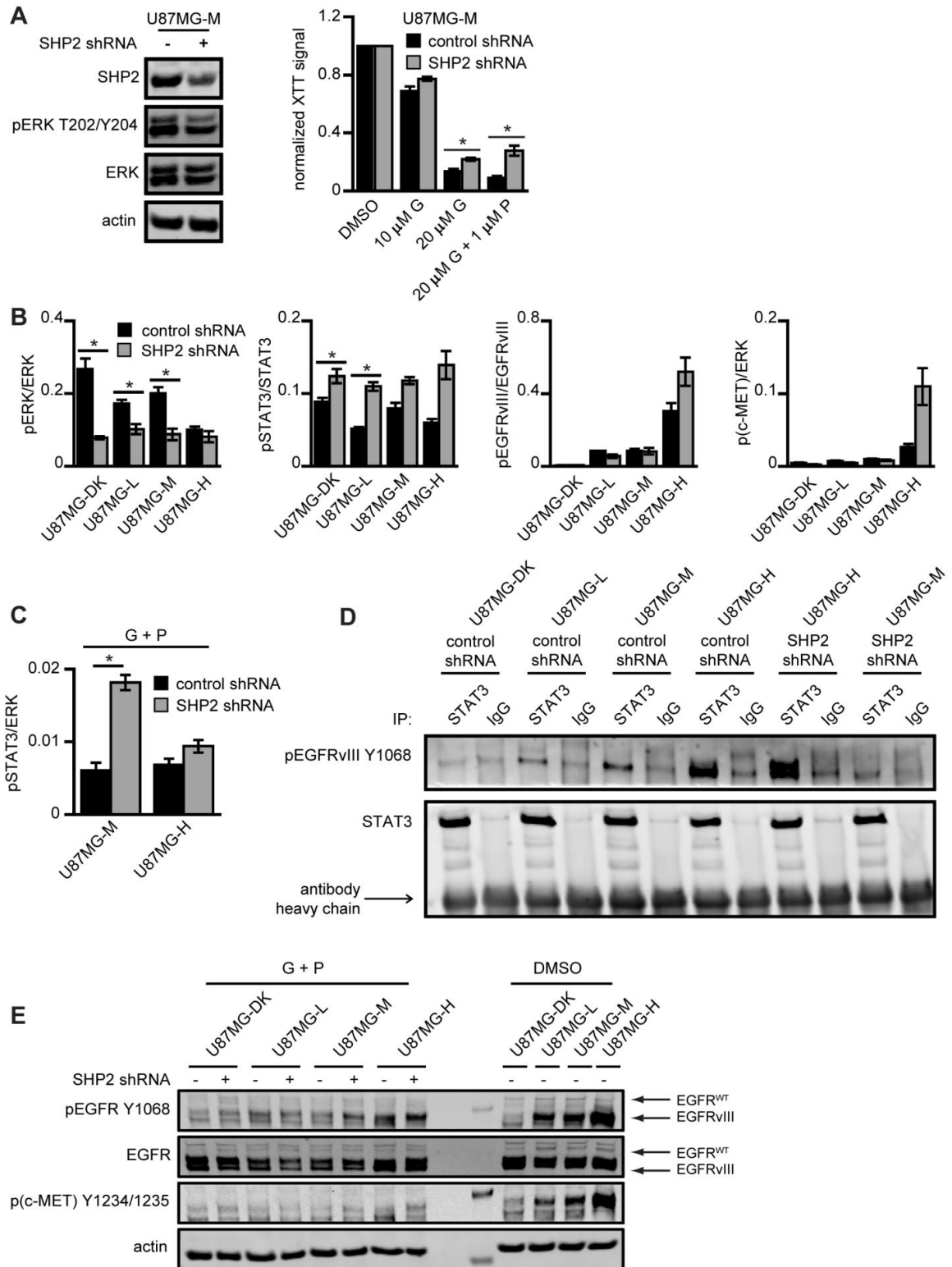


**Figure S3-9: SHP2's abilities to promote ERK phosphorylation in resting cells and to antagonize STAT3 phosphorylation in drug-treated cells are diminished with sufficiently high EGFRvIII expression.**

(A) U87MG-M cells expressing a control shRNA or an SHP2 shRNA distinct from the shRNA used in other experiments were lysed. Lysates were analyzed by western blotting using antibodies against the indicated proteins. These cells were also treated with the indicated concentrations of gefitinib (*G*) and/or PHA665752 (*P*) for 72 hrs, and cell proliferation was measured by XTT assay. XTT signal (y-axis) from cells in a given treatment condition was normalized by the signal measured from cells treated with DMSO. Data are represented as mean  $\pm$  s.e.m. for one experiment with six replicate wells ( $n = 6$ ); \* denotes  $p < 0.05$ . (B) Lysates prepared from U87MG-DK, -L, -M, and -H cells stably expressing control or SHP2-targeting shRNA grown in full media for 72 hrs were analyzed by western blotting using antibodies against the indicated proteins. Densitometry data are represented as mean  $\pm$  s.e.m. ( $n = 5$ ); \* denotes  $p < 0.05$ . (C) U87MG-M and -H cells with or without SHP2 knockdown were co-treated with 20  $\mu$ M gefitinib and 1  $\mu$ M PHA665752 for 24 hrs, and lysates were analyzed by western blotting using antibodies against the indicated proteins. Due to the large decrease in STAT3 expression in gefitinib/PHA665752-treated U87MG-H cells with SHP2 knockdown, pSTAT3 was normalized by ERK to compare total relative levels of phospho-STAT3 among cell lines. Data are represented as mean  $\pm$  s.e.m. ( $n = 3$ ); \* denotes  $p < 0.05$ . (D) U87MG-DK, -L, -M, and -H cells expressing a SHP2-targeting or non-targeting control shRNA were lysed. Lysates were immunoprecipitated with either a STAT3 antibody or a control antibody (IgG), and immunoprecipitates were analyzed by western blotting using antibodies against the indicated proteins. (E) U87MG-DK, -L, -M, and -H cells with or without SHP2 knockdown were treated with DMSO or 20  $\mu$ M gefitinib (*G*) and 1  $\mu$ M PHA665752 (*P*) for 24 hrs, and lysates were analyzed by western blotting using antibodies against the indicated proteins.

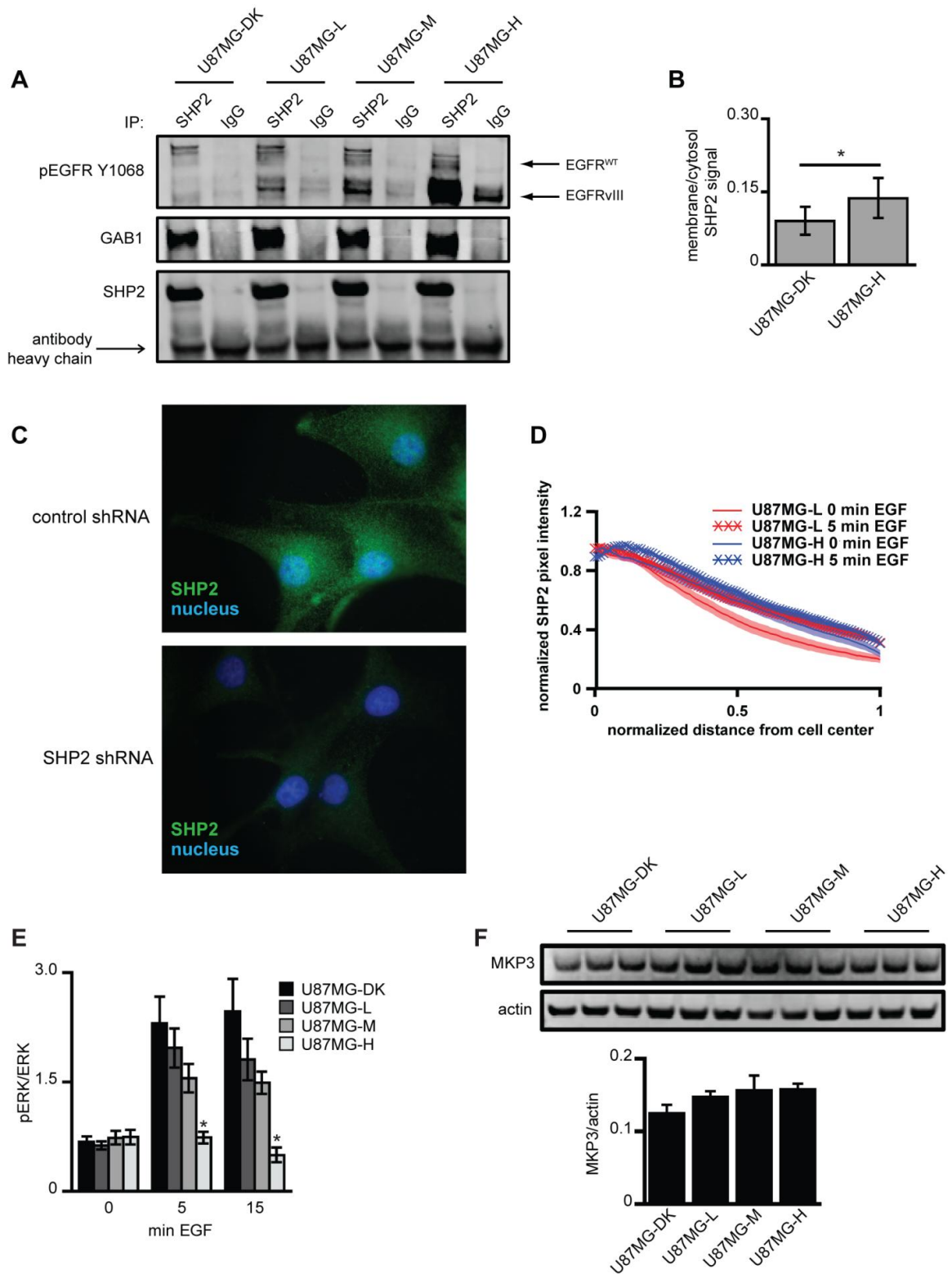


**Figure S3-10: With high levels of EGFRvIII expression, SHP2 becomes increasingly basally associated with EGFRvIII, SHP2 intracellular distribution is perturbed, and EGF-mediated ERK induction becomes impaired.**

(A) Serum-starved U87MG-DK, -L, -M, and -H cells treated with 10 ng/mL EGF for 5 min were lysed. Lysates were immunoprecipitated with either an SHP2 antibody or a control antibody (IgG), and immunoprecipitates were analyzed by western blotting using antibodies against the indicated proteins. (B) Membrane and cytosolic fractions from serum-starved U87MG-DK and -H cells were analyzed by western blotting. Data are represented as mean  $\pm$  s.e.m. ( $n = 4$ ); \* denotes  $p < 0.05$ . (C) Slides of serum-starved U87MG-M cells expressing a non-targeting control shRNA or an SHP2 shRNA were prepared for SHP2 immunofluorescence and subsequently imaged using the same exposure time. (D) Serum-starved U87MG-L and -H cells were treated with EGF and slides were prepared for SHP2 immunofluorescence. Intracellular pixel intensities from images were quantified as a function of normalized radial distance from cell centers ( $x = 0$ ) to the cell periphery ( $x = 1$ ). For seven images per condition, all cells contained within the image were analyzed. Lines represent mean and shaded areas represent s.e.m. ( $n \geq 10$  cells). (E) Lysates from serum-starved U87MG-DK, -L, -M, and -H cells treated with or without 10 ng/mL EGF for up to 15 min were analyzed by western blotting. Densitometry data are represented as mean  $\pm$  s.e.m. ( $n = 3$ ); \* denotes  $p < 0.05$  relative to DK cells. (F) U87MG-DK, -L, -M, and -H were lysed, and lysates were analyzed by western blotting using antibodies against the indicated proteins. Densitometry data are represented as mean  $\pm$  s.e.m. ( $n = 3$ ).

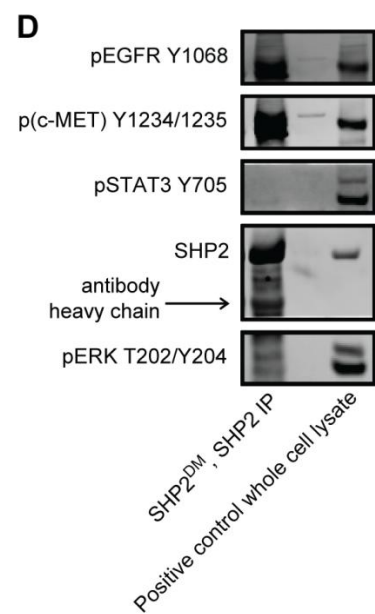
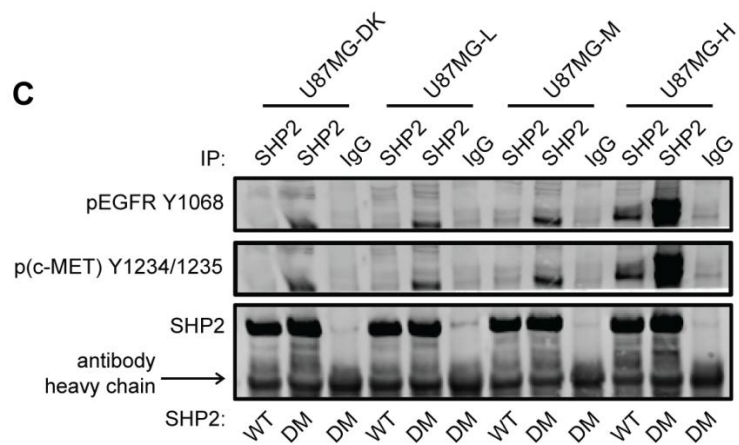
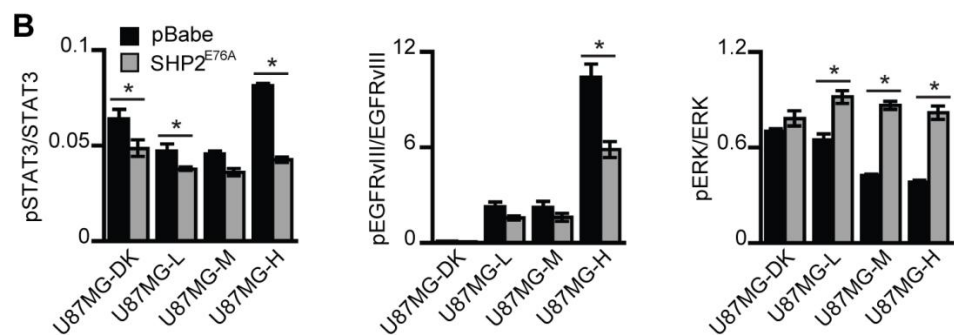
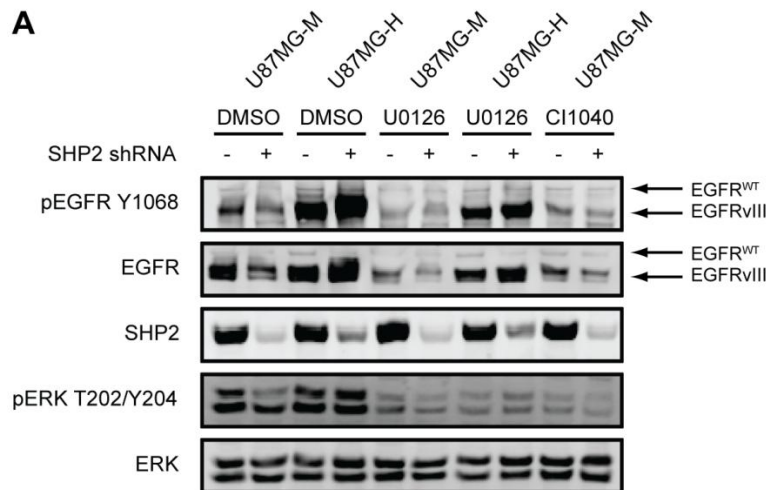


**Figure S3-11: SHP2 regulatory roles identified by SHP2 knockdown are confirmed by ectopic expression of SHP2 mutants.**

(A) U87MG-M and -H cells with or without SHP2 knockdown treated with 20  $\mu$ M U0126 or 3  $\mu$ M CI-1040 for 24 hrs were lysed. Lysates were analyzed by western blotting using antibodies against the indicated proteins. (B) U87MG-DK, -L, -M, and -H cells were transduced with an empty pBabe vector or a pBabe vector encoding SHP2<sup>E76A</sup>. Whole-cell lysates prepared from cells grown in complete media for 72 hrs were analyzed by western blotting using antibodies against the indicated proteins. Densitometry data are represented as mean  $\pm$  s.e.m. ( $n = 3$ ); \* denotes  $p < 0.05$ . (C) Serum-starved U87MG-DK, -L, -M, -H cells transiently transfected with SHP2<sup>WT</sup> or the double mutant SHP2<sup>D425A/C459S</sup> (SHP2<sup>DM</sup>) were lysed. Lysates were immunoprecipitated with either an SHP2 antibody or a control antibody (IgG), and immunoprecipitates were analyzed by western blotting using antibodies against the indicated proteins. Images are representative of three sets of biological replicates. (D) An SHP2 immunoprecipitate from U87MG-H cells expressing SHP2<sup>DM</sup> and a cell lysate positive for phospho-EGFR, phospho-MET, phospho-STAT3, and phospho-ERK were analyzed by western blotting using antibodies against the indicated proteins.

## **Chapter 4: EGFR-activated Kinases Counteract GAB1 Dephosphorylation to Maintain GAB1-SHP2 Complexes Distal from EGFR**

### **4-1 ABSTRACT**

Multi-membered complexes of signaling proteins nucleated in response to receptor activation are often represented as static assemblies held together by phosphotyrosine-SH2 domain and other interactions. However, reversible binding, phosphatase activity, and other topological details allow for dynamic modes of protein complex regulation that can significantly impact signal transduction. Here, we explore these aspects of signaling protein complex regulation using EGFR as a model system. Specifically, we demonstrate the ability of EGFR-activated SRC family kinases (SFKs) to repeatedly counteract GAB1 dephosphorylation to maintain the association of SHP2 with phosphorylated GAB1, which promotes SHP2 activity, in the cytosolic compartment distal from EGFR. Interpretation of our data using a computational model reveals that SFKs amplify EGFR activity to enable GAB1 phosphorylation and GAB1-SHP2 complexes to decay more slowly than EGFR phosphorylation. Interestingly, this SFK-dependent mechanism is not used downstream of c-MET. Thus, our results quantitatively describe a regulatory mechanism used by some receptors to control signaling complex persistence remotely.

## 4-2 INTRODUCTION

In receptor-mediated cell signaling, outside-in information transfer occurs because ligand-receptor binding in the extracellular compartment promotes intermolecular binding events in the cell interior mediated by phosphotyrosine-SH2 domain and other types of protein-protein interactions. Static textbook representations of this process belie the fact that phosphotyrosine-SH2 domain interactions (and other relevant protein-protein interactions) are reversible and relatively weak [64], and that phosphotyrosines can be regulated by protein tyrosine phosphatases (PTPs) with times scales that are small compared to the overall time scale for signal transduction [63, 64]. These issues, coupled with sometimes receptor- or cell context-dependent details of how specific downstream protein-protein interactions are regulated, create complexities that are typically absent in schematic representations of signaling pathways but which can have significant impact on signal transduction. Many investigators undoubtedly recognize these issues, but their full implications on the regulation of signaling protein complexes and overall signaling dynamics have not been widely pursued or quantitatively investigated. Here, we explore these issues to understand the ability of the epidermal growth factor receptor (EGFR) to drive and maintain the association of SRC homology 2 domain-containing phosphatase 2 (SHP2) with the adaptor protein GRB2-associated binder 1 (GAB1), a binding event that promotes SHP2 activity [52].

SHP2 regulates signaling through numerous pathways, with its most well-described function being to promote ERK activity [52]. SHP2 is basally auto-inhibited by an intramolecular interaction between its N-terminal SH2 domain and its PTP domain that limits PTP domain access to substrates [52]. Phosphotyrosine engagement of SHP2's

SH2 domains relieves this inhibition and activates SHP2 [52]. Downstream of EGFR, the most common event leading to SHP2 activation involves SHP2 binding to phosphorylated GAB1, which can complex with EGFR indirectly by binding with the EGFR adaptor GRB2 and be phosphorylated by receptor tyrosine kinases (RTKs) including EGFR [52, 65]. SHP2 binding to GAB1 occurs through phosphorylated GAB1 tyrosines 627 and 659, though binding of SHP2's N-terminal SH2 domain to GAB1 Y627 is thought to be the dominant event in promoting SHP2 activity [52]. Interestingly, compared to EGF, HGF promotes more sustained phosphorylation of GAB1 and ERK [89, 129], as well as more substantial redistribution of GAB1 to the cell periphery [130]. Thus, well-characterized differences in ERK activation by different RTKs may involve spatiotemporal differences in SHP2 engagement by GAB1.

Although GAB1-SHP2 complexes can be observed for 30 min or more in response to RTK activation [e.g., [55]], the complexes are unlikely to exist in a stable form for this amount of time since SH2 domain-containing proteins generally dissociate from phosphotyrosines within seconds after initial complex formation [61, 62]. Given that EGFR phosphotyrosines can be dephosphorylated with relatively small time scales [63], it seems likely that similarly rapid regulation of GAB1 tyrosines could occur. However, the kinetics of GAB1 dephosphorylation have not been quantified. If PTP-mediated regulation of GAB1 is relevant during the time scale of overall GAB1-SHP2 complex persistence, re-phosphorylation of GAB1 by a tyrosine kinase could play an important role in the persistence of GAB1-SHP2 complexes. Moreover, if RTKs were the only kinases able to play this role, GAB1-SHP2 complexes might exist mainly as membrane-associated species, as suggested by typical representations of the RTK-GRB2-

GAB1-SHP2 complex [e.g., [52, 54, 131]]. Conversely, the ability of a cytosolic kinase to drive GAB1 phosphorylation could extend the effective persistence time and length scales of GAB1-SHP2 complexes distal from a signal-initiating receptor.

Here, we identify a mechanism in adenocarcinoma cells wherein EGFR regulates the persistence of GAB1-SHP2 complexes distal from the receptor through many cycles of GAB1 dephosphorylation by activating SRC family kinases (SFKs), a substantial fraction of which are present in the cytosol. This picture stands in stark contrast to the typical view of EGFR-mediated SHP2 activation involving the linear multi-protein complex consisting of EGFR, GRB2, GAB1, and SHP2. To interpret our data, we constructed a kinetic model comprised of 386 reactions and characterized by parameters taken from the literature or fit to our data. To best recapitulate our data, the model requires that SFKs effectively amplify EGFR activity to buffer GAB1 phosphorylation, and thus GAB1-SHP2 association, against decreasing EGFR phosphorylation. This amplification is required even with perturbations to the model topology motivated by previously described feedback mechanisms involving SHP2's ability to promote SFK activity [55, 56] or to dephosphorylate GAB1 [132]. Interestingly, in response to HGF, GAB1-SHP2 complexes form in an SFK-independent manner and remain in complex with c-MET, suggesting that the mechanism identified downstream of EGFR may not be generic. Thus, our findings quantitatively describe a previously undocumented “remote control” mechanism wherein membrane-associated receptors amplify a signal originating from the membrane by activating intracellular kinases to regulate the persistence of functional protein complexes held together by phosphotyrosine-SH2 domain interactions.

## 4-3 MATERIALS AND METHODS

### Experiments

**Cell culture.** H1666 cells (American Type Culture Collection) were maintained in ACL4 [24]. 293T and HeLa cells (American Type Culture Collection) were maintained in DMEM supplemented with 10% fetal bovine serum (FBS). For serum starvation, cells were switched to media containing 0.1% FBS for 16-18 hrs.

**Immunoblotting.** Cell lysates were prepared using a standard buffer (Cell Signaling Technology, Danvers, MA, USA; #9803) supplemented with 1 mM PMSF, additional protease inhibitors (Sigma, St. Louis, MO, USA), and phosphatase inhibitors (Sigma). Proteins were resolved by SDS-PAGE and transferred to nitrocellulose membranes, which were blocked in Odyssey Blocking Buffer (OBB; LI-COR, Lincoln, NE, USA) and stripped with 0.2 M NaOH as needed. Images were obtained using a LI-COR Odyssey Infrared Imaging System.

**Immunoprecipitation.** Cell lysates were prepared per the immunoblotting protocol. 500 µg of total protein was incubated at 4°C overnight with agarose beads conjugated to SHP2 or control antibody. Beads were washed three times with lysis buffer, re-suspended in LDS sample buffer (Invitrogen), and boiled before immunoblotting.

**Stable shRNA and expression constructs.** The pLKO vector containing a short hairpin sequence targeting the 3' UTR of human *EGFR* (5'-AGAATGTGGAATACCTAAGG-3') was provided by Daniel Haber (Harvard Medical School). Lentivirus was produced by calcium phosphate-mediated transfection of 293FT cells (Invitrogen, Carlsbad, CA, USA) with vector and the packaging plasmids pCMV-

VSVG, pMDL-gp-RRE, and pRSV-Rev (Marilyn Farquhar, UCSD). Virus was harvested 48 and 72 hrs post-transfection and used to infect target cells, which were selected in puromycin. EGFR cDNA encoding Y845F EGFR (Sarah Parsons, University of Virginia) was inserted in the pMSCV vector. Retrovirus was produced by calcium phosphate-mediated transfection of amphotropic Phoenix cells (Gary Nolan, Stanford University) with vector. Virus was harvested 24, 30, and 48 hrs post-transfection and used to infect target cells, which were selected in hygromycin. Constructs were validated by sequencing. EGFR knockdown was validated by Western blot.

***Transient expression constructs.*** The p3xFlag-CMV-7.1 vector containing SRC<sup>Y527F</sup> cDNA was provided by Todd Miller (Stony Brook University). The pcDNA3 vector containing HA-tagged GAB1 was provided by Toshio Hirano (Osaka University). Cells were plated in 6-well plates in media lacking antibiotics, and were transfected the following day with 1 µg SRC<sup>Y527F</sup> DNA and 1 µg GAB1 DNA using 6 µL Lipofectamine 2000 (Invitrogen). Cells were switched to serum-free media 4 hrs later, and treated and lysed the next day before proceeding to immunoblotting/immunoprecipitation.

pCMV5 vector containing SRC<sup>WT</sup> and SRC<sup>K295R/Y527F</sup> cDNA were from Addgene (Joan Brugge, Harvard University). Cells were plated in 6-well plates in media lacking antibiotics, and were transfected the following day with 2 µg SRC DNA using 6 µL Lipofectamine 2000 (Invitrogen). Cells were switched to serum-free media 4 hrs later, and treated and lysed the next day before proceeding to immunoblotting.

***Antibodies and other reagents.*** EGFR antibody (Ab-12) was from Thermo Fisher Scientific (Waltham, MA, USA). ERK (#4695), pGAB1 Y627 (#3233), p-MET Y1234/1235 (#3126), and MET (#8198) antibodies were from Cell Signaling

Technology. SHP2 (sc-280), GAB1 (sc-9049), SRC (sc-8056; also detects the SFKs YES and FYN), and GRB2 (sc-255) antibodies were from Santa Cruz Biotechnology (Santa Cruz, CA, USA). Actin (MAB 1501) antibody was from Millipore. pEGFR Y1068 (#1727) antibody was from Epitomics (Burlingame, CA, USA). Infrared dye-conjugated secondary antibodies were from Rockland Immunochemicals (Gilbertsville, PA, USA) and Invitrogen, respectively. Gefitinib (LC Laboratories, Woburn, MA, USA), GDC-0941 (LC Laboratories), and PP2 (Sigma) were reconstituted in DMSO. Recombinant human EGF and HGF were from Peprotech (Rocky Hill, NJ, USA). Pervanadate was prepared as previously described [63].

***Subcellular fractionation.*** Membrane and cytosolic fractions were prepared as described previously [108].

***Statistics.*** Statistical analyses were performed using a paired two-tailed student's *t*-test.

### *Computational model*

***General model considerations and topology.*** The model consists of a set of coupled ordinary differential equations to describe the processes leading to EGFR phosphorylation, but includes the additions of the processes of SFK activation, GAB1 phosphorylation, and EGFR-GRB2, GRB2-GAB1, and GAB1-SHP2 associations. The model topology leading from EGF binding to EGFR phosphorylation is based in part upon a previously published model [63]. Essential processes and model parameters are summarized in Figure 4-5A and Table S4-1, respectively. In total, the model includes 386 reactions, 101 species, and 29 parameters.

***EGF binding and concentration.*** EGF binding at the plasma membrane was modeled as a reversible process characterized by association [133] and dissociation [134] rate constants. EGF was modeled at a constant concentration of 10 ng/mL.

***ATP and inhibitor binding.*** Association and dissociation rate constants for ATP and gefitinib with EGFR were previously calculated [63]. ATP was assumed to be at a constant cellular concentration of 1 mM [135]. Gefitinib, when included, was modeled at a constant cellular concentration of 1  $\mu$ M.

***EGFR dimerization.*** The EGFR dimerization rate constant was calculated as described previously [63] assuming  $6 \times 10^5$  EGFR per H1666 cell, which was estimated by a western blot based comparison of total EGFR levels in H1666 cells relative to PC9 cells, for which we have previously determined EGFR levels at the membrane using  $^{125}$ I-EGF. Dimer uncoupling rate constants in the presence or absence of EGF were described previously [136, 137]. All dimer species were assumed to be symmetric, with the exception of allowing for asymmetric EGF binding.

***EGFR phosphorylation.*** EGFR phosphorylation was modeled as a process which occurs between ATP-bound EGFR dimers where both receptors are simultaneously phosphorylated at a representative tyrosine which is able to bind GRB2, with distinct rate constants for phosphorylation occurring in the presence or absence of EGF [138].

***GAB1 phosphorylation.*** GAB1 phosphorylation at a representative tyrosine which is able to bind SHP2 was modeled as a process catalyzed by an active SFK. Because our experimental data suggest SFKs are the primary mediator of GAB1 phosphorylation in H1666 cells, we did not include the possibility of EGFR phosphorylating GAB1.

**PTP activity.** EGFR and GAB1 dephosphorylation were modeled as zeroth order with respect to PTPs, which precludes the requirement for considering distinct PTP species.

**EGFR degradation.** EGFR degradation was modeled as being permitted for any GRB2-bound EGFR species since GRB2 mediates the interaction of CBL with EGFR, which plays a primary role in ligand-mediated EGFR degradation [139]. Any proteins bound to EGFR targeted for degradation were assumed to become instantaneously unbound from that EGFR species.

**GRB2, GAB1, and SHP2 binding.** GRB2 was modeled as being able to bind phosphorylated EGFR using experimentally derived rate constants for association and dissociation [61]. GAB1 was modeled as being able to bind all GRB2 species through an SH3 domain-mediated interaction using previously described rate constants for association and dissociation [140]. SHP2 was modeled as being able to bind phosphorylated GAB1 using the same association and dissociation rate constants as for GRB2 binding EGFR, based on an assumption of similar SH2-domain mediated interactions for GRB2-EGFR and GAB1-SHP2.

**SFK activation.** The biochemical steps leading to SFK activation are complex, including separate steps for the dephosphorylation of a C-terminal regulatory tyrosine (e.g., SRC Y530), autophosphorylation of SRC Y418, and binding of SRC's SH2 domain to proteins including EGFR [141]. We simplified this to a first-order rate equation where phosphorylated EGFR activates SFK, using a previously derived  $k_{s,a}$  for EGF-bound EGFR [138], similar to topologies used in previous models [142]. Even with this simplification, our model fit is able to accurately recapitulate our experimental data,

indicating that our approach allows for sufficiently rapid SFK activation to reproduce the GAB1 phosphorylation kinetics observed experimentally. SFK inactivation was modeled as having c-SRC kinase (CSK) serve as the reaction enzyme, using a previously derived  $k_{S,i}$  for CSK [143, 144].

**Parameter fitting.** The four unknown parameters ( $k_{G1p}$ ,  $k_{G1dp}$ ,  $k_{dp}$ ,  $k_{deg}$ ) were determined by fitting the model to data gathered from parental H1666 cells, including the phosphorylation of GAB Y627 and association of GAB1 with SHP2 in response to 10 ng/ml EGF or EGF chased with 1  $\mu$ M gefitinib, dephosphorylation dynamics of EGFR in response to gefitinib, and degradation of EGFR in response to EGF. Parameter fitting was done using simulated annealing to minimize the total error between model output and experimental data. Error was computed as the sum of the squares of the differences between model outputs and the experimental values. The best-fit parameter results are included in Table S4-1.

**Sensitivity analysis.** Model sensitivity to changes in parameters was computed by increasing and decreasing parameter values by a factor of 10. Sensitivity was measured by summing the integrated differences between the original model and the two perturbed outputs over time. To compare differences among parameter perturbations, sensitivities were reported as percentages of the maximum perturbed parameter.

**Representative H1666 cell.** Calculations reflect  $6 \times 10^5$  EGFR per H1666 cell, as noted previously. GRB2, GAB1, SHP2, SFK, and CSK were also assumed to be at cellular concentrations of  $6 \times 10^5$  species per cell, which is within the range of previously reported intracellular protein concentrations [140].

**Model implementation.** Codes were generated and compiled using the Systems Biology Toolbox 2 (SBT2) package for MATLAB [145]. The *simulannealbnd* function in the Global Optimization Toolbox was used to fit the unknown rate constants to experimental data.

**Process timescale calculations.** Various process timescales ( $\tau$ ) were estimated as:

$\tau_{GAB1\_phos} = [(k_{G1p})(aSFK_{max})]^{-1}$ , where  $aSFK_{max}$  is the maximum concentration of active SFKs possible in response to EGF (10 ng/mL).

$$\tau_{GAB1,dephosphorylation} = k_{G1dp}^{-1}$$

$$\tau_{EGFR,phosphorylation} = k_{catE}^{-1}$$

$$\tau_{EGFR,dephosphorylation} = k_{dp}^{-1}$$

$\tau_{SHP2,binding} = [(k_{S2,f})(pGAB1_{max})]^{-1}$ , where  $pGAB1_{max}$  is the maximum concentration of phosphorylated GAB1 possible in response to EGF (10 ng/mL).

$$\tau_{SHP2,dissociation} = k_{S2,r}^{-1}$$

$\tau_{diffusioni} = r^2 / 6D_i$ , where  $r$  is the cell radius, and  $D_i$  is the diffusivity of species  $i$ .

#### 4-4 RESULTS

*In response to EGF, SHP2 remains in complex with GAB1 longer than with EGFR, and GAB1-SHP2 maintenance requires kinase activity to counteract multiple rounds of GAB1 dephosphorylation.* To understand the dynamics of SHP2-containing protein complex assembly in response to EGFR activation, we probed the phosphorylation of EGFR Y1068 and GAB1 Y627 over 120 min in response to 10 ng/mL EGF in SHP2 immunoprecipitates and whole cell lysates from H1666 lung adenocarcinoma cells, a cell line where the importance of SHP2 in driving ERK phosphorylation has been demonstrated [108]. EGFR and GAB1 both associated with SHP2 in response to EGF, but EGFR was lost more quickly than GAB1 from SHP2 immunoprecipitates, an effect that was most visible by western blot at  $t = 120$  min and which suggests a change in the stoichiometry of SHP2 complex assembly over time (Figure 4-1A). In whole cell lysates, we observed measureable amounts of phosphorylated EGFR at  $t = 120$  min (Figure 4-1B), prompting the question of how and why EGFR levels were so clearly reduced in SHP2 immunoprecipitates at 120 min. Similar, but even more pronounced, trends were observed in HeLa cells (Figure S4-8A).

To determine if these findings were related to a potential difference in EGFR and GAB1 dephosphorylation rates, we measured phosphorylated EGFR and GAB1 levels in EGF-treated cells chased with 1  $\mu$ M gefitinib, an EGFR kinase inhibitor. In response to gefitinib, EGFR dephosphorylation occurred within about 1 min, similar to the rate we previously observed in HeLa cells [63]. GAB1 dephosphorylation proceeded slightly more slowly, but the dephosphorylation timescale was one to two min for both proteins (Figures 4-1C and S4-8B), which is significantly shorter than the timescale with which

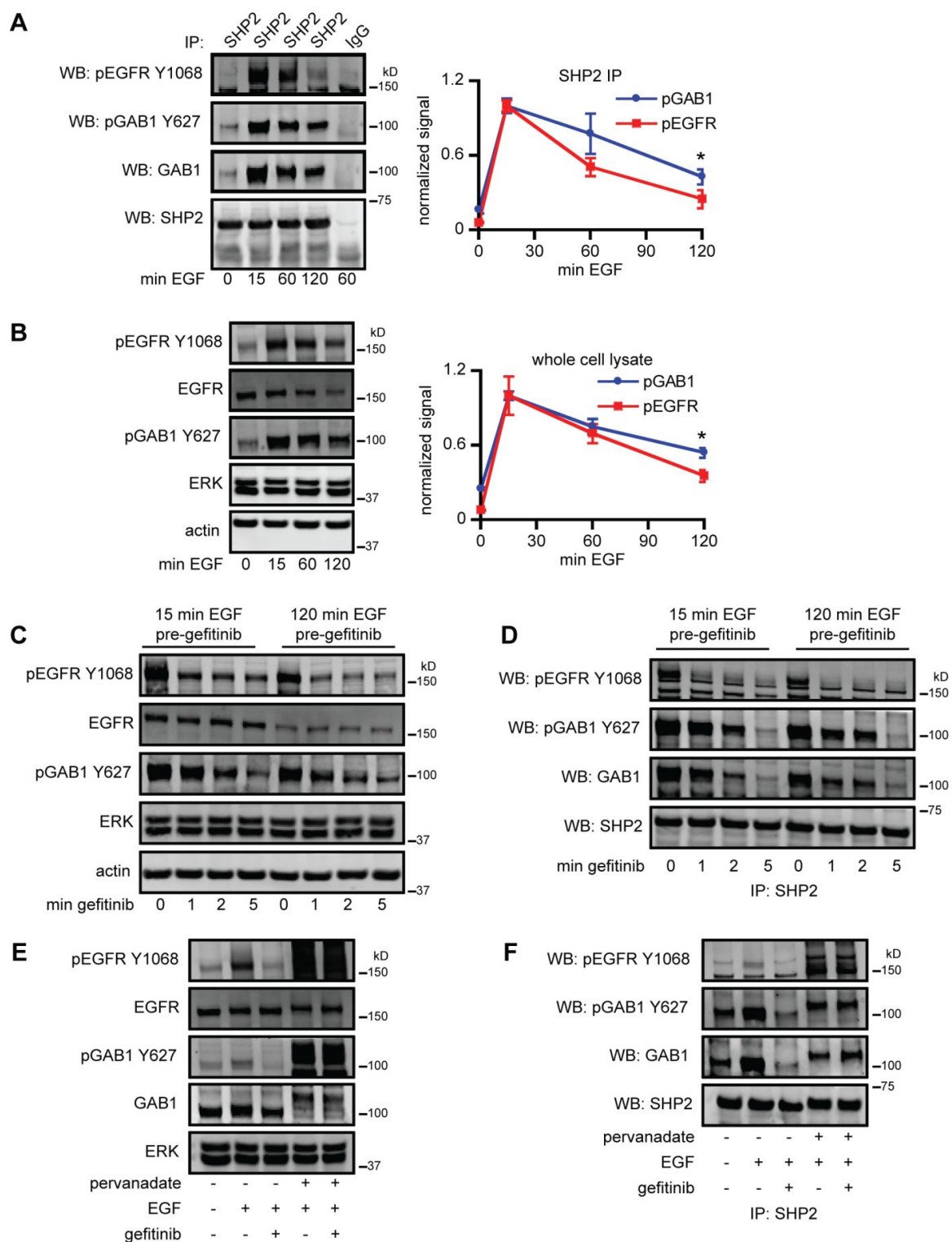


**Figure 4-1: Timescales of protein dephosphorylation and signaling complex disassembly.**

H1666 cells were treated with 10 ng/mL EGF for up to 120 min, and SHP2 immunoprecipitates (**A**) or whole cell lysates (**B**) were analyzed by western blotting with antibodies against the indicated proteins. (**C** and **D**) H1666 cells were treated with 10 ng/mL EGF for 15 or 120 min prior to a 1  $\mu$ M gefitinib chase for up to 5 min. Whole cell lysates and SHP2 immunoprecipitates were analyzed by western blotting with antibodies against the indicated proteins. (**E** and **F**) H1666 cells were treated with 10 ng/ml EGF for up to 15 min, with or without 100  $\mu$ M pervanadate, followed by a 1  $\mu$ M gefitinib chase for 5 min. Whole cell lysates and SHP2 immunoprecipitates were analyzed by western blotting with antibodies against the indicated proteins. Throughout the figure panels, blot signals for phosphorylated GAB1 were quantified and normalized by ERK signal (whole cell lysates) or SHP2 signal (SHP2 immunoprecipitates). All blot images are representative of three sets of biological replicates, and densitometry data are represented as mean  $\pm$  s.e.m. ( $n = 3$ ); \* denotes  $p < 0.05$  when comparing normalized pGAB1 signals to pEGFR signals at a given time point.

SHP2 appears to stay in complex with GAB1 even without EGFR in the complex. We also noted that GAB1 remained associated with SHP2 for several min following gefitinib treatment, at times when EGFR was no longer present in the immunoprecipitated complex (Figures 4-1D and S4-8C). Using pervanadate as a PTP inhibitor, we also demonstrated that PTP inhibition resulted in EGFR and GAB1 phosphorylation and EGFR-SHP2 and GAB1-SHP2 associations that were insensitive to EGFR inhibition (Figures 4-1E-F). The apparent decreased expression and electrophoretic mobility of GAB1 with pervanadate treatment have been reported in cells displaying elevated GAB1 phosphorylation [52, 90].

The results shown thus far demonstrate the need for multiple rounds of GAB1 re-phosphorylation to counteract the effects of PTPs in the maintenance of GAB1-SHP2 complexes over hours of EGF-mediated signaling. The fact that GAB1 can remain in

complex with SHP2 in the absence of EGFR, with GAB1 undergoing many rounds of dephosphorylation during the time of the maintenance of the complex, may suggest that kinases other than EGFR may be responsible for playing this re-phosphorylation role.

***SRC family kinases are required for EGFR-initiated GAB1 phosphorylation and maintenance of GAB1-SHP2 association.*** In COS7 cells, SRC family kinases (SFKs) play a major role in EGF-mediated GAB1 total tyrosine phosphorylation [52, 66]. We thus explored the possibility that SFKs play a role in maintaining GAB1 Y627 phosphorylation and GAB1-SHP2 association in response to EGF. We used H1666 cells with stable knockdown of endogenous EGFR and EGFR<sup>Y845F</sup> reconstitution to decouple SFK activity from regulation of EGFR activity, which arises through SRC's ability to phosphorylate EGFR Y845 [146]. Pretreating cells with the SFK inhibitor PP2 prior to EGF treatment did not affect EGFR phosphorylation, but it greatly reduced GAB1 phosphorylation and GAB1 binding to SHP2 (Figure 4-2A-B). We note that some pEGFR immunoprecipitated with SHP2 with PP2 treatment, but the amount was reduced relative to that found without PP2 and also dissociated from SHP2 with similar kinetics (Figure S4-9A). We interpret this result, which we discuss in further detail later, to indicate that some fraction of SHP2 associated with EGFR in a GAB1-independent manner, perhaps through direct SHP2-EGFR interaction. Chasing EGF-treated cells with PP2 also greatly reduced GAB1-SHP2 association (Figures 4-2C and S4-9B-C). In 293T cells expressing constitutively active SRC<sup>Y527F</sup>, GAB1 was constitutively phosphorylated

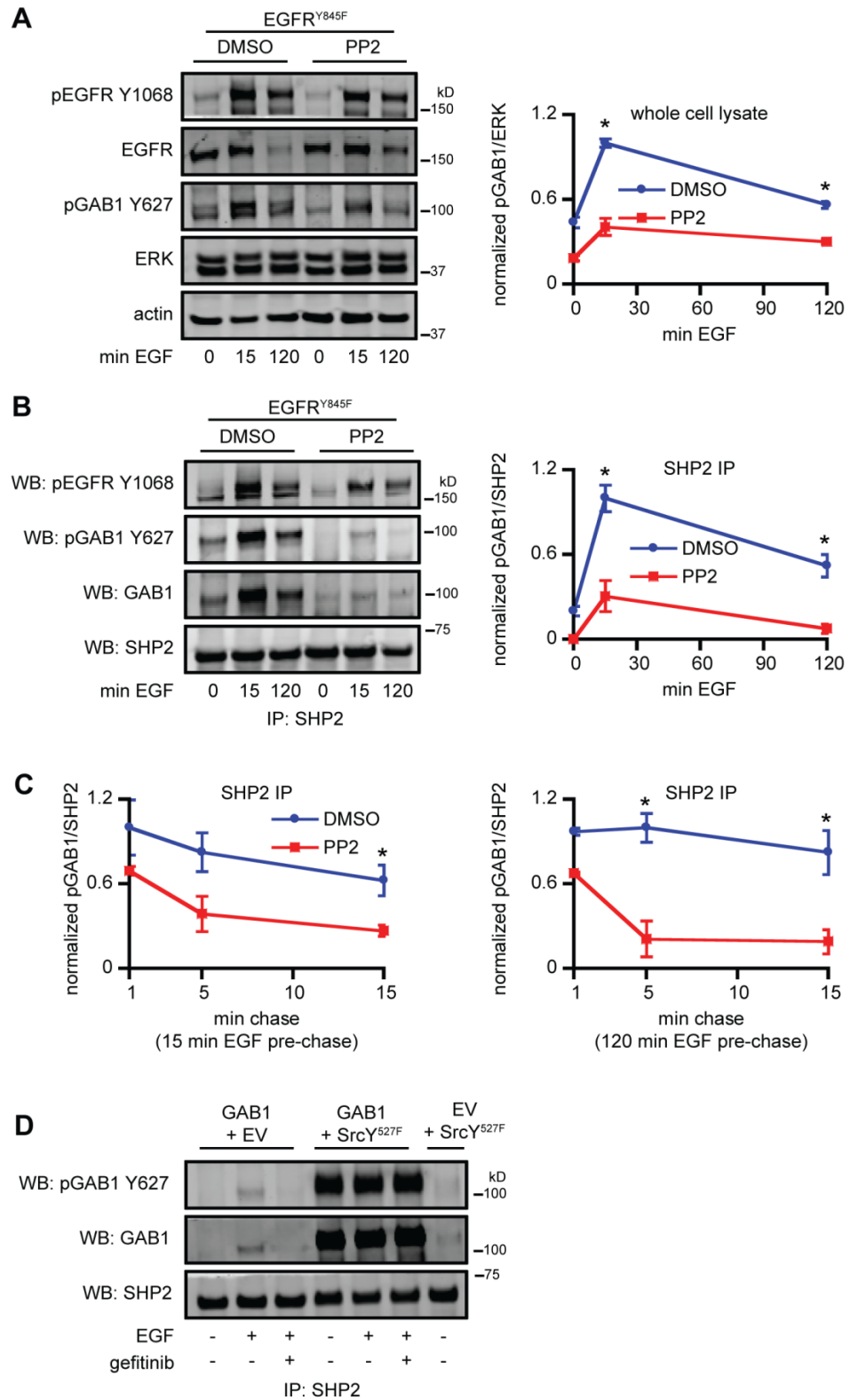


**Figure 4-2: Requirement of SFKs for EGF-initiated GAB1 phosphorylation and GAB1-SHP2 binding.**

(**A**, **B**, and **C**) H1666 cells with knockdown of endogenous EGFR and reconstitution with EGFR<sup>Y845F</sup> were pretreated with DMSO or 10  $\mu$ M PP2 for 30 min and subsequently treated with 10 ng/mL EGF for up to 120 min and lysed, or treated with 10 ng/mL EGF for up to 120 min and subsequently chased with DMSO or 10  $\mu$ M PP2 for up to 15 min prior to lysing cells. Whole cell lysates and SHP2 immunoprecipitates were analyzed by western blotting. Blot signals for phosphorylated GAB1 were quantified and normalized by ERK signal (whole cell lysate) or SHP2 signal (SHP2 immunoprecipitate). \* denotes  $p < 0.05$  when comparing normalized pGAB1 signals from DMSO-treated cells to signals from PP2-treated cells at a given time point. (**D**) 293T cells transiently expressing either: 1) GAB1 and p3xFlag empty vector (EV); 2) GAB1 and SRC<sup>Y527F</sup>; 3) pcDNA3 empty vector (EV) and SRC<sup>Y527F</sup>, were treated with 10 ng/mL EGF for 15 min and subsequently chased with 1  $\mu$ M gefitinib for 5 min prior to lysing cells. SHP2 immunoprecipitates were analyzed by western blotting with antibodies against the indicated proteins. Throughout the figure panels, all blot images are representative of three sets of biological replicates, and densitometry data are represented as mean  $\pm$  s.e.m. ( $n = 3$ ).

and constitutively associated with SHP2 in the absence of EGF and in the presence of gefitinib (Figures 4-2D and S4-9D). However, expression of dominant negative SRC<sup>K295R/Y527F</sup> did not impair GAB1 phosphorylation (Figure S4-9E), consistent with findings that SRC, YES, and FYN, the only three ubiquitously expressed SFK members [147], can compensate for one another [141]. Combined with the fact that the antibody used here detects SRC, FYN, and YES, these data create ambiguity regarding the specific SFK member that is primarily responsible for GAB1 phosphorylation. Accordingly, we will refer to SFKs as the intermediary species driving GAB1 phosphorylation henceforth.

***GAB1-SHP2 complexes exist mainly in the cytosol.*** The fact that GAB1-SHP2 complexes lacking EGFR can exist suggests, but does not guarantee, that GAB1-SHP2

complexes could be present in the cytosol. When we performed subcellular fractionation, essentially all EGF-induced GAB1-SHP2 complexes were found in the cytosolic fraction,

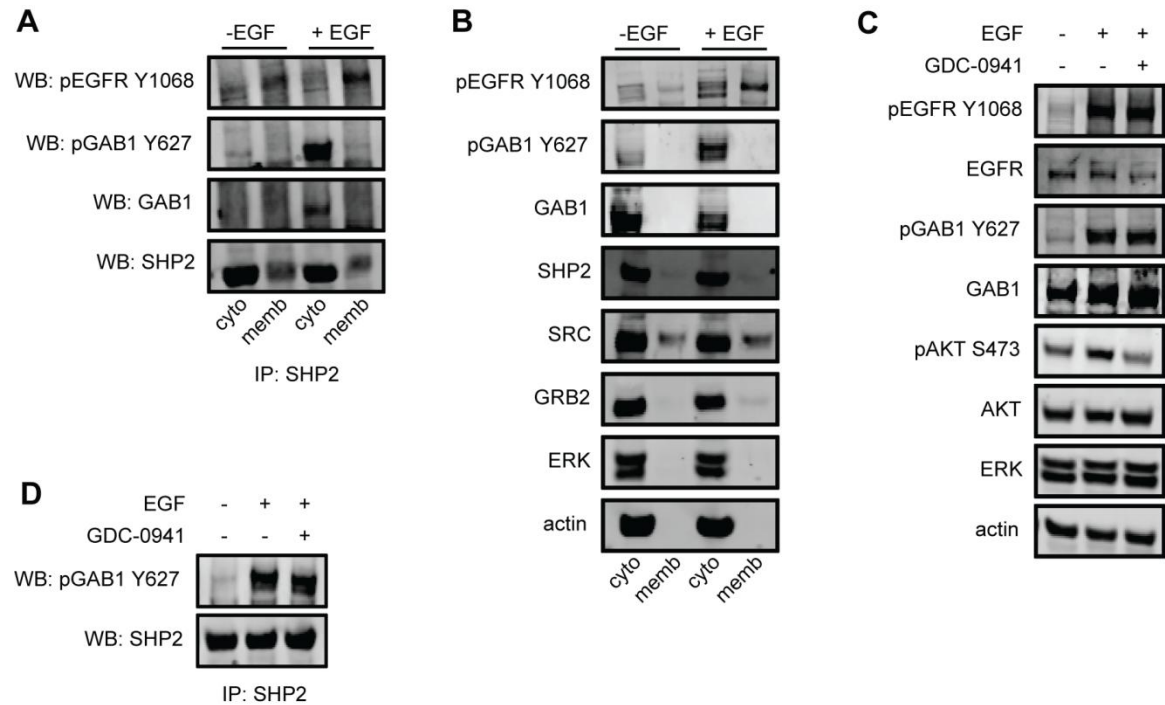


**Figure 4-3: Subcellular localization of GAB1-SHP2 complexes.**

(A and B) Membrane and cytosolic fractions were prepared from H1666 cells treated with or without 10 ng/mL EGF for 15 min. SHP2 immunoprecipitates (A) or whole cell lysates (B) were analyzed by Western blotting with antibodies against the indicated proteins. (C and D) H1666 cells were pretreated with DMSO or 0.5  $\mu$ M GDC-0941 for 30 min and subsequently treated with 10 ng/mL EGF for 15 min and lysed. Whole cell lysates (C) or SHP2 immunoprecipitates (D) were analyzed by western blotting with antibodies against the indicated proteins. All blot images are representative of three sets of biological replicates.

whereas essentially all SHP2 complexes containing EGFR were located in the membrane fraction (Figure 4-3A). While some reports suggest that SFKs are mainly located in the membrane due to myristoylation [148] and that a significant amount of GRB2 may be associated with EGFR in response to EGFR activation [149, 150], we also note that the

majority of SFKs and GRB2 were located in the cytosol, suggesting that SFKs can regulate GAB1 phosphorylation in the cytosol and that GRB2-GAB1-SHP2 (and GAB1-SHP2) complexes can exist there (Figure 4-3B). The presence of non-specific protein bands prevented the unequivocal detection of GRB2 in SHP2 immunoprecipitate western blots, but we assume GRB2 was present in at least some fraction of GAB1-SHP2 complexes due to the nature of the interaction between GRB2 and GAB1. Since the PI3K-dependent recruitment of GAB1 to the plasma membrane is essential for GAB1's function in some cell settings [130], we also probed the effect of PI3K inhibition on GAB1-SHP2 complexes, even though we did not detect a significant amount of GAB1 in membrane fractions. In H1666 cells treated with the PI3K inhibitor GDC-0941, EGF-mediated AKT S473 phosphorylation was inhibited but GAB1-SHP2 association was not impaired (Figure 4-3C-D).

*EGF and HGF promote different dynamics of GAB1-SHP2 complex persistence.* In some cell systems, GAB1 phosphorylation and GAB1-SHP2 association are sustained longer in response to HGF than EGF. This has been proposed as an explanation for HGF's ability to promote more sustained ERK phosphorylation in these cell systems [89, 129], but the mechanistic details by which c-MET and EGFR promote GAB1-SHP2 association for different time scales have not been fully explored. To compare GAB1-SHP2 association in response to EGF or HGF on a fair basis, we used equivalent dissociation constant-normalized concentrations of the ligands (38 or 50 ng/mL for EGF or HGF, respectively) [151, 152]. In H1666 cells, HGF promoted a lower but more persistent GAB1-SHP2 association than EGF, and c-MET remained in complex with SHP2 throughout the duration of GAB1-SHP2 binding (Figures 4-4A and S4-10A).

This may have occurred because c-MET phosphorylation was more persistent and the total protein level was more stable compared to EGFR (Figures 4-4B and S4-10B).

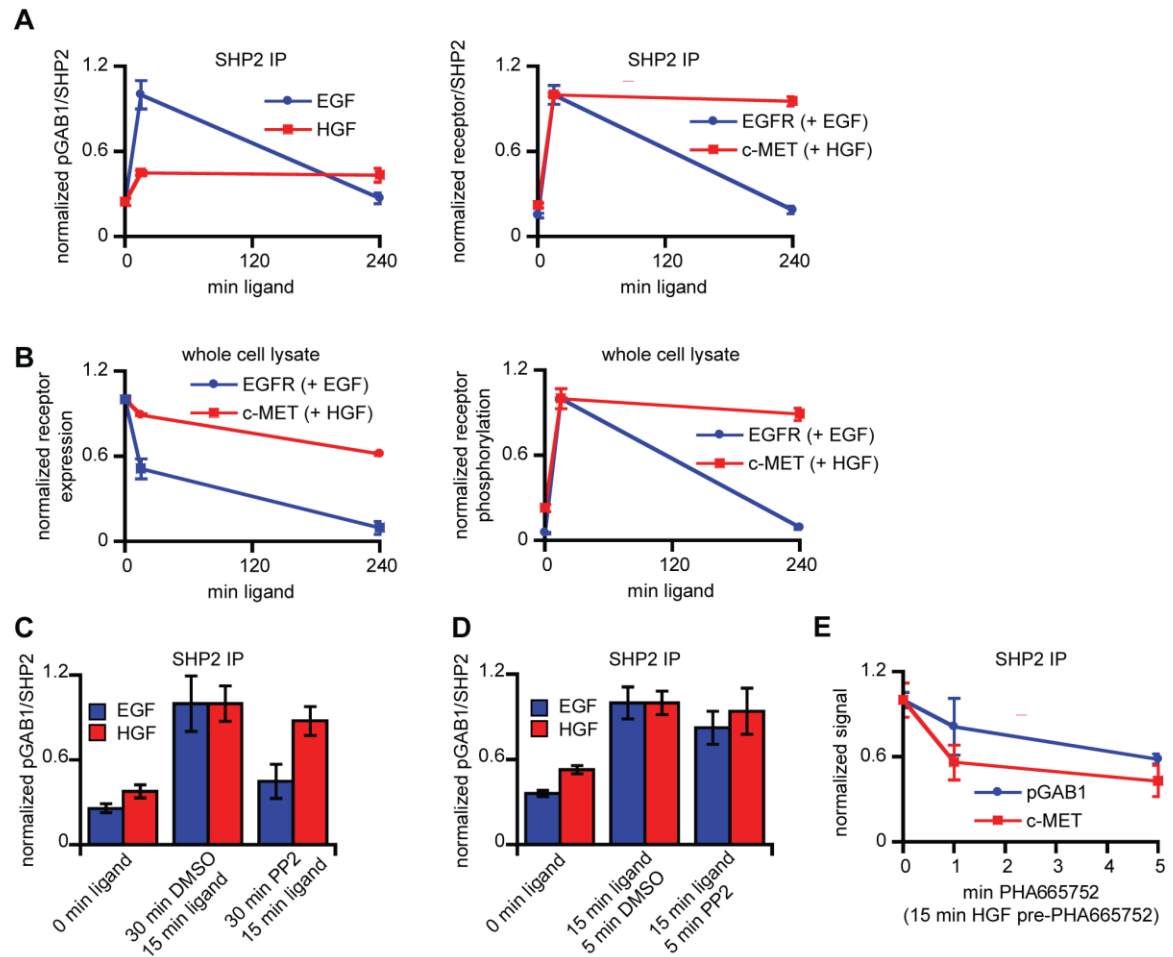


**Figure 4-4: Sustained association of GAB1 and SHP2 downstream of c-MET.**

H1666 cells were treated with 38 ng/mL EGF or 50 ng/mL HGF for up to 240 min, and SHP2 immunoprecipitates (**A**) or whole cell lysates (**B**) were analyzed by western blotting. Blot signals for MET, phospho-EGFR, and phospho-GAB1 were quantified and normalized by SHP2 signal (SHP2 immunoprecipitate loading control) for (**A**) and ERK signal (whole cell lysate loading control) for (**B**). (**C**) Cells were pretreated with DMSO or 10  $\mu$ M of the SFK inhibitor PP2 for 30 min and subsequently treated with HGF or EGF for 15 min and lysed, or treated with HGF or EGF for 15 min and subsequently chased with DMSO or 10  $\mu$ M PP2 for 5 min prior to lysing cells (**D**). SHP2 immunoprecipitates were analyzed by western blotting. Blot signals for c-MET and

phosphorylated GAB1 were quantified and normalized by SHP2 signal. (E) Cells were treated with HGF for 15 min and subsequently chased with 1  $\mu$ M PHA665752 for up to 5 min prior to lysing cells. SHP2 immunoprecipitates were analyzed by western blotting. Blot signals for c-MET and phosphorylated GAB1 were quantified and normalized by SHP2 signal (loading control). Throughout the figure panels, densitometry data are represented as mean  $\pm$  s.e.m. ( $n = 3$ ).

Although SFKs can be activated by c-MET [153], pretreating cells with PP2 prior to HGF addition or chasing HGF-treated cells with PP2 did not significantly reduce GAB1-SHP2 association, suggesting that a kinase other than a SFK (possibly c-MET itself) regulates GAB1 phosphorylation in response to HGF (Figures 4-4C-D and S4-10C-D). We note that the smaller effect of PP2 on EGF-mediated GAB1-SHP2 association observed in Figure 4-4 compared to that observed in Figure 4-2 is probably due to the larger EGF concentration used in Figure 4-4. Similar to observations with EGF treatments and gefitinib chases, GAB1-SHP2 association was prolonged relative to c-MET-SHP2 association in cells treated with HGF and chased with the c-MET inhibitor PHA665752 (Figures 4-4E and S4-10D).

***A computational model reveals that SFKs amplify EGFR activity to maintain GAB1-SHP2 complexes distal from EGFR.*** To quantitatively explore the relationships between EGFR and GAB1 phosphorylation, SFK activity, and GAB1-SHP2 binding, we developed a computational mechanistic model of GAB1-SHP2 complex dynamics that includes the processes of protein phosphorylation and dephosphorylation and reversible protein binding for the complexes shown in Figure 4-5A. Model development details are provided in *Materials and Methods* (Section 4-3). Most parameters were taken from the literature, as indicated in Table S4-1. Importantly, four key rate constants were

determined through fitting. The rate constant for EGFR dephosphorylation ( $k_{dp}$ ) was fit to the decrease in pEGFR levels throughout the course of a 5 min gefitinib treatment (Figure

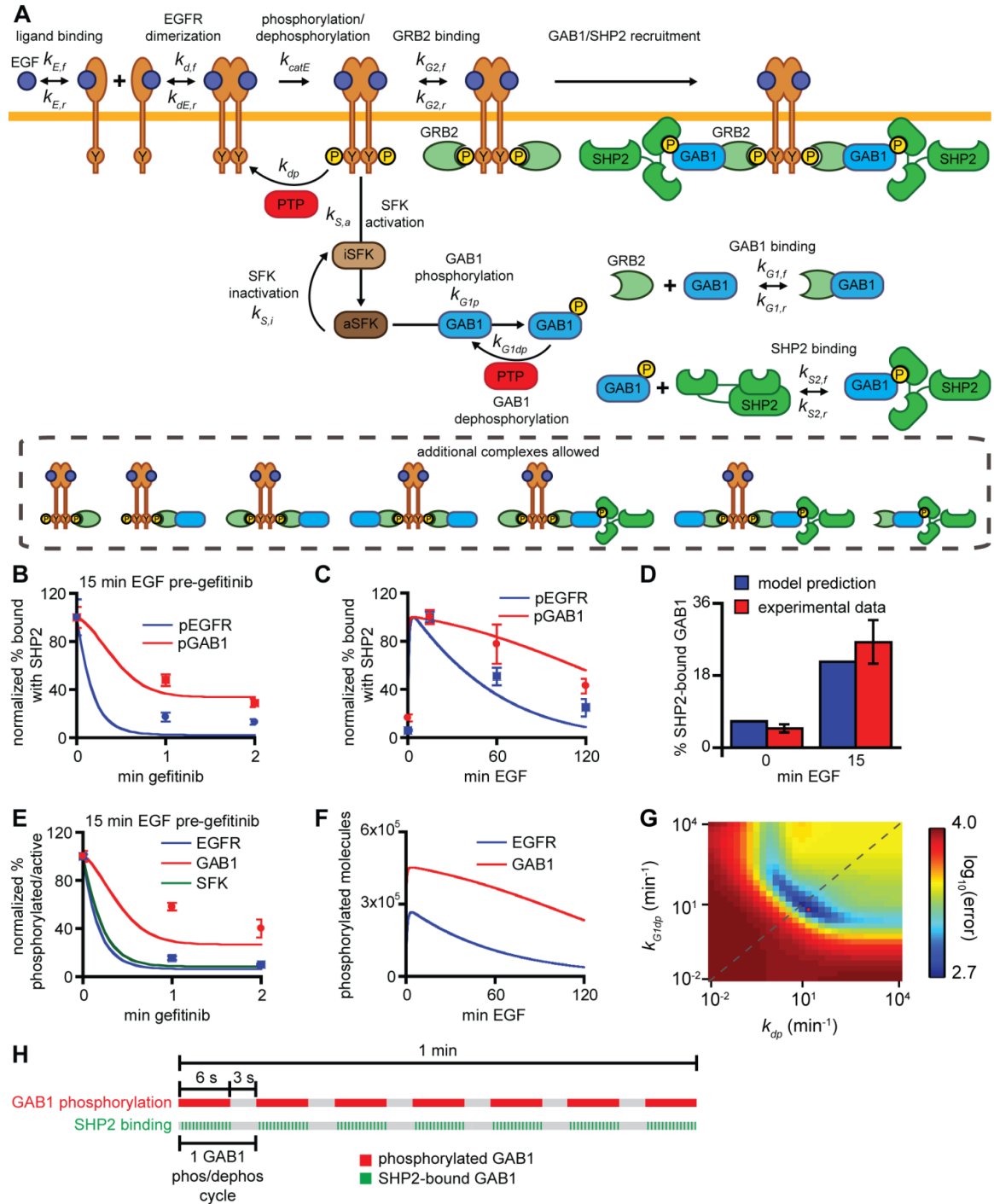


**Figure 4-5: Model topology and validation.**

(A) The model topology includes the depicted processes leading to EGFR and SFK phosphorylation and activation, respectively, as well as all allowed protein complexes which can exist with EGFR monomers (not shown) and dimers (shown). Model predictions for EGFR-SHP2 and GAB1-SHP2 association (lines) were compared to experimental data (points) from: (B) an EGF-pulse gefitinib-chase experiment and (C) an EGF stimulation time course. (D) H1666 cells were treated with 10 ng/mL EGF for 15 min, and lysates were immunoprecipitated with SHP2 antibody. Percent SHP2-bound GAB1 was determined for experimental data by first calculating the percent of GAB1 unbound with SHP2, which was calculated by dividing the normalized GAB1 signal in the SHP2 immunoprecipitate supernatant by that of the GAB1 signal in whole cell lysates. This value was subtracted from 100% to calculate percent SHP2-bound GAB1, which was then compared to the model prediction for percent SHP2-bound GAB1 in response to 15 min EGF. (E) Model predictions for normalized levels of phosphorylated EGFR and GAB1 and active SFK following a gefitinib chase were calculated. (F) Model predictions for the number of EGFR and GAB1 molecules phosphorylated throughout a 120 min EGF treatment were calculated. (G) Model error was calculated for ranges of  $k_{dp}$  and  $k_{G1dp}$ . Red circle indicates error minimum. (H) Based on rapid forward and reverse cycling of several cellular components leading to GAB1-SHP2 binding, the picture which emerges is that phosphorylation and binding events leading to SHP2 activation are exceedingly transient, rather than static.

S4-11A). The rate constants for GAB1 phosphorylation ( $k_{G1p}$ ) and dephosphorylation ( $k_{G1dp}$ ) were fit to the response of GAB1 Y627 phosphorylation and GAB1-SHP2 association to both long and short EGF treatments (Figures 4-1A-B and S4-11B) and an EGF-gefitinib pulse-chase experiment (Figures 4-1C-D). The rate constant for EGFR degradation ( $k_{deg}$ ), a process needed to allow pEGFR and pGAB1 levels to decrease with time (Figure S4-11C) because we assume a constant activity level of protein tyrosine

phosphatases, was fit to the response of EGFR levels over the course of a 2 hrs EGF treatment (Figure 4-1B).

Before proceeding, we note that the previously mentioned GAB1-independent mechanism of SHP2-EGFR association is not accounted for in our model topology. However, this omission should not affect model conclusions since our parameter fits do not rely upon EGFR-SHP2 association data. Moreover, since our data suggest EGFR and SHP2 dissociate immediately following a gefitinib chase (Figure 4-1D), and since GAB1-dependent and -independent EGFR-SHP2 complexes dissociate with similar kinetics over the course of a 2 hrs EGF treatment (Figure S4-9A), our model predictions for relative abundances of EGFR-SHP2 and GAB1-SHP2 complexes would be unchanged even if model fits did account for EGFR-SHP2 association data. We also note that approximately half of EGFR-SHP2 complexes are dependent on SFK activity and thus likely GAB1-dependent (Figure 4-2B). Therefore, the capacity for GAB1 to recruit SHP2 to EGFR is an important mechanism of EGFR-SHP2 complex formation and a valid inclusion for our model topology.

The parameterized model recapitulates differences in the rates of EGFR-SHP2 and GAB1-SHP2 dissociation following a gefitinib chase (Figure 4-5B). While both EGFR-SHP2 and GAB1-SHP2 complexes return to basal levels after 1-2 min of gefitinib treatment, EGFR-SHP2 complexes fall to 50% of their peak concentration approximately 5 times faster than do GAB1-SHP2 complexes. The model also accurately predicts differences in the relative abundances of EGFR-SHP2 and GAB1-SHP2 complexes over a 120 min EGF treatment time course (Figure 4-5C). The model further predicts that 22% of GAB1 was bound with SHP2 15 min after treatment with EGF, which is in line with

an experimental measurement of  $26 \pm 5\%$  (Figures 4-5D and S4-11D). Finally, the model predicts that even at peak levels of EGFR phosphorylation, only 1.5% of SHP2 exists in complex with EGFR (Figure S4-11E), which is qualitatively consistent with our experimental findings of SHP2 and GAB1-SHP2 complexes existing almost exclusively in the cytosol (Figures 4-3A-B).

Interestingly, the fitted rate constant for GAB1 dephosphorylation ( $k_{G1dp}$ ) is similar in magnitude to that for EGFR dephosphorylation ( $k_{dp}$ ), with each implying a dephosphorylation timescale of  $\sim 0.1$  min, despite a GAB1 dephosphorylation rate in cells that is smaller than the rate of EGFR dephosphorylation following a gefitinib chase (Table S4-1, Figure 4-1B, and Figure 4-5E). This apparent contradiction is explained by a time lag between the reductions in EGFR and GAB1 phosphorylation rates following gefitinib addition (Figure S4-11F), which arises because SFK inactivation, which is tied to EGFR phosphorylation, does not occur instantaneously after EGFR inactivation (Figure 4-5E). If SFKs are instead assumed to deactivate instantaneously upon EGFR inactivation, the rates of EGFR and GAB1 dephosphorylation are nearly identical, with GAB1 actually being slightly faster because of a difference in dephosphorylation rate constants (Figure S4-11G). Beyond this time lag in SFK inactivation, the difference in cellular EGFR and GAB1 dephosphorylation rates is exacerbated by an SFK-mediated amplification process that occurs in the parameterized model and generally produces a larger concentration of phosphorylated GAB1 (pGAB1) than pEGFR at any time, as can be seen in predictions of absolute phosphorylated levels of EGFR and GAB1 in response to EGF (Figure 4-5F). This amplification occurs as a combined result of a smaller timescale for the GAB1 phosphorylation step ( $\sim 3$  s) than for EGFR phosphorylation ( $\sim 4.5$  s) and as a result of the

relative slowness of other process steps leading to EGFR phosphorylation, including ligand binding and EGFR dimerization (Figure S4-11H). When parameter values are adjusted to remove this amplification process from the model, the difference between EGFR and GAB1 dephosphorylation rates is reduced, but not eliminated because of the time lag for SFK inactivation (Figure S4-11G).

Plotting the model error for a range of  $k_{G1dp}$  and  $k_{dp}$  values provides additional insight into the system's behavior (Figure 4-5G). While the error minimum is achieved for  $k_{G1dp}$  and  $k_{dp}$  of similar magnitudes, a relatively low model error is still achieved if one rate constant is increased and the other is decreased by up to an order of magnitude. Model error significantly increases when either rate constant is changed by more than an order of magnitude from its best-fit value. Thus, there is some capacity to explain the data by speeding one dephosphorylation process and slowing the other, but both rate processes must be fairly rapid to explain the experimental data reasonably.

Returning to the values of our fitted parameters for GAB1 phosphorylation and dephosphorylation and making some order of magnitude estimates, we note that the parameters suggest that when phosphorylation/dephosphorylation reaction rates are maximized, GAB1 Y627 undergoes ~6 cycles of dephosphorylation and re-phosphorylation per minute in response to EGF (Figure 4-5H), based on characteristic GAB1 phosphorylation and dephosphorylation times (see *Materials and Methods*). SHP2 cycles between GAB1-bound and -unbound states ~14 times during the time that GAB1 is phosphorylated in each GAB1 cycle, or ~100 times per minute at maximal rates.

***Robustness and sensitivity analyses confirm the need for an SFK-mediated amplification mechanism and reveal key processes controlling system behavior. To***

further explore model predictions surrounding the need for the amplification process that produces pGAB1/pEGFR ratios greater than one, we undertook two types of robustness analyses. Since we had no direct quantitative data available for the cellular

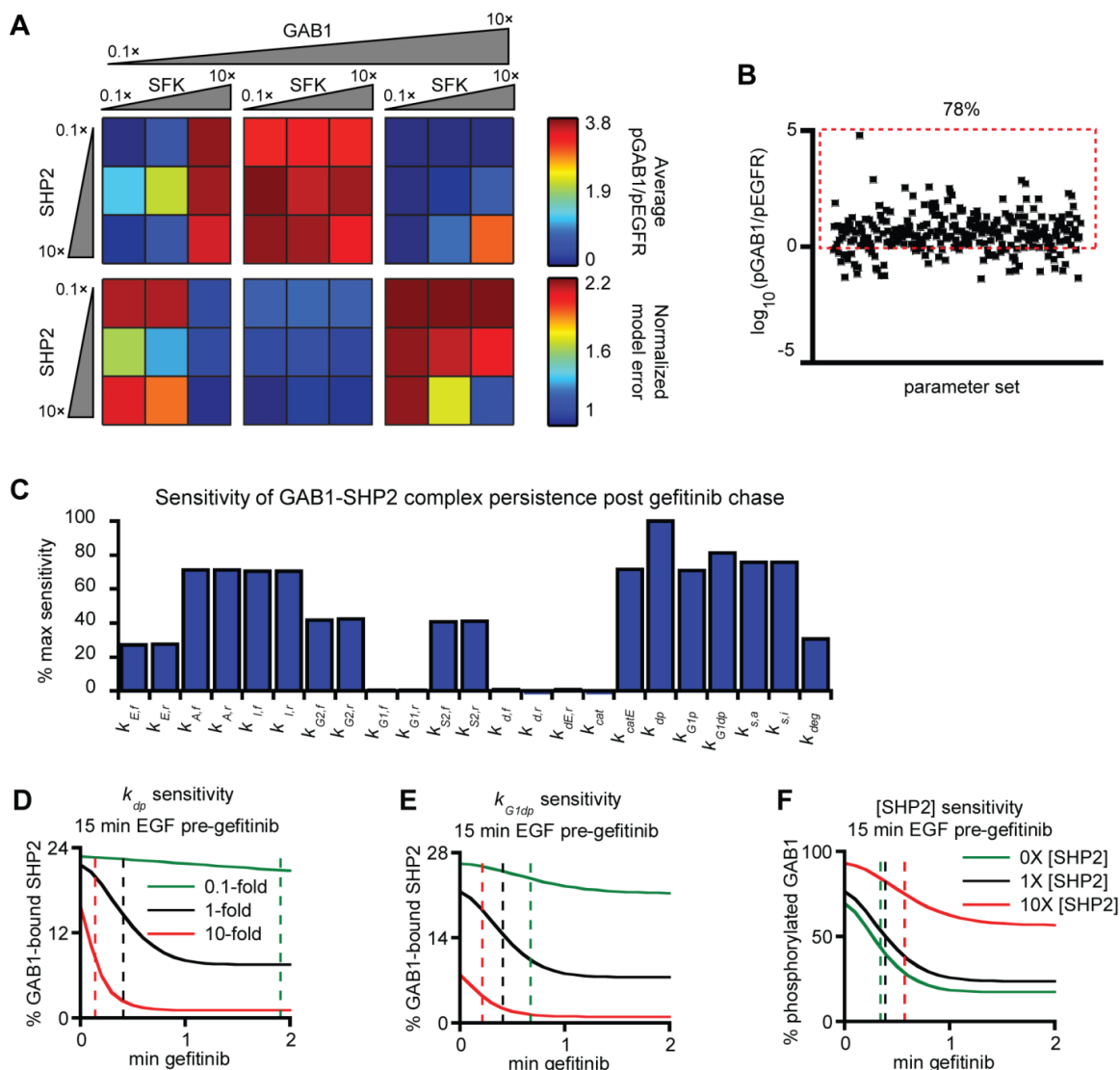


**Figure 4-6: Model requirement for SFK-mediated amplification of EGFR and model sensitivity.**

(A) A metric for the degree of amplified EGFR signal, pGAB1/pEGFR, and model error were calculated for 10-fold combinatorial variations in GAB1, SHP2, and SFK concentrations. (B) Model predictions for pGAB1/pEGFR were calculated for 300 random parameter sets, where each parameter was randomly varied up to an order of

magnitude above or below its base value. (C) Sensitivity of model predictions for time-integrated GAB1-SHP2 association for a 5 min, 1  $\mu$ M gefitinib-chase (preceded by a 15 min, 10 ng/mL EGF-pulse) to 10-fold changes in the model parameters was calculated. (D and E) Model predictions for the percent of GAB1-bound SHP2 following a gefitinib chase were compared with predictions when  $k_{dp}$  and  $k_{G1dp}$  were varied by a factor of 10. Representative times for GAB1-SHP2 dissociation (*dashed lines*) were calculated by determining the time at which 50% of dissociation had occurred relative to maximum and minimum values. (F) Model predictions for percent phosphorylated GAB1 and representative GAB1 dephosphorylation times following a gefitinib chase were calculated when SHP2 concentration was increased by a factor of ten or set to zero. Representative times for GAB1 dephosphorylation (*dashed lines*) were calculated by determining the time at which 50% of dephosphorylation had occurred relative to maximum and minimum values.

concentrations of GAB1, SHP2, and SFKs, we checked if our assumption of equivalent expression levels of these proteins could somehow be responsible for the model's identification of a need for the SFK-mediated amplification mechanism. For a range of GAB1, SHP2, and SFK concentrations, we refit the model and calculated errors and an average pGAB1/pEGFR ratio, a metric for amplification of EGFR's activity through SFKs. Across all combinations of concentrations tested, the smallest model errors were associated with amplification ( $\text{pGAB1/pEGFR} > 1$ ) (Figure 4-6A). We further tested the robustness of our model's prediction of SFK-mediated amplification by creating random parameter sets, where each parameter was randomly perturbed by up to an order of magnitude above or below its base value. For 78% of the parameter sets (234/300), pGAB1/pEGFR was greater than unity (Figure 4-6B). Therefore, even if the base model parameters are not well estimated, the model prediction of amplification of EGFR's signal by SFKs appears robust.

To further understand the processes that control amplification and its effects, we performed a parameter sensitivity analysis to identify processes controlling the persistence of GAB1-SHP2 complexes following a gefitinib chase (preceded by an EGF pulse), since complex persistence is augmented by the amplification processes, as we have already discussed. GAB1-SHP2 persistence had a strong dependence on a number of model parameters, but  $k_{dp}$  was chief among these (Figure 4-6C). EGF-gefitinib pulse-chase simulations show that either elevating or decreasing  $k_{dp}$  by an order of magnitude altered both the dynamic and steady state percentage of SHP2 bound by GAB1, as well as the rate at which GAB1-SHP2 dissociation occurred following a gefitinib-chase (Figure 4-6D). Analogous, but smaller, predicted effects were seen when altering  $k_{G1dp}$  (Figure 4-6E). The finding that altering  $k_{dp}$  has a larger effect on GAB1-SHP2 association than altering  $k_{G1dp}$  is further indication of the importance of the amplification of the EGFR signal by SFKs. Not surprisingly, the model was sensitive to perturbations to other parameters that affect EGFR phosphorylation, such as parameters for EGF, ATP, gefitinib, and GRB2 binding, and parameters that affect SFK activity including  $k_{S,a}$  and  $k_{S,i}$ . GAB1-SHP2 association was also sensitive to changes in  $k_{S2,f}$  and  $k_{S2,r}$ .

As others have shown that binding of SH2 domains to phosphotyrosines can protect them from dephosphorylation, as in the case of overexpression of PLC $\gamma$  SH2 domains preventing EGFR tyrosine dephosphorylation [154], we used the model to predict the consequences of SHP2 overexpression or depletion on the dynamics of GAB1 dephosphorylation (Figure 4-6F). Compared to the base model, elevating the cellular concentration of SHP2 by an order of magnitude resulted in little change to the dynamics of GAB1 dephosphorylation, but did produce a roughly two-fold increase in steady state

GAB1 phosphorylation. Conversely, complete removal of SHP2 from the model had relatively no effect on either the dynamics or steady state levels of GAB1 phosphorylation, suggesting that SHP2 offers little protection against GAB1 dephosphorylation at endogenous expression levels. This is due to the rate of SHP2 unbinding from GAB1 being over an order of magnitude faster than GAB1 dephosphorylation, such that GAB1 will generally be accessible to phosphatases unless there is a massive surplus of SHP2.

We went on to explore the potential effects of changes to the model topology motivated by several previously documented findings. Since SHP2 can promote SFK activity for some SFK members by preventing proper localization of c-SRC kinase (CSK) [55, 56], we updated the model to allow for active SHP2, in addition to EGFR, to activate SFKs. Relative to the base model (Figure S4-12A), allowing SHP2 activity to enhance SFK activity resulted in a significant effect on GAB1 phosphorylation (Figure S4-12B), as the rate constant for GAB1 phosphorylation needed to be reduced by several orders of magnitude to counteract the addition of this positive feedback loop. The rate constant for GAB1 dephosphorylation was unchanged with the model extension, as dephosphorylation kinetics were sufficiently rapid such that gefitinib addition still quickly returned GAB1 phosphorylation to basal levels. However, this topological addition did not reduce the minimum model error relative to the base model (Figures S4-12A-B). We also computed model error by adding in a distinct reaction for GAB1 dephosphorylation mediated by SHP2 [132], but this topological addition also did not result in an improved ability for the model to more accurately recapitulate the experimental data despite broadening the error basin (Figure S4-12C).

## 4-5 DISCUSSION

Here, we describe a mechanism in which EGFR drives the persistence of cytosolic GAB1-SHP2 complexes through many cycles of GAB1-SHP2 dissociation and GAB1 dephosphorylation via the ability of SFKs, activated by EGFR, to re-phosphorylate GAB1 repeatedly in a way that effectively amplifies EGFR activity (Figure 4-7). This mechanism may allow EGFR to control signaling processes via SHP2 at intracellular locations where it may not otherwise be able to do so because of EGFR's confinement to the cell surface or endomembrane compartments. Moreover, the amplification aspect of this process may enable a relatively small amount of activated EGFR to exert significant control over signaling events via GAB1-bound and active SHP2.

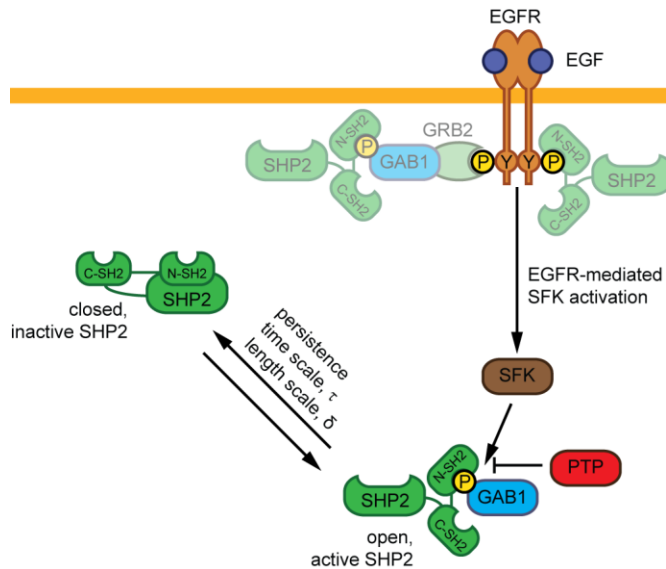


**Figure 4-7: Schematic of EGFR-mediated GAB1-SHP2 complex maintenance.**

Basally, SHP2 activity is suppressed through an intramolecular interaction between SHP2's N-terminal SH2 domain and the catalytic domain. When SHP2 SH2 domains engage tyrosine phosphorylated GAB1, the SHP2 intramolecular tethering is relieved and SHP2 activity increases. EGFR activation appears to promote this process primarily through the intermediary SFKs, which counteract many rounds of GAB1 tyrosine

dephosphorylation to enable GAB1-SHP2 complexes to persist distal from the receptor. With a lower abundance, GAB1-SHP2 complexes may also exist at the membrane in complex with EGFR, and some SHP2 may also engage with EGFR directly in GAB1-independent fashion.

The quantitative insights achieved here were possible because of the application of a mechanistic model in the interpretation of experimental data. In particular, the model provides confidence that an amplification step from EGFR to GAB1 is needed to fully explain the kinetics we measured and that this conclusion is robust even accounting for uncertainty in certain system properties (e.g., quantitative expression levels for certain proteins). The model also enables quantitative estimates of the phosphorylation cycles EGFR and GAB1 undergo in response to EGFR activation. Of course, other EGFR signaling models have been developed, with a few even considering EGFR-induced GAB1-SHP2 association [140, 142, 155]. However, none of those previous models included rigorous consideration of differential compartmentation of GAB1, SHP2, and the GAB1-SHP2 complex, realistic timescales for EGFR and GAB1 dephosphorylation, or the role for intermediary kinases in maintaining GAB1 phosphorylation.

The amplification mechanism described here bears some resemblance to ERK pathway amplification mechanisms wherein one RAF can promote the phosphorylation of a larger number of ERKs [156]. By analogy, our model requires that EGFR-activated SFKs effectively amplify EGFR activity such that stoichiometric ratios of pEGFR/pGAB1 exceed unity in order to explain our data reasonably well. It is worth noting that the model results reveal that there may be several ways to achieve such amplification. For example, SFKs need not be in stoichiometric excess of EGFR or GAB1 to produce an amplification from EGFR to GAB1 (Figure 4-6A), which appears to

be required for reasonable explanation of the data. Within the framework of our model, this is achieved by an increased fitted value of  $k_{Glp}$  permitting a decreased number of SFKs to phosphorylate GAB1 as efficiently as an elevated number of SFKs. Another commonly discussed feature of the ERK cascade is ultrasensitivity, which enables a graded input at the level of RAF to produce a switch-like output at the level of ERK [157]. The mechanism we describe here does not involve an analogous kind of ultrasensitivity. That is, a switch-like GAB1 phosphorylation response to increasing EGF concentration is not predicted by our model.

The specific location within the cell where SFKs phosphorylate GAB1 has important potential implications for how far within the cell GAB1-SHP2 complexes persist. While our results with PI3K inhibition may argue against a need for GAB1 to be membrane bound to be phosphorylated by SFKs, certain lines of evidence argue for SFK activity mainly at the membrane. Indeed, SFKs are typically thought of as membrane-bound species due in part to N-terminal myristoylation. Myristoylation itself may promote SFK activity [148], and some studies do suggest a requirement for SFKs to move to the membrane to become activated [158]. Still, in some cancer cell settings significant SFK fractions are found in the cytosol [159], as found here for H1666 cells, and other studies have demonstrated the presence of activated SFKs in the cytosol [160]. The potential importance of this detail can be further understood through order of magnitude estimates of specific process time scales. Assuming a cell radius of 10  $\mu\text{m}$  [161] and a diffusivity of 0.94  $\mu\text{m}^2/\text{s}$ , based on the diffusivity of tubulin and an adjustment due to estimated hydrodynamic radii of tubulin and the GAB1-SHP2 complex [162, 163], the characteristic time for a GAB1-SHP2 complex to diffuse from the plasma

membrane to the cell center is ~18 s. Comparison of that timescale with the characteristic time for GAB1 dephosphorylation of ~6 s, computed as the inverse of the rate constant for GAB1 dephosphorylation from our model fits, suggests that GAB1-SHP2 complexes formed exclusively at the plasma membrane may not persist over the entire cellular length scale. The ability of SFKs to drive GAB1 phosphorylation in the cytosol would overcome this limitation, potentially increasing SHP2's ability to regulate signaling processes over a larger intracellular length scale.

Of course, the endocytic trafficking of EGFR may also move the most upstream processes in this signaling pathway into the cell interior in ways that could help to overcome diffusional limitations that might otherwise limit GAB1-SHP2 complex access to intracellular locations. Along those lines, it should be noted that the ability of endocytosis-impaired and constitutively active EGFR mutants to sequester SHP2 at the cell periphery appears to antagonize SHP2's ability to participate fully in the activation of ERK [164]. To what extent this functional impairment of SHP2 activity involves a perturbation to the ability of GAB1-SHP2 complexes to exist distal from EGFR mutants remains unclear, but this will be worth pursuing in future studies.

The work presented here may also offer insight into the documented ability of HGF to drive more sustained GAB1 phosphorylation, GAB1-SHP2 association, and ERK activation than EGF [89, 129]. In our experiments, EGF-mediated EGFR activation resulted in relatively rapid degradation of EGFR over the course of an hour (55% degraded; Figure 4-1B), which may diminish GAB1 phosphorylation and GAB1-SHP2 association by reducing the pool of EGFR available to drive SFK activity. By comparison, c-MET degradation following HGF addition occurs quite slowly, which may

explain the more protracted downstream activation of ERK. Differences in the dynamics of HGF- and EGF-mediated ERK activation may also be due to differential recruitment of GAB1 to the cell periphery, given HGF but not EGF addition results in recruitment of GAB1 to the plasma membrane [130]. We also note that while SFKs are required for EGF-mediated GAB1 phosphorylation, our experiments suggest that SFKs are dispensable for GAB1 phosphorylation downstream of c-MET, suggesting there are different modes for RTK-mediated induction of GAB1-SHP2 association.

#### 4-6 ACKNOWLEDGEMENTS

We thank Dr. Daniel Haber, Dr. Marilyn Farquhar, Dr. Gary Nolan, Dr. Sarah Parsons, Dr. Todd Miller, Dr. Chris Chen, and Dr. Toshio Hirano for generously providing reagents. We also thank Alice Walsh and Calixte Monast for technical assistance.

#### 4-7 SUPPLEMENTARY MATERIAL

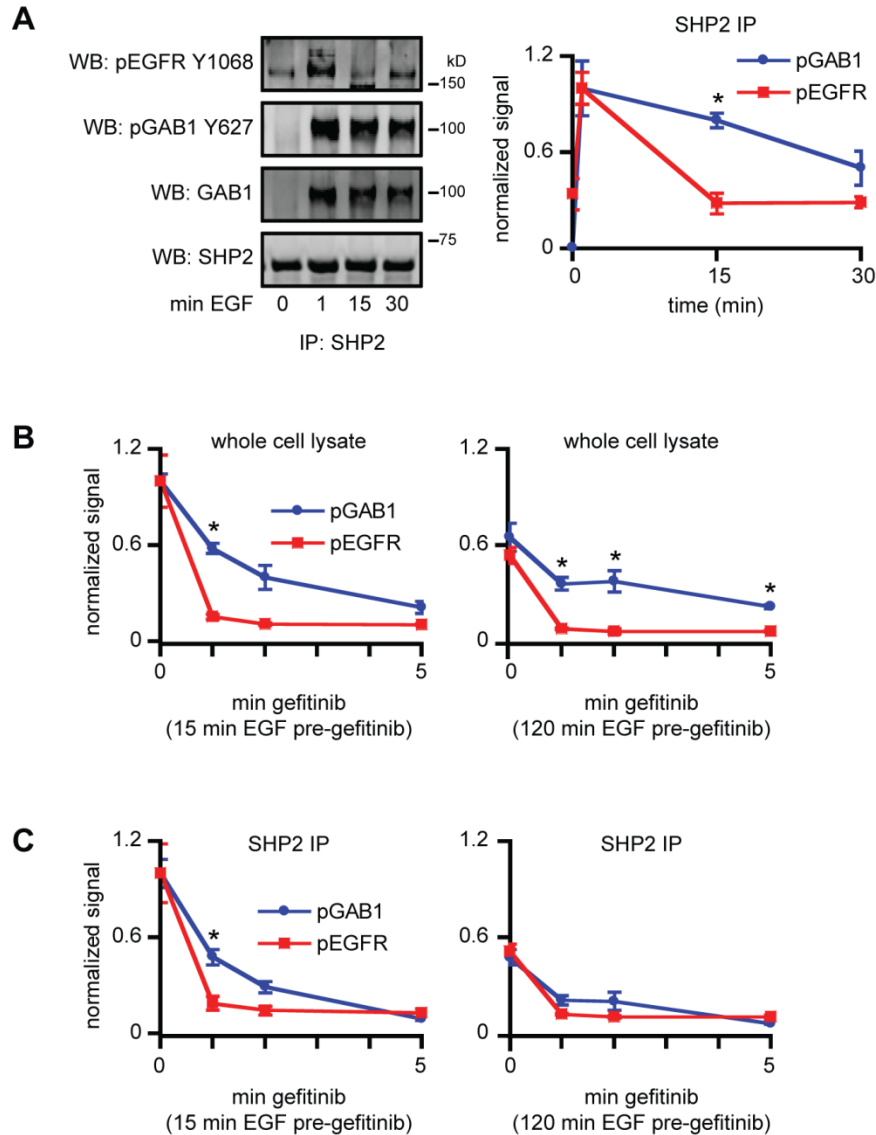


**Figure S4-8: Differential rates of EGFR-SHP2 and GAB1-SHP2 complex disassemblies.**

(A) HeLa cells were treated with 10 ng/mL EGF for up to 30 min, and lysates were immunoprecipitated with SHP2 antibody. Immunoprecipitates were analyzed by western blotting using antibodies against the indicated proteins. Blot signals for phosphorylated EGFR and GAB1 were quantified and normalized by SHP2 signal (loading control). (B and C) H1666 cells were treated with 10 ng/mL EGF for 15 or 120 min, and subsequently chased with 1  $\mu$ M gefitinib for up to 5 min prior to lysing cells. Whole cell lysates (B) and SHP2 immunoprecipitates (C) were analyzed by western blotting, and

blot signals for phosphorylated EGFR and GAB1 were quantified and normalized by ERK signal (whole cell lysate loading control) or SHP2 signal (SHP2 immunoprecipitate loading control). Throughout the figure panels, all blot images are representative of three sets of biological replicates, and densitometry data are represented as mean  $\pm$  s.e.m. ( $n = 3$ ); \* denotes  $p < 0.05$  when comparing normalized pGAB1 signals to pEGFR signals at a given time point.

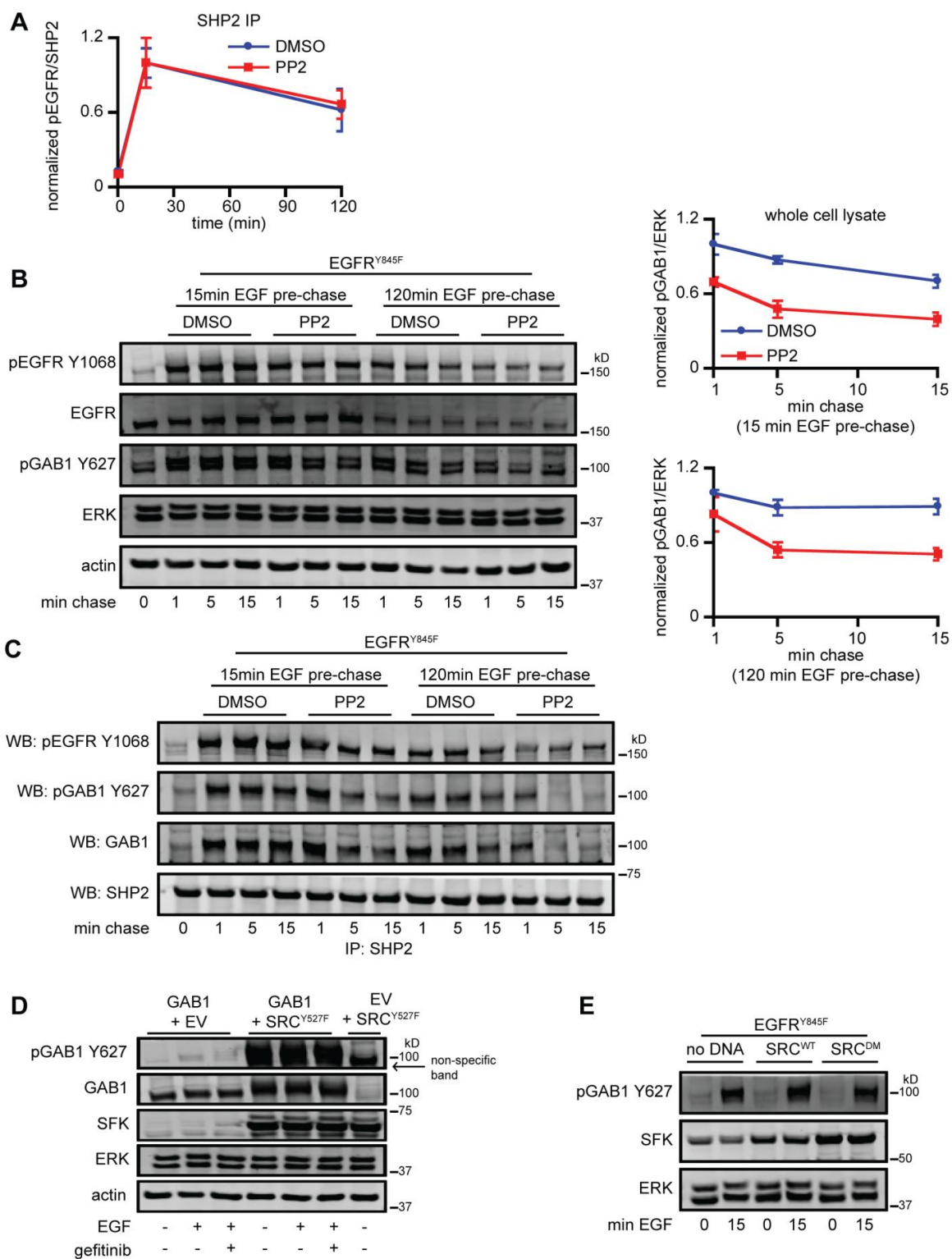


**Figure S4-9: SFK-mediated GAB1 phosphorylation and GAB1-SHP2 binding.**

(A) Blot signals for phosphorylated EGFR from Figure 2B were quantified and normalized by SHP2 signal. In order to compare pEGFR-SHP2 association kinetics with

or without PP2 pretreatment, all data points for each treatment condition were further normalized by their respective maximum pEGFR/SHP2 signal (i.e., pEGFR/SHP2 at 15 min EGF). **(B and C)** H1666 cells with knockdown of endogenous EGFR and reconstitution with EGFR<sup>Y845F</sup> were treated with 10 ng/mL EGF for up to 120 min and subsequently chased with DMSO or 10  $\mu$ M PP2 for up to 15 min prior to lysing cells. Whole cell lysates **(B)** and SHP2 immunoprecipitates **(C)** were analyzed by western blotting with antibodies against the indicated proteins. Blot signals from whole cell lysates for phosphorylated GAB1 were quantified and normalized by ERK signal (loading control). **(D)** 293T cells transiently expressing either: 1) GAB1 and p3xFlag empty vector (EV); 2) GAB1 and SRC<sup>Y527F</sup>; 3) pcDNA3 empty vector (EV) and SRC<sup>Y527F</sup>, were treated with 10 ng/mL EGF for 15 min and subsequently chased with 1  $\mu$ M gefitinib for 5 min prior to lysing cells. Whole cell lysates were analyzed by western blotting with antibodies against the indicated proteins. **(E)** H1666 cells with knockdown of endogenous EGFR and reconstitution with EGFR<sup>Y845F</sup> were transfected with SRC<sup>WT</sup> cDNA, SRC<sup>DM</sup> cDNA (dominant negative SRC<sup>K295R/Y527F</sup>), or no DNA and were treated with or without 10 ng/mL EGF for 15 min. Whole cell lysates were analyzed by western blotting with antibodies against the indicated proteins. Throughout the figure panels, all blot images are representative of three sets of biological replicates, and densitometry data are represented as mean  $\pm$  s.e.m. ( $n = 3$ ).

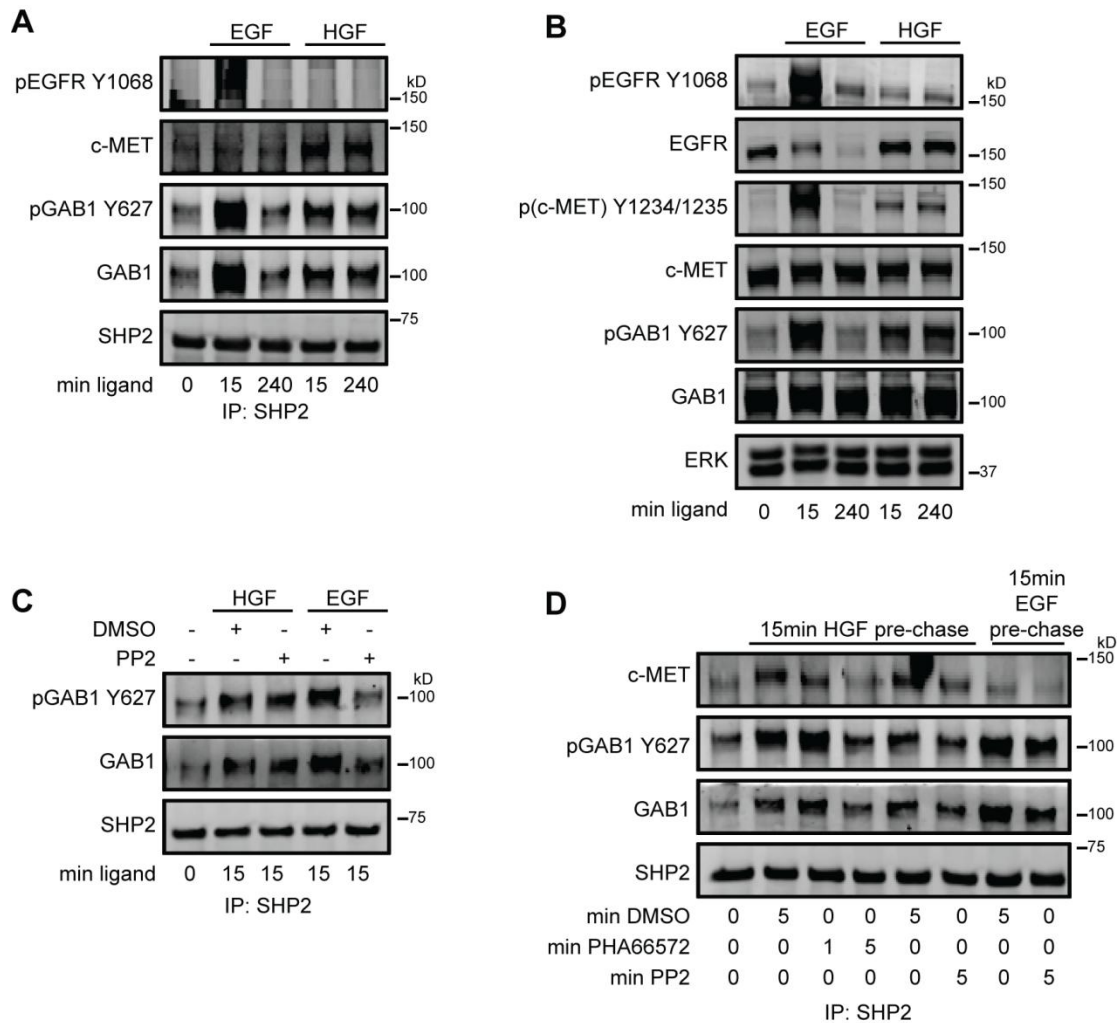


**Figure S4-10: Sustained HGF-mediated association of GAB1 and SHP2.**

H1666 cells were treated with 38 ng/mL EGF or 50 ng/mL HGF for up to 240 min, and SHP2 immunoprecipitates (**A**) or whole cell lysates (**B**) were analyzed by western blotting with antibodies against the indicated proteins. (**C** and **D**) Cells were pretreated with DMSO or 10  $\mu$ M PP2 for 30 minutes and subsequently treated with HGF or EGF for 15 min and lysed, or treated with HGF or EGF for 15 min and subsequently chased with DMSO, 10  $\mu$ M PP2, or 1  $\mu$ M PHA665752 for up to 5 min prior to lysing cells. SHP2 immunoprecipitates were analyzed by western blotting with antibodies against the indicated proteins. Throughout the figure panels, all blot images are representative of three sets of biological replicates.

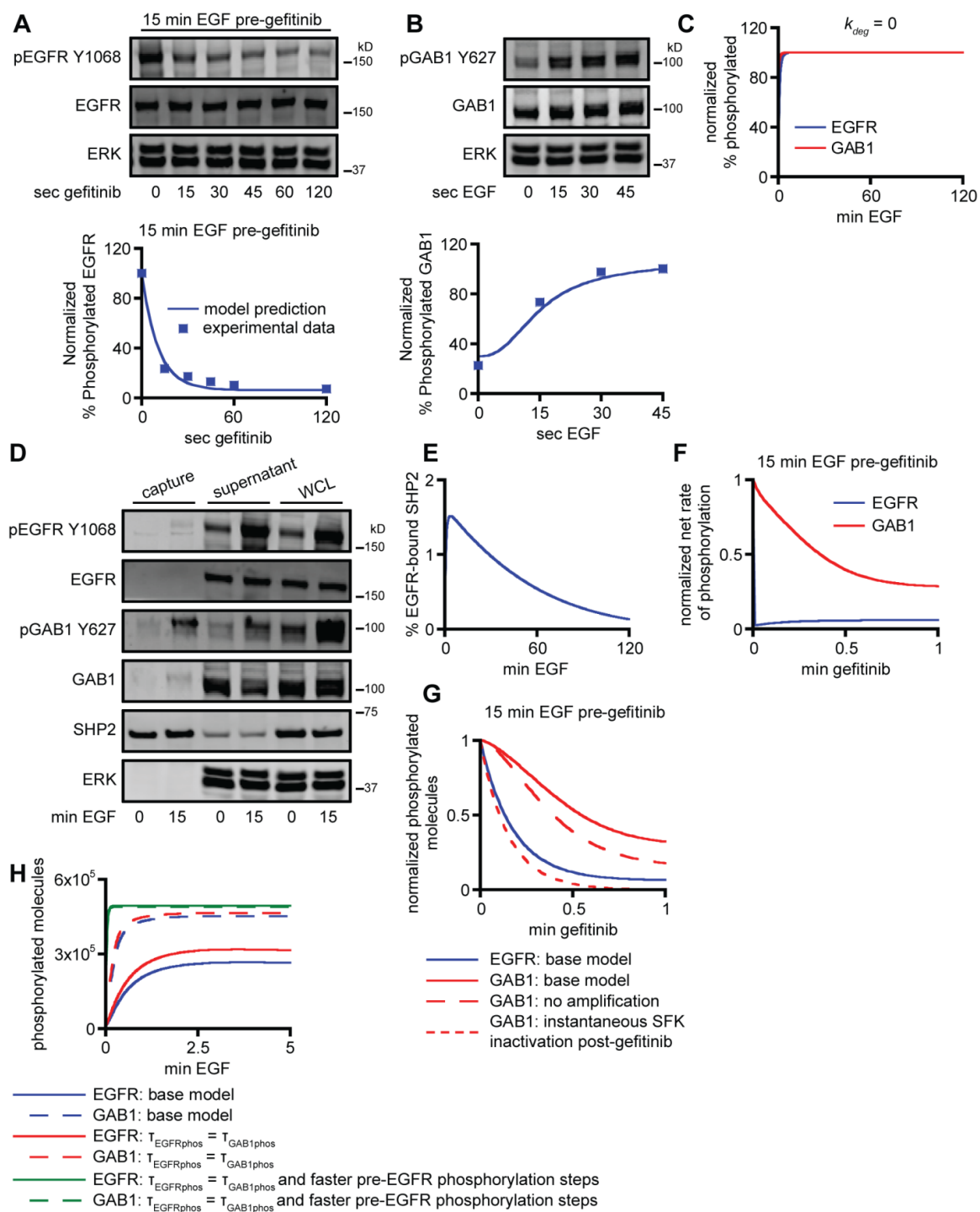


**Figure S4-11: Model fitting to experimental data.**

H1666 cells were treated with 10 ng/mL EGF for 15 min and subsequently chased with 1  $\mu$ M gefitinib for up to 2 min prior to lysing cells (A), or treated with 10 ng/mL EGF for up to 45 s and lysed (B). Lysates were analyzed by western blotting with antibodies against the indicated proteins. Blot signals for phosphorylated EGFR and GAB1 were

quantified and normalized by ERK signal (loading control), which were then compared with model predictions. **(C)** Normalized percent phosphorylated EGFR and GAB1 throughout a 2 hr EGF treatment model simulation were computed when EGFR degradation was neglected. **(D)** H1666 cells were treated with 10 ng/mL EGF for 15 min, and lysates were immunoprecipitated using an SHP2 antibody. Immunoprecipitates (capture), non-immunoprecipitated proteins (supernatant), and the original whole cell lysate were analyzed by western blotting using antibodies against the indicated proteins. **(E)** Model predictions for the percent of SHP2 bound with EGFR throughout a 120 min EGF treatment were calculated. **(F)** Normalized net rates of EGFR and GAB1 phosphorylation were predicted throughout a 1 min gefitinib treatment. **(G)** Model predictions for the normalized number of phosphorylated EGFR or GAB1 molecules throughout a 1 min gefitinib treatment were calculated, either for the base model topology, for a model topology where SFK-mediated amplification of GAB1 phosphorylation does not occur, or for a model topology where SFKs inactivate instantly following gefitinib addition. **(H)** Model predictions for the number of phosphorylated EGFR or GAB1 molecules throughout a 5 min EGF treatment were calculated, either for the base model parameters, for model parameters where the timescales for EGFR and GAB1 phosphorylation ( $\tau_{\text{EGFRphos}}$  and  $\tau_{\text{GAB1phos}}$ ) are equal, or for model parameters where both the EGFR and GAB1 phosphorylation timescales are equal and all forward and reverse rate constants for EGF binding, ATP binding, and EGFR dimerization are increased or decreased by an order of magnitude to speed up the processes which occur prior to EGFR phosphorylation. Throughout the figure panels, all blot images are representative of three sets of biological replicates, and densitometry data are represented as mean  $\pm$  s.e.m. ( $n = 3$ ).

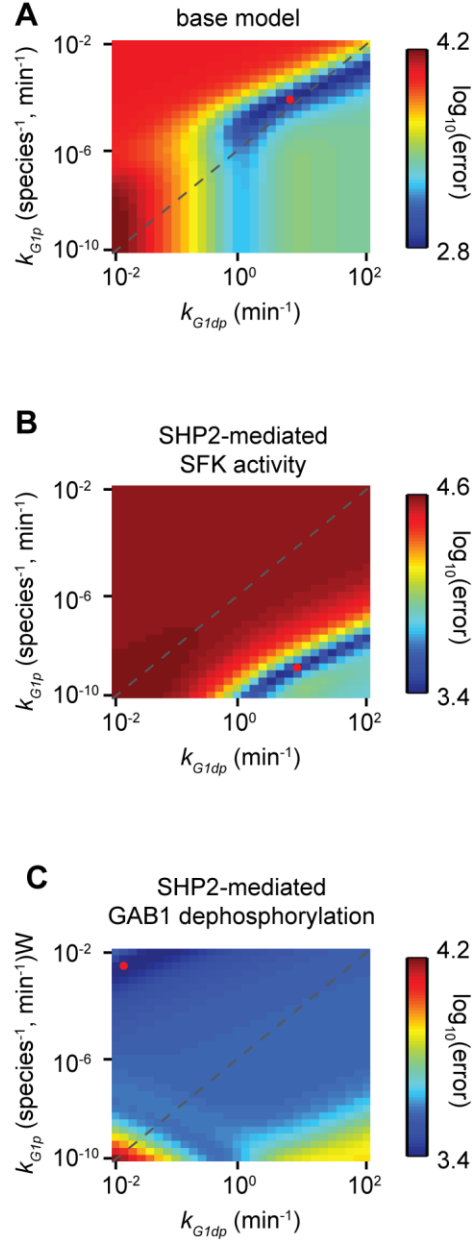


**Figure S4-12: Effect of variations in GAB1 phosphorylation ( $k_{Glp}$ ) and dephosphorylation ( $k_{Gldp}$ ) rate constants on model error.**

Model error was calculated for ranges of  $k_{Glp}$  and  $k_{Gldp}$  for the base model (**A**), a model which includes the capacity for GAB1-bound (active) SHP2 to contribute to SFK activity (**B**), and a model which includes the capacity for GAB1-bound (active) SHP2 to dephosphorylate GAB1 (**C**). Red circles indicate error minima.

**Table S4-1: Model parameters**

Parameter (units)	Description	Value	Source
$k_{E,f}$ ( $\mu\text{M}^{-1} \text{min}^{-1}$ )	EGF binding to EGFR, forward	$3.1 \times 10^2$	[133]
$k_{E,r}$ ( $\text{min}^{-1}$ )	EGF binding to EGFR, reverse	$8.0 \times 10^{-1}$	[134]
$k_{A,f}$ ( $\mu\text{M}^{-1} \text{min}^{-1}$ )	ATP binding to EGFR, forward	$1.0 \times 10^5$	[63]
$k_{A,r}$ ( $\text{min}^{-1}$ )	ATP binding to EGFR, reverse	$1.1 \times 10^7$	[63]
$k_{i,f}$ ( $\mu\text{M}^{-1} \text{min}^{-1}$ )	Gefitinib binding to EGFR, forward	$1.0 \times 10^5$	[63]
$k_{i,r}$ ( $\text{min}^{-1}$ )	Gefitinib binding to EGFR, reverse	$2.1 \times 10^2$	[63]
$k_{d,f}$ ( $\text{cell min}^{-1}$ )	EGFR dimerization, forward	$9.2 \times 10^{-4}$	Calculated
$k_{d,r}$ ( $\text{min}^{-1}$ )	EGFR dimerization, reverse, unoccupied	$1.4 \times 10^4$	[137]
$k_{dE,r}$ ( $\text{min}^{-1}$ )	EGFR dimerization, reverse, EGF-occupied	$1.0 \times 10^{-1}$	[136]
$k_{cat}$ ( $\text{min}^{-1}$ )	EGFR phosphorylation, unoccupied dimer	$2.7 \times 10^0$	[138]
$k_{catE}$ ( $\text{min}^{-1}$ )	EGFR phosphorylation, EGF-occupied dimer	$1.3 \times 10^1$	[138]
$k_{dp}$ ( $\text{min}^{-1}$ )	EGFR dephosphorylation	$8.0 \times 10^0$	Fit
$k_{S,a}$ ( $\text{cell min}^{-1}$ )	SFK activation	$1.3 \times 10^1$	[138]
$k_{S,i}$ ( $\text{cell min}^{-1}$ )	SFK inactivation	$1.0 \times 10^1$	[143, 144]
$k_{G2,f}$ ( $\text{cell min}^{-1}$ )	GRB2 binding to EGFR, forward	$3.8 \times 10^{-3}$	[61]
$k_{G2,r}$ ( $\text{min}^{-1}$ )	GRB2 binding to EGFR, reverse	$4.6 \times 10^2$	[61]
$k_{G1,f}$ ( $\text{cell min}^{-1}$ )	GAB1 binding to GRB2, forward	$2.4 \times 10^{-3}$	[140]
$k_{G1,r}$ ( $\text{min}^{-1}$ )	GAB1 binding to GRB2, reverse	$6.0 \times 10^1$	[140]
$k_{G1p}$ ( $\text{cell min}^{-1}$ )	GAB1 phosphorylation	$1.0 \times 10^{-4}$	Fit
$k_{G1dp}$ ( $\text{min}^{-1}$ )	GAB1 dephosphorylation	$9.5 \times 10^0$	Fit
$k_{S2,f}$ ( $\text{cell min}^{-1}$ )	SHP2 binding to phosphorylated GAB1, forward	$3.8 \times 10^{-3}$	[62]
$k_{S2,r}$ ( $\text{min}^{-1}$ )	SHP2 binding to phosphorylated GAB1, reverse	$4.6 \times 10^2$	[62]
$k_{deg}$ ( $\text{min}^{-1}$ )	EGFR degradation	$1.1 \times 10^{-1}$	Fit
ATP ( $\mu\text{M}$ )	Cellular ATP concentration	$1.0 \times 10^3$	[135]
EGF ( $\mu\text{M}$ )	Extracellular EGF concentration	$1.7 \times 10^{-3}$	See text
gefitinib ( $\mu\text{M}$ )	Gefitinib concentration	$1.0 \times 10^0$	See text
EGFR ( $\text{cell}^{-1}$ )	EGFR molecules per cell	$6.0 \times 10^5$	See text
GRB2 ( $\text{cell}^{-1}$ )	GRB2 molecules per cell	$6.0 \times 10^5$	[140]
GAB1 ( $\text{cell}^{-1}$ )	GAB1 molecules per cell	$6.0 \times 10^5$	[140]
SHP2 ( $\text{cell}^{-1}$ )	SHP2 molecules per cell	$6.0 \times 10^5$	[140]
SFK ( $\text{cell}^{-1}$ )	SFK molecules per cell	$6.0 \times 10^5$	[140]
CSK ( $\text{cell}^{-1}$ )	CSK molecules per cell	$6.0 \times 10^5$	[140]

## **Chapter 5: A Reaction-diffusion Model Predicts the Intracellular Length Scale Over Which EGFR-initiated GAB1-SHP2 Complexes Persist**

### **5-1 ABSTRACT**

Activation of receptor tyrosine kinases (RTKs) leads to the assembly of cytosolic protein complexes linked through interactions including those between phosphotyrosines and SH2 domains. However, these interactions are relatively weak and reversible, allowing for complex disassembly to occur on a time scale that permits intracellular phosphatases to dephosphorylate complex members and ultimately regulate complex persistence, which may limit the intracellular length scale over which RTKs can maintain the association of distal complexes. Here, we develop a computational reaction-diffusion model using the epidermal growth factor receptor (EGFR) as a model system to gain quantitative understanding of the regulation of cytosolic protein complexes containing SRC homology 2 domain-containing phosphatase 2 (SHP2) and GRB2-associated binder 1 (GAB1), the primary phosphorylated adapter protein which binds and activates SHP2 downstream of EGFR. The model predicts that by activating intermediary SRC family kinases (SFKs), which phosphorylate GAB1, EGFR can remotely maintain the association of GAB1 and SHP2 throughout the entire cell volume, a finding which is dependent on the capacity for SFKs to diffuse through the cytosol after being activated by EGFR at the plasma membrane. Further model investigation through a parameter sensitivity analysis identifies protein diffusivity and the rate constants for SFK

inactivation and GAB1 dephosphorylation as the most important parameters for determining the intracellular length scale of GAB1-SHP2 complex persistence. Based on calculations for characteristic protein diffusion, dephosphorylation, and dissociation times, our model suggests that each GAB1 molecule needs to be phosphorylated ~4 times throughout the cytosol to permit a GAB1-SHP2 complex originating from the plasma membrane to reach the cell center. Overall, our results suggest that GAB1-SHP2 complexes can persist distal from EGFR due to re-phosphorylation of GAB1 throughout the cytosol by EGFR-activated SFKs, which could allow membrane-bound EGFR to remotely control signaling events through SHP2 at subcellular locations where EGFR is not present.

## 5-2 INTRODUCTION

Receptor tyrosine kinases (RTKs), such as the epidermal growth factor receptor (EGFR), promote the activity of downstream signaling pathways by initially recruiting SH2 and PTB domain-containing cytosolic adapter proteins to RTK phosphotyrosines. However, receptor-adapter and other phosphorylation-dependent protein complexes exhibit rapid dissociation kinetics [61, 64], enabling protein tyrosine phosphatases (PTPs) to promote reversible complex disassembly by dephosphorylating tyrosines that participate in complex formation. In addition to directly binding cytosolic proteins to facilitate the formation of phosphorylation-dependent multi-membered protein complexes [150], RTKs can also activate cytosolic kinases to promote complex assembly (Chapter 4), which may serve as a means of extending the length scale of complex persistence distal from RTKs by counteracting the activity of cytosolic phosphatases that dephosphorylate key tyrosines. However, the intracellular length scales over which RTKs can remotely control the association of such complexes via this type of mechanism are unknown. Here, we use EGFR as a model RTK to computationally investigate the distance from the plasma membrane over which EGFR maintains the association of the cytosolic protein tyrosine phosphatase SRC homology 2 domain-containing phosphatase 2 (SHP2) with the adapter protein GRB2-associated binder 1 (GAB1) via the action of intermediary SRC family kinases (SFKs).

SHP2 is a key signaling intermediate responsible for promoting the activity of ERK downstream of many RTKs [28]. SHP2 is basally auto-inhibited by intramolecular interactions between its N-SH2 and PTP domains [28]. In most cell lines, activation of SHP2 downstream of EGFR primarily results from binding of SHP2 to phosphorylated

GAB1, where GAB1 phosphorylation can potentially occur through EGFR-activated SFKs (Chapter 4; [52, 66] ) or through the activity of EGFR itself [65]. GAB1-SHP2 association is mediated through binding of SHP2's N- and C-SH2 domains to phosphorylated GAB1 tyrosines 627 and 659, which disrupts auto-inhibitory SHP2 interactions and activates SHP2 [28]. In addition to activating SHP2, binding of SHP2 to GAB1 also permits the redistribution of cytosolic SHP2 to the plasma membrane through an EGFR-GRB2-GAB1-SHP2 protein linkage [54]. Via similar mechanisms receptor tyrosine kinases such as Ret, HER2, and c-MET can also recruit SHP2 to the plasma membrane [96, 131, 165]. However, some RTKs may more preferentially promote the association of GAB1 with SHP2 at the plasma membrane than others. Indeed HGF promotes more substantial recruitment of GAB1 to the plasma membrane than EGF in Madin-Darby canine kidney (MDCK) cells [130]. In a lung adenocarcinoma cell line, EGF-initiated GAB1-SHP2 complexes exist primarily in the cytosol with SFKs serving as the primary driver of GAB1 phosphorylation (Chapter 4).

As SFKs can be activated at the plasma membrane through events including binding of SRC's SH2 domain to EGFR [141], yet are inactivated within the cytosol through c-SRC kinase-mediated phosphorylation of negative regulatory tyrosines on SFKs [143], the number of active SFKs able to phosphorylate GAB1 may rapidly decline distal from the plasma membrane (i.e., towards the cell center). Furthermore, because GAB1 and SHP2 continuously dissociate and re-associate throughout the cytosol due to relatively fast rates of phosphotyrosine-SH2 domain binding/unbinding (Chapter 4; [64] ), which permits GAB1 to be dephosphorylated by cytosolic phosphatases throughout these binding cycles (Chapter 4), the local cytosolic concentration of GAB1-bound SHP2

may decline as this complex becomes inaccessible to active SFKs. Ultimately, the distance over which GAB1-SHP2 complexes persist distal from EGFR depends on how quickly SFKs and GAB1-SHP2 complexes are able to diffuse through the cytosol before becoming irreversibly inactivated and dissociated, respectively. Of course, in addition to diffusion, processes such as receptor internalization may also serve to extend the length scale of GAB1-SHP2 complexes distal from the plasma membrane, as others have shown that receptors including EGFR and TrkA continue to remain active and serve as nucleation sites for signaling complex formation within endosomes [67, 166-168].

Previous findings from our group suggest an important aspect of SHP2-mediated signaling involves the subcellular localization of active, GAB1-bound SHP2 [164, 169], although no prior studies have attempted to explore the spatial distribution of GAB1-SHP2 complexes throughout a cell. Here, we predict the spatiotemporal behavior of GAB1-SHP2 complexes within a representative EGF-treated cell by constructing a computational reaction-diffusion model of the processes that regulate GAB1-SHP2 complex assembly both at the plasma membrane and throughout the cytosol. The model predicts that GAB1 and SHP2 remain highly associated distal from EGFR, with the concentration of GAB1-SHP2 complexes at the cell center being 84% of the concentration of GAB1-SHP2 complexes at the plasma membrane. This result is sensitive to our assumption that EGFR-activated SFKs diffuse away from EGFR to phosphorylate GAB1 throughout the cytosol, as modifying the model topology to only permit GAB1 phosphorylation at the plasma membrane results in the concentration of GAB1-SHP2 complexes at the cell center being only 30% of that at the plasma membrane. A parameter sensitivity analysis further revealed that the total concentration

of GAB1-SHP2 complexes is most sensitive to perturbations in the rate constant for SHP2 binding GAB1, while the distance over which GAB1-SHP2 complexes persist distal from EGFR is most sensitive to perturbations in protein diffusivities and the rate constants for SFK inactivation and GAB1 dephosphorylation. Altogether, our findings suggest that in the absence of kinase activity distal from the plasma membrane, the extent of GAB1-SHP2 association rapidly decays due to the processes of GAB1-SHP2 unbinding and GAB1 dephosphorylation occurring more quickly than diffusion can permit GAB1-bound SHP2 to traverse the radius of a cell. Furthermore, our results suggest that EGFR-mediated activation of SFKs could permit membrane-localized EGFR to regulate signaling events at a distance through the cytosolic activity of SHP2.

### 5-3 MATERIALS AND METHODS

*General model considerations and topology.* The model consists of a set of coupled reaction-diffusion equations which describe the processes of protein diffusion, protein binding, and protein phosphorylation for a representative H1666 lung adenocarcinoma cell with a radius of 10  $\mu\text{m}$ . The resulting ordinary and partial differential equations for surface-associated proteins and cytosolic proteins, respectively, were solved in MATLAB using finite difference methods. Boundary conditions were also approximated using finite difference methods to solve for relevant protein concentrations at the cell surface and center. The system of equations was modeled in rectangular coordinates, based on the assumption of radial symmetry throughout the cell.

At a given time point, all partial differential equations for cytosolic proteins were approximated using an explicit finite difference method, where the first-order time and second-order space derivatives were approximated using forward and central differences, respectively. The system of algebraic equations which results from discretizing over the entire space domain was then explicitly solved for using known concentrations from the previous time point.

Next, the equations for surface-associated proteins and the boundary conditions for cytosolic proteins, which are coupled through the cell surface boundary, were simultaneously solved using an implicit finite difference method. The discretized boundary conditions for cytosolic proteins were evaluated first, where initial guesses for the concentrations of surface-associated proteins were provided. Subsequently, the discretized equations for surface-associated proteins were evaluated using the concentrations of cytosolic proteins previously solved for. This scheme was then

iterated, where the initial guess for concentrations of surface-associated was updated until convergence was reached.

This system of equations was then advanced to the next time point, where this process was repeated until the final time point was reached. The overall method is summarized according to the steps below:

- 1) All partial and ordinary differential equations for cytosolic and membrane-associated species, respectively, were discretized using finite difference methods.
- 2) Concentrations of all protein species were defined for the initial time.
- 3) The model was advanced one time step, and the concentrations of all cytosolic species were solved for throughout the bulk (i.e., everywhere except the cell center and cell surface boundaries).
- 4) At the same time step, the concentrations of all cytosolic species at the cell center were solved for using the appropriate boundary conditions at the cell center.
- 5) At the same time step, the concentrations of all cytosolic species at the cell surface were solved for using the appropriate boundary conditions at the cell surface, where initial guesses for concentrations of all membrane-associated species were provided.
- 6) The concentrations of all membrane-associated species were solved for using the concentrations of cytosolic species at the cell surface calculated in step 5.
- 7) Steps 5 and 6 were repeated, where the initial guesses for the concentrations of membrane-associated species in step 5 were updated using the

concentrations calculated in the previous iteration of step 6. This process was iterated until the concentrations solved for in step 5 and 6 converged.

8) Steps 3-7 were repeated until the final time point was reached.

**Boundary conditions.** No-flux boundary conditions were imposed on all cytosolic proteins at the cell center. The boundary conditions for SFKs at the cell surface consist of flux conditions, where the inward flux of inactive or active SFKs is equal to the reaction for EGFR-catalyzed conversion of inactive SFK to active SFK. Thus, the inward flux for inactive SFKs will be negative because inactive SFKs are being depleted at the surface, while the inward flux for active SFKs will be positive because active SFKs are being generated at the surface. The boundary conditions for all other cytosolic proteins at the cell surface consist of flux conditions, where the outward flux is equal to the reaction rate for these proteins binding to EGFR at the cell surface and the inward flux is equal to the reaction rate for these proteins unbinding from EGFR at the cell surface.

**Example equations.** Concentrations of cytosolic species were solved for as a function of time ( $t$ ) and space ( $x$ ) using equations of the following form:

$\frac{\partial C_i}{\partial t} = D_i \frac{\partial^2 C_i}{\partial x^2} + R_{vi}$ , where  $D_i$  and  $C_i$  correspond to the diffusivity and concentration of a given cytosolic protein, respectively, and  $R_{vi}$  corresponds to the net volumetric rate of production [moles per volume per time] for a given cellular process leading to the generation or consumption of the cytosolic species designated by  $C_i$ .

Boundary conditions at the cell center for cytosolic species were implemented using equations of the following form:

$D_i \frac{\partial C_i}{\partial x} = 0$ , which corresponds to no flux of the cytosolic species designated by  $C_i$

across the cell center boundary.

Boundary conditions at the plasma membrane for cytosolic species were implemented using equations of the following form:

$D_i \frac{\partial C_i}{\partial x} = R_{si}$ , where  $C_i$  corresponds to the concentration of a given cytosolic protein and

$R_{si}$  corresponds to the net volumetric rate of production at a surface [moles per area per time] for a given cellular process leading to the generation or consumption of that protein at the cell surface boundary.

Concentrations of membrane-associated species were solved for as a function of time ( $t$ ) only, based on the assumption that membrane-associated species do not diffuse through the plasma membrane or endocytose, using equations of the following form:

$\frac{\partial C_i}{\partial t} = R_{si}$ , where  $C_i$  corresponds to the concentration of a given membrane-associated

species and  $R_{si}$  corresponds to the net volumetric rate of production at a surface [moles per area per time] for a given cellular process leading to the generation or consumption of that protein.

**EGFR phosphorylation.** The process of EGFR phosphorylation was simplified to sequentially depend on the processes of EGF binding, EGFR dimerization, and EGFR phosphorylation. EGF binding at the plasma membrane was modeled as a reversible process characterized by association [133] and dissociation [134] rate constants. EGF was modeled at a constant concentration of 10 ng/mL. The EGFR dimerization rate constant was calculated as described previously (Chapter 4). Dimer uncoupling rate constants in the presence of EGF were described previously [137]. All dimer species were assumed

to be symmetric. EGFR phosphorylation was modeled as a process which occurs between EGF-bound EGFR dimers, where both receptors are simultaneously phosphorylated at a representative tyrosine (Y1068) which is able to bind GRB2. EGFR dephosphorylation was modeled as a zeroth order process with a previously described rate constant (Chapter 4).

***GAB1 phosphorylation.*** GAB1 phosphorylation at a representative tyrosine (Y627) which is able to bind SHP2 was modeled as a process catalyzed by active SFKs throughout the cytosol. GAB1 dephosphorylation was modeled as zeroth order and occurred throughout the cytosol.

***SFK activation.*** Similar to our previous model (Chapter 4), the process of SFK activation was modeled as a first-order rate equation where phosphorylated EGFR activates SFK, which only occurs at the cell surface boundary for this model. SFK inactivation was modeled as zeroth order and occurred throughout the cytosol.

***GRB2, GAB1, and SHP2 binding.*** Reactions for GRB2, GAB1, and SHP2 association/dissociation were described previously (Chapter 4).

***Phosphatase activity.*** EGFR and GAB1 dephosphorylation were modeled as zeroth order with respect to protein tyrosine phosphatases, which precludes the requirement for considering distinct phosphatase species.

***EGFR inhibition.*** Following treatment with EGF, EGFR inhibition was simulated by setting the rate constant for EGFR phosphorylation to zero at the desired timepoint post-EGF addition.

***Protein diffusivity.*** Diffusivities for each cytosolic protein monomer or complex were calculated based on the diffusivity of tubulin [162], which was adjusted based on

differences in the hydrodynamic radii of tubulin and a given protein monomer or complex [163].

**Parameter fitting.** Due to topological differences between this model and our previously developed model which did not include spatial considerations, we chose to refit parameters for SFK activation/inactivation and GAB1 phosphorylation/dephosphorylation to match our previous model's predictions for concentrations of phosphorylated GAB1 and active SFKs in response to EGF addition. The four relevant parameters ( $k_{G1p}$ ,  $k_{G1dp}$ ,  $k_{S,a}$ ,  $k_{S,i}$ ) were determined by computing the spatial average of [pGAB1] and [aSFK] in response to EGF and fitting these concentrations to prior predictions for [pGAB1] and [aSFK]. Parameter fitting was done using simulated annealing to minimize the total error between model output and experimental data. The error was computed as the square of the difference between model output and the experimental value. The best-fit results are included in Table 1.

**Sensitivity analysis.** Model sensitivity to changes in parameters was computed by increasing and decreasing parameter values by a factor of 10. Sensitivity was measured by summing the integrated differences between the original model and the two perturbed outputs over time. To compare differences among parameter perturbations, sensitivities were reported as percentages of the maximum perturbed parameter.

**Representative Cell.** EGFR, GRB2, GAB1, SHP2, and SFKs were assumed to be at cellular concentrations of  $6 \times 10^5$  species per cell, as described previously (Chapter 4). The cell radius was assumed to be 10  $\mu\text{m}$ , as described previously for other epithelial cells [161].

***Model implementation.*** Codes were generated and compiled in MATLAB. The *simulannealbnd* function in the Global Optimization Toolbox was used to fit the unknown rate constants. For all calculations, the space dimension was discretized into 100 nodes. For base model calculations, a time step of 0.00001s was used, while a time step of 0.000001s was used for parameter sensitivity analyses. To reduce the memory required to store solutions at every time point, solutions were only stored once per 100 time steps.

**Table 5-1: Model parameters**

Parameter (units)	Description	Value	Source
$k_{E,f}$ ( $\mu\text{M}^{-1} \text{min}^{-1}$ )	EGF binding to EGFR, forward	$3.1 \times 10^2$	[133]
$k_{E,r}$ ( $\text{min}^{-1}$ )	EGF binding to EGFR, reverse	$8.0 \times 10^{-1}$	[134]
$k_{d,f}$ ( $\text{cell min}^{-1}$ )	EGFR dimerization, forward	$9.2 \times 10^{-4}$	(Chapter 4)
$k_{dE,r}$ ( $\text{min}^{-1}$ )	EGFR dimerization, reverse	$1.0 \times 10^{-1}$	[136]
$k_{catE}$ ( $\text{min}^{-1}$ )	EGFR phosphorylation, EGF-occupied dimer	$1.3 \times 10^1$	[138]
$k_{dp}$ ( $\text{min}^{-1}$ )	EGFR dephosphorylation	$8.0 \times 10^0$	(Chapter 4)
$k_{S,a}$ ( $\text{cell min}^{-1}$ )	SFK activation	$4.0 \times 10^{-4}$	Fit
$k_{S,i}$ ( $\text{min}^{-1}$ )	SFK inactivation	$5.0 \times 10^0$	Fit
$k_{G2,f}$ ( $\text{cell min}^{-1}$ )	GRB2 binding to EGFR, forward	$3.8 \times 10^{-3}$	[61]
$k_{G2,r}$ ( $\text{min}^{-1}$ )	GRB2 binding to EGFR, reverse	$4.6 \times 10^2$	[61]
$k_{G1,f}$ ( $\text{cell min}^{-1}$ )	GAB1 binding to GRB2, forward	$2.4 \times 10^{-3}$	[140]
$k_{G1,r}$ ( $\text{min}^{-1}$ )	GAB1 binding to GRB2, reverse	$6.0 \times 10^1$	[140]
$k_{G1p}$ ( $\text{cell min}^{-1}$ )	GAB1 phosphorylation	$1.0 \times 10^{-4}$	Fit
$k_{G1dp}$ ( $\text{min}^{-1}$ )	GAB1 dephosphorylation	$9.5 \times 10^0$	Fit
$k_{S2,f}$ ( $\text{cell min}^{-1}$ )	SHP2 binding to phosphorylated GAB1, forward	$3.8 \times 10^{-3}$	[62]
$k_{S2,r}$ ( $\text{min}^{-1}$ )	SHP2 binding to phosphorylated GAB1, reverse	$4.6 \times 10^2$	[62]
EGF ( $\mu\text{M}$ )	Extracellular EGF concentration	$1.7 \times 10^{-3}$	See text
EGFR ( $\text{cell}^{-1}$ )	EGFR molecules per cell	$6.0 \times 10^5$	(Chapter 4)
GRB2 ( $\text{cell}^{-1}$ )	GRB2 molecules per cell	$6.0 \times 10^5$	[140]
GAB1 ( $\text{cell}^{-1}$ )	GAB1 molecules per cell	$6.0 \times 10^5$	[140]
SHP2 ( $\text{cell}^{-1}$ )	SHP2 molecules per cell	$6.0 \times 10^5$	[140]
SFK ( $\text{cell}^{-1}$ )	SFK molecules per cell	$6.0 \times 10^5$	[140]
$D_S$ ( $\mu\text{m}^2 \text{min}^{-1}$ )	Diffusivity of SFK molecules	$8.2 \times 10^1$	[162, 163]
$D_{G2}$ ( $\mu\text{m}^2 \text{min}^{-1}$ )	Diffusivity of GRB2 molecules	$1.3 \times 10^2$	[162, 163]
$D_{G2G1}$ ( $\mu\text{m}^2 \text{min}^{-1}$ )	Diffusivity of GRB2-GAB1 molecules	$6.1 \times 10^1$	[162, 163]
$D_{G2GIS2}$ ( $\mu\text{m}^2 \text{min}^{-1}$ )	Diffusivity of GRB-GAB1-SHP2 molecules	$5.5 \times 10^1$	[162, 163]
$D_{G1}$ ( $\mu\text{m}^2 \text{min}^{-1}$ )	Diffusivity of GAB1 molecules	$6.6 \times 10^1$	[162, 163]
$D_{GIS2}$ ( $\mu\text{m}^2 \text{min}^{-1}$ )	Diffusivity of GAB1-SHP2 molecules	$5.6 \times 10^1$	[162, 163]
$D_{S2}$ ( $\mu\text{m}^2 \text{min}^{-1}$ )	Diffusivity of SHP2 molecules	$7.8 \times 10^1$	[162, 163]
$R$ ( $\mu\text{m}$ )	Cell radius	$1.0 \times 10^1$	[161]

## 5-4 RESULTS

***Model predictions with baseline parameterization.*** To predict the concentration of GAB1-SHP2 complexes as a function of time and position following EGFR activation within a representative H1666 lung adenocarcinoma cell with an assumed radius of 10  $\mu\text{m}$ , we developed a computational model, the full details of which can be found in *Materials and Methods* (Section 5-3). The model considers cellular processes including EGFR phosphorylation, SFK activation, GAB1 phosphorylation, GAB1-SHP2 binding, and diffusion of cytosolic proteins. Model parameters were taken from a previous model we developed (Chapter 4), with the exception of parameters for SFK activation and inactivation and GAB1 phosphorylation and dephosphorylation, which were re-fit due to topological differences between the models. The rate constants for these processes were fit to predictions from our previously developed model to preserve similar average concentrations of active SFK and phosphorylated GAB1. The model thus fit is able to accurately recapitulate the previously predicted dynamics of SFK activation and GAB1 phosphorylation in response to EGF (Figure 5-1A). While the rate constants for GAB1 phosphorylation and dephosphorylation were relatively consistent between the models, the fitted parameters for SFK activation and inactivation had to be decreased by roughly four and six orders of magnitude, respectively. Consistent with our previous model's finding of amplification of SFK activity downstream of EGFR, this model predicts that each active EGFR molecule leads to the phosphorylation of an average of  $\sim 2$  GAB1 molecules throughout a 5 minute EGF treatment simulation (Figure 5-1B).

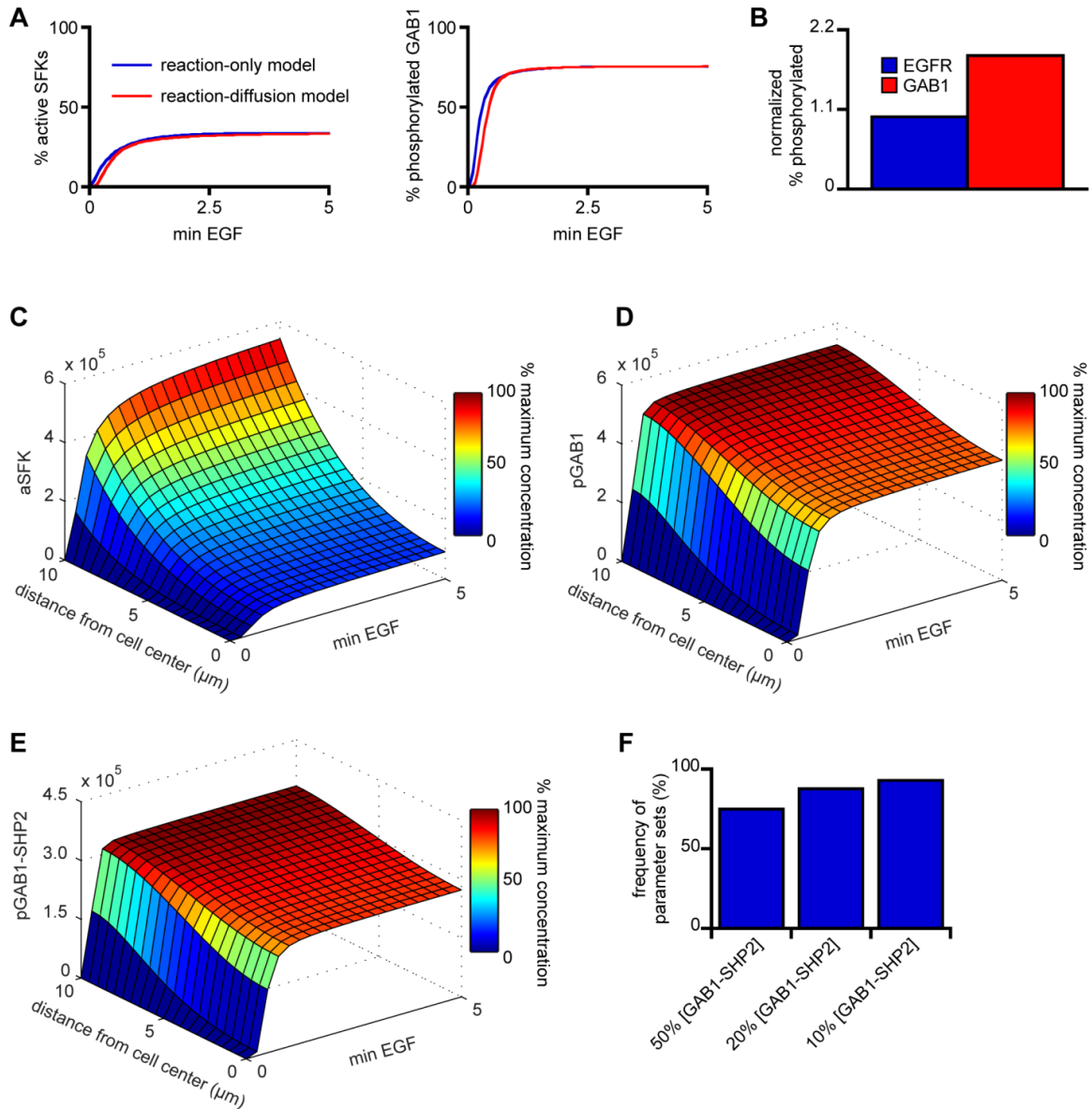


**Figure 5-1: Base model predictions and fits.**

(A) Reaction-diffusion model predictions for the spatially averaged concentrations of active SFKs and phosphorylated GAB1 were fit to predictions from our previous model (reaction-only), as described in *Materials and Methods*. (B) Average concentrations of phosphorylated EGFR and GAB1 throughout 5 min of EGF treatment were calculated and normalized to the average concentration of phosphorylated EGFR. (C-E) Model predictions for the cellular concentrations of active SFKs (aSFK), phosphorylated GAB1 (pGAB1), and GAB1-SHP2 complexes were plotted as a function of distance from the cell center and time following treatment with 10 ng/mL EGF. (F) For 100 random

parameter sets, the frequency with which the distance for the concentration of GAB1-SHP2 complexes to decay to 50%, 20%, or 10% of the plasma membrane GAB1-SHP2 concentration was greater than the cell radius  $R$  (10  $\mu\text{m}$ ) was calculated.

We next used the model to calculate protein concentrations as a function of distance from the cell surface. We found that the concentration of active SFKs rapidly decayed throughout the cytosol while the concentration of phosphorylated GAB1 remained relatively unchanged (Figures 5-1C-D). We also note that the concentration of GAB1-SHP2 complexes was essentially unchanged as a function of position within the cell, suggesting that EGFR-activated SHP2 retains its activity distal from the plasma membrane (Figure 5-1E). We tested the robustness of this prediction by creating random parameter sets, where each model parameter was randomly perturbed by up to an order of magnitude above or below its base value. For 75%, 88%, and 93% of the 100 parameter sets generated, the length scale for the concentration of GAB1-SHP2 complexes to reach 50%, 20%, and 10% of the maximal GAB1-SHP2 concentration at the cell surface, respectively, was greater than the cell radius  $R$  (10  $\mu\text{m}$ ; Figure 5-1F). Therefore, the model prediction of GAB1-SHP2 complexes being maintained distal from the cell surface appears robust even if the model parameters are not well estimated.

***Model parameter sensitivity.*** To identify model processes that strongly influence both the average concentration and concentration gradient of GAB1-SHP2 complexes within the cell, we performed a parameter sensitivity analysis for steady state GAB1-SHP2 complex formation in response to EGF treatment when individually perturbing each model parameter by a factor of ten (Figure 5-2A). We found that the average GAB1-SHP2 concentration was most sensitive to perturbations to the rate constants for

SHP2 binding to or unbinding from GAB1. To determine parameters which control the spatial distribution of GAB1-SHP2 complexes, we calculated the ratio of the concentration of GAB1-SHP2 complexes at the cell center to the cell surface and also defined  $r_{1/2}$  and  $r_{1/10}$  as length scales for GAB1-SHP2 association distal from the cell surface, which are the distances from the cell surface where the concentration of GAB1-SHP2 reaches 50% or 10% of its maximal value, respectively. Here, model predictions were exquisitely sensitive to changes in protein diffusivity, as well as rate constants for SFK inactivation and GAB1 dephosphorylation (Figure 5-2A-D).

We next performed a sensitivity analysis where the concentration of each protein considered in the model was perturbed by a factor of ten to determine which species most strongly control the steady state ratio of the GAB1-SHP2 concentration at the cell center to that at the cell surface. We noted that SFKs most strongly control the spatial distribution of GAB1-SHP2 complexes, while interestingly EGFR had relatively little control over the GAB1-SHP2 complex distribution (Figures 5-2E-F). Given that we previously identified the processes of SFK inactivation and GAB1 dephosphorylation as strong determinants of the GAB1-SHP2 length scale, we sought to determine the relationship between SFK concentration and the rates of these two processes in determining the GAB1-SHP2 length scale. As noted previously, a ten-fold increase in the rate constant for GAB1 dephosphorylation greatly reduces the GAB1-SHP2 persistence length scale, but, interestingly, a simultaneous ten-fold increase in SFK concentration negates the effect of an increased GAB1 dephosphorylation rate constant (Figure 5-2G). Similarly, a ten-fold increase in the rate constant for SFK inactivation also greatly reduces the GAB1-SHP2 length scale, but in this case an increase in SFK

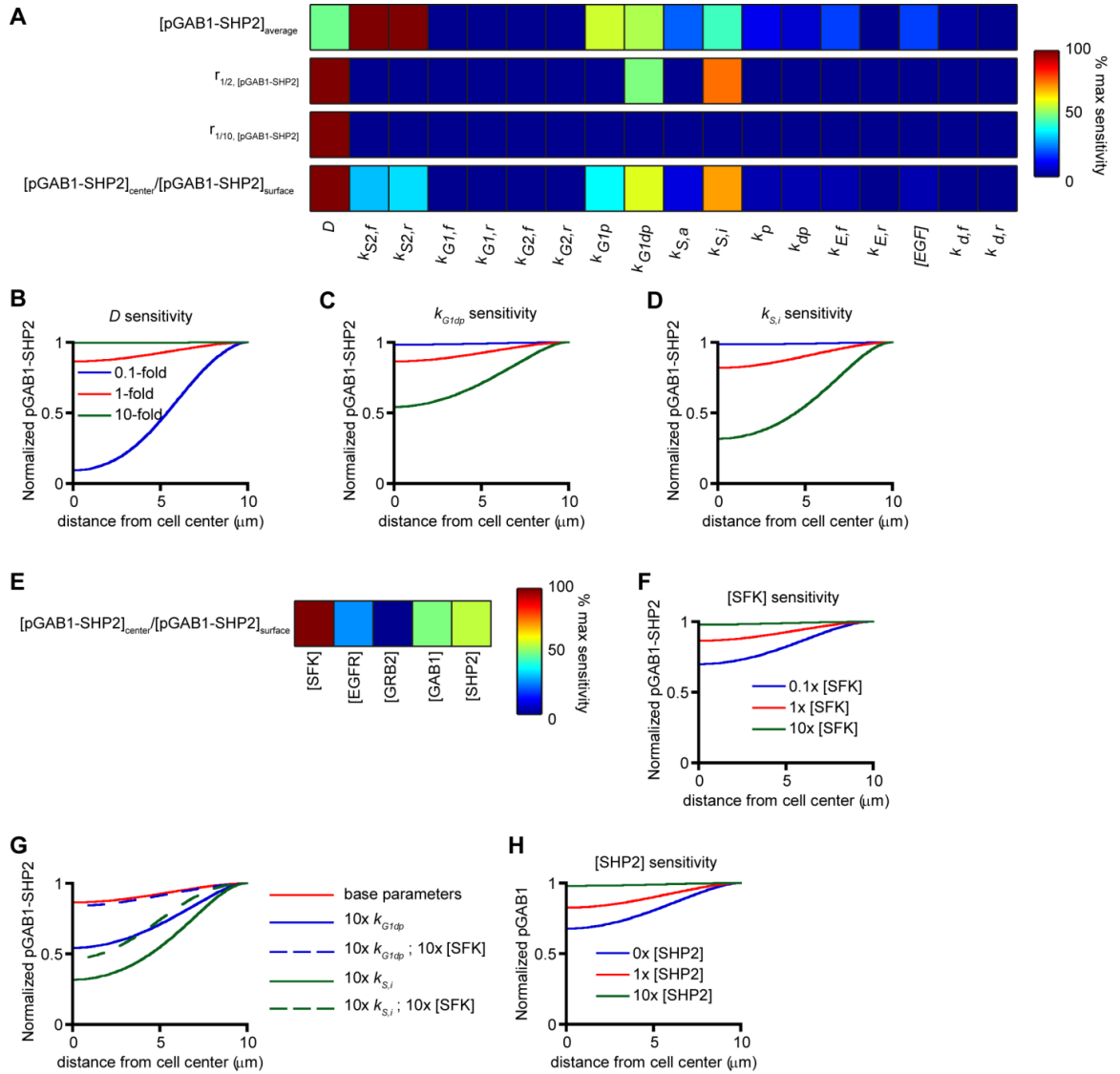


**Figure 5-2: Model sensitivity analysis.**

(A) The sensitivity of model predictions of the spatially averaged concentration of GAB1-SHP2 complexes, distances over which the GAB1-SHP2 concentration decays to 50% ( $r_{1/2}$ ) or 10% ( $r_{1/10}$ ) of the maximum GAB1-SHP2 concentration (i.e., at the cell surface), and the ratio of GAB1-SHP2 concentrations at the cell center to the cell surface to 10-fold changes in model parameters was calculated for a 5 min treatment with 10 ng/mL EGF. Sensitivity to diffusivity ( $D$ ) was calculated by making simultaneous 10-fold increases or decreases in the diffusivity of every cytosolic protein. Sensitivity of each model parameter was normalized to the maximum sensitivity for a given calculation. (B-D) Model predictions for the normalized concentration of GAB1-SHP2

after 5 min 10 ng/mL EGF treatment were compared with predictions when all protein diffusivities ( $D$ ),  $k_{G1dp}$ , and  $k_{S,i}$  were increased or decreased by a factor of 10. **(E)** The sensitivity of model predictions for the ratio of GAB1-SHP2 concentration at the cell center to the cell surface to 10-fold changes in the indicated protein concentrations was calculated for a 5 min 10 ng/mL EGF treatment. **(F-G)** Model predictions for the concentration of GAB1-SHP2 as a function of distance from the cell center, which was normalized to the concentration of GAB1-SHP2 at the plasma membrane, after 5 min EGF treatment were compared with predictions when the indicated parameters or protein concentrations were varied by a factor of 10. **(H)** Model predictions for the concentration of phosphorylated GAB1 as a function of distance from the cell center, which was normalized to the concentration of phosphorylated GAB1 at the plasma membrane, after a 5 min 10ng/mL EGF treatment were compared with predictions when the concentration of SHP2 was either increased 10-fold or set to zero.

concentration is unable to overcome a faster rate of SFK inactivation due to the elevated number of active SFKs generated at the plasma membrane becoming more quickly inactivated throughout the cytosol. Based on previous findings from our lab and others (Chapter 4; [154] ), we also sought to determine if SHP2's binding to GAB1 could protect GAB1 from being dephosphorylated throughout the cytosol. While our previous model, which did not take the spatial distribution of proteins into consideration, found very little effect of SHP2 depletion or overexpression on altering the total concentration of GAB1 phosphorylation, the current model predicts that both SHP2 depletion and overexpression can greatly change the extent of GAB1 phosphorylation throughout the cytosol (Figure 5-2H). This is due to the fact that in the current model, unbound and dephosphorylated GAB1 molecules near the cell center are in the proximity of a relatively low concentration of active SFKs compared to the cell surface, which makes

the protective effect of SHP2's binding to GAB1 much more apparent as there are fewer SFKs available to rephosphorylate GAB1 upon GAB1's dissociation from SHP2 and subsequent dephosphorylation.

***EGFR pulse-chase dynamics.*** To determine the consequences of acute EGFR inhibition on the spatiotemporal profile of GAB1-SHP2 complexes, we simulated a pulse-chase experiment where 10 ng/mL EGF was added for 5 min, followed by the simulated inhibition of EGFR modeled by setting the rate constant for EGFR phosphorylation to zero. We verified that this pulse-chase topology produced EGFR dephosphorylation kinetics similar to those achieved by our previous model, which explicitly included the EGFR inhibitor gefitinib in the model topology (Figure 5-3A; Chapter 4). When predicting the concentration of GAB1-SHP2 complexes as a function of cell position over a 2 min period following EGFR inhibition, we noted that this concentration decayed most rapidly near the cell surface throughout the chase (Figure 5-3B). A similar and even more pronounced trend was observed for the rate of SFK inactivation based on cell position (Figure 5-3C). Since our previous predictions suggest that both GAB1-SHP2 and active SFK concentrations are highest near the cell surface (Figures 5-1B and D), these data suggest that the net rate of GAB1-SHP2 dissociation and SFK inactivation are largest where these proteins and protein complexes are most highly concentrated. This result has interesting implications related to protein complex cycling, as this suggests that the total number of GAB1-SHP2 dissociation and re-association events, as well as GAB1 dephosphorylation and re-phosphorylation events, is largest closer to the cell surface over a given time interval.

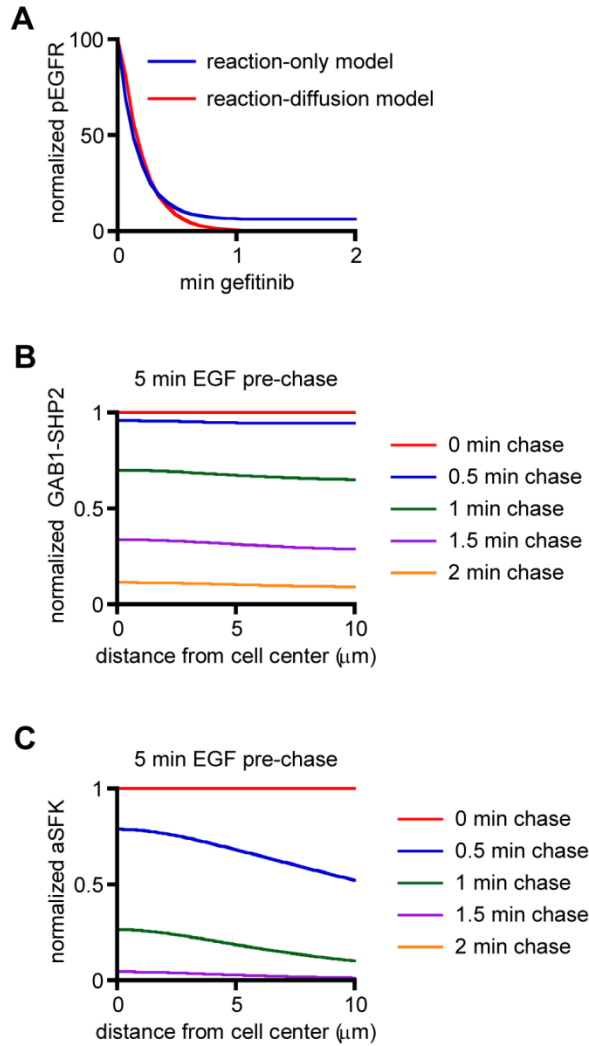
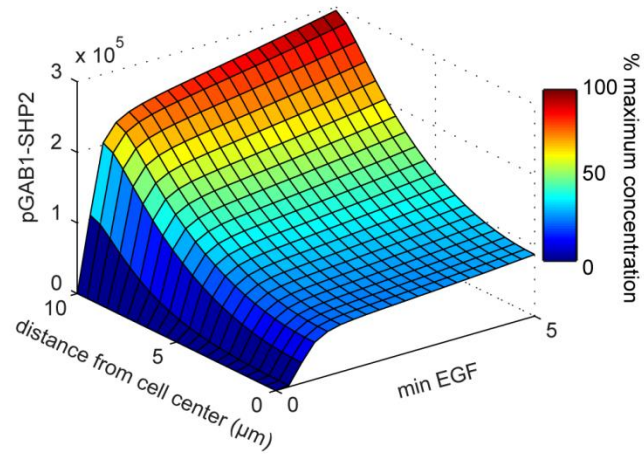


**Figure 5-3: EGF-pulse EGFR inhibition-chase predictions.**

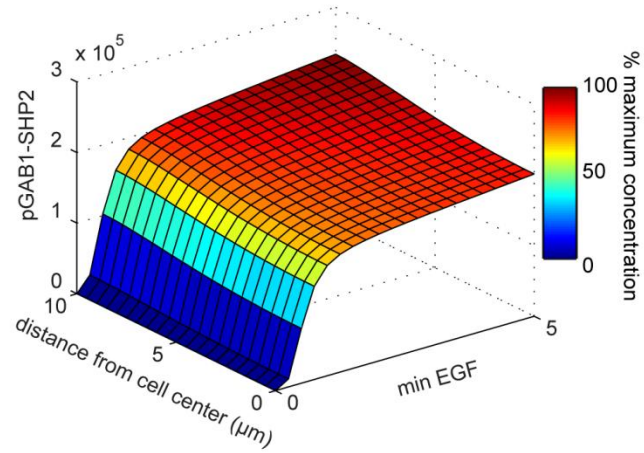
(A) The concentration of phosphorylated EGFR at the plasma membrane, which was normalized to the maximum phospho-EGFR concentration, was predicted for an EGF-pulse EGFR inhibitor-chase simulation, where a 5 min 10 ng/mL EGF treatment was followed by a 2 min EGFR inhibition simulation. The reaction-diffusion model prediction for the concentration of phosphorylated EGFR as a function of time following EGFR inhibition was compared to predictions from our previous model (reaction-only) where the EGFR inhibitor gefitinib was explicitly included in the model topology. (B-C) The concentrations of GAB1-SHP2 complexes and active SFKs at the indicated times following EGFR inhibition were normalized by their concentrations prior to EGFR inhibition and plotted as a function of distance from the cell center.

**Model extensions.** While our previous experimental data suggest that a significant fraction of SFKs exist within the cytosol (Chapter 4), where in some cases SFKs have been shown to be phosphorylated at the active site [160], other reports suggest that SFKs may only exist in an active state primarily at the plasma membrane due to SFK myristoylation [158]. To investigate how this aspect of SFK localization would affect our model prediction of the cellular GAB1-SHP2 length scale, we altered our model topology to allow SFKs to exist in an active state only at the plasma membrane. This change caused GAB1-SHP2 association to drop rapidly away from the cell surface (Figure 5-4A), with the length scale for GAB1-SHP2 association mirroring that for active SFKs from the base model topology (Figure 5-1C). The model parameters can be adjusted for this topology to generate a steady-state GAB1-SHP2 concentration gradient similar to that predicted by the base model, such as by increasing protein diffusivity or decreasing the GAB1 dephosphorylation rate constant (Figures 5-4B-C), however these adjustments do not fully recapitulate the average concentration of GAB1-SHP2 complexes or the precise dynamics of GAB1-SHP2 complex formation represented by the best-fit model.

**A** SFKs only active at plasma membrane; base model parameters



**B** SFKs only active at plasma membrane;  $10\times D$



**C** SFKs only active at plasma membrane;  $0.1\times k_{G1dp}$

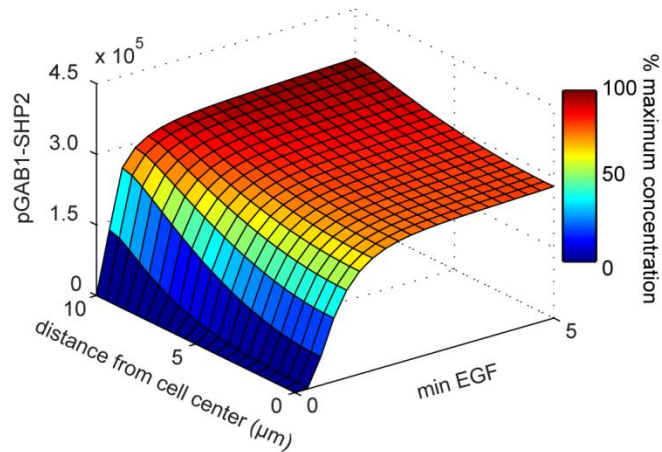


**Figure 5-4: Model predictions for SFKs only existing at the cell surface.**

(**A-C**) Model predictions for the concentrations GAB1-SHP2 complexes were plotted as a function of distance from the cell center and time following treatment with 10 ng/mL EGF when SFKs were only permitted to be active at the cell surface for either the base model parameters (**A**), a 10-fold increase in the diffusivity ( $D$ ) of all cytosolic proteins (**B**), or a 10-fold decrease in  $k_{G1dp}$  (**C**).

## 5-5 DISCUSSION

Our analysis reveals that GAB1 and SHP2 are predicted to remain associated throughout the cytosol to a significant degree due to the capacity for EGFR to activate intermediary SFKs to maintain cytosolic GAB1 phosphorylation throughout GAB1 phosphorylation/dephosphorylation cycles (Figure 5-5). This mechanism could permit EGFR to regulate signaling events through SHP2 at intracellular locations where EGFR is not present. Indeed, this possibility is suggested by a previous study which found that EGFR-activated SHP2 was required to dephosphorylate paxillin at focal adhesions, which themselves could be located a cell diameter away from EGFR if EGFR were activated at the apical membrane, rather than the basolateral membrane [55].

We note that the model conclusion of GAB1 and SHP2 remaining associated throughout the cytosol is based in part on this model's parameterization to previous experimental data gathered from a representative lung adenocarcinoma cell line expressing wild-type EGFR (Chapter 4), and that this conclusion may not be broadly applicable to EGFR-mediated induction of GAB1-SHP2 association in all cell backgrounds. This possibility is suggested by a previous study which noted impaired phosphorylation of the SFK member SRC at Y418 [24], an autophosphorylation site required for SRC activity, in an NSCLC cell line expressing a kinase-activated EGFR mutant, suggesting that SFK activity may be impaired in this setting. However, these cells still exhibited GAB1 phosphorylation on par with wild-type EGFR-expressing cells, which require SFKs for GAB1 phosphorylation (Chapter 4; [24] ). Thus, there may be a different mode of GAB1 phosphorylation in the context of *EGFR* mutation, potentially via direct phosphorylation of GAB1 by constitutively active mutant EGFR. Based on our

model predictions for GAB1 phosphorylation occurring only at the plasma membrane (Figure 5-4A), this mechanism would significantly decrease the length scale over which phospho-GAB1 and GAB1-SHP2 complexes extend into the cytosol away from the membrane. This possibility may offer additional insight into the impairment of SHP2's function observed in cells with *EGFR* mutation [164], as a previous study from our group revealed that SHP2 function is impaired in mutant EGFR-expressing cells through apparent sequestration of active SHP2 at the plasma membrane with internalization-impaired EGFR mutants [164].

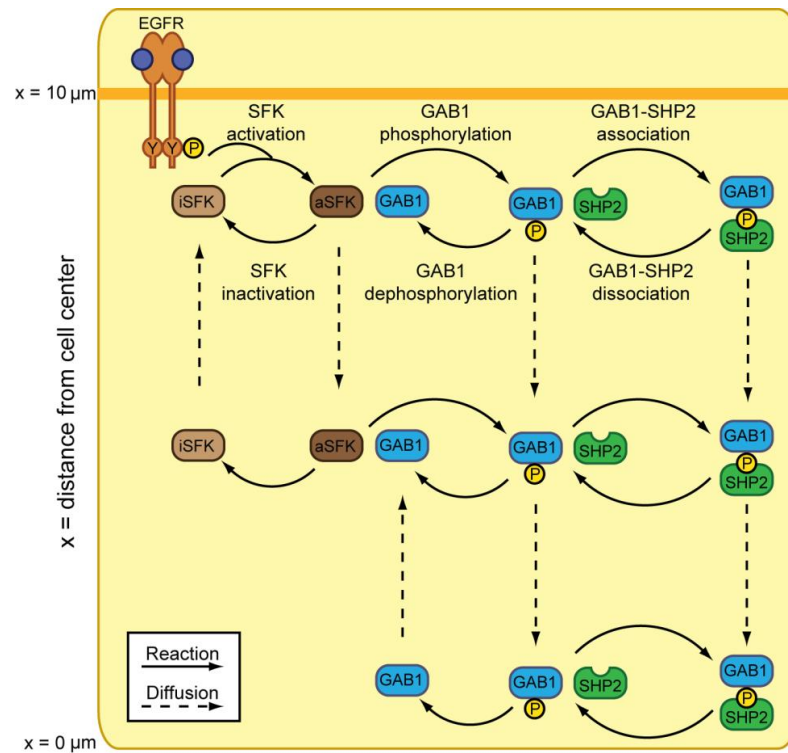


**Figure 5-5: Cytosolic SRC family kinases (SFKs) extend the intracellular GAB1-SHP2 length scale by rephosphorylating GAB1.**

Because SFKs can only be activated at the plasma membrane by EGFR and can be inactivated ubiquitously throughout the cytosol by c-SRC kinase, our model predictions suggest that the local cytosolic concentration of active SFKs drops steeply as a function

of distance from the plasma membrane. Conversely, while GAB1 and SHP2 dissociate and GAB1 is dephosphorylated throughout the cytosol, the length scale of GAB1 phosphorylation and GAB1-SHP2 association are extended relative to that of active SFKs due to the capacity for GAB1 to be phosphorylated throughout the cytosol.

Our analysis revealed that the GAB1-SHP2 length scale was sensitive to perturbations in the rate constants for SFK inactivation and GAB1 dephosphorylation, but interestingly was much less sensitive to the rate constants for SFK activation and GAB1 phosphorylation (Figure 5-2A). In fact, the rate constant for SFK activation had essentially no control over the steady state cellular distribution of GAB1-SHP2 complexes. This is likely the result of the model topology only permitting SFKs to be activated at the cell surface by membrane-bound EGFR, as SFKs will still be rapidly inactivated throughout the cytosol even if the surface concentration of active SFKs is increased or reaches steady state more quickly. This is similar to our finding that shows that despite the requirement for surface-associated EGFR to temporally activate cytosolic SFKs, EGFR only weakly controls the spatial gradient of GAB1-SHP2 complexes within the cell (Figure 5-2E). Our parameter analysis also revealed that an increased concentration of SFKs can offset a reduction in the GAB1-SHP2 length scale caused by an enhanced rate of GAB1 dephosphorylation, but not a reduction in this length scale caused by an enhanced rate of SFK inactivation, exemplifying that there are diverse relationships among cellular processes in dictating the spatial distribution of GAB1-SHP2 complexes.

Characteristic GAB1-SHP2 reaction-diffusion time scales based on the diffusivity of a GAB1-SHP2 complex and the rate constant for GAB1 dephosphorylation suggest that GAB1 needs to be phosphorylated ~4 times by SFKs throughout the cytosol to

permit an individual GAB1-SHP2 complex to diffuse to the cell center from the cell surface. While our model suggests that this does occur, as the concentration of GAB1-SHP2 complexes remain essentially the same at the cell center relative to the cell surface, the concentration of active SFKs is substantially reduced distal from the plasma membrane. However, even this relatively low concentration of intracellular active SFKs is still sufficient to permit the necessary number of GAB1 phosphorylation events required to maintain a much higher extent of GAB1 phosphorylation and GAB1-SHP2 association in proximity to the cell center, consistent with findings from our previous study which showed that SFKs amplify EGFR activity to maintain GAB1-SHP2 association at low levels of EGFR phosphorylation (Chapter 4).

While our model utilized parameters either taken from literature or fit to predictions from a model we previously developed (Chapter 4), the refinement and verification of this model's parameters will be aided by the generation of experimental data specifying the spatial distribution of GAB1-SHP2 complexes within a cell, such as data which could be obtained from FRET microscopy. While no such data currently exists, our previous findings show that GAB1-SHP2 complexes do exist primarily in the cytosol rather than membrane compartments (Chapter 4). It would also be beneficial to experimentally measure the diffusivity of all the cytosolic proteins included in the model by microscopy techniques such as fluorescence recovery after photobleaching (FRAP), as current predictions rely on the assumption of a previously reported estimate for protein diffusivity in the cytosol [161], which is assumed to be the same for all species in our model. In addition to the verification of model predictions through refining model parameters based on fitting to newly acquired experimental data, additional cellular

processes can be incorporated into the model to more completely recapitulate all cellular processes relevant to cytosolic protein complex assemblies. Some of these processes to consider which can control the spatial organization of multiprotein complexes include receptor internalization [166-168] and coordinated protein complex assembly via cytosolic scaffold proteins [170].

In a broad sense, the model described in this study offers a platform to study the spatial distribution of cytosolic phospho-proteins or protein complexes initiated by the activity of plasma membrane-associated receptors. In cases where experimental data is unavailable to compare against model predictions, the model can still be used to both identify individual cellular processes which strongly control a protein's spatial distribution and to study how multiple processes interact with or compensate for one another. The capacity for relevant model parameters to be fit to experimental data such as that which could be obtained by FRET microscopy will enable a more quantitative understanding of how the dynamics of cellular reactions such as dephosphorylation compete against diffusion to ultimately control the cellular length scale over which a receptor tyrosine kinase can orchestrate the assembly of cytosolic protein complexes.

## 5-6 ACKNOWLEDGEMENTS

We thank Dr. Talid R. Sinno for providing helpful feedback on development of the model.

## 5-7 SUPPLEMENTAL MODEL DEVELOPMENT

*Reaction-diffusion equations and initial and boundary conditions.* The equations and initial and boundary conditions for all protein monomers and complexes included in the model are described according to the following abbreviations:

### Concentrations of cytosolic protein monomers and complexes:

$C_{SFK,i}$  = inactive SFK  
 $C_{SFK,a}$  = active SFK  
 $C_{G1}$  = GAB1  
 $C_{PG1}$  = pGAB1  
 $C_{G2}$  = GRB2  
 $C_{G2G1}$  = GRB2-GAB1  
 $C_{G2PG1}$  = GRB2-pGAB1  
 $C_S$  = SHP2  
 $C_{PG1S}$  = pGAB1-SHP2  
 $C_{G2PG1S}$  = GRB2-pGAB1-SHP2

### Concentrations of membrane protein monomers and complexes:

$C_{mE}$  = EGFR monomer  
 $C_{mES}$  = EGF-bound EGFR monomer  
 $C_{mESmES}$  = EGF-bound EGFR dimer  
 $C_{E_p}$  = EGF-bound pEGFR dimer  
 $C_{EG2}$  = EGF-bound, GRB2-bound pEGFR dimer  
 $C_{EG2G1}$  = EGF-bound, GRB2-GAB1-bound pEGFR dimer  
 $C_{EG2PG1}$  = EGF-bound, GRB2-pGAB1-bound pEGFR dimer  
 $C_{EG2PG1S}$  = EGF-bound, GRB2-pGAB1-SHP2-bound pEGFR dimer

### Model parameters:

$D_S$  = SFK diffusivity  
 $D_{G2}$  = GRB2 diffusivity  
 $D_{G2G1}$  = GRB2-GAB1 diffusivity  
 $D_{G2G1S2}$  = GRB2-GAB1-SHP2 diffusivity  
 $D_{G1}$  = GAB1 diffusivity  
 $D_{G1S2}$  = GAB1-SHP2 diffusivity  
 $D_{S2}$  = SHP2 diffusivity  
 $k_{S,i}$  = SFK inactivation  
 $k_{S,a}$  = SFK activation  
 $k_{G1,f}$  = GAB1 binding, forward  
 $k_{G1,r}$  = GAB1 binding, reverse  
 $k_{G1p}$  = GAB1 phosphorylation  
 $k_{G1dp}$  = GAB1 dephosphorylation  
 $k_{G2,f}$  = GRB2 binding, forward  
 $k_{G2,r}$  = GRB2 binding, reverse

$k_{S2,f}$  = SHP2 binding, forward  
 $k_{S2,r}$  = SHP2 binding, reverse  
 $k_{E,f}$  = EGF binding, forward  
 $k_{E,r}$  = EGF binding, reverse  
 $k_{dE,f}$  = EGFR dimerization, forward  
 $k_{dE,r}$  = EGFR dimerization, reverse  
 $k_{catE}$  = EGFR phosphorylation  
 $k_{dp}$  = EGFR dephosphorylation  
 $[EGF]$  = EGF concentration

Equations and boundary conditions:

Equation and initial and boundary conditions for  $C_{SFk,i}$  as a function of time ( $t$ ) and space ( $x$ ), where  $t = 0$  corresponds to the initial time prior to EGF treatment,  $x = 0$  corresponds to the cell center, and  $x = 10$  corresponds to the cell surface:

$$\frac{\partial C_{SFk,i}}{\partial t} = D_s \frac{\partial^2 C_{SFk,i}}{\partial x^2} + k_{S,i} C_{SFk,a}$$

$$D_s \frac{\partial C_{SFk,i}}{\partial x}(10) = -k_{S,a} C_{SFk,i} C_{E\_tot}$$

$$D_s \frac{\partial C_{SFk,i}}{\partial x}(0) = 0$$

$$C_{SFk,i}(0) = 600,000$$

Equation and initial and boundary conditions for  $C_{SFk,a}$ :

$$\frac{\partial C_{SFk,a}}{\partial t} = D_s \frac{\partial^2 C_{SFk,a}}{\partial x^2} - k_{S,i} C_{SFk,a}$$

$$D_s \frac{\partial C_{SFk,a}}{\partial x}(10) = k_{S,a} C_{SFk,i} C_{E\_tot}$$

$$D_s \frac{\partial C_{SFk,a}}{\partial x}(0) = 0$$

$$C_{SFk,a}(0) = 0$$

Equation and initial and boundary conditions for  $C_{G1}$ :

$$\frac{\partial C_{G1}}{\partial t} = D_{G1} \frac{\partial^2 C_{G1}}{\partial x^2} - k_{G1,f} C_{G1} C_{G2} + k_{G1,r} C_{G2G1} - k_{G1p} C_{SFk,a} C_{G1} + k_{G1dp} C_{PG1}$$

$$D_{G1} \frac{\partial C_{G1}}{\partial x}(10) = k_{G1,f} C_{G1} C_{EG2} - k_{G1,r} C_{EG2G1}$$

$$D_{G1} \frac{\partial C_{G1}}{\partial x}(0) = 0$$

$$C_{G1}(0) = 600,000$$

Equation and initial and boundary conditions for  $C_{PG1}$ :

$$\begin{aligned} \frac{dC_{PG1}}{dt} = & D_{G1} \frac{\partial^2 C_{PG1}}{\partial x^2} - k_{G1,f} C_{PG1} C_{G2} + k_{G1,r} C_{G2PG1} + k_{G1p} C_{SFK,a} C_{G1} \\ & - k_{G1dp} C_{PG1} - k_{S2,f} C_{PG1} C_S + k_{S2,r} C_{PG1S} \end{aligned}$$

$$D_{G1} \frac{\partial C_{PG1}}{\partial x}(10) = k_{G1,f} C_{PG1} C_{EG2} - k_{G1,r} C_{EG2PG1}$$

$$D_{G1} \frac{\partial C_{PG1}}{\partial x}(0) = 0$$

$$C_{PG1}(0) = 0$$

Equation and initial and boundary conditions for  $C_{G2}$ :

$$\begin{aligned} \frac{dC_{G2}}{dt} = & D_{G2} \frac{\partial^2 C_{G2}}{\partial x^2} - k_{G1,f} C_{G1} C_{G2} + k_{G1,r} C_{G2G1} - k_{G1,f} C_{PG1} C_{G2} + k_{G1,r} C_{G2PG1} \\ & - k_{G1,f} C_{G2} C_{PG1S} + k_{G1,r} C_{G2PG1S} \end{aligned}$$

$$D_{G2} \frac{\partial C_{G2}}{\partial x}(10) = k_{G2,f} C_{G2} C_E - k_{G2,r} C_{EG2}$$

$$D_{G2} \frac{\partial C_{G2}}{\partial x}(0) = 0$$

$$C_{G2}(0) = 600,000$$

Equation and initial and boundary conditions for  $C_{G2G1}$ :

$$\frac{dC_{G2G1}}{dt} = D_{G2G1} \frac{\partial^2 C_{G2G1}}{\partial x^2} + k_{G1,f} C_{G1} C_{G2} - k_{G1,r} C_{G2G1} - k_{G1p} C_{SFK,a} C_{G2G1} + k_{G1dp} C_{G2PG1}$$

$$D_{G2G1} \frac{\partial C_{G2G1}}{\partial x}(10) = k_{G2,f} C_{G2G1} C_E - k_{G2,r} C_{EG2G1}$$

$$D_{G2G1} \frac{\partial C_{G2G1}}{\partial x}(0) = 0$$

$$C_{G2G1}(0) = 0$$

Equation and initial and boundary conditions for  $C_{G2PG1}$ :

$$\begin{aligned} \frac{dC_{G2PG1}}{dt} = & D_{G2G1} \frac{\partial^2 C_{G2PG1}}{\partial x^2} + k_{G1,f} C_{PG1} C_{G2} - k_{G1,r} C_{G2PG1} + k_{G1p} C_{SFK,a} C_{G2G1} \\ & - k_{G1dp} C_{G2PG1} - k_{S2,f} C_{G2PG1} C_S + k_{S2,r} C_{G2PG1S} \end{aligned}$$

$$D_{G2G1} \frac{\partial C_{G2PG1}}{\partial x}(10) = k_{G2,f} C_{G2PG1} C_E - k_{G2,r} C_{EG2PG1}$$

$$D_{G2G1} \frac{\partial C_{G2PG1}}{\partial x}(0) = 0$$

$$C_{G2PG1}(0) = 0$$

Equation and initial and boundary conditions for  $C_S$ :

$$\frac{dC_S}{dt} = D_{S2} \frac{\partial^2 C_S}{\partial x^2} - k_{S2,f} C_{PG1} C_S + k_{S2,r} C_{PG1S} - k_{S2,f} C_{G2PG1} C_S + k_{S2,r} C_{G2PG1S}$$

$$D_{S2} \frac{\partial C_S}{\partial x}(10) = k_{S2,f} C_S C_{EG2PG1} - k_{S2,r} C_{EG2PG1S}$$

$$D_{S2} \frac{\partial C_S}{\partial x}(0) = 0$$

$$C_S(0) = 600,000$$

Equation and initial and boundary conditions for  $C_{PG1S}$ :

$$\frac{dC_{PG1S}}{dt} = D_{G1S2} \frac{\partial^2 C_{PG1S}}{\partial x^2} + k_{S2,f} C_{PG1} C_S - k_{S2,r} C_{PG1S} - k_{G1,f} C_{G2} C_{PG1S} + k_{G1,r} C_{G2PG1S}$$

$$D_{G1S2} \frac{\partial C_{PG1S}}{\partial x}(10) = k_{G1,f} C_{PG1S} C_{EG2} - k_{G1,r} C_{EG2PG1S}$$

$$D_{G1S2} \frac{\partial C_{PG1S}}{\partial x}(0) = 0$$

$$C_{PG1S}(0) = 0$$

Equation and initial and boundary conditions for  $C_{G2PG1S}$ :

$$\begin{aligned} \frac{dC_{G2PG1S}}{dt} = & D_{G2G1S2} \frac{\partial^2 C_{G2PG1S}}{\partial x^2} + k_{S2,f} C_{G2PG1} C_8 - k_{S2,r} C_{G2PG1S} \\ & + k_{G1,f} C_{G2} C_{PG1S} - k_{G1,r} C_{G2PG1S} \end{aligned}$$

$$D_{G2G1S2} \frac{\partial C_{G2PG1S}}{\partial x}(10) = k_{G2,f} C_{G2PG1S} C_E - k_{G2,r} C_{EG2PG1S}$$

$$D_{G2G1S2} \frac{\partial C_{G2PG1S}}{\partial x}(0) = 0$$

$$C_{G2PG1S}(0) = 0$$

Equation and initial condition for  $C_{mE}$ :

$$\frac{dC_{mE}}{dt} = -[EGF]k_{E,f} C_{mE} + k_{E,r} C_{mES}$$

$$C_{mE}(0) = 600,000$$

Equation and initial condition for  $C_{mES}$ :

$$\frac{dC_{mES}}{dt} = [EGF]k_{E,f} C_{mE} - k_{E,r} C_{mES} - k_{dE,f} C_{mES} C_{mES} + k_{dE,r} C_{mESmES}$$

$$C_{mES}(0) = 0$$

Equation and initial condition for  $C_{mESmES}$ :

$$\frac{dC_{mESmES}}{dt} = k_{dE,f} C_{mES} C_{mES} - k_{dE,r} C_{mESmES} - k_{catE} C_{mESmES} + k_{dp} C_E$$

$$C_{mESmES}(0) = 0$$

Equation and initial condition for  $C_E$ :

$$\begin{aligned} \frac{dC_E}{dt} = & -k_{G2,f}C_{G2}C_E + k_{G2,r}C_{EG2} - k_{G2,f}C_{G2G1}C_E + k_{G2,r}C_{EG2G1} - k_{G2,f}C_{G2PG1}C_E \\ & + k_{G2,r}C_{EG2PG1} - k_{G2,f}C_{G2PG1S}C_E + k_{G2,r}C_{EG2PG1S} + k_{catE}C_{mESmES} - k_{dp}C_E \end{aligned}$$

$$C_E(0) = 0$$

Equation and initial condition for  $C_{EG2}$ :

$$\begin{aligned} \frac{dC_{EG2}}{dt} = & -k_{G1,f}C_{G1}C_{EG2} + k_{G1,r}C_{EG2G1} - k_{G1,f}C_{PG1}C_{EG2} + k_{G1,r}C_{EG2PG1} \\ & + k_{G2,f}C_{G2}C_E - k_{G2,r}C_{EG2} - k_{G1,f}C_{PG1S}C_{EG2} + k_{G1,r}C_{EG2PG1S} \end{aligned}$$

$$C_{EG2}(0) = 0$$

Equation and initial condition for  $C_{EG2G1}$ :

$$\begin{aligned} \frac{dC_{EG2G1}}{dt} = & k_{G1,f}C_{G1}C_{EG2} - k_{G1,r}C_{EG2G1} + k_{G2,f}C_{G1}C_{EG2} - k_{G2,r}C_{EG2G1} \\ C_{EG2G1}(0) = & 0 \end{aligned}$$

Equation and initial condition for  $C_{EG2PG1}$ :

$$\begin{aligned} \frac{dC_{EG2PG1}}{dt} = & k_{G1,f}C_{PG1}C_{EG2} - k_{G1,r}C_{EG2G1} + k_{G2,f}C_{G2PG1}C_E - k_{G2,r}C_{EG2PG1} \\ & - k_{S2,f}C_S C_{EG2PG1} + k_{S2,r}C_{EG2PG1S} \end{aligned}$$

$$C_{EG2PG1}(0) = 0$$

Equation and initial condition for  $C_{EG2PG1S}$ :

$$\begin{aligned} \frac{dC_{EG2PG1S}}{dt} = & k_{S2,f}C_S C_{EG2PG1} - k_{S2,r}C_{EG2PG1S} + k_{G1,f}C_{PG1S}C_{EG2} \\ & - k_{G2,r}C_{EG2PG1S} + k_{G2,f}C_{G2PG1S}C_E - k_{G2,r}C_{EG2PG1S} \end{aligned}$$

$$C_{EG2PG1S}(0) = 0$$

**Discretization scheme using finite difference methods.** Ordinary differential equations were discretized using a forward explicit finite difference method as follows, where  $h$  is the step size between two discretized time points ( $h = t_{i+1} - t_i$ ):

$$\frac{\partial C}{\partial t} = k_1 C$$

$$\frac{C_{i+1} - C_i}{h} = k_1 C_i$$

This discretized equation can then be rearranged to solve for  $C$  at time point  $t_{i+1}$ , given that values for  $C$  at time point  $t_i$  are known:

$$C_{i+1} = (h \cdot k_1 + 1)C_i$$

Partial differential equations were discretized using a forward explicit finite difference method for first-order derivatives, where  $h$  is the step size between two discretized time points ( $h = t_{i+1} - t_i$ ), and a central explicit finite difference method for second-order derivatives, where  $r$  is the step size between two discretized space points ( $r = x_{j+1} - x_j$ ), as follows:

$$\frac{\partial C}{\partial t} = D \frac{\partial^2 C}{\partial x^2}$$

$$\frac{C_{i+1,j} - C_{i,j}}{h} = D \frac{C_{i,j+1} - 2C_{i,j} + C_{i,j-1}}{r^2}$$

This discretized equation can then be rearranged to solve for  $C$  at time point  $t_{i+1}$  and space point  $x_j$ , given that values for  $C$  at space points  $x_{j-1}$ ,  $x_j$ , and  $x_{j+1}$  at time point  $t_i$  are known.

$$C_{i+1,j} = \left(1 - \frac{2D \cdot h}{r^2}\right)C_{i,j} + \frac{D \cdot h}{r^2}C_{i,j-1} + \frac{D \cdot h}{r^2}C_{i,j+1}$$

To simultaneously solve the discretized equations for membrane-associated species which are coupled with the discretized boundary conditions for cytosolic species,

an implicit finite difference method was utilized as follows, shown here for an example involving the discretized equations for two membrane-associated species ( $C1$  and  $C2$ ) and the discretized boundary condition for one cytosolic species ( $C3$ ):

Discretized equation for  $C1$ :

$$\frac{dC1}{dt} = -C3 \cdot C1 + C2$$

$$\frac{C1_{i+1} - C1_i}{h} = -C3_{i+1,j} \cdot C1_i + C2_i$$

Discretized equation for  $C2$ :

$$\frac{dC2}{dt} = C3 \cdot C1 - C2$$

$$\frac{C2_{i+1} - C2_i}{h} = C3_{i+1,j} \cdot C1_i - C2_i$$

Discretized boundary condition for  $C3$ :

$$D \frac{\partial C3}{\partial x} = C3 \cdot C1 - C2$$

$$D \frac{C3_{i+1,j} - C3_{i+1,j-1}}{r} = C3_{i+1,j-1} \cdot C1_{i+1} - C2_{i+1}$$

Due to the fact that  $C1_{i+1}$ ,  $C2_{i+1}$ , and  $C3_{i+1,j}$  are all unknown, initial guesses are provided for  $C1_{i+1}$  and  $C2_{i+1}$  to solve for  $C3_{i+1,j}$ , which is then used to solve for  $C1_{i+1}$  and  $C2_{i+1}$  according to the discretized equations above. These updated values are then used to resolve for  $C3_{i+1,j}$ , and this process is iterated until convergence is reached.

Discretization of boundary conditions for cytosolic species at the cell center results in the requirement for the concentration of a given cytosolic species to be equivalent at the cell center node and the space node immediately adjacent to it, as illustrated below:

$$D\frac{dC}{dx}(0) = 0$$

$$D\frac{C_{i+1}-C_i}{r} = 0$$

$$C_{i+1} = C_i$$

## **Chapter 6: Conclusions and Future Work**

### **6-1 SUMMARY**

One of the more clinically relevant findings of this thesis is that SHP2, as a driver of cell proliferative and survival through its activation of ERK, can promote resistance to the EGFR inhibitor gefitinib in wild-type EGFR-expressing NSCLC cells (Chapter 2). Consequently, NSCLC cells expressing kinase-activated EGFR mutants display enhanced cellular sensitivity to gefitinib at least partially due to impaired cellular function of SHP2. This study further identified a mechanism for impairment of SHP2's function in these cells via sequestration of biochemically active SHP2 with internalization-impaired mutant EGFR at the plasma membrane, a phenomenon that could also potentially be of relevance to other cytosolic signaling proteins that can either directly or indirectly bind EGFR. While this work identified SHP2 as a potential therapeutic target for subsets of NSCLCs, additional studies conversely identified SHP2 as a promoter of sensitivity to targeted therapeutics in GBM cells (Chapter 3). Despite the necessity of SHP2 expression for optimal response of GBM cells to EGFR/c-MET co-inhibition, SHP2 was also required for GBM tumorigenesis in a mouse xenograft model, potentially as a result of a newly discovered regulatory role for SHP2 in promoting the expression of hypoxia inducible factors. While previous studies have explored either oncogenic or tumor suppressor roles of SHP2 in various cell backgrounds [59, 71, 73, 109], this work provides the first evidence for SHP2 to simultaneously promote and antagonize proliferative/survival phenotypes in the same cell line.

Additional experimental and computational work undertaken in this thesis resulted in an improved understanding of the dynamics of SHP2's activation downstream of EGFR through SHP2's association with GAB1 (Chapter 4), as well as computational modeling predictions that suggest EGFR can potentially regulate SHP2's association with GAB1 throughout the entire cell volume as a result of EGFR's activation of cytosolic SFKs (Chapter 5). These results not only offer an updated view on how EGFR activates SHP2, which was traditionally considered to only be maintained in an active state when in complex with receptors such as EGFR [28], but may also offer broad insight into the means by which receptor proteins regulate the assembly of phosphorylation-dependent cytosolic signaling protein complexes, given that phosphotyrosine-SH2 domain interactions are exceedingly transient [61, 62] and cellular phosphatase activity is high [63, 64]. In the remainder of this chapter, we discuss the implications of our findings and suggest directions for future studies.

## 6-2 DEVELOPMENT AND APPLICATION OF SHP2 INHIBITORS

As SHP2 was shown to promote resistance to EGFR inhibitors in NSCLC cells and to promote tumorigenesis in GBM cells (Chapters 2 and 3), and also given that there exist numerous other reports detailing SHP2's oncogenic roles and overexpression in many cancers [69-71], it would be worthwhile to develop a specific and effective SHP2 inhibitor as a possible cancer therapeutic to use as either a single agent or in combination with other therapeutics such as EGFR inhibitors. While the development of specific and cell permeable small molecular inhibitors for protein kinases has been relatively successful, with 26 currently approved by the FDA, the development of inhibitors for

protein tyrosine phosphatases has been far more challenging. Due to the highly polar nature of the active site of phosphatases, compounds that tightly bind this site and inhibit phosphatase activity tend to be highly charged anionic phosphate mimics that are unable to pass through the plasma membrane [171]. In addition, since the phosphatase active site tends to be highly conserved among PTP family members, such as for PTP1B and TCPTP [171], the development of phosphatase inhibitors lacking undesirable off-target effects is also difficult.

Despite these challenges, several promising SHP2 inhibitors have been identified and tested in both cell culture and mouse models [171]. Among these include NSC-87877, an SHP2 inhibitor with a reported  $IC_{50}$  value of 0.3  $\mu M$  *in vitro* [172]. However, this inhibitor has not been widely used in laboratory studies, suggesting its specificity and efficacy may not be on par with other methods of antagonizing cellular SHP2 activity such as SHP2 knockdown. While this inhibitor was selective over most other phosphatases, it unfortunately also targets SHP1 [172], a submember of the SHP family of phosphatases that is highly homologous to SHP2 [28]. Additional screens that sought to identify SHP2 inhibitors that target both the active site of SHP2 as well as an adjacent region for specificity identified the inhibitor II-B08, that possesses an  $IC_{50}$  value of 5.5  $\mu M$  for SHP2 and includes the added benefit of selectivity against SHP1 [173]. While not an exceptionally potent inhibitor, a recent study found that II-B08 could slow proliferation of H1975 NSCLC cells *in vitro* and could also slightly reduce the growth rate of H1975 tumor xenografts [174]. Given the promising results from this study, it will be interesting to see if the development of improved SHP2 inhibitors will be able to more closely resemble the effects achieved with near complete knockdown of SHP2

observed with SHP2 shRNA or siRNA, which in some cases can completely inhibit the growth of certain tumors in mouse models [109].

As potent, selective, and cell permeable inhibitors developed for the phosphatase PTP1B have made it to clinical trial testing [171], the possibility for the development of similarly functional SHP2 inhibitors seems promising. While clinical trials involving the inhibition of SHP2 will require the development of better SHP2 inhibitors than currently available, it may still be useful now to examine whether SHP2 serves as a biomarker for cancer aggressiveness and patient survival. Due to the high frequency with which SHP2 has been found to be overexpressed in cancers including those of the lung and breast [69, 70, 175], it is highly likely that SHP2 plays an important role in the tumorigenesis and progression of solid tumors in humans, as suggested by the copious number of studies identifying oncogenic roles of SHP2 in cell culture and xenograft models [71]. Given that increasingly more paired data for protein expression with patient outcome is becoming publicly available through programs such as The Cancer Genome Atlas, we would recommend a study seeking to correlate the expression level of SHP2 in various cancers with patient outcomes including survival, metastasis, and response to therapy. Furthermore, it would be interesting to undertake additional studies similar to those performed in Chapters 2 and 3 of this thesis to explore the role of SHP2 in mediating therapeutic response, both for other cancers that are dependent on EGFR as well as cancers normally treated with chemotherapeutics or other targeted inhibitors. It would also be worthwhile to explore the potential requirement for SHP2 in the tumorigenesis of cancers originating from aberrant phosphorylation of SHP2 adapters, such as for

BCR/ABL-mediated lymphoid cancers requiring GAB2 hyperphosphorylation for transformation [176].

### 6-3 INVOLVEMENT OF SHP2 IN EPITHELIAL-TO-MESENCHYMAL TRANSITION

A recent study from Buonato and Lazzara showed that NSCLC cells require ERK for epithelial-to-mesenchymal transition (EMT) [177], a process whereby epithelial cells lose cell-cell adhesions to obtain a mesenchymal cell phenotype that imparts enhanced motility, invasiveness, and resistance to therapeutics [178, 179]. Specifically, Buonato and Lazzara showed that inhibiting ERK for a sufficiently long time caused NSCLC cells to revert from a mesenchymal phenotype to an epithelial phenotype, which enhanced cellular response to the EGFR inhibitor gefitinib [177]. Given that the study performed in Chapter 2 of this thesis showed that SHP2 strongly controls both ERK activity and cellular response to EGFR inhibition, it is possible that SHP2 also regulates EMT in a way which may connect SHP2's control over ERK with determining therapeutic response. While this hypothesis has not been explored in the context of NSCLC cells, other studies showed that SHP2 can regulate EMT in breast cancer cells [74], although the mechanism by which SHP2 regulated EMT and the implications of SHP2's control over EMT on dictating cellular response to therapeutics were not explored.

To investigate a possible link between SHP2 function and EMT in NSCLC cells, we propose a study that would first seek to measure the impact of SHP2 knockdown on the expression of epithelial and mesenchymal markers, such as E-cadherin and vimentin, respectively, in cells exhibiting a mesenchymal phenotype. Provided SHP2 regulates

EMT in these cells and SHP2 knockdown shifts cells to a more epithelial phenotype, it could then be determined whether SHP2 controls EMT in an ERK-dependent or – independent manner by attempting to restore cells to their basal mesenchymal status by expressing kinase-activated mutant MEK, the kinase immediately upstream of ERK in the MAPK cascade [180]. If constitutively active MEK expression overrides the effect of SHP2 knockdown on ERK phosphorylation and restores the mesenchymal status of cells, this would suggest that SHP2's control over ERK regulates EMT. However, if constitutively active MEK expression in SHP2-depleted cells restores ERK phosphorylation to basal levels but fails to revert cells back to a mesenchymal phenotype, this would suggest that SHP2 regulates EMT through an ERK-independent pathway.

Since the study by Buonato and Lazzara determined that cells co-treated with a MEK and EGFR inhibitor are optimally sensitized when initially pretreated with a MEK inhibitor to first induce a mesenchymal-to-epithelial transition before initiating treatment with an EGFR inhibitor [177], it would be worthwhile to relate this finding to the study performed in Chapter 2 of this thesis. Because our study utilized stable rather than transient knockdown of SHP2, it is likely that our study would have essentially mimicked that of Buonato and Lazzara in that SHP2-depleted cells would have had decreased levels of ERK activity and potentially an epithelial phenotype for a prolonged period of time prior to treatment with gefitinib. To determine whether SHP2 regulates response to EGFR inhibition by controlling cellular processes that occur over a long period of time, such as EMT, or solely by transiently controlling the activity of signaling pathways, such as ERK, we would recommend the use of an inducible SHP2 shRNA or an SHP2 inhibitor to transiently inhibit SHP2 immediately before treating cells with gefitinib.

Alternatively, if SHP2 is confirmed to regulate EMT in NSCLC cells, a study attempting to restore SHP2-depleted cells back to a mesenchymal phenotype through the overexpression of transcription factors known to be promote EMT, such as ZEB1, could be performed. It would be interesting to see if merely converting SHP2-depleted cells back to a mesenchymal phenotype is sufficient to prevent SHP2 knockdown from enhancing cellular response to gefitinib.

#### 6-4 INDUCIBLE KNOCKDOWN OF SHP2 IN GLIOBLASTOMA XENOGRAFTS

In Chapter 3 of this thesis, we sought to determine whether the net effect of SHP2 function in glioblastoma cells *in vitro*, where SHP2 simultaneously promotes proliferation and antagonizes cell survival in response to co-inhibition of EGFR and c-MET, could be reproduced *in vivo* through the use of a mouse xenograft model. While tumors arising from glioblastoma cells with SHP2 knockdown grew much more slowly than tumors arising from control cells, tumors consisting of cells with SHP2 knockdown never grew to a sufficient size to compare treatment with gefitinib and PHA665752 against control tumors. To confirm whether SHP2 function still enhances response to EGFR/c-MET co-inhibition *in vivo*, we propose the use of a xenograft model using cells where SHP2 can be conditionally knocked down using shRNA-expression systems such as pSico [86]. This would allow for tumors consisting of cells that conditionally express control or SHP2-targeted shRNA to grow to the appropriate size before inducing shRNA expression, at which point treatment with gefitinib and PHA665752 could begin after SHP2 protein levels are reduced in the appropriate tumors. While STAT3 appears to be the most important determinant downstream of SHP2 in dictating glioblastoma cell

response to EGFR/c-MET co-inhibition *in vitro*, it is possible that SHP2-mediated antagonism of STAT3 may be superseded by pro-survival functions of SHP2 *in vivo* such that tumors with reduced SHP2 expression respond as well if not better than control tumors to gefitinib and PHA665752.

## 6-5 ROLE OF SHP2 PHOSPHORYLATION

While not focused upon in this thesis, an additional purported aspect of SHP2 regulation besides from SHP2's association with adapter proteins such as GAB1 is the phosphorylation of SHP2 on C-terminal tyrosines 542 and 580 [28]. Some studies suggest that these tyrosines, when phosphorylated, enhance SHP2's catalytic activity and ability to activate ERK [29, 181]. When phosphorylated, Y542 and Y580 are suggested to recruit GRB2 [182] or bind SHP2's N-SH2 and C-SH2 domains, respectively, to mimic binding of SHP2 to an adapter protein and thus promote SHP2's catalytic activity [181, 182]. However, SHP2 phosphorylation does not appear to be required for SHP2-mediated ERK activation downstream of all receptor tyrosine kinases, including EGFR [29]. Consistent with this finding, the work performed in Chapter 2 of this thesis determined that rescue of SHP2-depleted NSCLC cells with re-expression of SHP2<sup>Y542F</sup> was able to restore ERK phosphorylation and reduce cellular response to gefitinib just as effectively as rescue with re-expression of wild-type SHP2 (Figure 2-3). However, this study also found that there was a diminished functional role of SHP2 in activating ERK in EGFR mutant-expressing cells exhibiting impaired phosphorylation of SHP2, although sequestration of SHP2 with internalization-impaired EGFR mutants is more likely the direct cause of reduced SHP2 function rather than impaired SHP2 phosphorylation [24].

Given the conflicting evidence for the role of SHP2 phosphorylation in regulating SHP2-mediated ERK activation, both from the work in this thesis and from other studies, additional work aimed at elucidating the importance of SHP2 phosphorylation in SHP2-mediated signaling would be worthwhile to undertake. It would be useful to screen for proteins besides GRB2 that bind phosphorylated SHP2, as GRB2-SHP2 binding does not appear to be required for ERK phosphorylation downstream of growth factor receptors where SHP2 phosphorylation itself is required for maximal ERK phosphorylation [29]. This screen could be accomplished through quantitative mass spectrometry experiments, where SHP2 immunoprecipitates obtained from ligand-treated cells expressing wild-type SHP2 are compared against SHP2 immunoprecipitates from cells expressing SHP2<sup>Y542F</sup>, SHP2<sup>Y580F</sup>, or SHP2<sup>Y542F/Y580F</sup> to determine differences in proteins that co-immunoprecipitate with wild-type or mutant SHP2.

## 6-6 LOCALIZATION OF SHP2 COMPLEXES IN MUTANT EGFR-EXPRESSING CELLS

While our initial work in NSCLC cells suggested that SHP2 function can be impaired via its sequestration with GAB1 and EGFR at the plasma membrane in cells expressing EGFR mutants (Chapter 2), our following studies in a representative cell line expressing wild-type EGFR found that nearly all GAB1-SHP2 complexes were present within the cytosol (Chapter 4). It will be interesting to perform the appropriate subcellular fractionation and subsequent SHP2 immunoprecipitation experiments to determine whether this also occurs in cells expressing mutant EGFR, or whether GAB1-bound SHP2 exists primarily at the plasma membrane as suggested by our hypothesis of

sequestration of activated SHP2 with membrane-bound EGFR. The fraction of bound SHP2 in mutant EGFR-expressing cells could potentially be shifted towards a higher ratio of EGFR:GAB1-bound SHP2 relative to wild-type cells, possibly through sequestration of SHP2 with EGFR in a GAB1-independent manner, such that cytosolic GAB1-SHP2 complexes only represent a small proportion of bound and active SHP2 in cells with *EGFR* mutation. Regardless of whether there are a significant number of GAB1-SHP2 complexes in the cytosol of mutant EGFR-expressing cells, it is clear that GAB1 and thus GAB1-SHP2 complexes are not required for ERK phosphorylation in these cells based on GAB1 knockdown experiments (Figure 2-6).

While we determined that SFKs were required for GAB1 phosphorylation in a wild-type EGFR-expressing NSCLC cell line (Chapter 4), data from a previous study by Lazzara et al. hints that this may not necessarily be true for NSCLC cells expressing mutant EGFR [24]. While GAB1 is phosphorylated to roughly similar extents in H1666 (EGFR<sup>WT</sup>) and H3255 (EGFR<sup>L858R</sup>) NSCLC cells, phosphorylation of the SFK member c-SRC at Y418, an autophosphorylation site required for c-SRC's activity, is severely impaired in H3255 cells relative to H1666 cells [24]. This suggests that there may potentially be different modes of GAB1 phosphorylation depending on *EGFR* mutation status, where wild-type EGFR utilizes cytosolic SFKs to promote GAB1 phosphorylation in the cytosol, while mutant EGFR can sufficiently phosphorylate GAB1 directly at the plasma membrane due to the enhanced kinase activity of this mutant receptor [22]. To test this hypothesis, mutant EGFR-expressing H3255 cells could be treated with the SFK inhibitor PP2 either in the presence or absence of EGF to determine whether SFKs are required for GAB1 phosphorylation in these cells. However, these results could be

confounded by several factors related to either non-specific effects related to PP2's potential inhibition of EGFR [183] or the capacity for SFKs to phosphorylate and increase the activity of EGFR [146], either of which would lead to the false conclusion that SFKs, rather than EGFR, are responsible for phosphorylating GAB1 in these cells. Similar to experiments performed in Chapter 4, H3255 cells would need to be engineered to have knockdown of endogenous EGFR<sup>L858R</sup> and ectopic expression of EGFR<sup>L858R/Y845F</sup> to decouple SFKs from promoting EGFR activity through SFK-mediated phosphorylation of EGFR at Y845. If PP2 addition still results in a significant effect on EGFR phosphorylation, which we did not see for cells expressing wild-type EGFR, either a more specific SFK inhibitor would need to be used, or the ubiquitously expressed SFK members SRC, YES, and FYN will need to be simultaneously knocked down instead, as has been done for previous studies seeking to draw conclusions about the net activity of all SFK members [184]. The results from this study could have important implications for better understanding the impaired functional role of SHP2 in mutant EGFR-expressing cells, which could occur not only due to impairments in the rate of cellular processes such as EGFR internalization (Chapter 2) but also by potential impairments in the activity of cytosolic kinases that regulate SHP2's activity. There also exists the possibility that impaired EGFR internalization prevents the activation of SFKs within the cytosol by endosomal EGFR in such a way that active SFKs are only located near the plasma membrane, as a previous study showed that the SFK member c-SRC traffics with activated EGFR following EGF stimulation [185]. Furthermore, if SFK activity is altered in EGFR mutant-expressing cells in such a way that SFK-mediated amplification of EGFR activity does not occur as it does in a representative cell line expressing wild-type

EGFR, this could cause GAB1-SHP2 dissociation and GAB1 dephosphorylation to occur more quickly in EGFR mutant-expressing cells relative to their wild-type counterparts. This could be tested by comparing the rates of GAB1 dephosphorylation and GAB1-SHP2 dissociation in these cells by western blotting and SHP2 immunoprecipitation EGF-pulse gefitinib-chase experiments, as performed in Chapter 4.

## 6-7 CYTOSOLIC DISTRIBUTION OF GAB1-SHP2 COMPLEXES

Experiments performed in Chapter 4 concluded that the majority of GAB1-SHP2 complexes exist in the cytosol, at least for a wild-type EGFR-expressing cell line. Computational studies performed in Chapter 5 predicted that these cytosolic GAB1-SHP2 complexes are present at a fairly constant concentration throughout the entire cell volume. Given our findings from Chapter 2 that suggest the importance of SHP2's activity within the cytosol, it will be essential to validate these computational predictions experimentally to determine if SHP2 is indeed active and GAB1-bound at a constant concentration throughout the cytosol. However, live-cell experiments that could measure the catalytic activity of SHP2 as a function of cellular localization would be impossible to develop. As an alternative, fluorescence resonance energy transfer (FRET) microscopy, a technique that utilizes the capacity for energy to be transferred between fluorophores located within 10-100 angstroms of one another [186], would be a much more feasible approach to determine where GAB1 and SHP2 are bound within a cell based on transfer of energy between fluorophore-tagged GAB1 and SHP2.

In fact, as part of this thesis work, we attempted to use fluorescence-lifetime imaging microscopy (FLIM), an imaging technique based on FRET principles, to

measure GAB1-SHP2 association in live cells by ectopically expressing fluorophore-tagged GAB1 and SHP2 fusion proteins, GAB1-YPET and SHP2-Cerulean, in cells. Despite attempting these measurements with: 1. all combinations of GAB1 and SHP2 fusion proteins with either N-terminal or C-terminal fluorophore tags, 2. all combinations of GAB1 and SHP2 fusion proteins with fluorophore-protein linkers consisting of either 6, 15, 25, or 35 amino acids, and 3. GAB1-Cerulean and SHP2-YPET instead of the original fluorophore-protein pairs, we were unable to obtain a positive signal from FLIM indicating interaction between GAB1 and SHP2, despite using conditions known to promote association between fluorescently-tagged GAB1 and SHP2 based on immunoprecipitation experiments. While FRET microscopy and FLIM are inherently challenging techniques [187], suggesting that technical issues may have potentially impeded our ability to detect association of GAB1-YPET and SHP2-Cerulean by live-cell microscopy, it is also possible that GAB1 and SHP2 are inherently poorly suited for FRET measurements. The requirement for an extremely small distance to exist between two fluorophores in order to elicit energy transfer, paired with the necessity for the fluorophores to be tagged on only the N- or C-terminus of GAB1 and SHP2, suggests the possibility that even when GAB1 and SHP2 are bound, their termini may not reach a sufficient distance from one another to permit the fluorophores to come within close enough proximity to generate a FRET signal.

Despite these experimental difficulties, additional considerations and topologies could also be added to our computational reaction-diffusion model in order to more completely represent all cellular processes that could regulate the spatial distribution of GAB1-SHP2 complexes. The parameter value for protein diffusivity, which we

estimated based on diffusion coefficients used in previous models [161], was considered to be constant among all the cytosolic proteins and protein complexes included in our model, which may or may not be a valid simplification. As the effective diffusivity of proteins such as GRB2 can be altered due to sequestration with phosphorylated EGFR at the plasma membrane [61], it may be worthwhile to experimentally measure relative rates of diffusion for GRB2, GAB1, SHP2, and a representative SFK member using microscopy techniques such as fluorescence recovery after photobleaching (FRAP). Additional model processes could also be included in the model topology such as the process of EGFR internalization, which has been incorporated in previous computational models of EGFR-mediated signaling [63]. As endosomal EGFR has been shown to retain its phosphorylation and capacity to bind GRB2 and regulate signaling pathways such as ERK [67], the propensity for endosomal EGFR to activate SFKs from within the cytosol could have a significant effect on the predicted intracellular distribution of GAB1-SHP2 complexes. The inclusion of this process in our reaction-diffusion model would require modifying the topology such that all EGFR species capable of internalizing, which could initially be simplified to include all phosphorylated EGFR, translocate from the plasma membrane through the cytosol. The velocity with which internalized EGFR traverses the cytosol could be approximated experimentally by using microscopy to measure the rate at which fluorescently-tagged EGFR moves through a cell following stimulation with EGF. However, fully modeling the process of EGFR internalization would necessitate many other considerations beyond a constant rate of EGFR trafficking, such as recycling of endosomal EGFR back to the plasma membrane and degradation of internalized EGFR.

## BIBLIOGRAPHY

1. Scott, J.D. and T. Pawson, *Cell signaling in space and time: where proteins come together and when they're apart*. Science, 2009. **326**(5957): p. 1220-4.
2. Hunter, T. and J.A. Cooper, *Protein-tyrosine kinases*. Annu Rev Biochem, 1985. **54**: p. 897-930.
3. Schlessinger, J. and M.A. Lemmon, *SH2 and PTB domains in tyrosine kinase signaling*. Sci STKE, 2003. **2003**(191): p. RE12.
4. Lippincott-Schwartz, J., E. Snapp, and A. Kenworthy, *Studying protein dynamics in living cells*. Nat Rev Mol Cell Biol, 2001. **2**(6): p. 444-56.
5. Tonks, N.K., *Protein tyrosine phosphatases: from genes, to function, to disease*. Nat Rev Mol Cell Biol, 2006. **7**(11): p. 833-46.
6. Lemmon, M.A. and J. Schlessinger, *Cell signaling by receptor tyrosine kinases*. Cell, 2010. **141**(7): p. 1117-34.
7. Hynes, N.E. and H.A. Lane, *ERBB receptors and cancer: the complexity of targeted inhibitors*. Nat Rev Cancer, 2005. **5**(5): p. 341-54.
8. Mukohara, T., S. Kudoh, S. Yamauchi, T. Kimura, N. Yoshimura, H. Kanazawa, K. Hirata, H. Wanibuchi, S. Fukushima, K. Inoue, and J. Yoshikawa, *Expression of epidermal growth factor receptor (EGFR) and downstream-activated peptides in surgically excised non-small-cell lung cancer (NSCLC)*. Lung Cancer, 2003. **41**(2): p. 123-30.
9. Fukuoka, M., S. Yano, G. Giaccone, T. Tamura, K. Nakagawa, J.Y. Douillard, Y. Nishiwaki, J. Vansteenkiste, S. Kudoh, D. Rischin, R. Eek, T. Horai, K. Noda, I.

- Takata, E. Smit, S. Averbuch, A. Macleod, A. Feyereislova, R.P. Dong, and J. Baselga, *Multi-institutional randomized phase II trial of gefitinib for previously treated patients with advanced non-small-cell lung cancer (The IDEAL 1 Trial) [corrected]*. J Clin Oncol, 2003. **21**(12): p. 2237-46.
10. Aldape, K.D., K. Ballman, A. Furth, J.C. Buckner, C. Giannini, P.C. Burger, B.W. Scheithauer, R.B. Jenkins, and C.D. James, *Immunohistochemical detection of EGFRvIII in high malignancy grade astrocytomas and evaluation of prognostic significance*. J Neuropathol Exp Neurol, 2004. **63**(7): p. 700-7.
  11. Frederick, L., X.Y. Wang, G. Eley, and C.D. James, *Diversity and frequency of epidermal growth factor receptor mutations in human glioblastomas*. Cancer Res, 2000. **60**(5): p. 1383-7.
  12. Ng, M. and D. Cunningham, *Cetuximab (Erbix)--an emerging targeted therapy for epidermal growth factor receptor-expressing tumours*. Int J Clin Pract, 2004. **58**(10): p. 970-6.
  13. Wakeling, A.E., S.P. Guy, J.R. Woodburn, S.E. Ashton, B.J. Curry, A.J. Barker, and K.H. Gibson, *ZD1839 (Iressa): an orally active inhibitor of epidermal growth factor signaling with potential for cancer therapy*. Cancer Res, 2002. **62**(20): p. 5749-54.
  14. Lynch, T.J., D.W. Bell, R. Sordella, S. Gurubhagavatula, R.A. Okimoto, B.W. Brannigan, P.L. Harris, S.M. Haserlat, J.G. Supko, F.G. Haluska, D.N. Louis, D.C. Christiani, J. Settleman, and D.A. Haber, *Activating mutations in the epidermal growth factor receptor underlying responsiveness of non-small-cell lung cancer to gefitinib*. N Engl J Med, 2004. **350**(21): p. 2129-39.

15. Sordella, R., D.W. Bell, D.A. Haber, and J. Settleman, *Gefitinib-sensitizing EGFR mutations in lung cancer activate anti-apoptotic pathways*. Science, 2004. **305**(5687): p. 1163-7.
16. Rich, J.N., D.A. Reardon, T. Peery, J.M. Dowell, J.A. Quinn, K.L. Penne, C.J. Wikstrand, L.B. Van Duyn, J.E. Dancey, R.E. McLendon, J.C. Kao, T.T. Stenzel, B.K. Ahmed Rasheed, S.E. Tourt-Uhlig, J.E. Herndon, 2nd, J.J. Vredenburgh, J.H. Sampson, A.H. Friedman, D.D. Bigner, and H.S. Friedman, *Phase II trial of gefitinib in recurrent glioblastoma*. J Clin Oncol, 2004. **22**(1): p. 133-42.
17. Lassman, A.B., M.R. Rossi, J.J. Raizer, L.E. Abrey, F.S. Lieberman, C.N. Grefe, K. Lamborn, W. Pao, A.H. Shih, J.G. Kuhn, R. Wilson, N.J. Nowak, J.K. Cowell, L.M. DeAngelis, P. Wen, M.R. Gilbert, S. Chang, W.A. Yung, M. Prados, and E.C. Holland, *Molecular study of malignant gliomas treated with epidermal growth factor receptor inhibitors: tissue analysis from North American Brain Tumor Consortium Trials 01-03 and 00-01*. Clin Cancer Res, 2005. **11**(21): p. 7841-50.
18. Kobayashi, S., T.J. Boggon, T. Dayaram, P.A. Janne, O. Kocher, M. Meyerson, B.E. Johnson, M.J. Eck, D.G. Tenen, and B. Halmos, *EGFR mutation and resistance of non-small-cell lung cancer to gefitinib*. N Engl J Med, 2005. **352**(8): p. 786-92.
19. Yun, C.H., K.E. Mengwasser, A.V. Toms, M.S. Woo, H. Greulich, K.K. Wong, M. Meyerson, and M.J. Eck, *The T790M mutation in EGFR kinase causes drug resistance by increasing the affinity for ATP*. Proc Natl Acad Sci U S A, 2008. **105**(6): p. 2070-5.

20. Pao, W., V.A. Miller, K.A. Politi, G.J. Riely, R. Somwar, M.F. Zakowski, M.G. Kris, and H. Varmus, *Acquired resistance of lung adenocarcinomas to gefitinib or erlotinib is associated with a second mutation in the EGFR kinase domain*. PLoS Med, 2005. **2**(3): p. e73.
21. Engelman, J.A., K. Zejnullahu, T. Mitsudomi, Y. Song, C. Hyland, J.O. Park, N. Lindeman, C.M. Gale, X. Zhao, J. Christensen, T. Kosaka, A.J. Holmes, A.M. Rogers, F. Cappuzzo, T. Mok, C. Lee, B.E. Johnson, L.C. Cantley, and P.A. Janne, *MET amplification leads to gefitinib resistance in lung cancer by activating ERBB3 signaling*. Science, 2007. **316**(5827): p. 1039-43.
22. Yun, C.H., T.J. Boggon, Y. Li, M.S. Woo, H. Greulich, M. Meyerson, and M.J. Eck, *Structures of lung cancer-derived EGFR mutants and inhibitor complexes: mechanism of activation and insights into differential inhibitor sensitivity*. Cancer Cell, 2007. **11**(3): p. 217-27.
23. Hendriks, B.S., G.J. Griffiths, R. Benson, D. Kenyon, M. Lazzara, J. Swinton, S. Beck, M. Hickinson, J.M. Beusmans, D. Lauffenburger, and D. de Graaf, *Decreased internalisation of erbB1 mutants in lung cancer is linked with a mechanism conferring sensitivity to gefitinib*. Syst Biol (Stevenage), 2006. **153**(6): p. 457-66.
24. Lazzara, M.J., K. Lane, R. Chan, P.J. Jasper, M.B. Yaffe, P.K. Sorger, T. Jacks, B.G. Neel, and D.A. Lauffenburger, *Impaired SHP2-mediated extracellular signal-regulated kinase activation contributes to gefitinib sensitivity of lung cancer cells with epidermal growth factor receptor-activating mutations*. Cancer Res, 2010. **70**(9): p. 3843-50.

25. Akca, H., M. Tani, T. Hishida, S. Matsumoto, and J. Yokota, *Activation of the AKT and STAT3 pathways and prolonged survival by a mutant EGFR in human lung cancer cells*. Lung Cancer, 2006. **54**(1): p. 25-33.
26. Guo, A., J. Villen, J. Kornhauser, K.A. Lee, M.P. Stokes, K. Rikova, A. Possemato, J. Nardone, G. Innocenti, R. Wetzel, Y. Wang, J. MacNeill, J. Mitchell, S.P. Gygi, J. Rush, R.D. Polakiewicz, and M.J. Comb, *Signaling networks assembled by oncogenic EGFR and c-Met*. Proc Natl Acad Sci U S A, 2008. **105**(2): p. 692-7.
27. Janmaat, M.L., J.A. Rodriguez, M. Gallegos-Ruiz, F.A. Kruyt, and G. Giaccone, *Enhanced cytotoxicity induced by gefitinib and specific inhibitors of the Ras or phosphatidyl inositol-3 kinase pathways in non-small cell lung cancer cells*. Int J Cancer, 2006. **118**(1): p. 209-14.
28. Neel, B.G., H. Gu, and L. Pao, *The 'Shp'ing news: SH2 domain-containing tyrosine phosphatases in cell signaling*. Trends Biochem Sci, 2003. **28**(6): p. 284-93.
29. Araki, T., H. Nawa, and B.G. Neel, *Tyrosyl phosphorylation of Shp2 is required for normal ERK activation in response to some, but not all, growth factors*. J Biol Chem, 2003. **278**(43): p. 41677-84.
30. Fenstermaker, R.A. and M.J. Ciesielski, *Deletion and tandem duplication of exons 2 - 7 in the epidermal growth factor receptor gene of a human malignant glioma*. Oncogene, 2000. **19**(39): p. 4542-8.
31. Sugawa, N., A.J. Ekstrand, C.D. James, and V.P. Collins, *Identical splicing of aberrant epidermal growth factor receptor transcripts from amplified rearranged*

- genes in human glioblastomas*. Proc Natl Acad Sci U S A, 1990. **87**(21): p. 8602-6.
32. Wong, A.J., J.M. Ruppert, S.H. Bigner, C.H. Grzeschik, P.A. Humphrey, D.S. Bigner, and B. Vogelstein, *Structural alterations of the epidermal growth factor receptor gene in human gliomas*. Proc Natl Acad Sci U S A, 1992. **89**(7): p. 2965-9.
  33. Garcia de Palazzo, I.E., G.P. Adams, P. Sundareshan, A.J. Wong, J.R. Testa, D.D. Bigner, and L.M. Weiner, *Expression of mutated epidermal growth factor receptor by non-small cell lung carcinomas*. Cancer Res, 1993. **53**(14): p. 3217-20.
  34. Moscatello, D.K., M. Holgado-Madruga, A.K. Godwin, G. Ramirez, G. Gunn, P.W. Zoltick, J.A. Biegel, R.L. Hayes, and A.J. Wong, *Frequent expression of a mutant epidermal growth factor receptor in multiple human tumors*. Cancer Res, 1995. **55**(23): p. 5536-9.
  35. Heimberger, A.B., R. Hlatky, D. Suki, D. Yang, J. Weinberg, M. Gilbert, R. Sawaya, and K. Aldape, *Prognostic effect of epidermal growth factor receptor and EGFRvIII in glioblastoma multiforme patients*. Clin Cancer Res, 2005. **11**(4): p. 1462-6.
  36. Zhang, X., W. Zhang, W.D. Cao, G. Cheng, and Y.Q. Zhang, *Glioblastoma multiforme: Molecular characterization and current treatment strategy (Review)*. Exp Ther Med, 2012. **3**(1): p. 9-14.

37. Sathornsumetee, S., D.A. Reardon, A. Desjardins, J.A. Quinn, J.J. Vredenburgh, and J.N. Rich, *Molecularly targeted therapy for malignant glioma*. Cancer, 2007. **110**(1): p. 13-24.
38. Furnari, F.B., T. Fenton, R.M. Bachoo, A. Mukasa, J.M. Stommel, A. Stegh, W.C. Hahn, K.L. Ligon, D.N. Louis, C. Brennan, L. Chin, R.A. DePinho, and W.K. Cavenee, *Malignant astrocytic glioma: genetics, biology, and paths to treatment*. Genes Dev, 2007. **21**(21): p. 2683-710.
39. Cecchi, F., D.C. Rabe, and D.P. Bottaro, *Targeting the HGF/Met signalling pathway in cancer*. Eur J Cancer, 2010. **46**(7): p. 1260-70.
40. Wen, P.Y., D. Schiff, T.F. Cloughesy, J.J. Raizer, J. Laterra, M. Smitt, M. Wolf, K.S. Oliner, A. Anderson, M. Zhu, E. Loh, and D.A. Reardon, *A phase II study evaluating the efficacy and safety of AMG 102 (rilotumumab) in patients with recurrent glioblastoma*. Neuro Oncol, 2011. **13**(4): p. 437-46.
41. Cohen, M.H., Y.L. Shen, P. Keegan, and R. Pazdur, *FDA drug approval summary: bevacizumab (Avastin) as treatment of recurrent glioblastoma multiforme*. Oncologist, 2009. **14**(11): p. 1131-8.
42. Nishikawa, R., X.D. Ji, R.C. Harmon, C.S. Lazar, G.N. Gill, W.K. Cavenee, and H.J. Huang, *A mutant epidermal growth factor receptor common in human glioma confers enhanced tumorigenicity*. Proc Natl Acad Sci U S A, 1994. **91**(16): p. 7727-31.
43. Lal, B., C.R. Goodwin, Y. Sang, C.A. Foss, K. Cornet, S. Muzamil, M.G. Pomper, J. Kim, and J. Laterra, *EGFRvIII and c-Met pathway inhibitors synergize*

- against PTEN-null/EGFRvIII+ glioblastoma xenografts*. Mol Cancer Ther, 2009. **8**(7): p. 1751-60.
44. Modjtahedi, H., D.K. Moscatello, G. Box, M. Green, C. Shotton, D.J. Lamb, L.J. Reynolds, A.J. Wong, C. Dean, H. Thomas, and S. Eccles, *Targeting of cells expressing wild-type EGFR and type-III mutant EGFR (EGFRvIII) by anti-EGFR MAb ICR62: a two-pronged attack for tumour therapy*. Int J Cancer, 2003. **105**(2): p. 273-80.
  45. Huang, H.S., M. Nagane, C.K. Klingbeil, H. Lin, R. Nishikawa, X.D. Ji, C.M. Huang, G.N. Gill, H.S. Wiley, and W.K. Cavenee, *The enhanced tumorigenic activity of a mutant epidermal growth factor receptor common in human cancers is mediated by threshold levels of constitutive tyrosine phosphorylation and unattenuated signaling*. J Biol Chem, 1997. **272**(5): p. 2927-35.
  46. Grandal, M.V., R. Zandi, M.W. Pedersen, B.M. Willumsen, B. van Deurs, and H.S. Poulsen, *EGFRvIII escapes down-regulation due to impaired internalization and sorting to lysosomes*. Carcinogenesis, 2007. **28**(7): p. 1408-17.
  47. Lo, H.W., X. Cao, H. Zhu, and F. Ali-Osman, *Constitutively activated STAT3 frequently coexpresses with epidermal growth factor receptor in high-grade gliomas and targeting STAT3 sensitizes them to Iressa and alkylators*. Clin Cancer Res, 2008. **14**(19): p. 6042-54.
  48. Huang, P.H., A. Mukasa, R. Bonavia, R.A. Flynn, Z.E. Brewer, W.K. Cavenee, F.B. Furnari, and F.M. White, *Quantitative analysis of EGFRvIII cellular signaling networks reveals a combinatorial therapeutic strategy for glioblastoma*. Proc Natl Acad Sci U S A, 2007. **104**(31): p. 12867-72.

49. Zhu, H., J. Acquaviva, P. Ramachandran, A. Boskovitz, S. Woolfenden, R. Pfannl, R.T. Bronson, J.W. Chen, R. Weissleder, D.E. Housman, and A. Charest, *Oncogenic EGFR signaling cooperates with loss of tumor suppressor gene functions in gliomagenesis*. Proc Natl Acad Sci U S A, 2009. **106**(8): p. 2712-6.
50. Antonyak, M.A., D.K. Moscatello, and A.J. Wong, *Constitutive activation of c-Jun N-terminal kinase by a mutant epidermal growth factor receptor*. J Biol Chem, 1998. **273**(5): p. 2817-22.
51. Moscatello, D.K., R.B. Montgomery, P. Sundareshan, H. McDanel, M.Y. Wong, and A.J. Wong, *Transformational and altered signal transduction by a naturally occurring mutant EGF receptor*. Oncogene, 1996. **13**(1): p. 85-96.
52. Gu, H. and B.G. Neel, *The "Gab" in signal transduction*. Trends Cell Biol, 2003. **13**(3): p. 122-30.
53. Shi, Z.Q., D.H. Yu, M. Park, M. Marshall, and G.S. Feng, *Molecular mechanism for the Shp-2 tyrosine phosphatase function in promoting growth factor stimulation of Erk activity*. Mol Cell Biol, 2000. **20**(5): p. 1526-36.
54. Montagner, A., A. Yart, M. Dance, B. Perret, J.P. Salles, and P. Raynal, *A novel role for Gab1 and SHP2 in epidermal growth factor-induced Ras activation*. J Biol Chem, 2005. **280**(7): p. 5350-60.
55. Ren, Y., S. Meng, L. Mei, Z.J. Zhao, R. Jove, and J. Wu, *Roles of Gab1 and SHP2 in paxillin tyrosine dephosphorylation and Src activation in response to epidermal growth factor*. J Biol Chem, 2004. **279**(9): p. 8497-505.
56. Zhang, S.Q., W. Yang, M.I. Kontaridis, T.G. Bivona, G. Wen, T. Araki, J. Luo, J.A. Thompson, B.L. Schraven, M.R. Philips, and B.G. Neel, *Shp2 regulates SRC*

- family kinase activity and Ras/Erk activation by controlling Csk recruitment. Mol Cell*, 2004. **13**(3): p. 341-55.
57. Shi, Z.Q., W. Lu, and G.S. Feng, *The Shp-2 tyrosine phosphatase has opposite effects in mediating the activation of extracellular signal-regulated and c-Jun NH2-terminal mitogen-activated protein kinases. J Biol Chem*, 1998. **273**(9): p. 4904-8.
  58. Wu, C.J., D.M. O'Rourke, G.S. Feng, G.R. Johnson, Q. Wang, and M.I. Greene, *The tyrosine phosphatase SHP-2 is required for mediating phosphatidylinositol 3-kinase/Akt activation by growth factors. Oncogene*, 2001. **20**(42): p. 6018-25.
  59. Bard-Chapeau, E.A., S. Li, J. Ding, S.S. Zhang, H.H. Zhu, F. Princen, D.D. Fang, T. Han, B. Bailly-Maitre, V. Poli, N.M. Varki, H. Wang, and G.S. Feng, *Ptpn11/Shp2 acts as a tumor suppressor in hepatocellular carcinogenesis. Cancer Cell*, 2011. **19**(5): p. 629-39.
  60. Kholodenko, B.N., J.F. Hancock, and W. Kolch, *Signalling ballet in space and time. Nat Rev Mol Cell Biol*, 2010. **11**(6): p. 414-26.
  61. Morimatsu, M., H. Takagi, K.G. Ota, R. Iwamoto, T. Yanagida, and Y. Sako, *Multiple-state reactions between the epidermal growth factor receptor and Grb2 as observed by using single-molecule analysis. Proc Natl Acad Sci U S A*, 2007. **104**(46): p. 18013-8.
  62. Barua, D., J.R. Faeder, and J.M. Haugh, *Structure-based kinetic models of modular signaling protein function: focus on Shp2. Biophys J*, 2007. **92**(7): p. 2290-300.

63. Monast, C.S., C.M. Furcht, and M.J. Lazzara, *Computational analysis of the regulation of EGFR by protein tyrosine phosphatases*. Biophys J, 2012. **102**(9): p. 2012-21.
64. Mayer, B.J., *Perspective: Dynamics of receptor tyrosine kinase signaling complexes*. FEBS Lett, 2012. **586**(17): p. 2575-9.
65. Lehr, S., J. Kotzka, A. Herkner, E. Klein, C. Siethoff, B. Knebel, V. Noelle, J.C. Bruning, H.W. Klein, H.E. Meyer, W. Krone, and D. Muller-Wieland, *Identification of tyrosine phosphorylation sites in human Gab-1 protein by EGF receptor kinase in vitro*. Biochemistry, 1999. **38**(1): p. 151-9.
66. Daub, H., C. Wallasch, A. Lankenau, A. Herrlich, and A. Ullrich, *Signal characteristics of G protein-transactivated EGF receptor*. EMBO J, 1997. **16**(23): p. 7032-44.
67. Fortian, A. and A. Sorkin, *Live-cell fluorescence imaging reveals high stoichiometry of Grb2 binding to the EGF receptor sustained during endocytosis*. J Cell Sci, 2014. **127**(Pt 2): p. 432-44.
68. Chan, R.J. and G.S. Feng, *PTPN11 is the first identified proto-oncogene that encodes a tyrosine phosphatase*. Blood, 2007. **109**(3): p. 862-7.
69. Zhou, X., J. Coad, B. Ducatman, and Y.M. Agazie, *SHP2 is up-regulated in breast cancer cells and in infiltrating ductal carcinoma of the breast, implying its involvement in breast oncogenesis*. Histopathology, 2008. **53**(4): p. 389-402.
70. Zhan, X., H. Dong, C. Sun, L. Liu, D. Wang, and Z. Wei, *[Expression and clinical significance of SHP2 in the tumor tissues of smokers with lung cancer]*. Zhongguo Fei Ai Za Zhi, 2010. **13**(9): p. 877-81.

71. Mohi, M.G. and B.G. Neel, *The role of Shp2 (PTPN11) in cancer*. Curr Opin Genet Dev, 2007. **17**(1): p. 23-30.
72. Hatakeyama, M., *Oncogenic mechanisms of the Helicobacter pylori CagA protein*. Nat Rev Cancer, 2004. **4**(9): p. 688-94.
73. Zhan, Y., G.J. Counelis, and D.M. O'Rourke, *The protein tyrosine phosphatase SHP-2 is required for EGFRvIII oncogenic transformation in human glioblastoma cells*. Exp Cell Res, 2009. **315**(14): p. 2343-57.
74. Zhou, X.D. and Y.M. Agazie, *Inhibition of SHP2 leads to mesenchymal to epithelial transition in breast cancer cells*. Cell Death Differ, 2008. **15**(6): p. 988-96.
75. Yang, J. and R.A. Weinberg, *Epithelial-mesenchymal transition: at the crossroads of development and tumor metastasis*. Dev Cell, 2008. **14**(6): p. 818-29.
76. Tsuji, T., S. Ibaragi, and G.F. Hu, *Epithelial-mesenchymal transition and cell cooperativity in metastasis*. Cancer Res, 2009. **69**(18): p. 7135-9.
77. Bentires-Alj, M., J.G. Paez, F.S. David, H. Keilhack, B. Halmos, K. Naoki, J.M. Maris, A. Richardson, A. Bardelli, D.J. Sugarbaker, W.G. Richards, J. Du, L. Girard, J.D. Minna, M.L. Loh, D.E. Fisher, V.E. Velculescu, B. Vogelstein, M. Meyerson, W.R. Sellers, and B.G. Neel, *Activating mutations of the noonan syndrome-associated SHP2/PTPN11 gene in human solid tumors and adult acute myelogenous leukemia*. Cancer Res, 2004. **64**(24): p. 8816-20.

78. Keilhack, H., F.S. David, M. McGregor, L.C. Cantley, and B.G. Neel, *Diverse biochemical properties of Shp2 mutants. Implications for disease phenotypes.* J Biol Chem, 2005. **280**(35): p. 30984-93.
79. Tartaglia, M., E.L. Mehler, R. Goldberg, G. Zampino, H.G. Brunner, H. Kremer, I. van der Burgt, A.H. Crosby, A. Ion, S. Jeffery, K. Kalidas, M.A. Patton, R.S. Kucherlapati, and B.D. Gelb, *Mutations in PTPN11, encoding the protein tyrosine phosphatase SHP-2, cause Noonan syndrome.* Nat Genet, 2001. **29**(4): p. 465-8.
80. Sturla, L.M., P.O. Zinn, K. Ng, M. Nitta, D. Kozono, C.C. Chen, and E.M. Kasper, *Src homology domain-containing phosphatase 2 suppresses cellular senescence in glioblastoma.* Br J Cancer, 2011. **105**(8): p. 1235-43.
81. de la Iglesia, N., S.V. Puram, and A. Bonni, *STAT3 regulation of glioblastoma pathogenesis.* Curr Mol Med, 2009. **9**(5): p. 580-90.
82. Kontaridis, M.I., K.D. Swanson, F.S. David, D. Barford, and B.G. Neel, *PTPN11 (Shp2) mutations in LEOPARD syndrome have dominant negative, not activating, effects.* J Biol Chem, 2006. **281**(10): p. 6785-92.
83. Engelman, J.A., P.A. Janne, C. Mermel, J. Pearlberg, T. Mukohara, C. Fleet, K. Cichowski, B.E. Johnson, and L.C. Cantley, *ErbB-3 mediates phosphoinositide 3-kinase activity in gefitinib-sensitive non-small cell lung cancer cell lines.* Proc Natl Acad Sci U S A, 2005. **102**(10): p. 3788-93.
84. Chan, G., D. Kalaitzidis, and B.G. Neel, *The tyrosine phosphatase Shp2 (PTPN11) in cancer.* Cancer Metastasis Rev, 2008. **27**(2): p. 179-92.
85. Vieira, A.V., C. Lamaze, and S.L. Schmid, *Control of EGF receptor signaling by clathrin-mediated endocytosis.* Science, 1996. **274**(5295): p. 2086-9.

86. Ventura, A., A. Meissner, C.P. Dillon, M. McManus, P.A. Sharp, L. Van Parijs, R. Jaenisch, and T. Jacks, *Cre-lox-regulated conditional RNA interference from transgenes*. Proc Natl Acad Sci U S A, 2004. **101**(28): p. 10380-5.
87. Wickrema, A., S. Uddin, A. Sharma, F. Chen, Y. Alsayed, S. Ahmad, S.T. Sawyer, G. Krystal, T. Yi, K. Nishada, M. Hibi, T. Hirano, and L.C. Platanias, *Engagement of Gab1 and Gab2 in erythropoietin signaling*. J Biol Chem, 1999. **274**(35): p. 24469-74.
88. Salvi, M., A. Stringaro, A.M. Brunati, E. Agostinelli, G. Arancia, G. Clari, and A. Toninello, *Tyrosine phosphatase activity in mitochondria: presence of Shp-2 phosphatase in mitochondria*. Cell Mol Life Sci, 2004. **61**(18): p. 2393-404.
89. Maroun, C.R., M.A. Naujokas, M. Holgado-Madruga, A.J. Wong, and M. Park, *The tyrosine phosphatase SHP-2 is required for sustained activation of extracellular signal-regulated kinase and epithelial morphogenesis downstream from the met receptor tyrosine kinase*. Mol Cell Biol, 2000. **20**(22): p. 8513-25.
90. Turke, A.B., K. Zejnullahu, Y.L. Wu, Y. Song, D. Dias-Santagata, E. Lifshits, L. Toschi, A. Rogers, T. Mok, L. Sequist, N.I. Lindeman, C. Murphy, S. Akhavanfard, B.Y. Yeap, Y. Xiao, M. Capelletti, A.J. Iafrate, C. Lee, J.G. Christensen, J.A. Engelman, and P.A. Janne, *Preexistence and clonal selection of MET amplification in EGFR mutant NSCLC*. Cancer Cell, 2010. **17**(1): p. 77-88.
91. Yano, S., W. Wang, Q. Li, K. Matsumoto, H. Sakurama, T. Nakamura, H. Ogino, S. Kakiuchi, M. Hanibuchi, Y. Nishioka, H. Uehara, T. Mitsudomi, Y. Yatabe, and S. Sone, *Hepatocyte growth factor induces gefitinib resistance of lung*

- adenocarcinoma with epidermal growth factor receptor-activating mutations.* Cancer Res, 2008. **68**(22): p. 9479-87.
92. Coldren, C.D., B.A. Helfrich, S.E. Witta, M. Sugita, R. Lapadat, C. Zeng, A. Baron, W.A. Franklin, F.R. Hirsch, M.W. Geraci, and P.A. Bunn, Jr., *Baseline gene expression predicts sensitivity to gefitinib in non-small cell lung cancer cell lines.* Mol Cancer Res, 2006. **4**(8): p. 521-8.
  93. Wang, S.E., A. Narasanna, M. Perez-Torres, B. Xiang, F.Y. Wu, S. Yang, G. Carpenter, A.F. Gazdar, S.K. Muthuswamy, and C.L. Arteaga, *HER2 kinase domain mutation results in constitutive phosphorylation and activation of HER2 and EGFR and resistance to EGFR tyrosine kinase inhibitors.* Cancer Cell, 2006. **10**(1): p. 25-38.
  94. Offterdinger, M. and P.I. Bastiaens, *Prolonged EGFR signaling by ERBB2-mediated sequestration at the plasma membrane.* Traffic, 2008. **9**(1): p. 147-55.
  95. Hendriks, B.S., L.K. Opresko, H.S. Wiley, and D. Lauffenburger, *Coregulation of epidermal growth factor receptor/human epidermal growth factor receptor 2 (HER2) levels and locations: quantitative analysis of HER2 overexpression effects.* Cancer Res, 2003. **63**(5): p. 1130-7.
  96. Zhou, X. and Y.M. Agazie, *Molecular mechanism for SHP2 in promoting HER2-induced signaling and transformation.* J Biol Chem, 2009. **284**(18): p. 12226-34.
  97. Paulsen, C.E., T.H. Truong, F.J. Garcia, A. Homann, V. Gupta, S.E. Leonard, and K.S. Carroll, *Peroxide-dependent sulfenylation of the EGFR catalytic site enhances kinase activity.* Nat Chem Biol, 2011. **8**(1): p. 57-64.

98. Ren, Y., Z. Chen, L. Chen, B. Fang, H. Win-Piazza, E. Haura, J.M. Koomen, and J. Wu, *Critical role of Shp2 in tumor growth involving regulation of c-Myc*. Genes Cancer, 2010. **1**(10): p. 994-1007.
99. Sharma, S.V., D.W. Bell, J. Settleman, and D.A. Haber, *Epidermal growth factor receptor mutations in lung cancer*. Nat Rev Cancer, 2007. **7**(3): p. 169-81.
100. Janes, K.A., J.G. Albeck, S. Gaudet, P.K. Sorger, D.A. Lauffenburger, and M.B. Yaffe, *A systems model of signaling identifies a molecular basis set for cytokine-induced apoptosis*. Science, 2005. **310**(5754): p. 1646-53.
101. Kumar, N., A. Wolf-Yadlin, F.M. White, and D.A. Lauffenburger, *Modeling HER2 effects on cell behavior from mass spectrometry phosphotyrosine data*. PLoS Comput Biol, 2007. **3**(1): p. e4.
102. Lazzara, M.J. and D.A. Lauffenburger, *Quantitative modeling perspectives on the ErbB system of cell regulatory processes*. Exp Cell Res, 2009. **315**(4): p. 717-25.
103. Wolf-Yadlin, A., N. Kumar, Y. Zhang, S. Hautaniemi, M. Zaman, H.D. Kim, V. Grantcharova, D.A. Lauffenburger, and F.M. White, *Effects of HER2 overexpression on cell signaling networks governing proliferation and migration*. Mol Syst Biol, 2006. **2**: p. 54.
104. Schmitz, J., M. Weissenbach, S. Haan, P.C. Heinrich, and F. Schaper, *SOCS3 exerts its inhibitory function on interleukin-6 signal transduction through the SHP2 recruitment site of gp130*. J Biol Chem, 2000. **275**(17): p. 12848-56.
105. Bard-Chapeau, E.A., S. Li, J. Ding, S.S. Zhang, H.H. Zhu, F. Princen, D.D. Fang, T. Han, B. Bailly-Maitre, V. Poli, N.M. Varki, H. Wang, and G.S. Feng,

- Ptpn11/Shp2 acts as a tumor suppressor in hepatocellular carcinogenesis.* Cancer Cell, 2012. **19**(5): p. 629-39.
106. Zhang, S.Q., W.G. Tsiaras, T. Araki, G. Wen, L. Minichiello, R. Klein, and B.G. Neel, *Receptor-specific regulation of phosphatidylinositol 3'-kinase activation by the protein tyrosine phosphatase Shp2.* Mol Cell Biol, 2002. **22**(12): p. 4062-72.
  107. Cai, T., K. Nishida, T. Hirano, and P.A. Khavari, *Gab1 and SHP-2 promote Ras/MAPK regulation of epidermal growth and differentiation.* J Cell Biol, 2002. **159**(1): p. 103-12.
  108. Furcht, C.M., A.R. Munoz Rojas, D. Nihalani, and M.J. Lazzara, *Diminished functional role and altered localization of SHP2 in non-small cell lung cancer cells with EGFR-activating mutations.* Oncogene, 2012.
  109. Aceto, N., N. Sausgruber, H. Brinkhaus, D. Gaidatzis, G. Martiny-Baron, G. Mazzarol, S. Confalonieri, M. Quarto, G. Hu, P.J. Balwierz, M. Pachkov, S.J. Elledge, E. van Nimwegen, M.B. Stadler, and M. Bentiresh-Alj, *Tyrosine phosphatase SHP2 promotes breast cancer progression and maintains tumor-initiating cells via activation of key transcription factors and a positive feedback signaling loop.* Nat Med, 2012. **18**(4): p. 529-37.
  110. Roberts, P.J. and C.J. Der, *Targeting the Raf-MEK-ERK mitogen-activated protein kinase cascade for the treatment of cancer.* Oncogene, 2007. **26**(22): p. 3291-310.
  111. Hodge, D.R., E.M. Hurt, and W.L. Farrar, *The role of IL-6 and STAT3 in inflammation and cancer.* Eur J Cancer, 2005. **41**(16): p. 2502-12.

112. Zhan, Y. and D.M. O'Rourke, *SHP-2-dependent mitogen-activated protein kinase activation regulates EGFRvIII but not wild-type epidermal growth factor receptor phosphorylation and glioblastoma cell survival*. Cancer Res, 2004. **64**(22): p. 8292-8.
113. De Witt Hamer, P.C., *Small molecule kinase inhibitors in glioblastoma: a systematic review of clinical studies*. Neuro Oncol, 2010. **12**(3): p. 304-16.
114. Argyriou, A.A. and H.P. Kalofonos, *Molecularly targeted therapies for malignant gliomas*. Mol Med, 2009. **15**(3-4): p. 115-22.
115. Lund, K.A., L.K. Opresko, C. Starbuck, B.J. Walsh, and H.S. Wiley, *Quantitative analysis of the endocytic system involved in hormone-induced receptor internalization*. J Biol Chem, 1990. **265**(26): p. 15713-23.
116. Wiley, H.S. and D.D. Cunningham, *The endocytotic rate constant. A cellular parameter for quantitating receptor-mediated endocytosis*. J Biol Chem, 1982. **257**(8): p. 4222-9.
117. Amin, A.R., V.S. Thakur, R.K. Paul, G.S. Feng, C.K. Qu, H. Mukhtar, and M.L. Agarwal, *SHP-2 tyrosine phosphatase inhibits p73-dependent apoptosis and expression of a subset of p53 target genes induced by EGCG*. Proc Natl Acad Sci U S A, 2007. **104**(13): p. 5419-24.
118. Chung, J., E. Uchida, T.C. Grammer, and J. Blenis, *STAT3 serine phosphorylation by ERK-dependent and -independent pathways negatively modulates its tyrosine phosphorylation*. Mol Cell Biol, 1997. **17**(11): p. 6508-16.
119. Shao, H., H.Y. Cheng, R.G. Cook, and D.J. Tweardy, *Identification and characterization of signal transducer and activator of transcription 3 recruitment*

- sites within the epidermal growth factor receptor*. Cancer Res, 2003. **63**(14): p. 3923-30.
120. Fan, Q.W., C.K. Cheng, W.C. Gustafson, E. Charron, P. Zipper, R.A. Wong, J. Chen, J. Lau, C. Knobbe-Thomsen, M. Weller, N. Jura, G. Reifenberger, K.M. Shokat, and W.A. Weiss, *EGFR phosphorylates tumor-derived EGFRvIII driving STAT3/5 and progression in glioblastoma*. Cancer Cell, 2013. **24**(4): p. 438-49.
  121. Agazie, Y.M. and M.J. Hayman, *Development of an efficient "substrate-trapping" mutant of Src homology phosphotyrosine phosphatase 2 and identification of the epidermal growth factor receptor, Gab1, and three other proteins as target substrates*. J Biol Chem, 2003. **278**(16): p. 13952-8.
  122. Krens, S.F., M. Corredor-Adamez, S. He, B.E. Snaar-Jagalska, and H.P. Spaink, *ERK1 and ERK2 MAPK are key regulators of distinct gene sets in zebrafish embryogenesis*. BMC Genomics, 2008. **9**: p. 196.
  123. Dauer, D.J., B. Ferraro, L. Song, B. Yu, L. Mora, R. Buettner, S. Enkemann, R. Jove, and E.B. Haura, *Stat3 regulates genes common to both wound healing and cancer*. Oncogene, 2005. **24**(21): p. 3397-408.
  124. Yu, H. and R. Jove, *The STATs of cancer--new molecular targets come of age*. Nat Rev Cancer, 2004. **4**(2): p. 97-105.
  125. Lu, Z. and S. Xu, *ERK1/2 MAP kinases in cell survival and apoptosis*. IUBMB Life, 2006. **58**(11): p. 621-31.
  126. Zhang, W. and H.T. Liu, *MAPK signal pathways in the regulation of cell proliferation in mammalian cells*. Cell Res, 2002. **12**(1): p. 9-18.

127. Tykocinski, E.S., R.A. Grant, G.S. Kapoor, J. Krejza, L.E. Bohman, T.A. Gocke, S. Chawla, C.H. Halpern, J. Lopinto, E.R. Melhem, and D.M. O'Rourke, *Use of magnetic perfusion-weighted imaging to determine epidermal growth factor receptor variant III expression in glioblastoma*. *Neuro Oncol*, 2012. **14**(5): p. 613-23.
128. Vivanco, I., H.I. Robins, D. Rohle, C. Campos, C. Grommes, P.L. Nghiemphu, S. Kubek, B. Oldrini, M.G. Chheda, N. Yannuzzi, H. Tao, S. Zhu, A. Iwanami, D. Kuga, J. Dang, A. Pedraza, C.W. Brennan, A. Heguy, L.M. Liao, F. Lieberman, W.K. Yung, M.R. Gilbert, D.A. Reardon, J. Drappatz, P.Y. Wen, K.R. Lamborn, S.M. Chang, M.D. Prados, H.A. Fine, S. Horvath, N. Wu, A.B. Lassman, L.M. DeAngelis, W.H. Yong, J.G. Kuhn, P.S. Mischel, M.P. Mehta, T.F. Cloughesy, and I.K. Mellinghoff, *Differential sensitivity of glioma- versus lung cancer-specific EGFR mutations to EGFR kinase inhibitors*. *Cancer Discov*, 2012. **2**(5): p. 458-71.
129. Maroun, C.R., M. Holgado-Madruga, I. Royal, M.A. Naujokas, T.M. Fournier, A.J. Wong, and M. Park, *The Gab1 PH domain is required for localization of Gab1 at sites of cell-cell contact and epithelial morphogenesis downstream from the met receptor tyrosine kinase*. *Mol Cell Biol*, 1999. **19**(3): p. 1784-99.
130. Maroun, C.R., M.A. Naujokas, and M. Park, *Membrane targeting of Grb2-associated binder-1 (Gab1) scaffolding protein through Src myristoylation sequence substitutes for Gab1 pleckstrin homology domain and switches an epidermal growth factor response to an invasive morphogenic program*. *Mol Biol Cell*, 2003. **14**(4): p. 1691-708.

131. Schaeper, U., N.H. Gehring, K.P. Fuchs, M. Sachs, B. Kempkes, and W. Birchmeier, *Coupling of Gab1 to c-Met, Grb2, and Shp2 mediates biological responses*. J Cell Biol, 2000. **149**(7): p. 1419-32.
132. Cunnick, J.M., L. Mei, C.A. Doupnik, and J. Wu, *Phosphotyrosines 627 and 659 of Gab1 constitute a bisphosphoryl tyrosine-based activation motif (BTAM) conferring binding and activation of SHP2*. J Biol Chem, 2001. **276**(26): p. 24380-7.
133. Waters, C.M., K.C. Oberg, G. Carpenter, and K.A. Overholser, *Rate constants for binding, dissociation, and internalization of EGF: effect of receptor occupancy and ligand concentration*. Biochemistry, 1990. **29**(14): p. 3563-9.
134. French, A.R., D.K. Tadaki, S.K. Niyogi, and D.A. Lauffenburger, *Intracellular trafficking of epidermal growth factor family ligands is directly influenced by the pH sensitivity of the receptor/ligand interaction*. J Biol Chem, 1995. **270**(9): p. 4334-40.
135. Zamaraeva, M.V., R.Z. Sabirov, E. Maeno, Y. Ando-Akatsuka, S.V. Bessonova, and Y. Okada, *Cells die with increased cytosolic ATP during apoptosis: a bioluminescence study with intracellular luciferase*. Cell Death Differ, 2005. **12**(11): p. 1390-7.
136. Hendriks, B.S., L.K. Opresko, H.S. Wiley, and D. Lauffenburger, *Quantitative analysis of HER2-mediated effects on HER2 and epidermal growth factor receptor endocytosis: distribution of homo- and heterodimers depends on relative HER2 levels*. J Biol Chem, 2003. **278**(26): p. 23343-51.

137. Shan, Y., M.P. Eastwood, X. Zhang, E.T. Kim, A. Arkhipov, R.O. Dror, J. Jumper, J. Kuriyan, and D.E. Shaw, *Oncogenic mutations counteract intrinsic disorder in the EGFR kinase and promote receptor dimerization*. Cell, 2012. **149**(4): p. 860-70.
138. Fan, Y.X., L. Wong, T.B. Deb, and G.R. Johnson, *Ligand regulates epidermal growth factor receptor kinase specificity: activation increases preference for GAB1 and SHC versus autophosphorylation sites*. J Biol Chem, 2004. **279**(37): p. 38143-50.
139. Huang, F., D. Kirkpatrick, X. Jiang, S. Gygi, and A. Sorkin, *Differential regulation of EGF receptor internalization and degradation by multiubiquitination within the kinase domain*. Mol Cell, 2006. **21**(6): p. 737-48.
140. Kiyatkin, A., E. Aksamitiene, N.I. Markevich, N.M. Borisov, J.B. Hoek, and B.N. Kholodenko, *Scaffolding protein Grb2-associated binder 1 sustains epidermal growth factor-induced mitogenic and survival signaling by multiple positive feedback loops*. J Biol Chem, 2006. **281**(29): p. 19925-38.
141. Abram, C.L. and S.A. Courtneidge, *Src family tyrosine kinases and growth factor signaling*. Exp Cell Res, 2000. **254**(1): p. 1-13.
142. Borisov, N., E. Aksamitiene, A. Kiyatkin, S. Legewie, J. Berkhout, T. Maiwald, N.P. Kaimachnikov, J. Timmer, J.B. Hoek, and B.N. Kholodenko, *Systems-level interactions between insulin-EGF networks amplify mitogenic signaling*. Mol Syst Biol, 2009. **5**: p. 256.
143. Okada, M. and H. Nakagawa, *A protein tyrosine kinase involved in regulation of pp60c-src function*. J Biol Chem, 1989. **264**(35): p. 20886-93.

144. Cole, P.A., P. Burn, B. Takacs, and C.T. Walsh, *Evaluation of the catalytic mechanism of recombinant human Csk (C-terminal Src kinase) using nucleotide analogs and viscosity effects*. J Biol Chem, 1994. **269**(49): p. 30880-7.
145. Schmidt, H. and M. Jirstrand, *Systems Biology Toolbox for MATLAB: a computational platform for research in systems biology*. Bioinformatics, 2006. **22**(4): p. 514-5.
146. Biscardi, J.S., M.C. Maa, D.A. Tice, M.E. Cox, T.H. Leu, and S.J. Parsons, *c-Src-mediated phosphorylation of the epidermal growth factor receptor on Tyr845 and Tyr1101 is associated with modulation of receptor function*. J Biol Chem, 1999. **274**(12): p. 8335-43.
147. Thomas, S.M. and J.S. Brugge, *Cellular functions regulated by Src family kinases*. Annu Rev Cell Dev Biol, 1997. **13**: p. 513-609.
148. Patwardhan, P. and M.D. Resh, *Myristoylation and membrane binding regulate c-Src stability and kinase activity*. Mol Cell Biol, 2010. **30**(17): p. 4094-107.
149. Jiang, X., F. Huang, A. Marusyk, and A. Sorkin, *Grb2 regulates internalization of EGF receptors through clathrin-coated pits*. Mol Biol Cell, 2003. **14**(3): p. 858-70.
150. Sorkin, A., M. McClure, F. Huang, and R. Carter, *Interaction of EGF receptor and grb2 in living cells visualized by fluorescence resonance energy transfer (FRET) microscopy*. Curr Biol, 2000. **10**(21): p. 1395-8.
151. Lokker, N.A. and P.J. Godowski, *Generation and characterization of a competitive antagonist of human hepatocyte growth factor, HGF/NK1*. J Biol Chem, 1993. **268**(23): p. 17145-50.

152. Klein, P., D. Mattoon, M.A. Lemmon, and J. Schlessinger, *A structure-based model for ligand binding and dimerization of EGF receptors*. Proc Natl Acad Sci U S A, 2004. **101**(4): p. 929-34.
153. Chan, P.C., Y.L. Chen, C.H. Cheng, K.C. Yu, L.A. Cary, K.H. Shu, W.L. Ho, and H.C. Chen, *Src phosphorylates Grb2-associated binder 1 upon hepatocyte growth factor stimulation*. J Biol Chem, 2003. **278**(45): p. 44075-82.
154. Rotin, D., B. Margolis, M. Mohammadi, R.J. Daly, G. Daum, N. Li, E.H. Fischer, W.H. Burgess, A. Ullrich, and J. Schlessinger, *SH2 domains prevent tyrosine dephosphorylation of the EGF receptor: identification of Tyr992 as the high-affinity binding site for SH2 domains of phospholipase C gamma*. EMBO J, 1992. **11**(2): p. 559-67.
155. Tasaki, S., M. Nagasaki, H. Kozuka-Hata, K. Semba, N. Gotoh, S. Hattori, J. Inoue, T. Yamamoto, S. Miyano, S. Sugano, and M. Oyama, *Phosphoproteomics-based modeling defines the regulatory mechanism underlying aberrant EGFR signaling*. PLoS One, 2010. **5**(11): p. e13926.
156. Ferrell, J.E., Jr., *Tripping the switch fantastic: how a protein kinase cascade can convert graded inputs into switch-like outputs*. Trends Biochem Sci, 1996. **21**(12): p. 460-6.
157. Huang, C.Y. and J.E. Ferrell, Jr., *Ultrasensitivity in the mitogen-activated protein kinase cascade*. Proc Natl Acad Sci U S A, 1996. **93**(19): p. 10078-83.
158. Sandilands, E., V.G. Brunton, and M.C. Frame, *The membrane targeting and spatial activation of Src, Yes and Fyn is influenced by palmitoylation and distinct RhoB/RhoD endosome requirements*. J Cell Sci, 2007. **120**(Pt 15): p. 2555-64.

159. Sirvent, A., C. Benistant, J. Pannequin, L. Veracini, V. Simon, J.F. Bourgaux, F. Hollande, F. Cruzalegui, and S. Roche, *Src family tyrosine kinases-driven colon cancer cell invasion is induced by Csk membrane delocalization*. *Oncogene*, 2010. **29**(9): p. 1303-15.
160. Dittmann, K., C. Mayer, R. Kehlbach, and H.P. Rodemann, *Radiation-induced caveolin-1 associated EGFR internalization is linked with nuclear EGFR transport and activation of DNA-PK*. *Mol Cancer*, 2008. **7**: p. 69.
161. Kholodenko, B.N., *MAP kinase cascade signaling and endocytic trafficking: a marriage of convenience?* *Trends Cell Biol*, 2002. **12**(4): p. 173-7.
162. Pepperkok, R., M.H. Bre, J. Davoust, and T.E. Kreis, *Microtubules are stabilized in confluent epithelial cells but not in fibroblasts*. *J Cell Biol*, 1990. **111**(6 Pt 2): p. 3003-12.
163. Erickson, H.P., *Size and shape of protein molecules at the nanometer level determined by sedimentation, gel filtration, and electron microscopy*. *Biol Proced Online*, 2009. **11**: p. 32-51.
164. Furcht, C.M., A.R. Munoz Rojas, D. Nihalani, and M.J. Lazzara, *Diminished functional role and altered localization of SHP2 in non-small cell lung cancer cells with EGFR-activating mutations*. *Oncogene*, 2013. **32**(18): p. 2346-55, 2355 e1-10.
165. Incoronato, M., A. D'Alessio, S. Paladino, C. Zurzolo, M.S. Carlomagno, L. Cerchia, and V. de Franciscis, *The Shp-1 and Shp-2, tyrosine phosphatases, are recruited on cell membrane in two distinct molecular complexes including Ret oncogenes*. *Cell Signal*, 2004. **16**(7): p. 847-56.

166. Wang, Y., S. Pennock, X. Chen, and Z. Wang, *Endosomal signaling of epidermal growth factor receptor stimulates signal transduction pathways leading to cell survival*. Mol Cell Biol, 2002. **22**(20): p. 7279-90.
167. Miaczynska, M., L. Pelkmans, and M. Zerial, *Not just a sink: endosomes in control of signal transduction*. Curr Opin Cell Biol, 2004. **16**(4): p. 400-6.
168. Ye, H., R. Kuruvilla, L.S. Zweifel, and D.D. Ginty, *Evidence in support of signaling endosome-based retrograde survival of sympathetic neurons*. Neuron, 2003. **39**(1): p. 57-68.
169. Furcht, C.M., J.M. Buonato, N. Skuli, L.K. Mathew, A. Munoz Rojas, M.C. Simon, and M.J. Lazzara, *Multivariate signaling regulation by SHP2 differentially controls proliferation and therapeutic response in glioma cells*. J Cell Sci, 2014.
170. Good, M.C., J.G. Zalatan, and W.A. Lim, *Scaffold proteins: hubs for controlling the flow of cellular information*. Science, 2011. **332**(6030): p. 680-6.
171. Barr, A.J., *Protein tyrosine phosphatases as drug targets: strategies and challenges of inhibitor development*. Future Med Chem, 2010. **2**(10): p. 1563-76.
172. Chen, L., S.S. Sung, M.L. Yip, H.R. Lawrence, Y. Ren, W.C. Guida, S.M. Sebt, N.J. Lawrence, and J. Wu, *Discovery of a novel shp2 protein tyrosine phosphatase inhibitor*. Mol Pharmacol, 2006. **70**(2): p. 562-70.
173. Zhang, X., Y. He, S. Liu, Z. Yu, Z.X. Jiang, Z. Yang, Y. Dong, S.C. Nabinger, L. Wu, A.M. Gunawan, L. Wang, R.J. Chan, and Z.Y. Zhang, *Salicylic acid based small molecule inhibitor for the oncogenic Src homology-2 domain containing protein tyrosine phosphatase-2 (SHP2)*. J Med Chem, 2010. **53**(6): p. 2482-93.

174. Xu, J., L.F. Zeng, W. Shen, J.J. Turchi, and Z.Y. Zhang, *Targeting SHP2 for EGFR inhibitor resistant non-small cell lung carcinoma*. Biochem Biophys Res Commun, 2013. **439**(4): p. 586-90.
175. Tang, C., D. Luo, H. Yang, Q. Wang, R. Zhang, G. Liu, and X. Zhou, *Expression of SHP2 and related markers in non-small cell lung cancer: a tissue microarray study of 80 cases*. Appl Immunohistochem Mol Morphol, 2013. **21**(5): p. 386-94.
176. Sattler, M., M.G. Mohi, Y.B. Pride, L.R. Quinnan, N.A. Malouf, K. Podar, F. Gesbert, H. Iwasaki, S. Li, R.A. Van Etten, H. Gu, J.D. Griffin, and B.G. Neel, *Critical role for Gab2 in transformation by BCR/ABL*. Cancer Cell, 2002. **1**(5): p. 479-92.
177. Buonato, J.M. and M.J. Lazzara, *ERK1/2 blockade prevents epithelial-mesenchymal transition in lung cancer cells and promotes their sensitivity to EGFR inhibition*. Cancer Res, 2014. **74**(1): p. 309-19.
178. Thomson, S., E. Buck, F. Petti, G. Griffin, E. Brown, N. Ramnarine, K.K. Iwata, N. Gibson, and J.D. Haley, *Epithelial to mesenchymal transition is a determinant of sensitivity of non-small-cell lung carcinoma cell lines and xenografts to epidermal growth factor receptor inhibition*. Cancer Res, 2005. **65**(20): p. 9455-62.
179. Thiery, J.P., *Epithelial-mesenchymal transitions in tumour progression*. Nat Rev Cancer, 2002. **2**(6): p. 442-54.
180. Johnson, G.L. and R. Lapadat, *Mitogen-activated protein kinase pathways mediated by ERK, JNK, and p38 protein kinases*. Science, 2002. **298**(5600): p. 1911-2.

181. Lu, W., D. Gong, D. Bar-Sagi, and P.A. Cole, *Site-specific incorporation of a phosphotyrosine mimetic reveals a role for tyrosine phosphorylation of SHP-2 in cell signaling*. Mol Cell, 2001. **8**(4): p. 759-69.
182. Sun, J., S. Lu, M. Ouyang, L.J. Lin, Y. Zhuo, B. Liu, S. Chien, B.G. Neel, and Y. Wang, *Antagonism between binding site affinity and conformational dynamics tunes alternative cis-interactions within Shp2*. Nat Commun, 2013. **4**: p. 2037.
183. Hanke, J.H., J.P. Gardner, R.L. Dow, P.S. Changelian, W.H. Brissette, E.J. Weringer, B.A. Pollok, and P.A. Connelly, *Discovery of a novel, potent, and Src family-selective tyrosine kinase inhibitor. Study of Lck- and FynT-dependent T cell activation*. J Biol Chem, 1996. **271**(2): p. 695-701.
184. Klinghoffer, R.A., C. Sachsenmaier, J.A. Cooper, and P. Soriano, *Src family kinases are required for integrin but not PDGFR signal transduction*. EMBO J, 1999. **18**(9): p. 2459-71.
185. Donepudi, M. and M.D. Resh, *c-Src trafficking and co-localization with the EGF receptor promotes EGF ligand-independent EGF receptor activation and signaling*. Cell Signal, 2008. **20**(7): p. 1359-67.
186. Sekar, R.B. and A. Periasamy, *Fluorescence resonance energy transfer (FRET) microscopy imaging of live cell protein localizations*. J Cell Biol, 2003. **160**(5): p. 629-33.
187. Wallrabe, H. and A. Periasamy, *Imaging protein molecules using FRET and FLIM microscopy*. Curr Opin Biotechnol, 2005. **16**(1): p. 19-27.